IAEA-TECDOC-337

INORGANIC ION EXCHANGERS AND ADSORBENTS FOR CHEMICAL PROCESSING IN THE NUCLEAR FUEL CYCLE

PROCEEDINGS OF A TECHNICAL COMMITTEE MEETING
ON INORGANIC ION EXCHANGERS AND ADSORBENTS
FOR CHEMICAL PROCESSING IN THE NUCLEAR FUEL CYCLE
ORGANIZED BY THE
INTERNATIONAL ATOMIC ENERGY AGENCY
AND HELD IN VIENNA, 12–15 JUNE 1984

A TECHNICAL DOCUMENT ISSUED BY THE
INTERNATIONAL ATOMIC ENERGY AGENCY, VIENNA, 1985

INORGANIC ION EXCHANGERS AND ADSORBENTS
FOR CHEMICAL PROCESSING IN THE NUCLEAR FUEL CYCLE
IAEA, VIENNA, 1985
IAEA-TECDOC-337

Printed by the IAEA in Austria
July 1985

PLEASE BE AWARE THAT
ALL OF THE MISSING PAGES IN THIS DOCUMENT
WERE ORIGINALLY BLANK

The IAEA does not maintain stocks of reports in this series. However, microfiche copies of these reports can be obtained from

INIS Clearinghouse
International Atomic Energy Agency
Wagramerstrasse 5
P.O. Box 100
A-1400 Vienna, Austria

Orders should be accompanied by prepayment of Austrian Schillings 80.00 in the form of a cheque or in the form of IAEA microfiche service coupons which may be ordered separately from the INIS Clearinghouse.

FOREWORD

Radioactive off-gases and low- to high-activity liquid and solid wastes arise from the operation of power reactors, spent fuel reprocessing plants and other nuclear fuel cycle facilities. The safe treatment and disposal of radioactive wastes is, therefore, an important engineering task. So is the extraction and recovery of useful fission products and actinides from various sources. Inorganic ion-exchangers and adsorbents have been receiving attention for these purposes because of their strong chemical affinity, high retention capacity for certain radionuclides and high resistance to irradiation.

In response to the growing interest in these topics, the IAEA convened the Technical Committee Meeting on "Inorganic Ion-Exchangers and Adsorbents for Chemical Processing in the Nuclear Fuel Cycle" at its Headquarters from June 12 to 15, 1984 with the attendance of 29 participants from 15 Member States. This Technical Document contains the 20 papers presented during the Meeting. A variety of inorganic ion-exchangers and adsorbents have been reported: zeolites, ammonium molybdophosphate, magnetite, sodium titanate, zinc-charcoal mixtures, polyantimonic acid, titanium phosphate, zirconium phosphate, hydrated alumina, silica, bentonites, mordenite, hydrous titanium oxide and others. The potential usefulness of these inorganic compounds has been proved in various areas of nuclear fuel cycle technology, especially in the separation and fixation of fission products and actinides and in the treatment of effluents from nuclear power plants and of dissolver off-gases. The use of the inorganic ion-exchangers and adsorbents can entail many advantages over conventional processes in the areas of radioactive waste treatment and in the recovery of fission products and of actinides.

The Agency wishes to thank all the scientists, engineers and institutions who contributed to this Meeting with their papers and their participation. Special thanks are due to the General Chairman, Mr. H.J.Ache (Federal Republic of Germany) and to the Session Chairmen, Messrs. L. Szirtes (Hungary), E.W. Hooper (United Kingdom), C. Madic (France), Weng Haomin (China) and M. Abe (Japan).

The officer of the IAEA responsible for this Meeting was M. Ugajin of the Division of Nuclear Fuel Cycle. Assistance in preparing the final document was provided by S. Ajuria.

EDITORIAL NOTE

In preparing this material for the press, staff of the International Atomic Energy Agency have mounted and paginated the original manuscripts as submitted by the authors and given some attention to the presentation.

The views expressed in the papers, the statements made and the general style adopted are the responsibility of the named authors. The views do not necessarily reflect those of the governments of the Member States or organizations under whose auspices the manuscripts were produced.

The use in this book of particular designations of countries or territories does not imply any judgement by the publisher, the IAEA, as to the legal status of such countries or territories, of their authorities and institutions or of the delimitation of their boundaries.

The mention of specific companies or of their products or brand names does not imply any endorsement or recommendation on the part of the IAEA.

Authors are themselves responsible for obtaining the necessary permission to reproduce copyright material from other sources.

CONTENTS

INTRODUCTION

In spite of a slowing down of construction of new power plants in comparison to previous forecasts, nuclear energy continues to be a proven source of electricity and an essential component of the energy balance of many countries. By the end of 1983 there were 317 nuclear power reactors in operation, which produced about 12% of the world's electricity. The total capacity of these reactors was 191 gigawatts (GWe). The IAEA now estimates that the total installed nuclear capacity in the world will amount to 275 GWe by 1985, to 380 GWe by 1990 and between 380 and 850 GWe by the turn of the century.

This development of nuclear power will depend on the safe and efficient operation of power reactors and supporting fuel cycle facilities. Nuclear power production generates actinides, fission products and activation products that have to be safely managed to protect the public. Radioactive off-gases and low - to high-activity liquid and solid wastes inevitably arise from the operations of power reactors and plants for uranium ore processing, fuel fabrication, spent fuel reprocessing and other nuclear fuel cycle activities.

Waste treatment is, therefore, one of the great engineering tasks that the nuclear industry has to face. Other important tasks are to extract and recover useful fission products and fissile and fertile materials from irradiated nuclear fuels and other sources.

In response to the growing interest in these topics and as a result of the increasing use of nuclear power, the IAEA decided to hold this Technical Committee Meeting within the framework of the Agency's activities on nuclear materials and fuel cycle technology. The application of inorganic ion-exchangers and adsorbents to both waste treatment and the recovery of fission products and actinides were of primary concern in this meeting. Because of the importance of the scientific knowledge needed to develop successful technical processes, the meeting covered the two major fields of fundamental studies and industrial applications.

It has been shown that inorganic ion-exchangers and adsorbents have high selectivity and high exchange capacity for certain elements which are important in the nuclear industry. Moreover, they are virtually non-combustible and generally immune to radiation damage and biological degradation, which are significant advantages over the organic ion-exchangers currently in use. There are reasonable possibilities to use inorganic exchangers for processes involving extraction, purification and retention of radioactive materials. Because of their versatility, inorganic ion-exchangers and adsorbents will play an important role in nuclear fuel cycle technology in the near future.

The main objectives of the meeting were to provide an opportunity for experts involved in chemical processing in the nuclear fuel cycle to exchange information on experimental results and experiences and to discuss the specific problems facing them. This was the first meeting organized by the Agency to deal with these topics.

SODIUM TITANATE – A HIGHLY SELECTIVE INORGANIC ION EXCHANGER FOR STRONTIUM

J. LEHTO, J.K. MIETTINEN,
Department of Radiochemistry,
University of Helsinki,
Helsinki, Finland

Abstract

A strontium-selective inorganic ion exchanger, sodium titanate, has been synthetized from an industrial intermediate of a titanium dioxide pigment process. The distribution coefficient of sodium titanate for strontium is high, nearly 10^5 at a pH above 7. The sorption capacity is also high: 1.4 mmol of strontium per gram of exchanger. The effect of high concentrations of sodium chloride, boric acid, sodium citrate and EDTA on the sorption has been studied. The sorption rate of strontium in sodium titanate has been found to be rather high. The exchanger is highly resistant to gamma radiation. A gamma irradiation dose of 10^7 Gy has practically no effect on its structure and sorption properties. Decontamination factors higher than 100 have been obtained for strontium from two actual nuclear power plant waste solutions.

1. Introduction

In the past twenty years a great number of synthetic inorganic ion exchangers have been developed for processing nuclear waste solutions. Inorganic ion exchangers have many important advantages in this field. First, most of them withstand high temperatures and radiation doses. Thus, unlike organic ion exchange resins, they can be loaded with radionuclides to a high degree and can be utilized in the treatment of hot solutions. Second, some of them, like titanates and zeolites, can be ceramized to a solid final waste product. The best known ceramic waste product is the titanate mineral based SYNROC (1). Third, many inorganic ion exchangers are highly selective to certain key radionuclides, like some zeolites are to cesium.

Sodium titanate is known to be effective in the separation of strontium. However, it has often been synthetized from expensive chemicals like titanium tetrachloride and titanium alcoxides (2,3). In this paper is described a sodium titanate product which was produced from an intermediate of an industrial titanium dioxide pigment process. The raw material is cheap and readily available. The synthesis, as well as sorption and radiation resistance properties of sodium titanate, are described.

2. Experimental

Sodium titanate was synthetized from "titanium hydrate" which is an intermediate from the titanium dioxide pigment process, the so called sulphate process used at a plant of Kemira Co., Finland. The raw material was slurried in hot butanol and sodium hydroxide was added as a 30 w-% water solution.

The mixture was stirred at 93 °C for a few hours. After the product had settled, it was filtered, washed with water and finally dried at 105 °C (4).

The sorption capacity of sodium titanate for strontium and the stoichiometry of the Sr^{2+} - Na^{+} exchange were studied using column experiments. Sr^{2+} solution (0.01-M, pH 5) was pumped at a flow rate of 0.6 ml/min through 3.0 g sodium titanate columns. The grain size of the sodium titanate was 0.315-0.850 mm, as in all other experiments. The Sr^{2+} and Na^{+} concentrations in the 18 ml fractions collected from the eluate were measured by means of an atomic absorption spectrometer (AAS). Using the eluate volume, where the Sr^{2+} concentration was 50 % (50 % breakthrough) of the concentration in the feed solution, the sorption capacity was calculated with the following formula:

$$\text{Capacity (mmol/g)} = \frac{V(50\ \%) \times C_o}{m},$$

where
$V(50\ \%)$ = eluate volume at the 50 % breakthrough
C_o = Sr^{2+} concentration in the feed solution (0.01-M)
m = exchanger mass (3.0 g)

The stoichiometry of the Sr^{2+} - Na^{+} exchange was calculated by comparing the total amount of Sr^{2+} absorbed to the total amount of Na^{+} eluted from the column.

The distribution coefficient (K_D) of strontium in sodium titanate, as a function of pH, was determined with a batch method as follows: 0.2 g samples of exchanger were shaken with 20 ml of 0.0005-M Sr^{2+} solution containing ^{85}Sr tracer. The pH's of the solutions were adjusted to different values using nitric acid. After two hours shaking, the mixtures were centrifuged and the pH's of the solutions were measured. The ^{85}Sr activities of the solutions were measured using a NaI crystal and a single channel analyser. The distribution coefficients were calculated with the following formula:

$$K_D\ (\text{ml/g}) = \frac{A_o - A}{A} \times \frac{V}{m},$$

where
A_o = ^{85}Sr activity in the solution before shaking
A = ^{85}Sr activity in the solution after shaking
V = solution volume (20 ml)
m = exchanger mass (0.2 g)

The effect of boric acid on the sorption of strontium as a function of pH was studied at two different boric acid concentrations. The experiments were carried out as described above for K_D measurements, but the 0.0005-M Sr^{2+} solutions were either 0.5-M or 1.0-M with regard to boric acid.

The effect of different sodium ion concentrations on the sorption of strontium was tested by stirring 1.0 g samples of sodium titanate in 100 ml of 0.0005-M Sr^{2+} solutions (pH 5) which where 0.0005, 0.005, 0.05, 0.5, 2.0 or 4.0 molaric with regard to sodium chloride (5). The distribution coefficients were calculated as described earlier.

The effect of organic complex forming agents, EDTA and sodium citrate, on the sorption of strontium was studied as a function of pH at two different EDTA and sodium citrate concentrations. The experiments were carried out by stirring 1.0 g samples of exchanger in 100 ml of 0.0005-M Sr^{2+} solutions of different pH values. The Sr^{2+} solutions contained these complex forming agents in molarities of 0.05 or 0.005. The Sr^{2+} concentrations of the solutions before and after two hours stirring were measured using AAS. The sorption percentages were calculated with the formula: $(A_o - A/A_o) \times 100\ \%$, where A is the strontium concentration left in the solutions after stirring and A_o is the initial strontium concentration in the solutions (4).

The sorption rate of strontium in sodium titanate was studied by stirring 1.0 g samples of exchanger in 100 ml of Sr^{2+} solution. Aliquots of 1 ml volume were drawn from the solution at different time intervals and the ^{85}Sr activities of the aliquots were measured, as described earlier. The sorption half times $T_{1/2}$ were calculated as the times during which the concentration of strontium in the solution decreases by a factor of two. The effects of the exchanger grain size and of the Sr^{2+} concentration were tested (5).

The effects of gamma irradiation on the structure and the sorption properties of sodium titanate were studied. Sodium titanate samples were irradiated with a ^{60}Co source. The total absorbed gamma dose was 10^7 Gy and the dose rate 35 kGy/h. After the irradiation, the structure was studied using X-ray diffraction, IR spectrometric and thermoanalytical methods. The specific surface area was determined. The effect on the sorption of strontium was tested by determining the distribution coefficient as a function of pH as described earlier (6).

The efficiency of sodium titanate for the separation of strontium from two actual power plant (Loviisa, Finland) waste solutions was tested. The waste solutions contained high amounts of these inactive salts: boric acid, sodium and potassium ions. The total salt contents were 215 g/l and 2 g/l. The pH values of the solutions were 12.5 and 10.0, respectively. The solution with pH 12.5, having the higher salt content, is a waste concentrate obtained by evaporation from the solution with pH 10.0. This solution originates from various sources like leakages in the primary circuits, and from decontaminations. ^{85}Sr tracer was added to these waste solutions. Samples of 450 ml volume from the solutions were eluted through sodium titanate columns of masses of 1.0 g and 2.0 g. The elution rate was 1 ml/min. The ^{85}Sr activities in the eluates were measured using a Ge(Li) crystal and a multichannel analyzer. The decontamination factors (D.F.) were calculated as the ratios of the strontium concentration in the feed solution to the concentration in the eluate.

3. Results and discussion

Fig. 1 shows a breakthrough curve of strontium from a sodium titanate column. The breakthrough curve depicts the concentrations of Sr^{2+} and Na^{+} in the eluate as a function of the eluate volume.

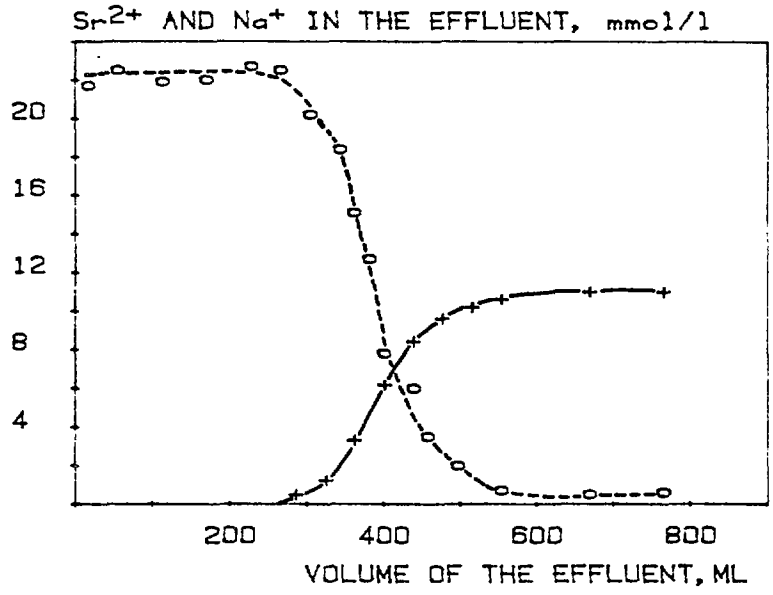

Fig. 1. A breakthrough curve of strontium from a 3.0 g sodium titanate column. Sr^{2+} concentration in the feed solution: 0.0106-M, pH: 5. Elution rate: 0.6 ml/min. Solid line (+) = Sr^{2+}, dashed line (o) = Na^{+}.

The sorption capacity of sodium titanate for strontium, calculated using the 50 % breakthrough value of strontium, was fairly high, 1.4 $\pm$ 0.1 mmol/g.

In Fig. 1 it can be clearly seen that when Sr^{2+} was absorbed in the sodium titanate column, Na^{+} was simultaneously eluted out. When Sr^{2+} began to break through, the Na^{+} concentration in the eluate decreased respectively. The molar ratio of Na^{+} eluted from the column to Sr^{2+} absorbed in the column was 2.0 $\pm$ 0.1 averaged from two experiments. This ratio and the shapes of the curves in Fig. 1 indicate a stoiciometric chemical ion exchange of two Na^{+} ions by one Sr^{2+} ion.

Fig. 2 shows the distribution coefficient K_D of strontium in sodium titanate as a function of pH. At the acidic region, K_D increases steeply and reaches a constant high value of nearly 10^5 at a pH above 7.

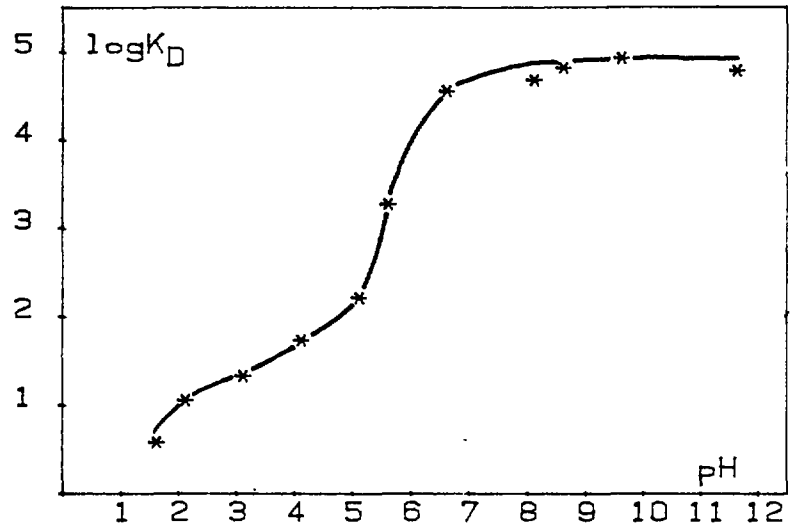

Fig. 2. The distribution coefficient K_D of Sr^{2+} in sodium titanate, as a function of pH. The initial Sr^{2+} concentration in the solution 0.0005-M.

Boric acid is used as a neutron absorber in nuclear power reactors and thus it might be found in high concentrations in low- and medium-level power plant waste solutions. The effect of boric acid on the sorption of strontium in sodium titanate is shown in Fig. 3. Up to pH 6 there is no effect. Above this pH value, the boric acid concentration of 1.0-M reduces the distribution coefficient by a factor of 10.

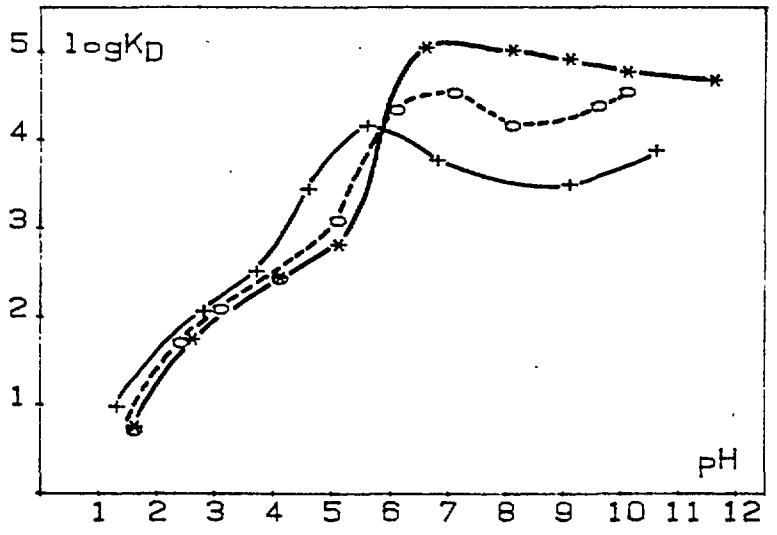

Fig. 3. The distribution coefficient K_D of Sr^{2+} in sodium titanate, as a function of pH, at two different boric acid concentrations. The initial Sr^{2+} concentration in the solution: 0.0005-M. * = 0-M H_3BO_3, o = 0.5-M H_3BO_3 (dashed line), + = 1.0-M H_3BO_3.

Nuclear waste solutions often contain high amounts of sodium. A high concentration of 4.0-M of sodium decreases the distribution coefficient of strontium in sodium titanate only by a factor of 10, as can be seen in Fig. 4. Dosch obtained a similar result with sodium titanate synthetized in the Sandia National Laboratories (7).

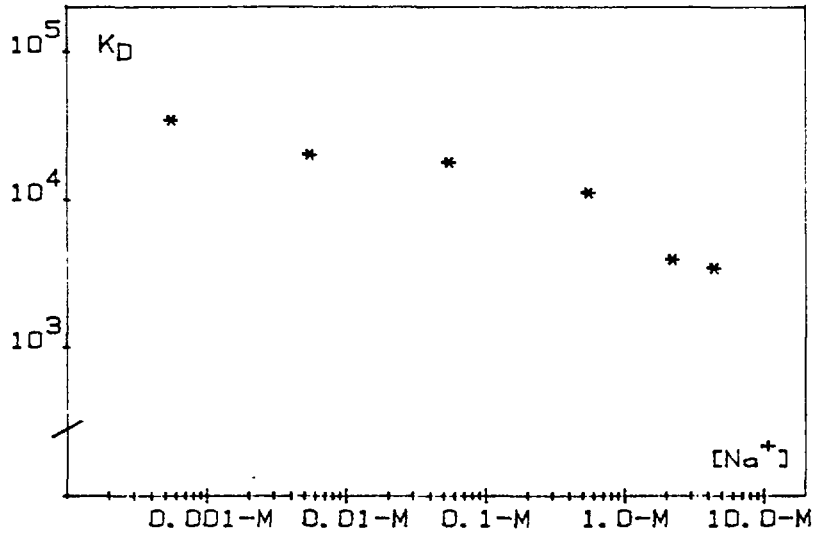

Fig. 4. The distribution coefficient K_D of Sr^{2+} in sodium titanate, as a function of Na^+ concentration. The initial Sr^{2+} concentration in the solution: 0.0005-M, pH: 5 (5).

In order to fix waste nuclides in inorganic ion exchangers, the nuclides first have to be eluted from spent organic reactor resins. This elution can be carried out by using organic complex forming agents. Methods based on this principle have been developed in Sweden (8). Figs. 5 and 6 show the effects of two complex forming agents on the sorption of Sr^{2+} in sodium titanate. EDTA decreases sorption to a great extent, and thus it can be excluded as a possible eluting agent. Sodium citrate for its part affects sorption only slightly at pH<6.

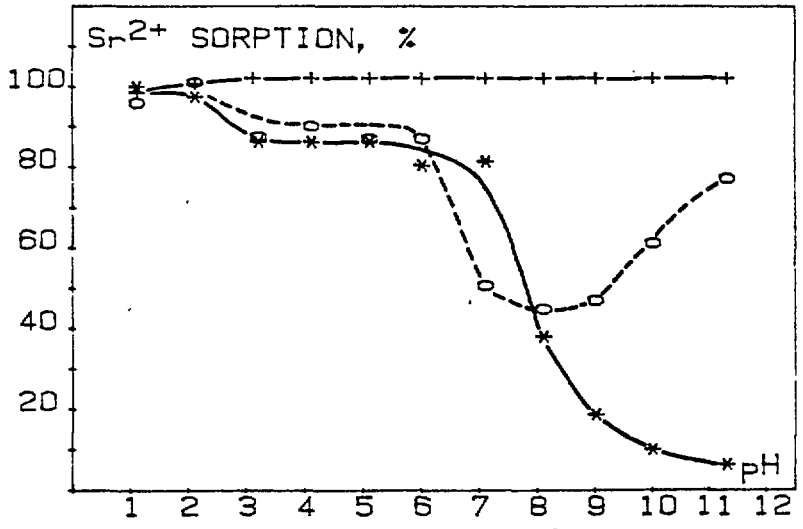

Fig. 5. The sorption percentage of Sr^{2+} in sodium titanate, as a function of pH, at two different EDTA concentrations. The initial Sr^{2+} concentration in the solution: 0.0005-M. + = 0-M EDTA, o = 0.005-M EDTA (dashed line), * = 0.05-M EDTA (4).

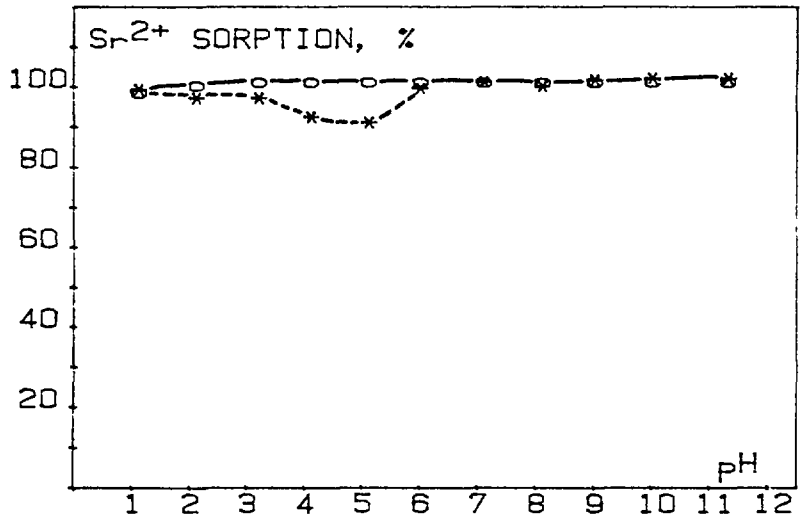

Fig. 6. The sorption percentage of Sr^{2+} in sodium titanate, as a function of pH, at two different sodium citrate concentrations. The initial Sr^{2+} concentration in the solution: 0.0005-M. o = 0.005-M sodium citrate, * = 0.05-M sodium citrate (dashed line)(4).

Sodium titanate is highly resistant to gamma radiation. Practically no change was found in its structure and in its specific surface area, when samples of the exchanger were exposed to a gamma irradiation dose of 10^7 Gy. No effect on the sorption of strontium was found either, as can be seen in Fig. 7. Kenna found a 50 % decrease in the strontium capacity of the sodium titanate synthetized in the Sandia National Laboratories after having irradiated the exchanger with a gamma irradiation dose of 2×10^7 Gy (9).

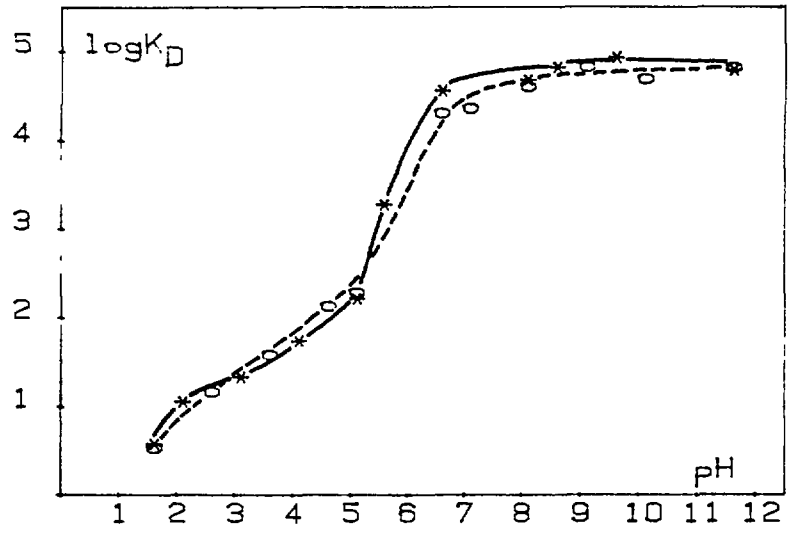

Fig. 7. The distribution coefficient K_D of Sr^{2+} in sodium titanate, as a function of pH, when the exchanger was exposed to a gamma irradiation dose of 10^7 Gy (dashed line(o)) and when not exposed (solid line (*)). The initial Sr^{2+} concentration in the solution: 0.0005-M (6).

The sorption rate of Sr^{2+} in sodium titanate is satisfactorily high considering the use of the exchanger in column operations. Sorption half time of 1.6 ± 0.2 min was obtained for sorption from a 0.001-M Sr^{2+} solution in sodium titanate with a grain size of 0.315-0.850 mm. The half time decreases when smaller grain sizes are used and increases when the Sr^{2+} concentration gets higher.

The experiments on the separation of strontium from the two nuclear power plant waste solutions, using sodium titanate, gave satisfactory results. The decontamination factors and the volume reduction factors obtained are compiled in Table I.

Table I. The decontamination factors (D.F.) and the volume reduction factors (V.R.F.) obtained from the column experiments using sodium titanate for the separation of strontium from two waste solutions taken from the Loviisa nuclear power plant, Finland. 450 ml of the solutions were eluted through the columns. The flow rate was 1 ml/min.

Salt content of the waste solution	Mass of the exchanger	D.F.	V.R.F.
215 g/l	1 g	40 ± 10	280
215 g/l	2 g	170 ± 40	140
2 g/l	1 g	130 ± 20	280
2 g/l	2 g	270 ± 50	140

4. Conclusions

Sodium titanate is highly selective toward strontium. The capacity and the distribution coefficient are high, remaining sufficient even at high concentrations of boric acid and sodium chloride. Thus this exchanger is suitable for separation of strontium from nuclear waste solutions containing high amounts of inactive salts.

The use of the industrial intermediate "titanium hydrate" as a raw material in sodium titanate synthesis reduces preparation costs significantly compared with other synthesis methods. "Titanium hydrate" is available in large amounts and is cheap. Furthermore the synthesis of sodium titanate from "titanium hydrate" is rather straightforward.

Separation of waste nuclides using sodium titanate has an additional advantage in that the loaded exchanger can be turned into a solid final waste form. One method is hot pressing used, for example, in the SYNROC process. Another method developed in our laboratory includes mixing the titanate with clay and firing the mixture at 1000 C° to a solid form (10). This method also gives a highly resistant waste form.

5. Acknowledgement

This study was supported by the Ministry of Commerce and Industry, Finland.

6. References

(1). Ringwood, A.E., et al., Nucl. Chem. Waste Manag. 2(1981)287.
(2). Forberg, S. and Olsson, P.-J., Method of Preparing Titanates Suitable as Ion-Exchange Material, U.S.Patent 4.161.513, 1979.
(3). Lynch, R.W., et al., The Sandia Solidification Process-A Broad Range Aqueous Waste Solidification Method, in Management of Radioactive Wastes from the Nuclear Fuel Cycle, IAEA, Vienna, 1976, p. 361.
(4). Heinonen, O.J., Lehto, J. and Miettinen, J.K., Radiochim. Acta 28(1981)93.
(5). Lehto, J., Heinonen, O.J. and Miettinen, J.K., Radiochem. Radioanal. Letters 46(1981)381.
(6). Lehto, J. and Szirtes, L., Radiochem. Radioanal. Letters 50(1982)375.
(7). Dosch, R.G., Final Report on the Application of Titanates, Niobates and Tantalates to Neutralized Defense Waste Decontamination - Materials Properties, Physical Forms and Regeneration Techniques, Sandia National Laboratories, Report SAND-80-1212, 1980.
(8). Forberg, S., et al., Fixation of Medium-Level Wastes in Titanates and Zeolites: Progress Towards a System for Transfer of Nuclear Reactor Activities from Spent Organic to Inorganic Ion Exchangers, in Scientific Basis for Nuclear Waste Management, Vol. 2., ed. C.J.M. Northrup, Plenum Publishing Co., 1980, p. 867.
(9). Kenna, B.T., Radiation Stability of Sodium Titanate Exchanger Materials, Sandia National Laboratories, Report SAND-79-0199, 1979.
(10).Lehto, J., Heinonen, O.J. and Miettinen, J.K., Ceramization of Inorganic Ion Exchangers Loaded with Nuclear Waste into Red Clay Tiles, in Scientific Basis for Nuclear Waste Management VI, ed. D.G. Brookins, Elsevier Science Publishing Co., 1983, p. 589.

THE EFFECT OF GAMMA RADIATION ON VARIOUS INORGANIC ION EXCHANGERS

L. SZIRTES
Institute of Isotopes,
Hungarian Academy of Sciences,
Budapest, Hungary

Abstract

The effect of gamma radiation in the range of 5×10^3 to 10^7 Gy has been studied for the following inorganic ion-exchangers: amorphous zirconium, titanium and chromium phosphates, zirconium tellurate and crystalline zirconium and cerium phosphates. The solubility in acidic solutions, the ion-exchange capacity and the specific surface area of these compounds were examined before and after irradiation. Zirconium phosphate has a very stable crystalline structure which remains unchanged during the irradiation process. The crystal lattice of cerium arsenates is partly destroyed during irradiation but the relatively high stability of the bands of AsO^{3-} groups prove that no chemical change accompanies this process. The cerium phosphate crystal is completely destroyed and becomes amorphous after irradiation.

Using ion exchangers in radiochemical practice in many cases they are exposed to high doses from charged particles and/or gamma radiation. The organic ion exchangers are submitted to radiolysis which results in changes of different properties, i.e. swelling, capacity etc. For example a Russian anion exchanger type AV-17 lossed 50% of its original capacity after irradiation with a dose of about 5×10^6 Gy (1). Other observations in this field were collected later on in the book of Yegoroff (2). These facts made difficulties in using ion exchange procedures in radiochemical practice, at least in cases when high activity level exists.

It is a pitiable fact that in contrast to the general view that all inorganic ion exchangers have a good resistance against both charged particles and gamma-rays only some works were found treating this subject (3-5).

Therefore, several years ago we made some investigations on amorphous chromium, titanium, zirconium phosphates and circonium tellurate and on crystalline zirconium, cerium phosphates and cerium arsenate (6-9).

EXPERIMENTAL

The amorphous zirconium, titanium, chromium phosphates and the zirconium tellurate were synthetized by the methods described by us earlier (10-12). The crystalline zirconium phosphate was prepared by the method of Clearfield (13), while cerium phosphate and arsenate were synthetized according to Alberti (14-15). The samples were irradiated with gamma-rays using the K-80 type gamma irradiation facility of the Institute of Isotopes (source: ^{60}Co, dose rate: 10^4 Gy/hr). The samples were irradiated for various time in such a way that they were exposed to $5x10^3$, 10^4, 10^6 and 10^7 Gy dose, respectively. Doses were controlled by chlorobenzene dosimetry (17). All experiments were carried out after irradiation in parallel on the treated and original samples.

The amounts of the components were determined by analytical chemical methods, i.e. zirconium, titanium and chromium by usual gravimetric method as oxides; cerium was determined spectrophotochemically (17) while phosphate and tellurate colorimetrically (18) and arsenic iodometrically in the usual way. The X-ray diffractograms were obtained using a DRON-2 type high-angle powder diffractometer with CuK_α (Ni-filter) radiation (λ = 0,15418 nm).

The i.r. investigations were carried out at room temperature (200-4000 cm^{-1}) using a Perkin-Elmer 225 type spectrophotometer. The spectra of the solid samples were obtained from mults in Nujol, hexachlorbutadiene and Voltalef.
The weight losses were determined by thermal analysis using MOM type derivatograph in temperature interval 25-1000°C by a heating rate of 5°C/min.

The specific surface areas of the amorphous materials were determined by the krypton adsorption method, using a volumetric gas adsorption apparatus at liquid nitrogen

temperature and were analysed by the BET method with a computer program.

The ion uptake was examined using tracer technique as follows: several samples of the ion exchangers (0.1 g. each) were equilibrated with 10 ml of 0.2 M (MCl + MOH) solution, where M denotes Na^+, K^+, Rb^+ and Cs^+ respectively. After shaking at room temperature till attaining equilibrium (usually two days); the amount of alkaline metals in the samples of the supernatant liquid were determined by measuring the radioactivities of the initial and equilibrated solutions, while for assay of the phosphate, tellurate and arsenic content the methods mentioned before were used; the process was controlled and the pH measured by Radiometer type automatic titrimeter. For labelling ^{24}Na, ^{42}K, ^{86}Rb and ^{131}Cs nuclides of high specific activities were used.

Results and Discussion

The ratios of the ligands to the central metal ions of the examined materials - both initial and irradiated - and the formulae calculated from the analytical data are collected in Table 1.

The solubility data in various acidic solvents are collected in Table 2.

The values of specific surface area of the amorphous materials are given in Table 3.

Table 1.

Ratios of ligands/metal for various materials

Ion exchanger	Formulae	Ratios	
		original	irradiated*
a.) amorphous			
Zirconium phosphate (ZPa)	$Zr(HPO_4)_2 \times H_2O$	1.95	1.95
Titanium phosphate (TP)	$Ti(HPO_4)_2 \times 1.32\ H_2O$	1.90	1.85
Chromium phosphate (CrP)	$Cr_2O(HPO_4)_2 \times 3H_2O$	1.10	1.04
Zirconium tellurate (ZTe)	$ZrO(HTeO_4)_2 \times 2H_2O$	1.22	1.20
b.) crystalline			
Zirconium phosphate (ZP)	$Zr(HPO_4)_2 \times 1.33H_2O$	2.00	1.98
Cerium phosphate (CeP)	$Ce(HPO_4)_2 \times 0.33H_2O$	1.99	-
Cerium arsenate (CeAs)	$Ce(HAsO_4)_2 \times 1.00H_2O$	2.01	1.97

*absorbed dose is 1×10^7 Gy.

Table 2.

Solubility data in various acidic solvents (mmole PO_4 or TeO_4 or As/g. ion exchanger)

Ion exchange materials	H_2SO_4		HCl		$HClO_4$		Remarks
	0.05M	0.5M	0.1M	1.0M	0.1M	1.0M	
ZP_a original	0.04	0.05	0.02	0.03	0.02	0.02	in all cases the solubility of the materials is strougly increased above pH > 8
irradiated	0.05	0.05	0.02	0.02	0.03	0.03	
TP original	0.05	0.06	0.04	0.07	0.05	0.07	
irradiated	0.05	0.05	0.06	0.06	0.07	0.06	
CrP original	0.12	0.10	0.12	0.11	0.12	0.13	
irradiated	0.11	0.10	0.12	0.13	0.13	0.11	
ZTe original	0.08	0.07	0.08	0.10	0.09	0.07	
irradiated	0.10	0.08	0.09	0.09	0.07	0.07	
ZP original	0.02	0.05	0.02	0.01	0.02	0.03	
irradiated	0.03	0.05	0.03	0.02	0.02	0.03	
CeP original	0.27	0.28	0.20	0.40	0.18	0.25	
irradiated	1.57	3.24	1.60	2.42	1.65	1.78	
CeAs original	0.08	0.61	0.12	0.25	0.10	0.22	
irradiated	0.29	0.92	0.34	0.37	0.35	0.39	

Table 3.

Specific surface area values

Ion Exchanger		S(m^2/g) before irradiation	S(m^2/g) after irradiation
Zirconium phosphate	(ZP_a)	10.8	10.0
Titanium phosphate	(TP)	8.7	1.3
Chromium phosphate	(CrP)	26.8	2.12
Zirconium tellurate	(ZTe)	16.5	1.0

The thermoanalytical data of amorphous materials are shown in Fig. 1. (dotted lines for irradiated samples).

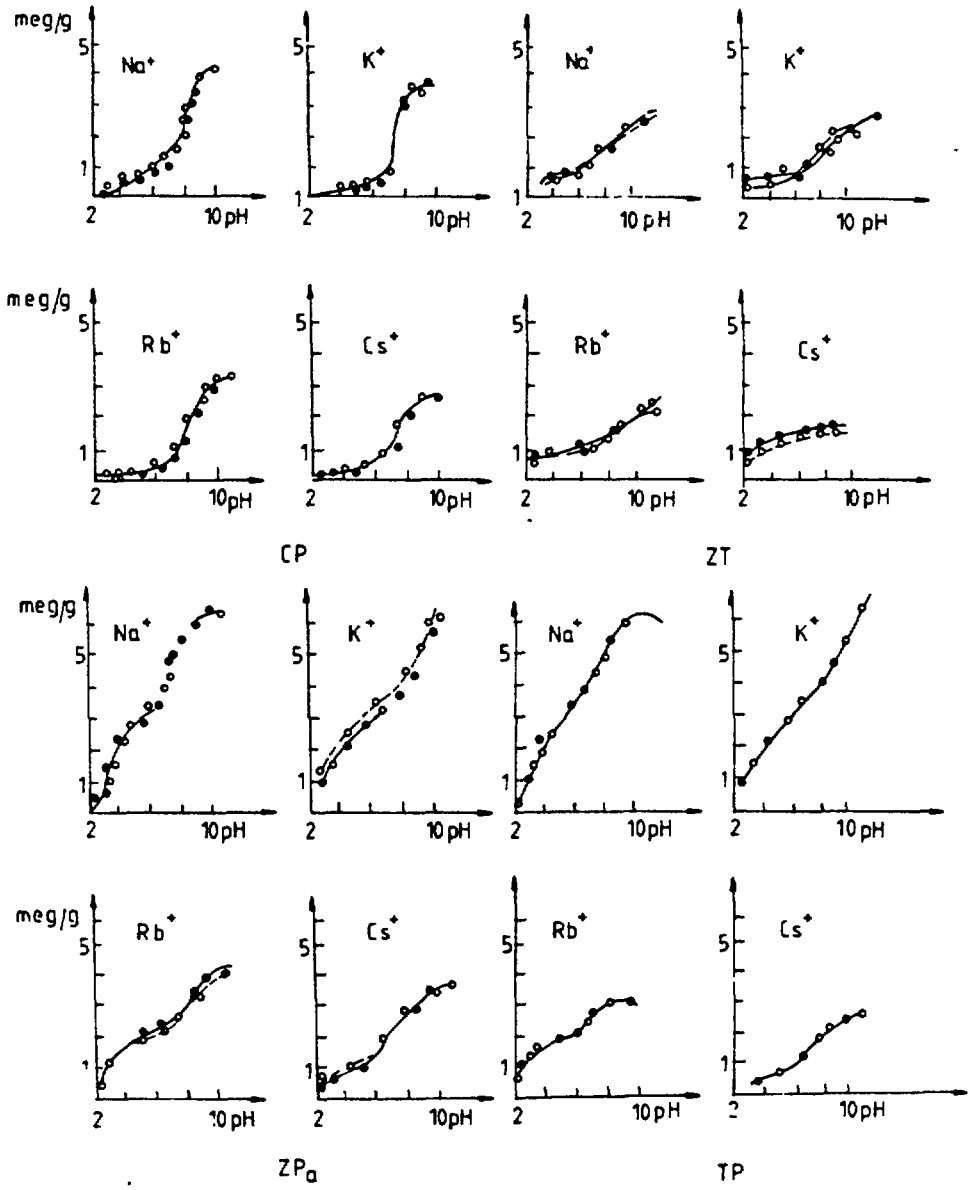

Fig. 1. Ion uptake of alkali metals on amorphous materials

The ion uptake data for alkaline metals are shown in Fig. 2.

From the data it can be seen that no characteristic changes occur in solubility, the ion uptake and thermal behaviour of the zirconium, titanium phosphates and zirconium tellurate.

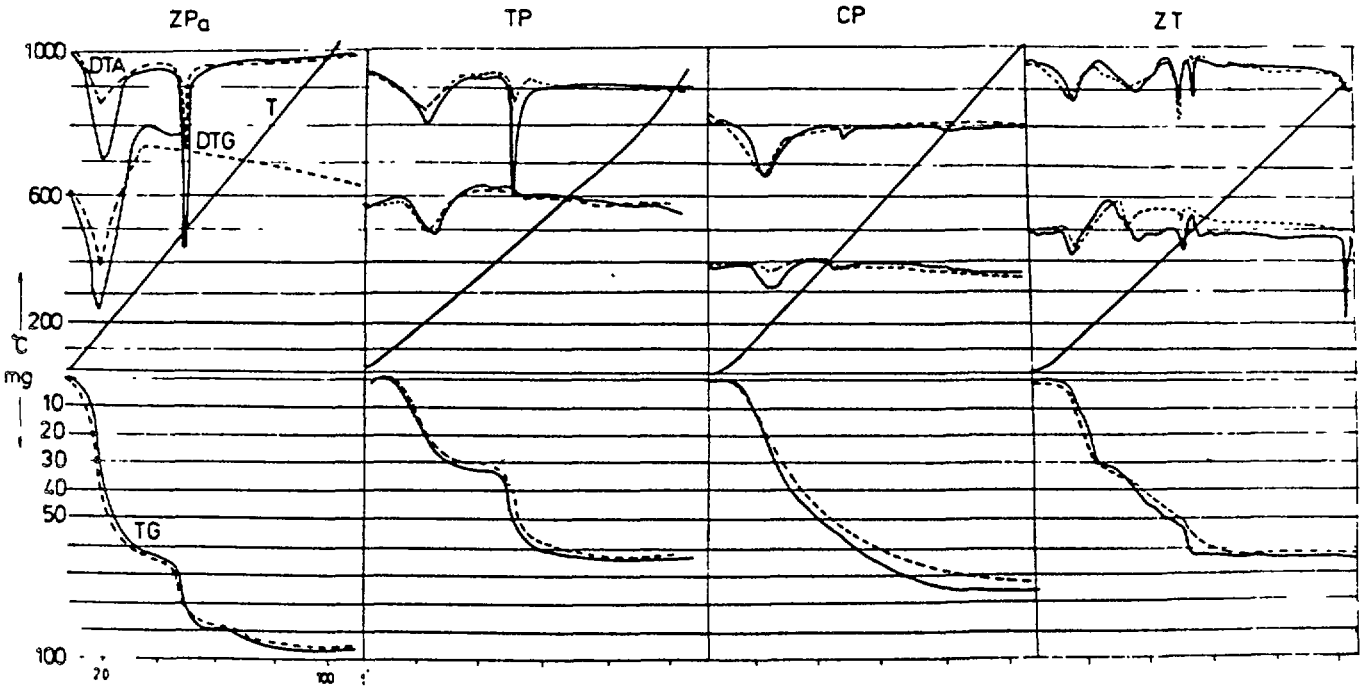

Fig. 2. Thermograms of amorphous materials (dotted line for irradiated samples)

In case of chromium phosphate under the irradiation the specific area value decreased about one order of magnitude and the exothermic process existing at 250°C on the thermogram of the initial sample was not to be found on that of the irradiated one.

This phenomenon can be explained by supposing that the polimer chain $\left[-/Cr-HPO_4-Cr/_x-H_2PO_4\right]_4$ was broken during the irradiation process. In case of crystalline materials further X-ray and i.r. spectrometric investigations were carried out. The results of these measurements are shown in Figs.3 and 4.

As it can be seen after irradiation zirconium phosphate revealed exactly the same diffractogram as the original sample; in case of cerium arsenate some extra very weak

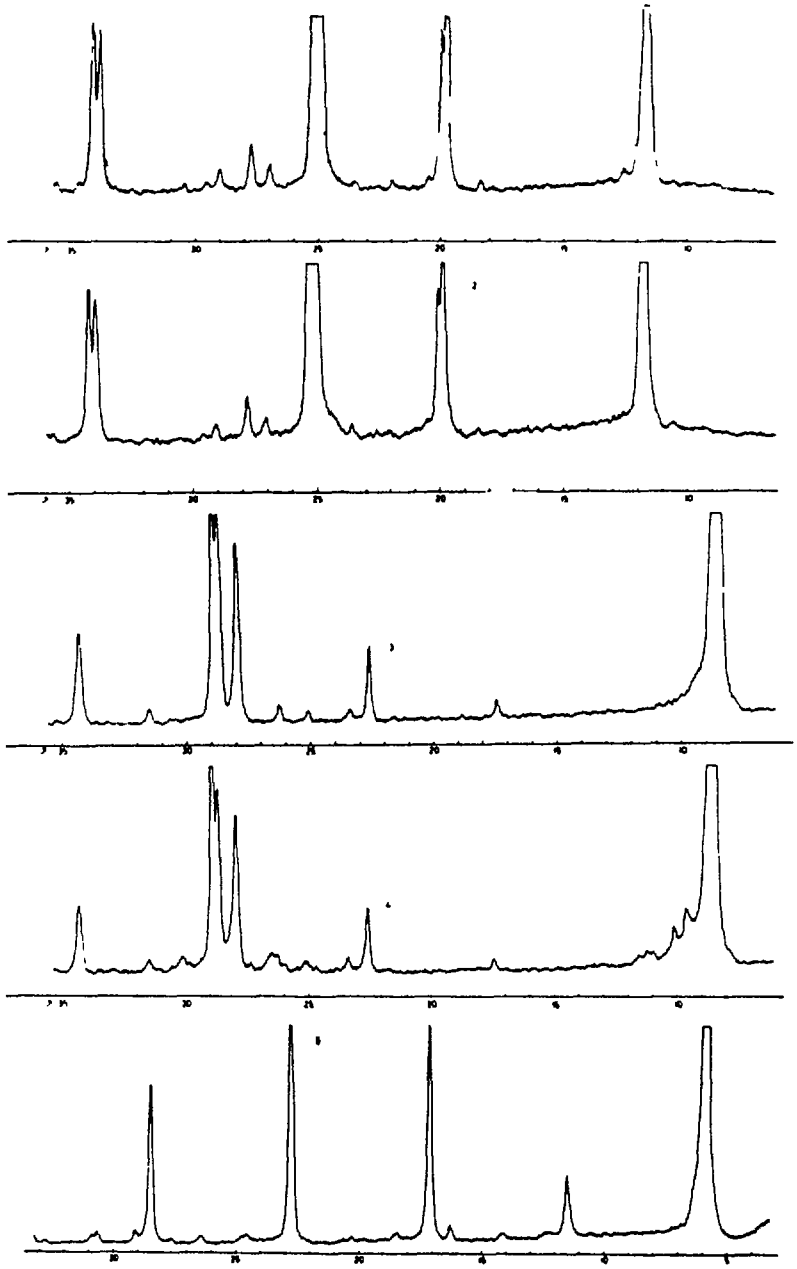

Fig. 3. X-ray diffractograms of crystalline materials 1-zirconium phosphate, 2-irradiated zircónium phosphate, 3-cerium arsenate, 4-irradiated cerium arsenate, 5-cerium phosphate, 6-irradiated cerium phosphate.

peaks appeared and the diffractogram of cerium phosphate contained no peaks et all.

The i.r. spectra of zirconium phosphate (Fig. 4) showed practially no difference between the initial and irradiated samples. In case of cerium arsenate changes only in the character of the bands due to As-OH groups (2880, 2360 and 1245 cm^{-1}) and H_2O (3590, 3485 and 1595 cm^{-1}) were found.

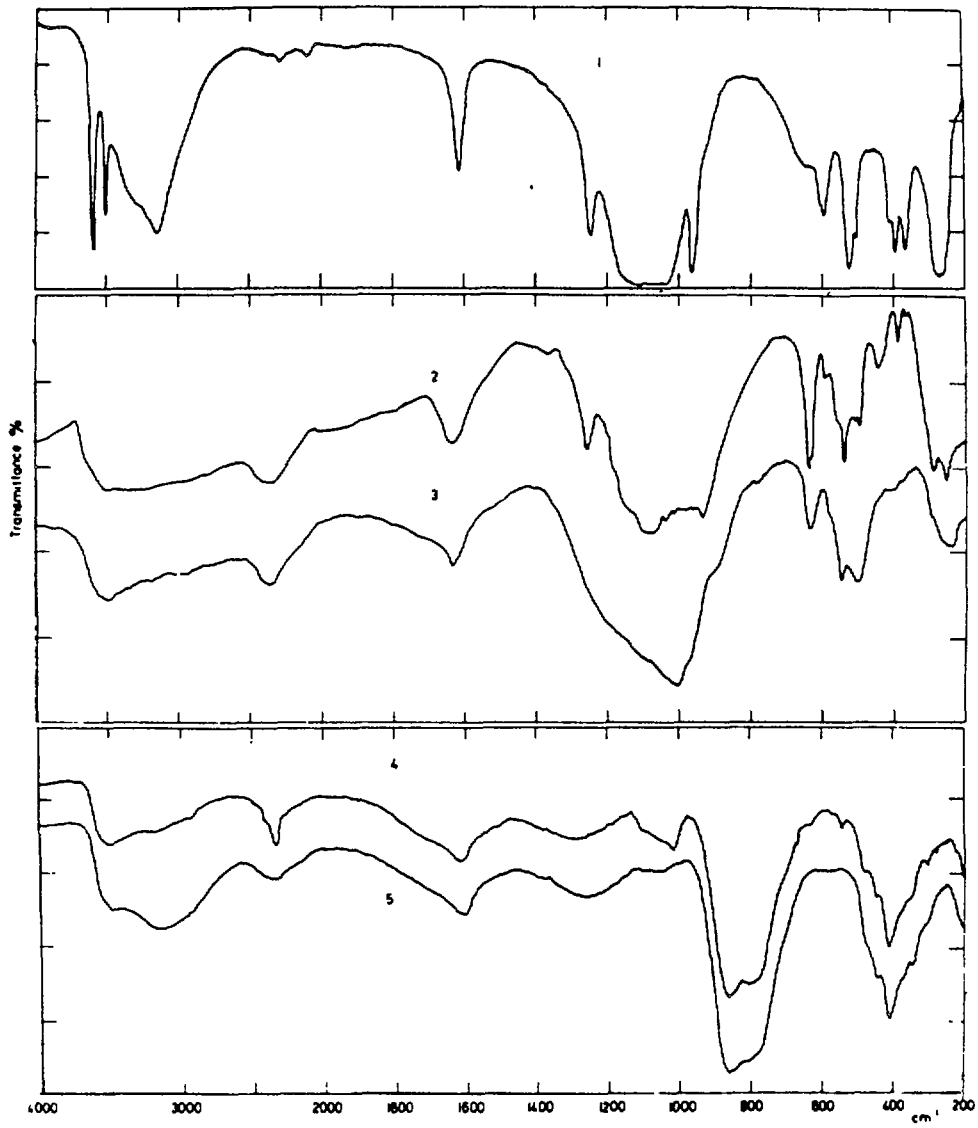

Fig. 4. Infrated spectra of crystalline materials 1-zirconium phosphate (both original and irradiated) 2-cerium phosphate, 3-irradiated cerium phosphate, 4-cerium arsenate, 5-irradiated cerium arsenate

For cerium phosphate the following changes were observed: absence of the band at 1420 cm^{-1} (P-OH in plane deformation) and the presence of a new band at 980 cm^{-1} which is due to a P-O-P structure.

The weight loss data got by thermal analysis are shown in Fig. 5. As it can be ssen both zirconium phosphate and cerium arsenate have practically the same water content before and after irradiation, while the cerium phosphate after irradiation had about twice higher weight loss than the initial sample.

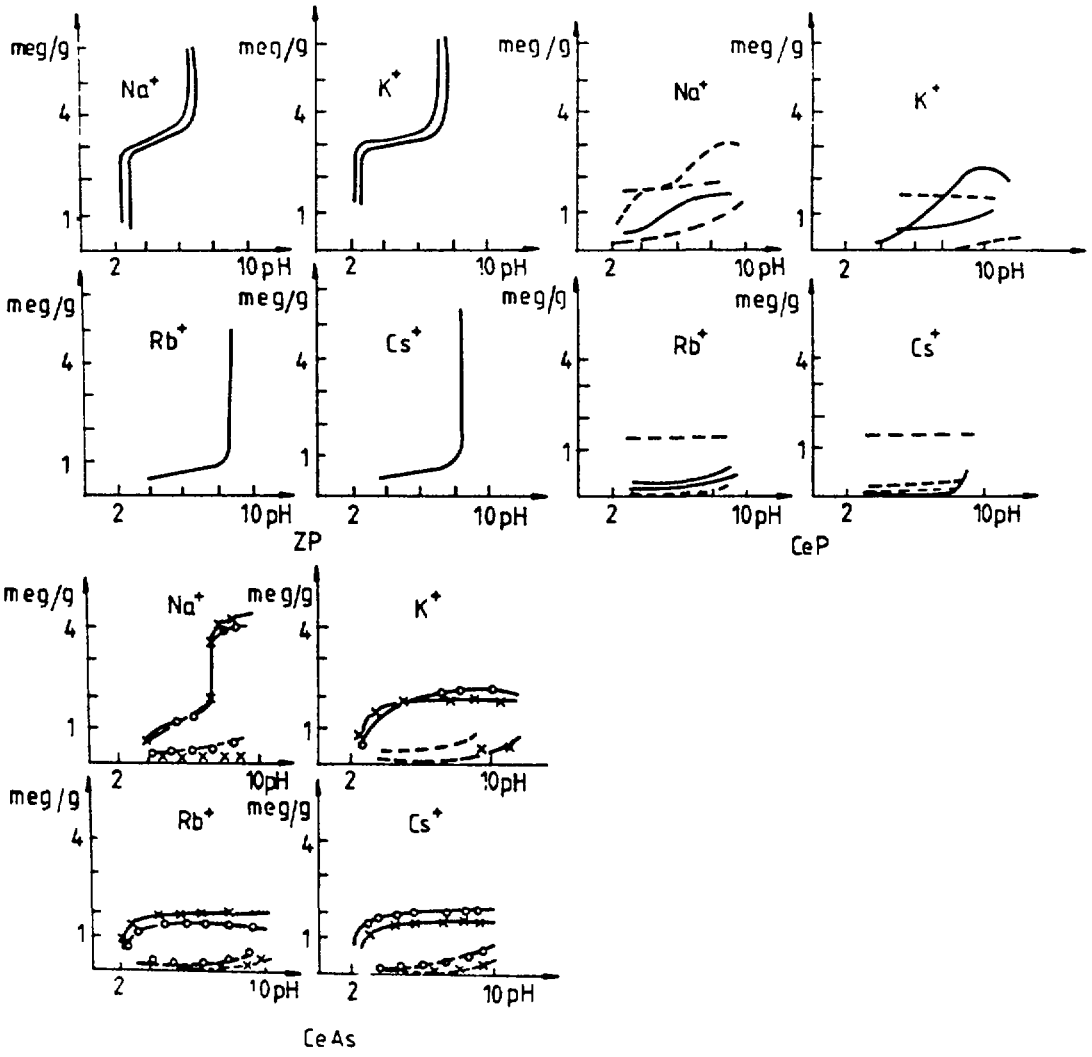

Fig. 5. Ion uptake of alkali metals on crystalline materials (dotted line shows the solubility)

Comparing the results of these three measurements the following conclusions can be drawn:

1. zirconium phosphate has a very stable crystalline structure which remains unchanged during the whole irradiation process.

2. The results concerning cerium arsenate indicated that in this case the crystal lattice was partly destroyed during irradiation but the relatively high stability of the bands of AsO_4^{3-} groups prove that no chemical change accompanies this process.

3. The cerium phosphate crystal lattice is completely destroyed after irradiation and according to the X-ray diffractogram the material became amorphous.

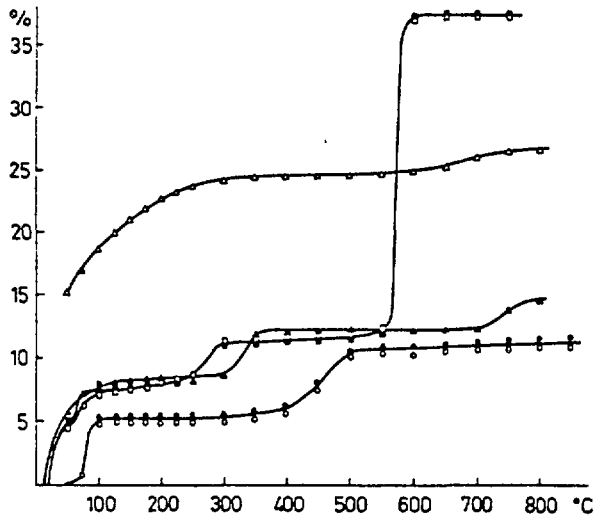

Fig. 6. Weight losses of the crystalline materials ●-●-●- zirconium phosphate, o-o-o- irradiated phosphate, ▲-▲-▲- cerium phosphate, △-△-△- irradiated cerium phosphate, ■-■-■- cerium arsenate, □-□-□- irradiated cerium arsenate

Moreover the i.r. spectra indicate an intensive decrease of HPO_4^{2-} and $H_2PO_4^-$ groups and presence of P-O-P structural elements.

The observations suggest that as a result of irradiation the original structure is split and different phosphorus--oxygen compounds are formed, which are usually rather volatile (19). This assumption seems to be strenghtened by the ion uptake (Fig. 6) and weight loss data; i.e. the higher amount of soluble materials, the higher extent of water-loss and the character of this process (the weight loss starts at a relatively low temperature and it is practically finished at 350°C).

Based on the above mentioned it can be stated that the examined amorphous materials except chromium phosphate do not change their basic behavious under the irradiation process.

The investigated crystalline materials showed individual behaviours under their irradiation with gamma rays.

Taking into consideration these facts, finishing my lecture I want to emphasize that we must not generalize the good resistance of inorganic ion exchangers against gamma radiation, but before using them we must investigate their behaviour under the irradiation. We must make this first of all in case of newly synhetized materials.

REFERENCES

[1] KISELEVA, E.D., Z. Fizicheskoi Khimii (USSR) 36 (1962) 2465

[2] YEGOROFF, E.V., NOVIKOV, P.D., Deistvie ionizinyuschih islutsenii ha ionoobmennie materiali Atomizdat Moscov 1965 (in Russian)

[3] AMPHLETT C.B., Proc. 2nd Int. Conf. on Peaceful Uses of Atomic Energy Geneva 28 (1958) 17.

[4] YASUSHI, I., Bull. Chem. Soc. Japan 36 (1963) 1316

[5] GROMOV, V.V., SPICIN, V.I., Atomn. Energ. (USSR) 14 (1963) 491.

[6] ZSINKA, L., SZIRTES, L., STENGER, V., Radiochem. Radioanal Letters 4 (1970) 257

[7] ZSINKA, L., SZIRTES, L., MINK, J., KÁLMÁN J., Inorg. Nucl. Chem. 36 (1974) 1147

[8] SZIRTES, L., ZSINKA, L., J. Radioanal. Chem. 21 (1974) 267

[9] ZSINKA, L., SZIRTES, L., MINK, J., J. Radioanal. Chem. 30 (1976) 139

[10] SZIRTES, L., ZSINKA, L., ZABORENKO, K.B., IOFA, B.Z., Acta Chim. Hung. 54 (1967) 215

[11] ZSINKA, L., SZIRTES, L., Acta Chim. Hung. 69 (1971) 249

[12] SZIRTES, L., ZSINKA, L., Radiochem. Radioanal. Lett. 7 (1971) 61.

[13] CLEARFIELD, A., STYNES, J.A., J. Inorg. Nucl. Chem. 26 (1964) 257

[14] ALBERTI, G., COSTANTINO, U., DIGREGORIO, F., GALLI, P., TORRACCA, E., J. Inorg. Nucl. Chem. 30 (1968) 295

[15] ALBERTI, G., COSTANTINO, U., DIGREGORIO, F., TORRACCA, E., J. Inorg. Nucl. Chem. 31 (1969) 3195

[16] HORVÁTH, Z., BÁNYAI, É., FÖLDIÁK, G., Radiochim. Acta 13 (1970) 150

[17] GREENHOUSE, H.C., FEINBUSH, E.M., GORDON, L., Analyt. Chem. 29 (1957) 1531

[18] BERNHARDT, D.N-, WREATH, A.R., Analyt. Chem. 27 (1955) 440

[19] VAN WASER, J.R., Phoshorus and Its Compounds Vol I pp. 217 Interscience, New York (1958)

TECHNOLOGY AND ROLE OF Cs AND Sr SEPARATION IN DISPOSAL STRATEGY OF HIGH LEVEL WASTE

L.H. BAETSLE
Centre d'étude de l'énergie nucléaire,
Mol, Belgium

Abstract

The separation of Cs and Sr from the HLW by inorganic ion exchangers has been extensively studied in the sixties as a treatment method to separate "long lived" fission products from short lived. This approach needs very high decontamination factors and a subsequent partitioning of α-emitters. The separation of Cs and Sr in acid medium was thoroughly investigated at S.C.K./C.E.N. Mol and the results obtained are briefly discussed in the perspective of an over-all waste management strategy. Based on the existing technical information different flow sheets are discussed which identify the results to be aimed at for each of the separation steps involved. Though Cs and Sr separation from HLW showed to be of little additional advantage unless it is quantitative i.e. involving very high decontamination factors, a semi-quantitative separation approach showed to be very attractive in easing the terminal disposal problem.

Any separation of both radionuclides from HLW reduces in a proportional way the heat output of the residual waste fraction and decreases the Cs contamination problems during vitrification. One of the limiting factors in disposal of vitrified HLW in conjunction with MLW and α-waste, is the decay heat emitted by the canisters. Roughly 1 KW/TEQU after 10 years and 0.6 KW/TEQU after 50 years, a 90 o/o removal of both heat producing radionuclides (^{137}Cs and ^{90}Sr) can shorten the standard cooling time in engineered structures from 50 to 20 year, or less depending on the thermal load of the formation, the separated Cs and Sr fractions have to be α-free (i.e. below 100 n Ci/g) and may not use more than 10 o/o of the initial equivalent glass volume. These requirements are fundamental and call for very specific ion exchangers with high absorption capacity. These matrices constitute after drying and conditioning a first choice storage form during 300 years. Beyond that period the radiation hazard becomes negligeable.

1. INTRODUCTION

Separation of Cs and Sr from High Level Waste (HLW) solution is a subject which was intensively studied some 20 years ago. The use of inorganic ion exchangers as separation method seemed obvious because none of the classical partition processes e.g. liquid extraction or precipitation could achieve sufficiently high decontamination factors.

The main aim of the studies was the development of inorganic ion exchangers which possessed sufficiently high selectivity coefficients for the two most important fission products ^{137}Cs and ^{90}Sr and a reasonably high uptake capacity.

In the frame work of waste treatment it was at that time hoped that by separating Cs and Sr from HLW with Decontamination Factors (DF) of 10^4 the effluent from this process could be treated as Medium Level Waste (MLW) for which adequate conditioning and disposal methods were available.

The presence of α-emitters in HLW at concentrations which are not compatible with MLW compositions was at the beginning not recognised as a very important fact, but gradually, with increasing fuel burn-up, it infused the scientific community that even the most perfect Cs-Sr partition method could not transform HLW into MLW.

2. STATUS OF Cs and Sr SEPARATION FROM HLW IN BELGIUM AROUND THE MIDDLE SIXTIES

2.1. Separation of Cs

Several inorganic ion exchangers displaying high selectivities for Cs in concentrated HNO_3 solution were developed.

- Zirconium phosphate [1][2][3]
- Titanium phosphate [4][5]
- Ferro-cyanide molybdate [6][7]

The first selective inorganic ion exchanger capable of separating Cs from simulated HAW solutions (see fig. 1 for composition and general PUREX flow sheets) was zirconium phosphate. The product was characterized as an amorphous or semi-crystalline ion exchanger with mono functional phosphate groups. The acidity of HAW or IWF being about 1 M HNO_3 and the chemical composition of the solution rather diluted, zirconium phosphate is technically usable for Cs removal. However the introduction of a Cs partition module between the HAW and IWF or between the IWF and the high activity concentrator is a real technological problem which cannot be realized unless the reprocessing process has planned the partition module during the design phase of the plant. Experiments with real HAW solutions have shown that Cs can be removed from the solution by using a zirconium phosphate cartridge but that the adsorption is rather irreversible. Regeneration and repetitive use of the same zirconium phosphate cartridge seemed to be problematic.

About simultaneously a second generation ion exchange product "titanium phosphate" was developed and showed to be superior to zirconium phosphate. The functional groups acidity of titanium phosphate was higher and the reaction kinetics of the ion exchanger was several times faster than that of zirconium phosphates. Cs separation experiments were conducted in hot cell conditions with High Activity Waste Concentrate (HAWC) solutions produced by the Eurochemic facility in 1966-1967. These solutions typical of PUREX HAWC stream contain 7 M HNO_3 and a wide variety of chemical impurities as shown in fig. 2 (composition 1). The composition 2 was artificially prepared with a tenfold lower Al-concentration because this element was not considered typical of a PUREX HAWC product but occurred in the Eurochemic waste solution. Volume reduction factors of about 50

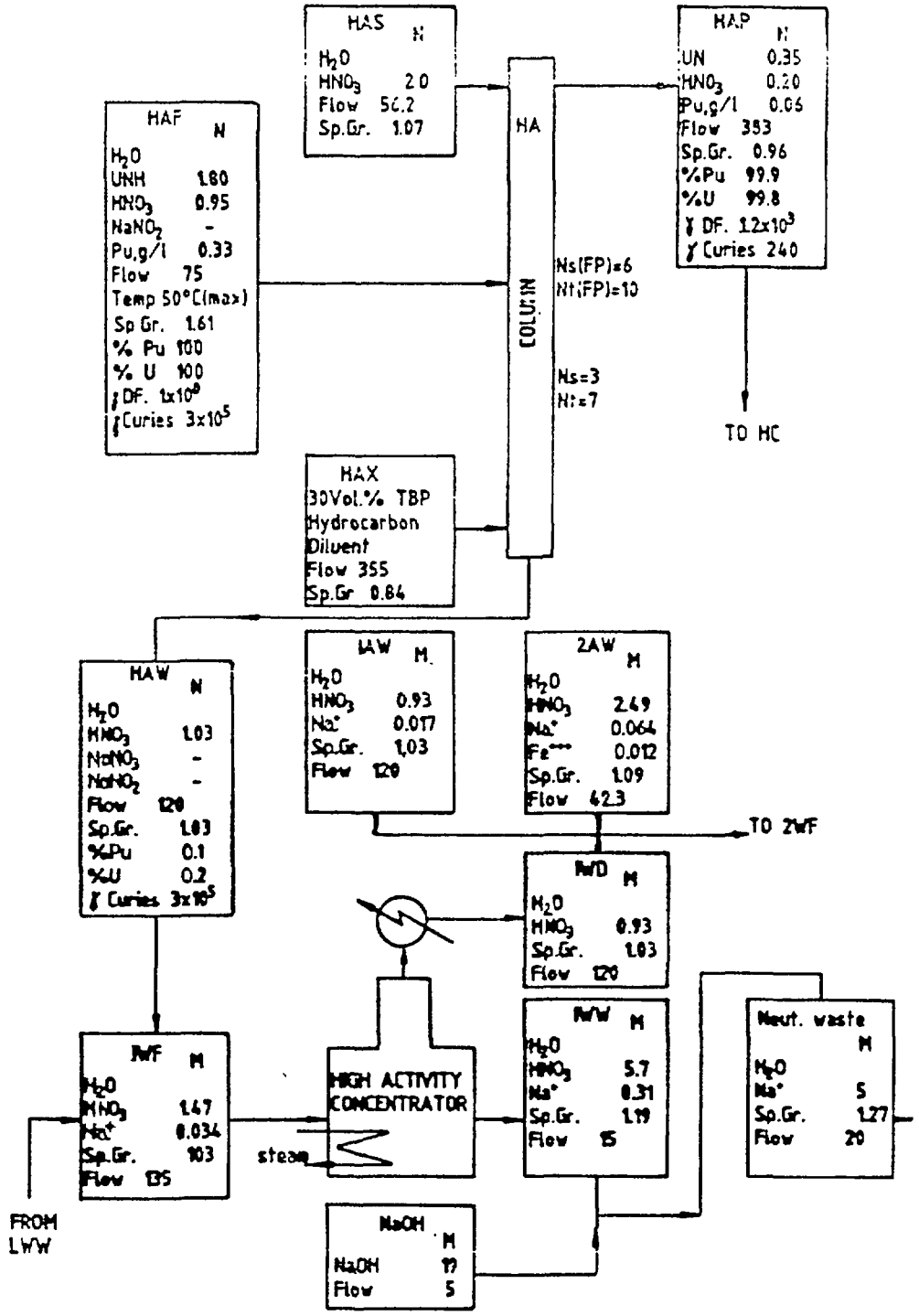

FIG. 1.

with DF's exceeding 100 have been experimentally obtained in real hot conditions. The definition of the volume reduction factor is the ratio between the volume of feed solution and that of the ion exchange cartridge on which selectively all Cs ions present in the feed solution have been concentrated. Repeated use of one cartridge was shown to be feasible and therefore the use of titanium phosphate was much more focussed on the separation of ^{137}Cs from fission product solutions as a means of cheaply producing ^{137}Cs sources for irradiation purposes.

COMPOSITION OF HAW SOLUTIONS

Element	I g/l	II g/l
Fe	1.25	1.25
Cr	0.54	0.54
Ni	0.94	0.94
Mn	0.02	0.02
Mo	1.35	1.35
Cu	0.035	0.035
Zr	5.45	0.0545
Al	22.6	0.226
U	3.35	3.35
Pu	—	—
RE	7.2	7.2
Cs	1.9	1.9
Sr	0.83	0.83
Na	8.8	0.88
Si	0.032	0.032
$SO_4^{=}$	1.34	1.34
NH_4^{+}	0.144	0.144
$PO_4^{\equiv}$	1.5	1.5
H^{+}	7.M	7.M

FIG. 2.

A third type of ion exchange material is an acid coprecitate of molybdenum and ferro-cyanides. This type of compound is much more crystalline than the M(IV) phosphates and displays the highest selectivity towards Cs in acid solution. This ion exchange material called for simplicity "Ferro-cyanide molybdate" is specifically suited for immobilization of ^{137}Cs in view of final storage. The product is chemically less stable than the M(IV) phosphates and must consequently be used in a continuous mode feed operation. The reaction kinetics is similar to that of titanium phosphate but the sorption reaction is to be considered as irreversible. Tests with real HAWC solution have been carried out till plugging of the cartridge because discontinuous mode feed operations had been imposed in hot cell.

In conclusion of the Cs sorption paragraph it may be stated that according to 1965 state-of-the-art two ion exchange materials behaved quite well in real hot cell conditions : titanium phosphate and ferro cyanide molybdate ; the first being preferred because of chemical stability.

2.2. Separation of ^{90}Sr from HLW [8]

A much more difficult partition process to be developed was the separation of Sr from HAWC solutions. None of those at that time known sorbents permitted a relatively selective separation of Sr in such a complex mixture of ions and at such high acidity. The discovery in 1965 of polyantimonic acid as Sr sorbent in acid medium constituted a real breakthrough in this field. Laboratory tests with simulated HAWC solution showed the sorption capacity to be high but the reaction kinetics very slow.

By working at higher temperature (up to 80 °C) a reasonnably good adsorption kinetics was obtained. The main ion exchange competition came from the rare earths and from sodium ions if present in solution. By continuous mode feed operation at very low flow rates practical ion exchange saturation can be achieved and volume reduction factors of 15 to 20 according to the accepted breakthrough percentage have been obtained with HAWC solutions.

As a conclusion of the previous paragraphs describing the state of-the-art on Cs and Sr partitioning from HLW in the 1960's in Belgium it can be stated that selective separation on irreversibly loaded inorganic ion exchange materials was feasible with HAWC solutions representative of typical PUREX-HLW solutions. However a better result can be obtained by installing a Cs-Sr partition module between the HAW tank and the 1 WW evaporator. A schematic flow sheet with typical adsorption data for titanium phosphate (TiP) and polyantimonic acid (PA) is given in Fig. 3. The block diagramme shows that the ^{137}Cs volume reduction factor is adequate but that the ^{90}Sr sorption capacity ought to be increased if the combined Cs + Sr cartridge is to become smaller than the initial waste vitrification volume (120 l/TeqU),[9].

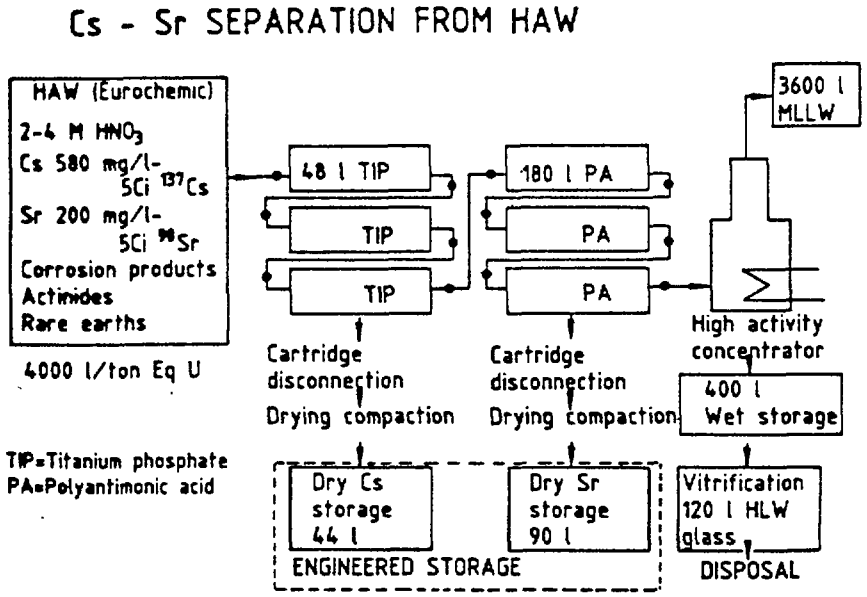

FIG. 3.

3. ROLE OF Cs-Sr SEPARATION ON LIQUID HLW HANDLING AND STORAGE

- The heat output produced by HLW as a function of time is shown on Fig. 4. It clearly illustrates the fact that from 5 till 100 years storage the heat problem is dominated by the presence of ^{137}Cs and ^{90}Sr. Indeed during this period the over-all heat output curve practically coincides with the Cs-Sr curve and starts deviating consistently from 160 years on, at which moment the heat output produced by actinides (^{241}Am and ^{243}Am essentially) equals that of the fission products.

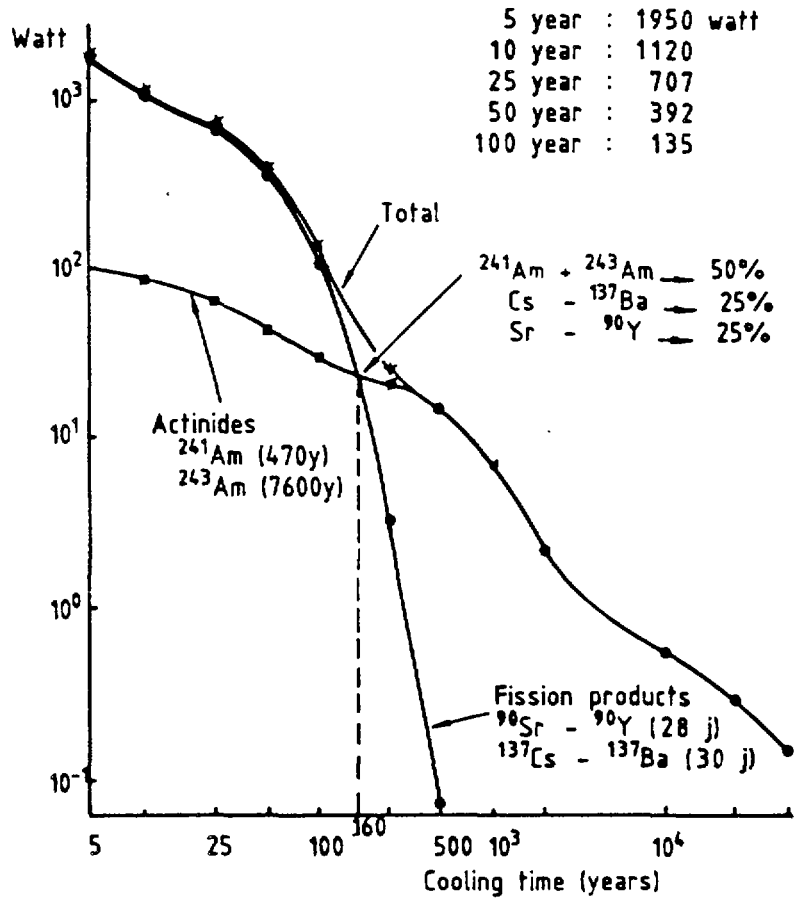

FIG. 4. THERMAL OUTPUT OF A STANDARD HLW GLASS BLOCK CORRESPONDING TO 1 TON Eq. URANIUM

- In the early storage period, between 5 and 10 years, after discharge from the reactor the HLW solution is stored in liquid form in specially equipped HLW storage tanks (see Fig. 5). The safety aspects related to this type of storage surpasses by all means those associated with the entire PUREX processing schemes A cost benefit analysis of the Cs-Sr separation might therefore help to endorse the thesis that even at short notice the simplified construction of HLW storage tanks might outweigh the construction of the Cs-Sr partition module.

- During the vitrification process liquid HLW solution is heated up at temperatures of 1150-1200 °C causing a partial evaporation of ^{137}Cs (15 to 30 %) which is partly recycled into the melter partly plated out on the cool surfaces of the ventilation system. Suppression of ^{137}Cs deposition on cold surfaces and reduction of liquids recycling is another advantage of initial Cs separation from HAW solutions as promoted in this paper. However it is difficult to evaluate the over-all benefit compared to the HLW vitrification as a stand alone process since also MLW treatment costs have to be taken into account.

SKETCH OF HIGH-LEVEL LIQUID WASTE
STORAGE TANK AT TOKAI, JAPAN

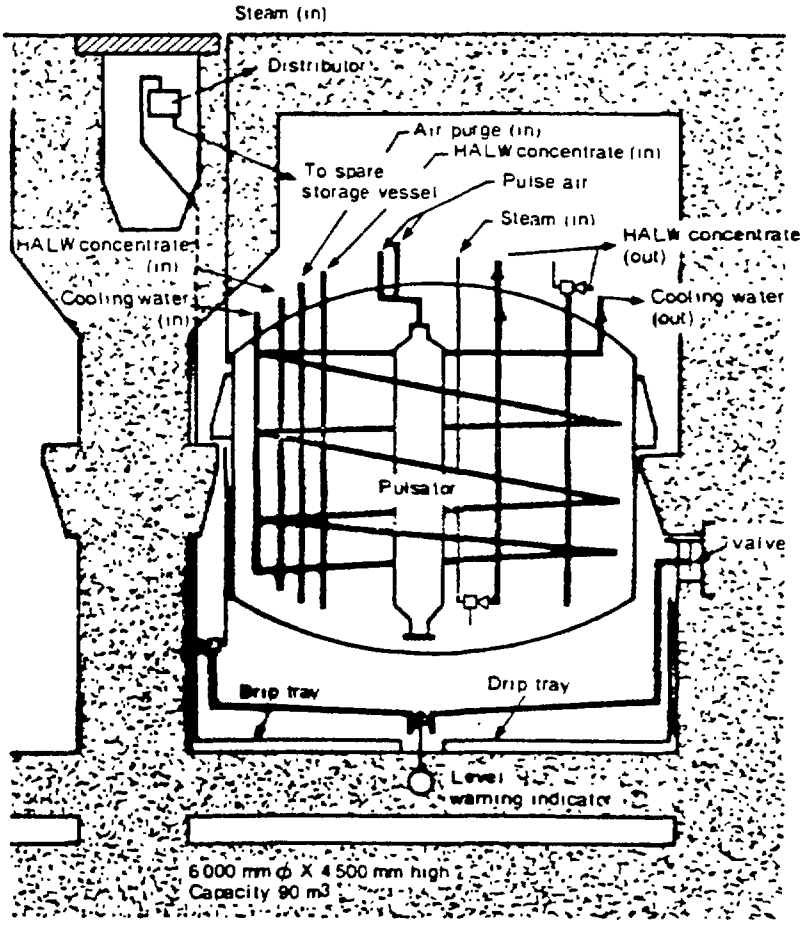

FIG. 5.

4. ROLE OF Cs-Sr PARTITIONING ON LONG TERM STORAGE OF VITRIFIED HLW

Solidified HLW resulting from the vitrification process contains all the fission products and as a consequence (explained in the previous paragraph) produces lots of heat (see Fig. 4) which have to be dissipated into the geological formation.

The actinides in the HLW produce a much lower heat which does not decrease substantially beyond 500 years.

Several scenarios (see Fig. 6) have been considered for geological disposal of HLW and α-waste resulting from a 30 year nuclear electricity production programme. For each scenario discharge from the reactor is supposed to be the origin of the time graph at t = 0, reprocessing with simultaneous production of α-wastes and liquid HLW occurs at t = 5 years and vitrification at t = 10 years.

SCENARIO 1

Disposal of α-waste 10 years after t = 0 and disposal of HLW at t = 50 years.

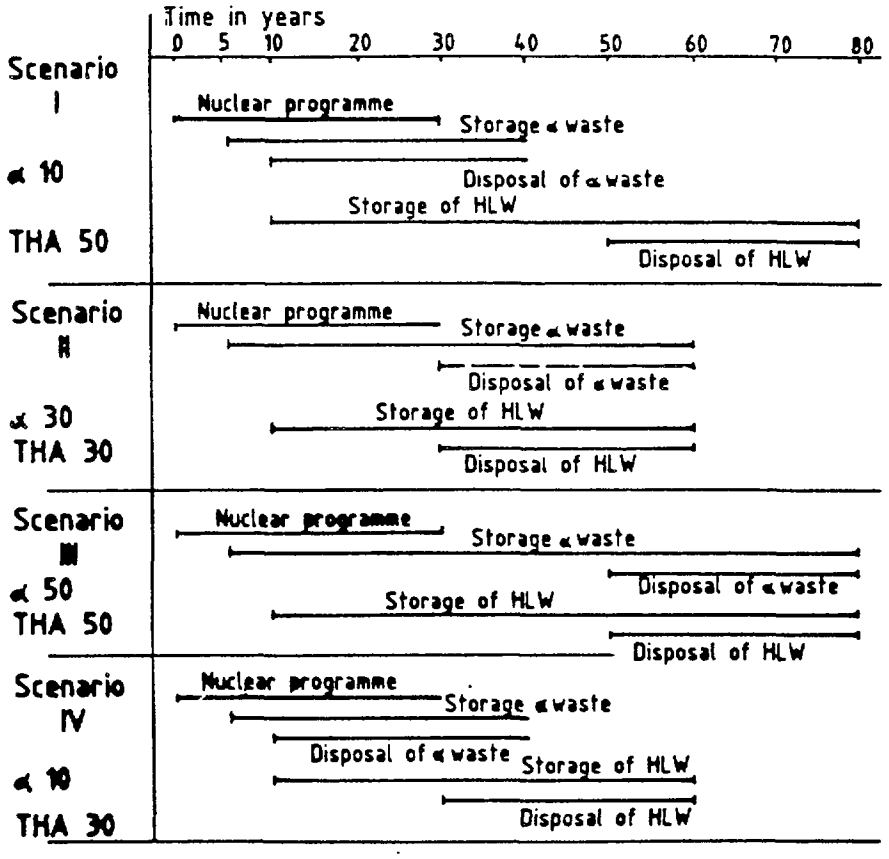

STORAGE SCENARIO' S OF REPROCESSING WASTE

FIG. 6.

SCENARIO 2

Simultaneous disposal of HLW and α-wastes at t = 30 years after discharge.

SCENARIO 3

Simultaneous disposal of HLW and α-waste at t = 50 years.

SCENARIO 4

Disposal of α-waste at t = 10 years and disposal of HLW at t = 30 years.

The limiting factor in all scenario's is without any doubt the permissible heat load of the geological formation which limits the number of canisters per unit volume or surface to be disposed off at a given time.

The earliest disposal scenario for HLW is scheduled at t = 30 years and stretches out till 50 years after the first fuel element discharge from the reactor. The α-wastes can be disposed off in a

suitable geologic formation as soon as the repository is available. Economic considerations have shown that simultaneous disposal of alpha and HLW wastes is preferable to consecutive disposal of α-wastes and HLW wastes. The economic benefits of simultaneous disposal can be deduced from the operation cost of a repository beyond the period necessary for α-wastes. In scenario 1 the time span considered amounts to 40 years whereas in scenario 4 (a formation with high thermal load) the interval between the end of the α-waste disposal period and the end of HLW disposal amounts to 20 years. Every year a repository has to be kept in operation requires the services of about 100 skilled technicians. By integrating these services over 20 respectively 40 years a total expenditure benefit of 2000 resp. 4000 man year is obtained. By disposing α-wastes together with Cs-Sr from HLW another over-all gain in disposal expenditures is expected from the size of the repository.

Presently the repository site is mainly determined by the spacing of heat sources rather than by the total volume of α-waste though these are 10 times more important in volume than HLW. By pursuing the Cs-Sr from HLW option the small HLW volumes have merely to be added to the α-waste volume which increases then with 10 % and the design differences between HLW and α-waste galleries disappear in the safety margin of the project.

In order to illustrate the influence of the heat load on the uptake capacity of a repository for HLW canisters a typical example connected to the currently investigated Boom-clay layer situated at 180-280 m below the nuclear site of Mol, Belgium is discussed in some detail, [10].

The following constraints were imposed on the design criteria : the temperature at the contact between HLW canister and the clay formation may not exceed 120 °C to avoid drying and local collapse, the temperature increase at the interface between clay and sandy layers may not exceed 5 °C in order to avoid convective currents in the sandy aquifer and finally the ground surface temperature increase may not exceed 0.5 °C.

Taking into account these very conservative hypotheses and relying on an experimental heat transfer coefficient in clay of 1.69 W/m °C it was calculated that these design conditions lead to a maximum thermal load of 22 kW per hA (hA = 10.000 m^2).

After 30 years each HLW canister (corresponding to 1.5 TeqU) still has a heat output of 1 kW which corresponds to 22 canisters per hA or the equivalent yearly HLW production of 1 GWel cooled during 30 years.

By waiting 50 years the heat output per canister decreases to 0.6 kW or each hectare has room for 36 canisters.

The removal of the heat producing fission products has the same effect as a cooling time. By removing 5 years after discharge from the reactor 50 % of the Cs-Sr or 100 % of ^{137}Cs or ^{90}Sr corresponds to a cooling of about 20 years.

Cs - Sr SEPARATION FROM FISSION PRODUCTS
REQUIRED DECONTAMINATION FACTORS

1 TEQ. HLW 50 YEARS COOLING 390 W.

DF	EQUIVALENT COOLING TIME reduced to : years
100	7.5
95	8
90	8.5
80	9.9
50	24
0	50

DECONTAMINATION FACTOR OF α EMITTERS

BASIS : 100 n Ci/g Ion exchanger
Vol. red. fact. : 50
} — 4 m Ci

α Activity { Ci 674 443
{ decay 250 years 500 years

$$\boxed{DF} = \frac{558\ Ci}{4.10^{-3} Ci} = \boxed{1.4 \cdot 10^5}$$

FIG. 7.

Fig. 7 shows systematically the influence of the removal percentage of Cs-Sr on the equivalent cooling time. It clearly shows that 80 % removal of both heat producing isotopes is sufficient to produce waste canisters which can be disposed off into a geological formation immediately after their vitrification, i.e. at t = 10 years.

The existing separation technology developed earlier is capable of providing the necessary base for the removal of Cs-Sr from HAW streams. Eighty percent removal corresponds in "ion exchange" terms to a DF = 5 which is very easy to obtain in industrial circumstances.

The question arises what to do with the separated Cs and Sr fractions ? Two aspects have to be addressed : the volume and the purity of the separated fractions.

As already shown in Fig. 3 the separation technique of Cs is sufficiently developed to put it into operation since the volume of the separated Cs cartridge is only 33 % of that of the vitrified waste (40 l compared to 120 l glass). A decontamination factor of 20 (95 % removal) can easily be guaranteed in pilot scale facilities and this separation alone reduces the cooling time of the residual vitrified waste to about 24 years.

Further R & D has to be performed in order to bring the Sr separation technique at the same chemical and technological level as that of Cs.

The second aspect which needs some further comment is the purity of the separated Cs or Sr fraction. If the separation technique has to offer new perspectives in the field of geological disposal it must provide pure Cs and Sr fractions free of long-lived α-emitters.

As shown in Fig. 7 the decontamination factors of α-emitters must be very high in order to get a cartridge whose residual α-activity is equal or lower than 100 nCi/g ion exchanger. This α-activity is now considered necessary to keep the separated fractions below the limit of α-waste which must otherwise be disposed off in geological formation. The second most important R & D task is the development of ion exchange techniques capable to cope with these severe restrictions on the α-purity of the separated Cs-Sr isotopic fraction.

If the Cs-Sr separation technique can be improved up to the point where the total volume of Cs + Sr fraction does not exceed 20 to 30 % of the regular glass volume and if these fractions are free of α-emitters their storage in bunkers during 300 years is sufficient to reduce their health hazard to a low level waste type which may be dispersed in the biosphere.

In these circumstances the nuclear electricity production has disposed off safely all the α-emitters in deep geological formation and the short-lived fission products can be stored safely during a period which is short in comparison with the lifetime of a civilisation.

REFERENCES

[1] BAETSLE, L.H., PELSMAEKERS, J. J. Inorg. Nucl. Chem. (21) pp. 124-132 (1961).

[2] BAETSLE, L.H., HUYS, D., J. Inorg. Nucl. Chem. (21) pp. 131-140 (1961).

[3] BAETSLE, L.H., J. Inorg. Nucl. Chem. (25) pp. 271-282 (1963).

[4] PIRET, J., HENRY, J., BALOU, G., BEAUDET, C., Bull. Soc. Chim. Fr. , p. 3590, (1965).

[5] BAETSLE, L.H., MARKL MUSYL, L., HUYS, D., "Ion Exchange in the Process Industries", Soc. Chem. Ind. pp. 209-215 (1970).

[6] BAETSLE, L.H., VAN DEYCK, D., HUYS, D., J. Inorg. Nucl. Chem. (27) pp. 683-695 (1965).

[7] BAETSLE, L.H., HUYS, D., VAN DEYCK D., J. Inorg. Nucl. Chem. (28) pp. 2385-2394 (1966).

[8] BAETSLE, L.H., HUYS, D., J. Inorg. Nucl. Chem. (30) pp. 636-649 (1968).

[9] BAETSLE, L.H., HUYS, D., SPEECKAERT, Ph., Belgian Report from S.C.K./C.E.N., BLG 487 (1973).

[10] COMMISSION OF THE EUROPEAN COMMUNITIES, "Nuclear Science and Technology : Admissible Thermal Loading in Geological Formations. Consequences on Radio-active Waste Disposal Methods", Vol. 1 Synthesis Report. Report EUR 8179 (1982).

EVALUATION OF ZEOLITE MIXTURES FOR DECONTAMINATING HIGH-ACTIVITY-LEVEL WATER AT THE THREE MILE ISLAND UNIT 2 NUCLEAR POWER STATION

E.D. COLLINS, D.O. CAMPBELL, L.J. KING, J.B. KNAUER
Oak Ridge National Laboratory,*
Oak Ridge, Tennessee

R.M. WALLACE
Savannah River Laboratory,**
Aiken, South Carolina

United States of America

Abstract

Mixtures of Linde™ Ionsiv™ IE-96 and Ionsiv™ A-51 zeolites were evaluated for use in the Submerged Demineralizer System (SDS) that was installed at the Three Mile Island Unit 2 Nuclear Power Station to decontaminate ~2780 m^3 of high-activity-level water (HALW). The original SDS flowsheet was conservatively designed for removal of cesium and strontium and would have required the use of ~60 SDS columns. Mixed zeolite tests, which were made on a 10^{-5} scale, indicated that the appropriate ratio of IE-96/A-51 was 3:2. A mathematical model was used to predict the performance of the mixed zeolite columns in the SDS configuration and with the intended method of operation. Actual loading results were similar to those predicted for strontium and better than those predicted for cesium. The number of SDS columns needed to process the HALW was reduced to ~10.

1. INTRODUCTION

Large volumes of high-activity-level water (HALW), containing >100 Ci/m^3, were created by the accident at Three Mile Island, Unit 2 (TMI-2). This HALW consisted of two bodies — that in the reactor coolant system (~340 m^3) and that which was spilled into the reactor building floor (~2440 m^3). Early selection of a flowsheet for decontamination of the HALW was necessary so that process design and equipment fabrication could be initiated. After careful consideration, the TMI-2 Technical Advisory Group selected a flowsheet that was based primarily on adsorption of the bulk of the radioactive contaminants, cesium and strontium, onto an inorganic ion exchanger. This exchanger, Linde™ Ionsiv™ IE-95, is a commercially available chabazite type of zeolite, having a history of successful, large-scale usage.

---

* Operated by the Martin Marietta Energy Systems, Inc., under contract DE-AC05-840R21400 with the U.S. Department of Energy.

** Operated by E.I. Du Pont de Nemours & Co. under contract DE-AC09-76SR00001 with the U.S. Department of Energy.

The processing system was designed by Allied Chemical Nuclear Services for the Chem Nuclear Company, the prime contractor for equipment fabrication and installation. The system was designed so that the equipment items containing high levels of activity were housed in one of the spent fuel handling pools in order to use the pool water for shielding. Therefore, the process was called the "Submerged Demineralizer System," or SDS, although the process was not intended to demineralize the water during its decontamination.

The SDS process flowsheet was evaluated in a series of tests made at Oak Ridge National Laboratory during early 1980, using 3 L of TMI-2 HALW.[1] The tests showed that the bulk of the cesium and strontium was effectively adsorbed on the zeolite, but that subsequent treatment with organic-based polishing resins did not provide additional decontamination from cesium and strontium or removal of the minor contaminants, ^{125}Sb and ^{106}Ru, which are anionic in nature.

The original SDS flowsheet called for the contaminated water to be clarified and then passed through a series of ion exchange columns, as illustrated in Fig. 1. Four small columns, each containing ~230 L of sorbent, were to be located within the spent fuel pool. The first three were to contain IE-96 zeolite, the fourth a strong-acid type cation exchange resin.

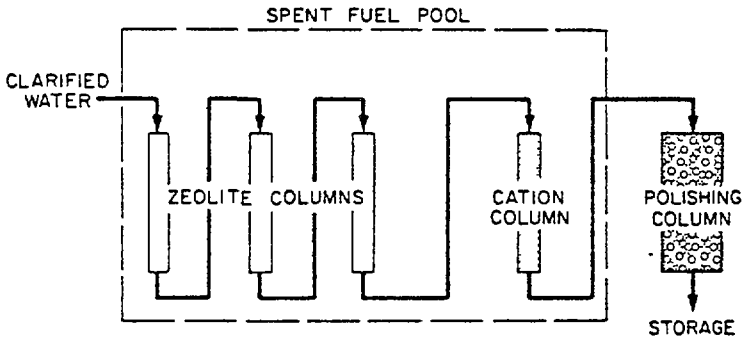

FIG. 1 ORIGINAL SDS FLOWSHEET.

The IE-96 zeolite was found to be an excellent sorbent for cesium and adequate for strontium, if the contact time between the water and zeolite was sufficiently long (>20 min). Therefore, the manner of operation of the proposed SDS was designed to accommodate the needed contact time.

The columns were modular and were intended to be used as the radioactive waste containers after being loaded. The flowsheet called for the columns to be moved after each 45,000 L of water had been processed. This is equivalent to 200 bed volumes, based on each column. At that point, the column in the first position was to be discharged, the other two moved forward one position, countercurrent to the flow of water, and a new column installed in the third position. In this manner, the cesium would be loaded in the column in the first position and all three columns would provide a sufficient contact time for strontium sorption.

2. EXPERIMENTAL PROCEDURES

2.1. Consideration for increased loading of cesium and strontium on zeolite

The original flowsheet was conservatively designed with respect to cesium and strontium removal and would have required at least 60 columns to process all of the HALW. Thus, a U.S. Department of Energy Task Force[2] evaluated the technical and financial benefits of loading the columns with cesium to a higher level than that specified by the original flowsheet. This higher level was limited by the loading characteristics of strontium.

During evaluation of the original SDS flowsheet, a 1000-bed volume test had been made. The results indicated that as many as ~600 bed volumes could be processed before strontium breakthrough from the third column would occur. Since the organic cation resin, which was to be used originally in the fourth column, was found to be ineffective for providing additional decontamination, consideration was given to using zeolite in the fourth column in order to increase the capacity of the system. Then, the throughput could be increased to 600 bed volumes, while maintaining a sufficient safety margin. This would reduce the number of SDS columns needed to ~25.

2.2. Consideration and evaluation of the use of mixed zeolites

A further increase in loading was envisioned after a more "strontium-specific" zeolite, Linde™ Ionsiv™ A-51, was identified.[3] The use of IE-96 zeolite for cesium sorption and A-51 zeolite for strontium sorption in either mixed beds, layered beds, or alternate columns was considered. The use of alternate columns would involve maintaining two types of columns that might require different treatment during subsequent waste solidification operations. If layered columns were used, and if flow distribution at the bottom of the column was poor, the bottom layer could be adversely affected. Therefore, the use of mixed columns appeared to be most appropriate.

A 1500-bed volume test was made with TMI-2 HALW and a mixed zeolite bed containing equal parts of IE-96 and A-51. The breakthrough curves obtained for cesium and strontium, using this mixture, were compared with those obtained when using only IE-96 zeolite (Fig. 2). The cesium breakthrough, when using only IE-96, was <0.01% during the entire 1000-bed volume throughput of that test.

These results show that, when using the mixed zeolite, the capacity for strontium sorption is increased by a factor of ~10, even though the kinetics of the strontium sorption, as indicated by the lesser slope of the breakthrough curve, are somewhat slower. The capacity for cesium is adequate for a throughput of up to ~2000 bed volumes. That loading would represent a factor of 10 increase over the original flowsheet design.

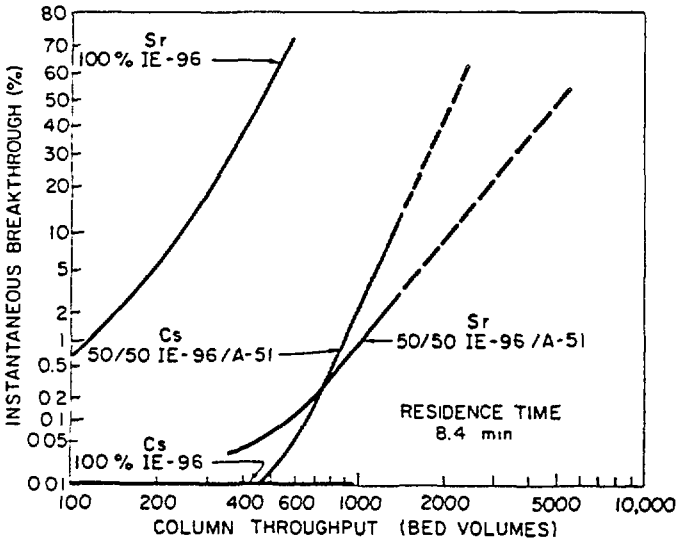

FIG. 2. COMPARISON OF PERFORMANCE OF SINGLE ZEOLITE AND MIXED ZEOLITE.

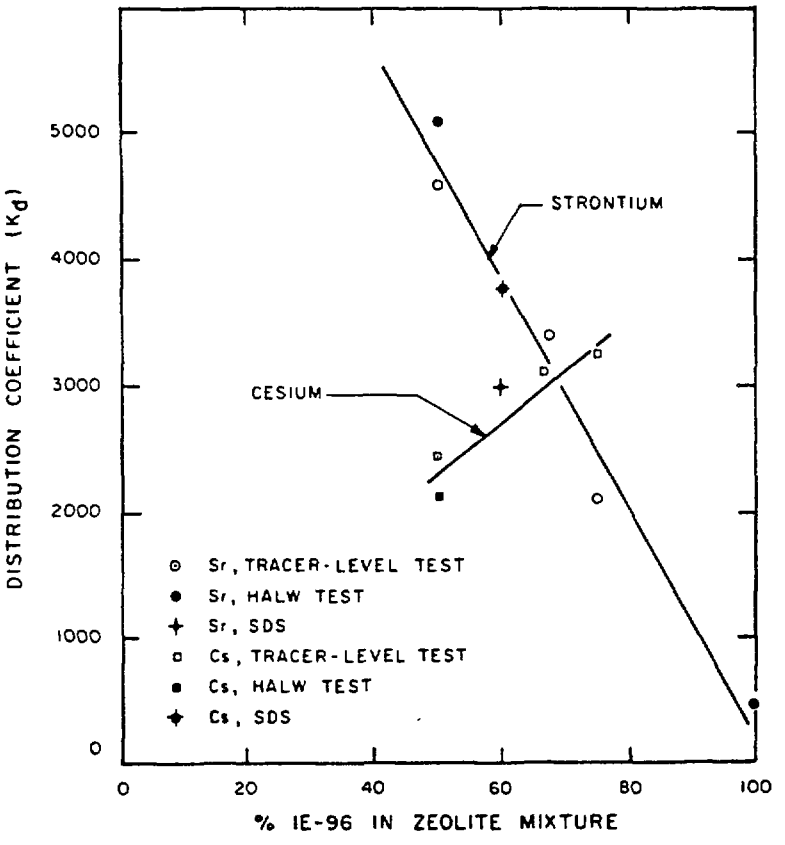

FIG. 3. CESIUM AND STRONTIUM DISTRIBUTION COEFFICIENTS OBTAINED WITH VARIOUS ZEOLITE MIXTURES.

The proportions of the two zeolites necessary to achieve balanced loadings of cesium and strontium were determined by means of a series of tracer-level tests. A synthetic solution formulated to a composition similar to the TMI-2 HALW (2000 ppm of boron, 1600 ppm of sodium, and minor amounts of other elements, with ^{137}Cs and $^{89-90}Sr$ added as radioactive tracers) was used with

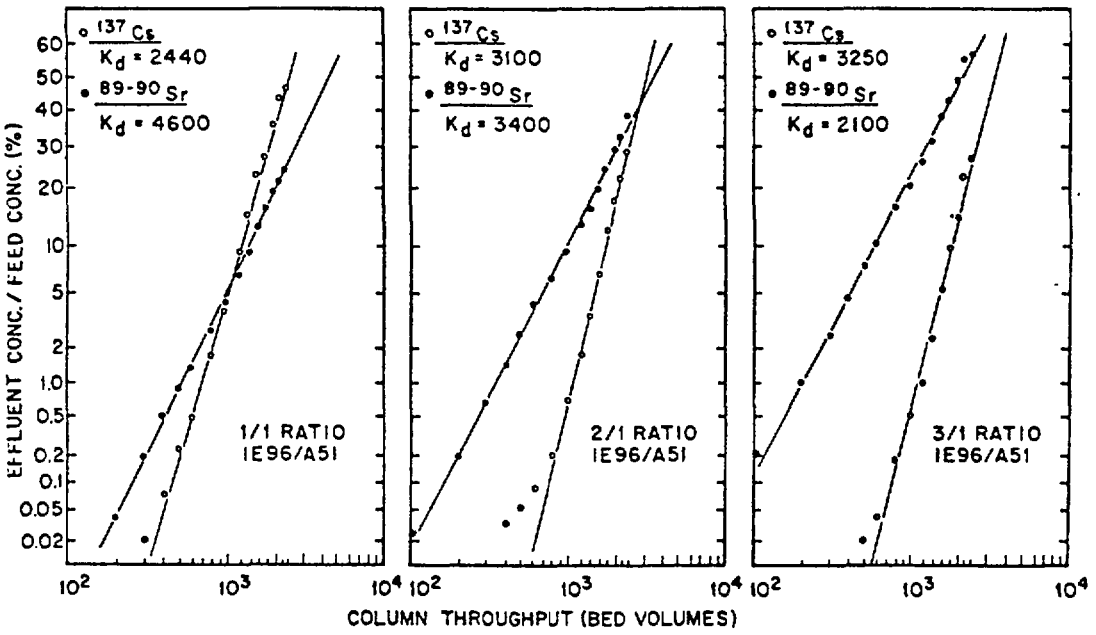

FIG. 4. RESULTS OF TRACER-LEVEL COLUMN TESTS.

the volume of TMI-2 HALW available was sufficient for only one test. That test was made with a 1:1 zeolite mixture, as described above. One of the tracer-level tests was also made with a 1:1 zeolite mixture and produced results which were not substantially different from those obtained with the actual HALW. Other tracer-level tests were made with 2:1 and 3:1 ratios of IE-96/A-51. A correlation of distribution coefficients obtained for cesium and strontium with different zeolite mixtures is shown in Fig. 3, while cesium and strontium breakthrough data are shown on a comparative basis for the series of tests in Fig. 4. These data indicate that the proper ratio for balanced loading is between 1:1 and 2:1. Thus, a mixture containing 60% of IE-96 and 40% of A-51 (a ratio of 3:2) was selected.

2.3. Modeling

The tests provided breakthrough data for only one column. Therefore, the data were fitted by means of the J-function, using the constant separation factor model developed by Thomas,[4] to enable calculation of the mass transfer coefficients and extrapolation of the data to obtain the estimated performance of a second, third, and fourth column in series.

The general Thomas equation for the reaction kinetics of ion exchange in a fixed bed is as follows:

$$-\left(\frac{\partial X}{\partial N}\right)_{NT} = \left(\frac{\partial Y}{\partial NT}\right)_{N} = X(1 - Y) - RY(1 - X) , \qquad (1)$$

where X and Y are the dimensionless concentrations of the solute ion in the fluid and solid phases, respectively, and R is the

separation factor. The variable X is defined as C/C_0, where C and C_0 are the concentrations of the solute ion of interest in the effluent and feed solutions, respectively. The variable Y is defined as q/q^*, where q is the actual concentration in the solid phase, and q^* is the concentration in the solid phase when it is in equilibrium with fluid at the inlet concentration, C_0. When the concentration of the solute ion is small relative to the concentration of the replaceable ion in the feed (as it is in this case), R approaches unity, and the isotherm is linear.

The variable N represents the length of the exchange column in transfer units and is defined by the expression

$$N = K_d' \rho_B K_a / (f/v) \ , \tag{2}$$

in which K_d' is the distribution coefficient when X = 1, ρ_B is the bulk density of the ion-exchanger, K_a is the mass-transfer coefficient characteristic of the system, f is the rate of flow of solution through the column, and v denotes the overall volume of the sorbent bed, including the void spaces. The throughput parameter, T, is defined approximately by:

$$T = (V/v)/K_d' \rho_B \ , \tag{3}$$

where V is the volume of solution processed through the column. Note that V/v is the number of "bed volumes" of solution.

Since ρ_B is essentially constant, it is convenient to define a volume-basis distribution coefficient, $K_d = q_v/C_0$, where q_v is the concentration of the solute ion per unit volume of the sorbent bed (sorbent plus void space) and C_0 is the concentration in the feed solution. Equations (2) and (3) can then be expressed as

$$N = K_d K_a / (f/v) \ , \tag{2a}$$

and

$$T = (V/v)/K_d \ . \tag{3a}$$

Equation (1) has been integrated [Eq.(16-128a) in ref. 5] for the special case of reversible second-order reaction kinetics (appropriate to ion exchange) with the solution being

$$X = C/C_0 = \frac{J(RN,NT)}{J(RN,NT) + [1-J(N,RNT)] \exp[(R-1)N(T-1)]} \ , \tag{4}$$

where J is a mathematical function[5] related to the Bessel function, I_0.

For large values of RN (a condition approached in SDS operation and in the small-scale tests), C/C_0 = ~0.5 when T = 1, independent of the values of RN. This characteristic can be employed in the data analysis. Experimental data can be used to construct logarithmic-probability plots of C/C_0 vs V/v. These plots are nearly linear and can be used to estimate K_d, which is approximately equal to V/v at the point where $C/C_0 = 0.5$. Values of R and N can then be obtained from the experimental data through the iterative use of Eqs. (3a) and (4).

A numerical solution model of the Thomas equation was developed to accept input data in a form that simulates the cyclical mode of operation proposed for the SDS. A numerical solution was required to analyze the multibed system in which the partially loaded columns are moved forward (countercurrent to the water flow) periodically, because an analytic solution is not practical unless the initial loading on each bed is zero.

The four columns of the SDS were represented in the model by two 4000-point arrays (one each for X and for Y), using 1000 points for each column. Calculations were carried out to simulate the passage of the desired volume of feed through the four columns in series, with initial values of zero for X(n) and Y(n) for all points.

At the end of the first feed cycle, the values of X(n) and Y(n) were replaced by the previously calculated values of X(n + 1000) and Y(n + 1000) for values of n between 1 and 3000 and were set equal to zero for values of n between 3001 and 4000. This procedure simulated removing the first column, moving the last three columns forward one position, and putting a new column in the fourth position. The calculations were then repeated for another cycle, using this configuration as the initial condition. This modeled rotation procedure was repeated for the number of cycles necessary to process the total volume of HALW.

2.4. Predicted and actual SDS performance

By interpolating between the experimentally derived distribution coefficients and the calculated mass transfer coefficients and separation factors for 1:1 and 2:1 zeolite mixtures, values were derived for the 3:2 mixture. These values are shown in Table I, along with corrected values obtained from early SDS operations. The observed differences were not greatly significant, even though the scaleup factor from the test column size to the SDS column size was ~10^5. Whereas the test column data indicated nearly balanced loading of cesium and strontium, the actual data showed similar performance for strontium but better performance for cesium. As shown in Table II, using the early SDS data, cesium and strontium breakthroughs were calculated for six loading cycles in which 2760 m^3 of HALW are processed (460 m^3 in each cycle). Although the strontium breakthrough continued to increase throughout the six cycles, the breakthrough from the fourth column did not exceed the concentration (0.1%) of a nonexchangeable species of strontium observed in the HALW. The number of zeolite columns used to process the bulk of the HALW at TMI-2 was reduced to ~10.

Table I. Comparison of predicted and actual performance parameters for cesium and strontium

Parameter	Test column data		SDS column data	
	Cesium	Strontium	Cesium	Strontium
Distribution coefficient (K_d)	2805	3760	3800	3000
Mass transfer coefficient (K_a)	8.0×10^{-4}	2.9×10^{-4}	2.2×10^{-3}	5.6×10^{-3}
Separation factor (R)	1.15	1.65	1.0	1.0

Table II. Calculated cumulative breakthrough of cesium and strontium for six cycles of column replacement

Cycle number	Cumulative breakthrough (% of feed)							
	Cesium				Strontium			
	Column 1	Column 2	Column 3	Column 4	Column 1	Column 2	Column 3	Column 4
1	0.62	a	a	a	13.8	0.18	a	a
2	0.71	a	a	a	22.9	0.92	a	a
3	0.73	a	a	a	29.5	2.14	a	a
4	0.73	a	a	a	34.5	3.62	0.17	a
5	0.73	a	a	a	38.3	5.21	0.35	a
6	0.73	a	a	a	41.4	6.81	0.60	a

[a]Calculated breakthrough less than observed concentrations (0.003% of cesium and 0.1% of strontium) of nonexchangeable species.

3. SUMMARY

The original SDS flowsheet at TMI-2 was conservatively designed for the removal of cesium and strontium and would have required the use of ~60 SDS columns to decontaminate the HALW. As a process improvement, the use of mixed zeolites to enable increased, balanced loadings of cesium and strontium was evaluated. Tests made on a 10^{-5} scale indicated that the appropriate ratio of Linde™ Ionsiv™ IE-96 and Ionsiv™ A-51 was 3:2. A mathematical model was used to predict the performance of the mixed zeolite columns in the SDS configurations and with the intended method of operation. Actual loading results were similar to those predicted for strontium and better than those predicted for cesium. The number of SDS columns needed to process the HALW was then reduced to ~10.

4. ACKNOWLEDGMENTS

This work was performed at the Oak Ridge National Laboratory and the Savannah River Laboratory under contracts DE-AC05-840R21400 and DE-AC09-76SR00001, respectively, with the U.S. Department of Energy.

REFERENCES

[1] CAMPBELL, D. O., et al., "Evaluation of the Submerged Demineralizer System (SDS) Flowsheet for Decontamination of High-Activity Level Water at Three Mile Island Unit 2 Nuclear Power Station," ORNL/TM-7448 (1980).

[2] Evaluation of Increased Cesium Loading on Submerged Demineralizer Systems (SDS) Zeolite Beds, DOE/SDS Task Force, DOE/NE-0012 (1981).

[3] COLLINS, E. D., et al., "Water Decontamination Process Improvement Tests and Considerations," AIChE Symposium Series 213, 78 (1982) 9.

[4] HIESTER, N. K., VERMEULEN, T., KLEIN, G., Chemical Engineers' Handbook, Fourth ed. (PERRY, J. H., et al., Eds) McGraw-Hill, New York (1963) 16-2.

[5] HIESTER, N. K., VERMEULEN, T., Chem. Eng. Prog., 48 (1952) 505.

APPLICATION OF SILVER-FREE ZEOLITES TO REMOVE IODINE FROM DISSOLVER OFF-GASES IN SPENT FUEL REPROCESSING PLANTS

T. SAKURAI, Y. KOMAKI, A. TAKAHASHI, M. IZUMO
Japan Atomic Energy Research Institute,
Tokai-mura, Ibaraki-ken,
Japan

Abstract

The present work dealt with the interaction of zeolite 13X with such organic iodides as CH_3I and C_2H_5I in the presence of NO_2 with the intention of applying silver-free zeolites to the iodine removal process of the dissolver off-gas. On the assumption that the dissolver off-gas would be dried for the purpose of removal of tritium, the experiments were carried out under a dry condition.

Zeolite 13X removes dilute CH_3I from a process gas stream with high efficiencies at ≅25 °C. It was found that NO_2 decomposed CH_3I on the zeolite. Infrared analysis and mass spectrometry confirmed that the following reaction took place on zeolite 13X and also on a silver-exchanged zeolite at ≅25 °C.

$$CH_3I + 2\ NO_2 \longrightarrow CH_3NO_3 + 1/2\ I_2 + NO.$$

A similar reaction occurs also for C_2H_5I on the zeolites:

$$C_2H_5I + 2\ NO_2 \longrightarrow C_2H_5NO_3 + 1/2\ I_2 + NO.$$

When a simulated dissolver off-gas (containing ≅100 ppm $-I_2$, ≅10 ppm-CH_3I and ≅1 %-NO_2) was supplied to a zeolite 13X bed, the I_2 which was produced by the decomposition of CH_3I was adsorbed at the same place of the bed as another I_2 which was originally included in the gas.

At ≅100 °C, the zeolite 13X bed traps only iodine and NO_2 passes through the bed without being adsorbed: the zeolite can separate iodine chromatographically from NO_2. On the basis of these experimental results, an iodine removal process was discussed.

I. Introduction

Caustic scrubbing was probably the first iodine removal process used and has been adopted in most of the nuclear reprocessing plants in the world. Because of its relatively poor net trapping efficiency (especially for organic iodides), caustic scrubbers require a secondary iodine trapping process if high efficiencies are needed.

Recently, several new iodine removal processes with higher efficiencies have been developed in many countries, as an alternative to the caustic scrubbing technique [1]. Among these alternative processes, a dry process which uses silver-exchanged zeolites or silver-impregnated adsorbents has been considered to be promising by many workers. Both elemental

iodine (I_2) and organic iodides form stable complexes or compounds with the silver in these adsorbents [1 ~ 3]. The disadvantage is in that silver is valuable and expensive; a successful recovery process of the adsorbent has not been developed yet [1].

On the other hand, silver-free zeolites, e.g. zeolite 13X, are placed in a low position in the field of the off-gas treatment. The reason seems to be that silver-free zeolites lose their iodine removal efficiencies when co-adsorption of water occurs. Wilhelm has reported that there was no useful removal efficiency for methyl iodide (CH_3I) when zeolite 13X bed was allowed to reach water adsorption equilibrium with the normal laboratory air (relative humidity 30 ~ 60 %) and at higher relative humidity (85 %) [3].

In order to remove tritium, however, there is a possibility in the near future that a filter bed of silica gel is installed in the off-gas treatment system of the dissolver off-gas (DOG). When this filter bed is realized, the water concentration of the process gas entering the iodine removal process decreases to considerably low levels. This situation makes us reconsider the use of less expensive silver-free zeolites for the iodine removal process of DOG.

On this assumption, we have been studying silver-free zeolites in order to probe their potential abilities of adsorbing iodine in the presence of NO_x. It has been already confirmed that some kinds of silver-free zeolites adsorb elemental iodine with high efficiencies [4]. Our next concern is in behavior of organic iodides on the zeolites, which would constitute 1 ~ 10 % of the total iodine quantity in DOG. No experimental data are available for the interaction of organic iodide with silver-free zeolites in the presence of NO_x. The main species of the organic iodide has been postulated to be methyl iodide (CH_3I) [5].

The present work was carried out to obtain the information about the interactions of organic iodides with silver-free zeolites in the presence of NO_x; zeolite 13X was used as the sample. A dynamic method was applied for most part of the present work with the aid of a tracer technique using radioiodine ^{131}I. A static method was adopted as occasion demanded.

II. Experimental

1. Materials

The zeolites used were: (i) zeolite 13X in the form of 1/16" pellets, and (ii) a silver-exchanged zeolite AgX in the form of 1 mmϕ particles for reference.

Commercial grade methyl iodide (CH_3I), ethyl iodide (C_2H_5I), and nitrogen dioxide (NO_2) were used without further purification.

Radioiodine, ^{131}I, was purchased from Japan Radioisotope Association in the form of a carrier-free $Na^{131}I$ solution.

2. Preparations of radioactive methyl iodide (CH_3I^*) and elemental iodine (I_2^*)

The methyl iodide was prepared through the liquid-phase reaction between dimethyl sulfate ($(CH_3)_2SO_4$) and sodium iodide (NaI) labeled with $Na^{131}I$ [6]. The product was dried on a zealite 3A bed at 100 °C.

Heating a mixture of $K_2Cr_2O_7$ and NaI labeled with $Na^{131}I$ to 400 °C yielded radioactive elemental iodine [6], which was also dried on zeolite 3A.

Their specific activities were ≅2 mCi/g-CH_3I and ≅300 μCi/g-I_2.

3. Apparatus and procedure for the dynamic method

The dissolver off-gas entering the iodine removal process of the reprocessing plants, has been postulated to include ≅1 % of NO_x and 50 ~ 200 ppm of iodine. Organic iodides constitute 1 ~ 10 % of the total iodine quantity.

In the first stage of the experiments, the removal efficiency of zeolite 13X for CH_3I was studied by supplying an air stream containing CH_3I (10 ~ 100 ppm) and NO_2 (≅1 %) to an adsorption column (15 mm i.d. x 200 mm length) packed with ≅25 g of zeolite 13X. In the second stage, a simulated DOG was fed into the adsorption column in order to predict the behavior of organic iodides in the dissolver off-gas. Figure 1 illustrates the apparatus for feeding a simulated DOG, together with experimental conditions. (In the case of the first stage experiments, the I_2-feeding line was closed.) The main air stream was dried with a zeolite 3A bed. Prior to use, the zeolite bed was heated at 400 °C for 1 h in an air flow.

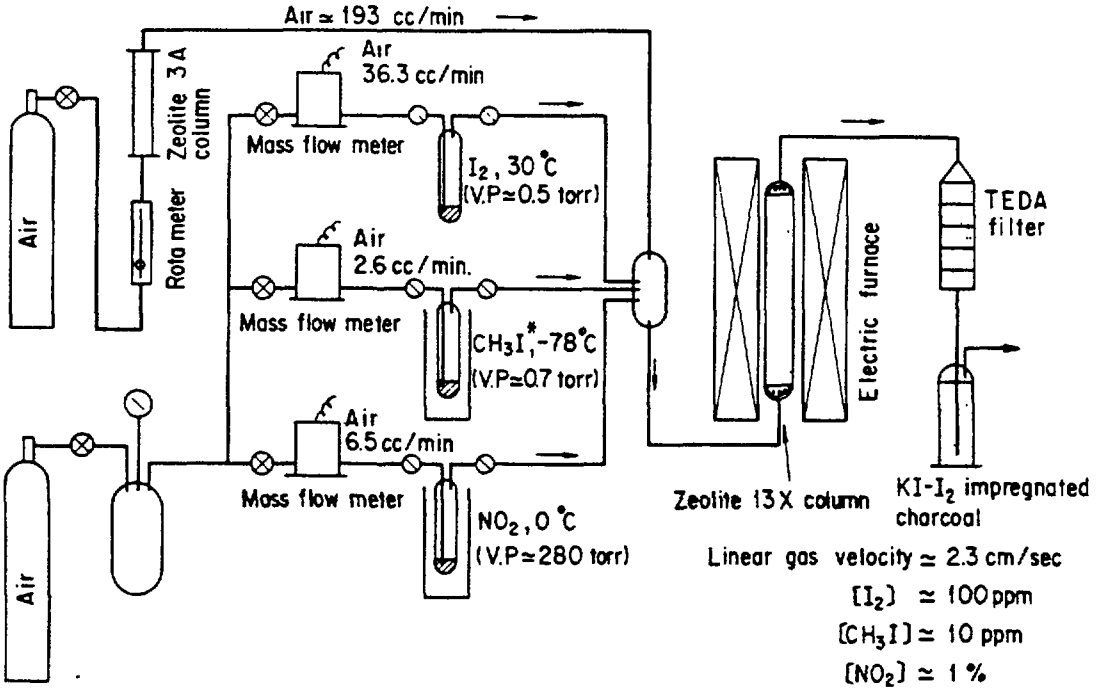

Fig. 1 Apparatus for feeding the simulated dissolver off-gas.
(V.P. = Vapor pressure)

Nitrogen dioxide represented NO_x in the present work. This would not affect validity of the results obtained, because NO_2 is a main component of NO_x and also another component NO is partly oxidized to NO_2 by oxygen and partly passed through the zeolite bed without being adsorbed.

The mass flowmeters 'Model SEC-LU' from Standard Technology Co. measured the flow rates of the air flows. Since no experimental data had been available for the vapor pressure of CH_3I at -78 °C, we checked it with a pressure gauge 'MKS Baratron pressure measurement system' from MKS Instruments INC. and obtained a value (0.7 torr or 93 Pa) close to the one extrapolated from Antoine's formula [7]. The triethylenediamine (TEDA) filter and the $KI-I_2$-impregnated charcoal captured iodine released from the adsorption column.

After the gas supply of prescribed time, distribution of ^{131}I was examined along the length of the adsorption column and the filter. In measuring radioactivity, a γ-scintillation counter (NaI) was shielded with Pb blocks of 50 mm thick so as to count it only through a slit of 10 mm wide in the front Pb block.

4. Apparatus and procedure for the static method

The interactions between CH_3I and zeolites were also studied by means of a static method. The experimental apparatus consisted of a CH_3I container (Monel), a NO_2 container (Pyrex glass), a Monel reactor to be loaded with zeolite samples (24 mm i.d. x 150 mm depth), a Monel cylinder to control the amounts of the gaseous reactants, a pressure gauge (Monel) and a vacuum manifold.

About 500 mg of the zeolite 13X was put in the reactor and dried at 400 °C for 1 h in a high vacuum. The reactor was closed and cooled with $liq-N_2$. On the other hand, CH_3I and NO_2 were introduced into the cylinder until the prescribed pressure of each gas was reached therein. The gaseous mixture was then transferred to the reactor and was condensed at its entrance end. The cold trap was removed from the reactor and the system was kept at room temperature (≅25 °C) for ≅1 h, in order to allow the zeolite to adsorb the gas. Subsequently, the reactor was detached from the apparatus for analysis of the reaction products. The infrared analysis and mass spectrometry of the products were carried out.

III. Results and discussion

1. Removal efficiency of zeolite 13X for CH_3I

The interaction of zeolite 13X with CH_3I was studied by the dynamic method in the presence of NO_2. An air flow including ≅100 ppm-CH_3I^* and ≅1 %-NO_2 was fed into the adsorption column (25 °C) at a linear gas velocity of 2.3 cm/sec. In order to realize a CH_3I^* concentration of ≅100 ppm, the CH_3I^* container (Fig. 1) was cooled to -50 °C and an air flow was passed through it at a rate of 2.6 cc/min. Distribution of ^{131}I in the column was measured at every 5 h intervals during the gas supply. Figure 2 shows the results. The abscissa of the figure denotes the

distance from the inlet of the column and the ordinate the amount of CH_3I adsorbed at each position along the length of the column.

Methyl iodide was adsorbed near the inlet of the column and accumulated there with elapse of time. On the other hand, no radioactivity was detected at the TEDA filter downstream of the column. It is therefore evident that zeolite 13X is capable of retaining successfully CH_3I^* at room temperature; a maximum amount of the adsorbed CH_3I^* exceeded 50 mg/g-zeolite 13X. In a different run, a CH_3I^* concentration of 10 ppm, almost equivalent to that in DOG, was realized by cooling the CH_3I^* container to -78 °C. The same results were obtained as to the feature of ^{131}I distribution in the adsorption column.

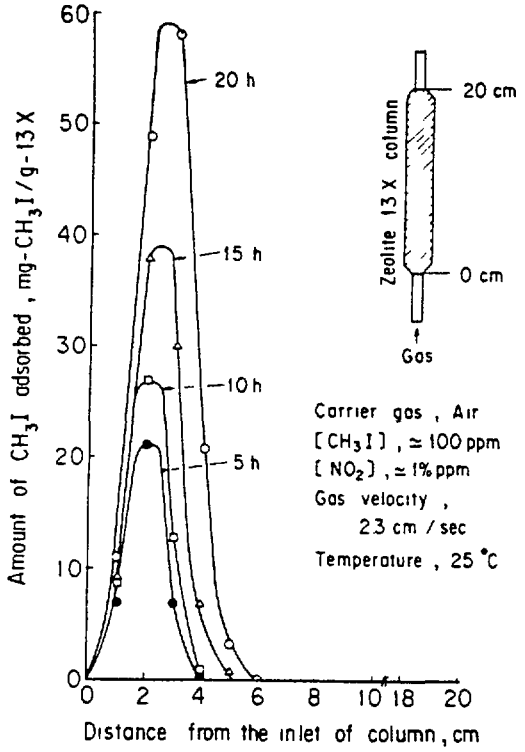

Fig. 2 Distribution of CH_3I^* in the zeolite 13X column after the gas supply of 5, 10, 15 and 20 h.

When supply of the gas was started, a yellow adsorption band of NO_2 was first noticed at the bottom of the zeolite bed. Behind this band, the zeolite bed turned pink due to the adsorption of iodine. When the air stream containing CH_3I^* alone (100 ppm) was supplied to another adsorption column, CH_3I^* was also adsorbed on the zeolite, showing a peak of ^{131}I distribution at the same position as in Fig. 2. However, in this case, the zeolite bed was not colored at all. Therefore, appearance of the pink adsorption band described above means that the decomposition of CH_3I^* into I_2^* took place in the presence of NO_2. The position of the pink adsorption band coincided with that of the peak in the figure. The adsorption front of NO_2 traveled much faster than that of I_2^* in the direction of flow: after 20 h of the gas supply, the former reached a position of 14 cm distant from the inlet of the column, whereas the latter was at a dstance of only 3.5 cm from the inlet.

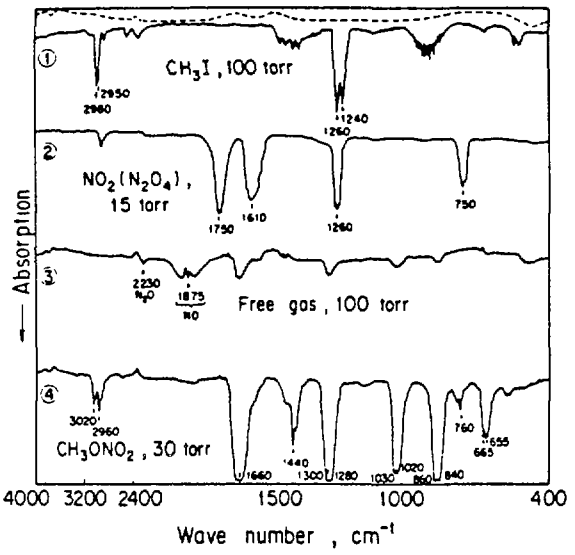

Fig. 3 Infrared spectra of ① CH_3I, ② NO_2, ($2\ NO_2 \rightleftharpoons N_2O_4$), ③ the free gas remaining after the adsorption process, and ④ CH_3NO_3.

Heating the adsorption column in an air flow resulted in the release of NO_2 at 100 ~ 200 °C and then desorption of iodine beyond 300 °C. A large amount of iodine (I_2^*) crystallized in the Pyrex tubing between the adsorption column and the TEDA filter. Hence, it became clear that CH_3I was decomposed by NO_2 on the zeolite:

Another adsorption column charged with zeolite 13X was treated with the process gas at 100 °C for 5 h. Methyl iodide was adsorbed completely, showing a peak of ^{131}I distribution centered at the position of 3 cm from the inlet of the column; however, the yellow adsorption band of NO_2 no longer appeared anywhere in the column. Keeping the column at 100 °C in an air flow caused the adsorption band of I_2^* to travel gradually in the direction of flow with elapse of time. Zeolite 13X separates iodine chromatographically from NO_2 at around 100 °C.

2. Reaction of CH_3I and C_2H_5I with NO_2

Since NO_2 was found to decompose CH_3I, we tried to identify the reaction pruduct by means of infrared analysis and mass spectrometry. Figure 3 shows the results of the infrared analysis.

Fig. 3 - ① and ② are the spectra of CH_3I and NO_2, respectively. Fig. 3 - ③ shows the spectrum of the free gas which remained in the reactor after the adsorption process. In this case, a gaseous mixture of CH_3I and NO_2 in a volume ratio of 1:2 was introduced into the reactor. The amounts of CH_3I and NO_2 were 119.4 mg and 17.4 mg, respectively. The spectrum reveals presence of NO, N_2O and other unknown substances. Mass spectrometry indicated that the main component of the remaining gas was NO and the amount of N_2O was very small. It further revealed that no free oxygen was present in the gas. After the analyses, the free gas was evacuated by pumping.

Fig. 3 - ③ suggests the presence of other products adsorbed on the zeolite; so the reactor was warmed slowly in order to desorb the unknown products. Beyond 50 °C, their desorption became observable; the pressure increased gradually with increasing temperature and reached a value of 30 torr (4 kPa) at 120 °C. Fig. 3 - ④ shows the spectrum of the gas desorbed. Analyses of the infrared and mass spectra revealed that the gas desorbed was methyl nitrate (CH_3NO_3) in an almost pure form [8].

When a gaseous mixture of CH_3I and NO_2 was kept in the absence of the zeolite for one hour, its infrared spectrum was merely a superposition of those of the two substances. The reaction of CH_3I with NO_2 needs the presence of the zeolite; it is therefore written down as follows.

$$CH_3I + 2NO_2 \xrightarrow[\text{zeolite}]{\cong 25\ ^\circ C} (1/2)I_2 + CH_3NO_3 + NO.$$

In different runs, the silver-exchanged zeolite (AgX) was treated with the CH_3I - NO_2 mixture under the same experimental conditions as described already. The same reactions were noticed thereof.

When the $[NO_2]/[CH_3I]$ ratio was increased to four in a different run, the infrared spectra obtained consisted of the absorption bands of CH_3NO_3, NO, and excess NO_2.

Although CH_3I has been postulated to be the main component of the organic iodides in DOG, there is still a possibility that other organic iodides having molecular weights greater than that of CH_3I may be present therein, e.g. ethyl iodide (C_2H_5I). So the same experiments were performed for C_2H_5I. The result was formation of ethyl nitrate ($C_2H_5NO_3$), I_2, and NO:

$$C_2H_5I + 2NO_2 \xrightarrow[\text{zeolite}]{\cong 25\ ^\circ C} (1/2)I_2 + C_2H_5NO_3 + NO.$$

Thus, the present work has confirmed that such organic iodides as CH_3I and C_2H_5I react with NO_2 in the presence of zeolites, producing I_2, the alkyl nitrates and NO.

3. Behavior of CH_3I in the simulated DOG on zeolite 13X

In order to obtain the information about the reaction rate, a simulated DOG was supplied to the adsorption column (25 °C) at a linear gas velocity of ≅2.3 cm/sec. The experimental conditions were described in Figure 1. Prior to the experiments, either I_2 or CH_3I was labeled with ^{131}I in order to distinguish their behaviors. In the experiments, the simulated DOG was supplied for 25 h at room temperature, and then the column was heated at 400 °C for 1 h; finally the gas was again supplied to the column for 6 h at room temperature. At the end of each step, distribution of ^{131}I was examined.

Figure 4 shows the results. The "I_2 in the gas stream" curve in the figure shows the distribution of the I_2 which was trapped directly from the gas stream during 25 h of the gas supply. The "I_2 from CH_3I" curve corresponds to the distribu-

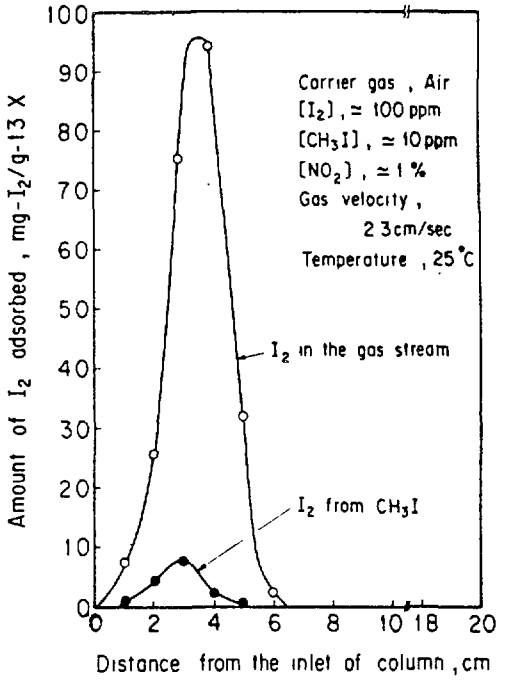

Fig. 4 Distribution of the adsorbed iodine (I_2) along the length of the zeolite 13X column. (The gas supply, 25 h)

tion of the I_2 which originally came from CH_3I in the stream through its reaction with NO_2 during the first gas supply (25 h). The location of the two peaks coincides each other: in both cases, iodine concentrated in the vicinity of the inlet and no radioactivity was detectable on the TEDA filter. There are two findings available for assuming the reaction mechanism:

(i) as described already, the CH_3I - NO_2 reaction does not take place in gas-phase, and

(ii) zeolite 13X adsorbs CH_3I itself and there is little difference in $^{131}I_2$ distribution between adsorptions of CH_3I alone and of a CH_3I - NO_2 mixture.

Therefore, the first step of the reaction would be adsorption of CH_3I on the zeolite and then NO_2 oxidizes in situ the CH_3I adsorbed.

Heating the column in air flow resulted in the desorption of NO_2 beyond 100 °C and also in small migration of the adsorbed iodine in the zeolite bed. At 400 °C, more than 90 % of the iodine was desorbed from the bed within 1 h.

Subsequently the simulated DOG was again supplied to the zeolite column for 6 h. The I_2 in the gas stream and the I_2 from CH_3I were also located at the same position of the column as in the first adsorption. The zeolite can be used repeatedly in removing iodine from DOG.

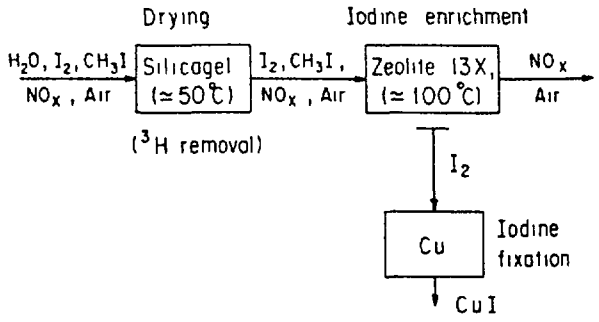

Fig. 5 An iodine removal process using zeolite 13X.

IV. Conclusion

Zeolite 13X removes both I_2 and CH_3I with high efficiencies under the dry condition; so long as NO_2 coexists, the presence of such organic iodides as CH_3I and C_2H_5I does not bring about additional problems. The stability of adsorbed iodine is however considerably lower for zeolite 13X than for AgX and other silver-impregnated adsorbents. For the long-term storage, the iodine adsorbed on zeolite 13X should be transferred to an appropriate solid material to form stable complexes or compounds.

We are considering an iodine removal process illustrated in Figure 5. The dissolver off-gas which was dried with a filter bed of silica gel is fed to a zeolite 13X bed at ≅100 °C, where iodine is trapped and NO_x passes through the bed without being adsorbed. The adsorbed iodine is then desorbed from the bed at ≅400 °C and is allowed to react with copper to form CuI, which would be fed to the long-term storage.

REFERENCES

[1] Burger, L. L. and Scheele, R. D., "The Status of Radioiodine Control for Nuclear Fuel Reprocessing Plants", PNL-4689 (1983).

[2] Maeck, W. J., Pence, D. T. and Keller, J. H., "A Highly Efficient Inorganic Adsorber for Airborne Iodine Species (Silver zeolite development studies)", CONF-680821, (1968) 185.

[3] Wilhelm, J. G., "Trapping of Fission Product Iodine with Silver Impregnated Molecular Sieves", KFK-1065, (1969).

[4] Sakurai, T., Izumo, M., Takahashi, A. and Komaki, T., J. Nucl. Sci. Technol., 20 (1983) 784.

[5] Atkins, D. H. F. and Eggleton, A. E. J., "Iodine Compounds Formed on Release of Carrier-Free Iodine-131", AERE-M-1211, (1963).

[6] Noguchi, H., Murata, M., Tsuchiya, Y., Matsui, H. and Kokubu, M., "A Method of Quantitative Measurement of Radioiodine Species Using Maypack Sampler", JAERI-M-9408, (1981).

[7] Lange, N. A. (Ed.), "Handbook of Chemistry", Handbook Publishers, Inc., Sandusk, OHIO, (1956) 1424.

[8] Strinhagen, E., Abrahamsson, S. and Mclafferty, F. W., "Atlas of Mass Spectral Data", Vol. 1, Interscience publishers, New York, (1969) 97.

RADIOACTIVE RUTHENIUM REMOVAL FROM LIQUID WASTES OF ^{99}Mo PRODUCTION PROCESS USING ZINC AND CHARCOAL MIXTURE

R. MOTOKI, M. IZUMO, K. ONOMA, S. MOTOISHI, A. IGUCHI,
T. SATO*, T. ITO
Japan Atomic Energy Research Institute,
Tokai-mura, Ibaraki-ken, Japan

Abstract

The production of ^{99}Mo by the reaction of ^{235}U(n,f) using UO_2 as target material was carried out in JAERI. Medium- and high-level liquid wastes arising from this production process contained U, Pu and fission products in which radioactive ruthenium in various valency and complex states was included.

For the removal of radioactive ruthenium, after testing various combinations of adsorbents, a novel method using a column packed with adsorbents composed of zinc and activated charcoal (charcoal) was developed. The effects of composition of mixtures, flow rates, pH of feed solutions, washing, and repeat use on ruthenium removal efficiency were investigated. A feature of this column method is that the efficiency of removal can be recovered by washing with dilute nitric acid and it is possible to treat a large quantity of liquid wastes. It was found that this column method was also effective for the removal of U, ^{239}Pu, ^{144}Ce, ^{155}Eu and ^{125}Sb.

This method was applied to the treatment of actual medium- and high-level liquid wastes, the quantities of which were 600L and 124L respectively. After the removal of U, Pu and fission products by conventional removal methods such as coprecipitation, filtration, electrolysis and adsorption with inorganic adsorbents, residual ^{106}Ru was removed by using the column packed with a mixture of zinc and charcoal. Decontamination factors for ^{106}Ru ranging from 10^2 to 10^4 were obtained. The concentration of U, ^{239}Pu, ^{144}Ce, ^{155}Eu, and ^{125}Sb after treatment were found to be below the limit of detection.

1. Introduction

Through 1977 into 1979, weekly production of 20Ci ^{99}Mo from fission product of ^{235}U was carried out in JAERI. In the production, irradiated UO_2 was dissolved in nitric acid and ^{99}Mo was extracted from the solution with di-2-ethylhexyl phosphoric acid. As the ^{99}Mo production procedure was similar to the Purex process, the liquid wastes resulting from the production were also very much like that from the nuclear fuel reprocessing.

It has been well-known that radioactive ruthenium might be present in multiple valence and complex states simultaneously in nitric acid solution [1-7] and it is one of the most questionable nuclides in the treatment of radioactive wastes [8-15]. Development of an efficient method of removal of radioactive ruthenium, therefore, has been much expected.

In the course of the treatment of the radioactive wastes arising from the ^{99}Mo production, a novel procedure [16,17] was developed for the removal of radioactive ruthenium on the basis

---

* On leave from Mitsui Mining & Smelting Co., Ltd.

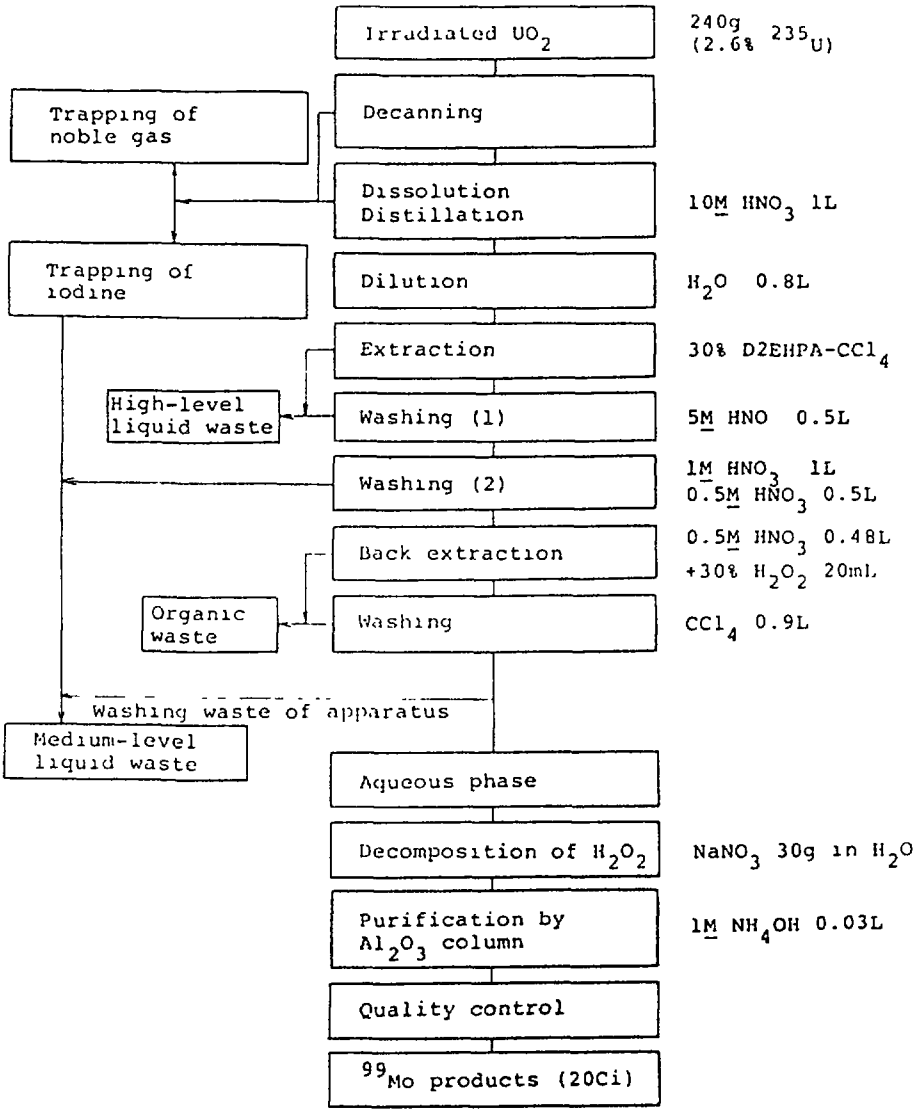

Fig.1 Flow chart of ^{99}Mo production from irradiated UO_2

of columns packed with a mixture of activated charcoal (charcoal) and metal powder, of which zinc was found to be most effective. The usefulness of this method was demonstrated by the successful results obtained in the treatment of total amount of actual wastes. It is natural that the radioactive ruthenium removal procedure developed here should be applicable to the treatment of wastes occurring from the various phases of the nuclear fuel cycle.

The present paper describes the results of development of, and of the treatment of the actual wastes with, the novel procedure of radioactive ruthenium removal.

2. The nature and amount of liquid wastes from ^{99}Mo production

The procedure of ^{99}Mo production and the origins of wastes in the procedure are shown in Fig.1. The amount and characteristics of liquid wastes are summarized in Table I together with the decontamination factor necessary for each nuclide to be disposed as low-level liquid wastes.

Table I Radioactivity concentration of liquid wastes and decontamination factor (DF) necessary for disposal as low-level liquid wastes (β-γ:10^{-3}~10^{-5}μCi/mL, α:<5×10^{-5}μCi/mL)

Medium-level liquid waste

(Assayed in March 1981)

Nuclide	Radioactivity concentration (μCi/mL)	DF
^{106}Ru	6×10^{-2}	60
^{137}Cs	1×10^{-1}	100
^{144}Ce	2×10^{-2}	20
α	2×10^{-4}	4
β-γ	4×10^{-1}	400

pH : ~13 $NaNO_2$: 0.027M

U : 3.0mg/L volume : 600L

$NaNO_3$: 0.3M

High-level liquid waste

(Assayed in July 1981)

Nuclide	I		II	
	Radioactivity concentration (μCi/mL)	DF	Radioactivity concentration (μCi/mL)	DF
^{106}Ru	2.5	2.5×10^3	5	5×10^3
^{137}Cs	11	11 "	14	14 "
^{144}Ce	22	22 "	55	55 "
^{125}Sb	0.22	0.2 "	0.34	0.3 "
^{155}Eu	0.21	0.2 "	0.28	0.3 "
^{90}Sr	11	11 "	14	14 "
^{147}Pm	~3	~3 "	~3	~3 "
α	0.03	0.6×10^3	0.05	1×10^3
β-γ	48	48×10^3	89	89×10^3

U : 23mg/mL volume : I:73L, II:51L

HNO_3 : I:3.8M, II:4.5M

The medium-level liquid waste consisted of the scrub solution of sodium hydroxide used for the removal of radioactive iodine and dilute nitric acid used for washing of the apparatus. This waste contained a considerable amount of sodium nitrate and was supposed to be equivalent to the washing effluent in the nuclear fuel reprocessing plant in terms of the radioactivity level [18]. Since this waste was somewhat alkaline, some part of radioactive ruthenium of chemical forms that was prone to precipitate was supposed to have formed coprecipitate with sodium uranate. While the high-level liquid waste consisted of the nitric acid solution of irradiated UO_2 from aqueous phase after extraction with organic solvents (di-2-ethylhexyl phosphoric acid and carbon tetrachloride) and washing solution of the organic solvents and was stored in two tanks, tank-I and -II. The high-level liquid waste here was equivalent to the medium-level liquid waste from the nuclear fuel reprocessing.

In order to decrease the radioactivity concentration in these liquid wastes to the acceptable levels of the low-level liquid wastes defined in our Institute, ^{106}Ru decontamination factors of >60, $>2.5x10^3$, and $>5x10^3$ were required respectively for the medium-level, high-level liquid wastes-I, and -II (see Table I).

3. Development of ^{106}Ru removal techniques

In preliminary experiments, no effective method was found for the removal of ^{106}Ru of chemical forms whose separation were difficult by conventional means such as coprecipitation, adsorbent columns, and ion exchangers as previously reported on treatment of liquid wastes from nuclear fuel reprocessing. In the experiments above, it was observed that several kinds of metal powders and charcoal were considerably effective for the removal of radioactive ruthenium when used separately. Based on these experiences, a method using a column packed with a mixture of metal powders and charcoal was devised and tested. In the experiments a mixture of zinc powder and charcoal was found to have high removal efficiency for ^{106}Ru.

3.1. Radioactivity measurement and decontamination factor

Decontamination factor of each nuclide was calculated from the ratio of concentration before and after removal treatment of sample solutions. The concentration was obtained respectively by measuring γ-ray intensity with a γ-ray pulse-height analyzer using NaI(Tℓ) and Ge(Li) detectors, α-ray intensity with a 2π gas flow counter, and β-γ ray intensities with a gas flow GM counter.

3.2. Waste solutions used for experiments

Various chemical species of ruthenium were contained in nitric acid solution and in solution of sodium nitrate and species which could be removed without difficulty by coprecipitation and filtration were also included. In order to examine the efficiency of removal of ruthenium in the form of anions or in abnormal chemical state where it is difficult to be separated from the solution, ruthenium components which could be removed easily should be separated by pretreatment in advance. Such components were coprecipitated with aluminium hydroxide flocculate generated from electrolysis and filtered in the case of medium-level liquid waste, and they were coprecipitated with sodium uranate by neutralization of nitric acid with sodium hydroxide in the case of high-level liquid waste. Decontamination factors of ^{106}Ru obtained by these coprecipitation methods were ~4, ~20, and $\sim10^2$ for the medium-level, high-level liquid wastes-I, and -II respectively.

Each solution obtained by the pretreatment was named the pretreated medium-level, high-level liquid waste-I, and -II respectively.

The pH of these waste sample solutions was adjusted with nitric acid or sodium hydroxide prior to experiments. For the preparation of solution containing all chemical species of ^{106}Ru, uranium and ^{239}Pu were extracted from the high-level liquid waste-II with 30% tri-n-butyl phosphate in kerosine. All chemical species of ^{106}Ru appeared to remain dissolved in the residual aqueous solution since no ^{106}Ru radioactivity was detected in organic phase. This solution was named the extracted solution. The pH and sodium nitrate concentration were controlled by adding sodium hydroxide.

Table II Decontamination factor of fission products with metal powder-charcoal column and pH of solution

No.	Metal \ nuclide	α	^{155}Eu	^{144}Ce	^{125}Sb	^{106}Ru	^{137}Cs	pH
1	Al	2	1	1	1	8.3×10^3	1	4.5
2	Sn	> 53	2.9×10^3	16	1.4×10^3	8.3×10^3	1	6.3
3	Cu	1	1	1	2	32	3	3.1
4	Fe	2	2.8×10^3	1.0×10^5	1.3×10^3	8.3×10^3	1	6.0
5	Zn	>340	4.9×10^3	1.9×10^5	2.2×10^3	1.6×10^4	1	8.4

$NaNO_3$: No. 1~4 : 1.6 M, No. 5 : 2.5 M

Flow rate : 0.24~0.4 cm/min

pH of feed : No. 1~4 : 2.7, No. 5 : 1.5

For other detailes, see text.

3.3. Removal of ^{106}Ru using zinc-charcoal column

In order to find a combination for an adsorbent of metal powder and charcoal suitable for ^{106}Ru removal, mixtures of tin, iron, zinc, or copper powder and charcoal were tested. Metal powders having a purity of 99.9% and a grain size of <100 mesh and charcoal (Tsurumicoal Co., Ltd. GVA) of 60 to 300 mesh were mixed in water and packed in columns of a diameter of 8 or 18mm. For the purpose of investigating the removal efficiencies for all chemical species of ^{106}Ru 100mL of the extracted solution prepared above was passed through each column packed with a mixture of 3g each of metal powder and charcoal and the decontamination factors of each nuclide and the change of pH of solutions were evaluated as shown in Table II. Decontamination factor of 10^4 for ^{106}Ru was obtained by using these adsorbents except a mixture of copper and charcoal and among these a mixture of zinc and charcoal indicated the highest removal efficiency for all nuclides. No peaks of ^{144}Ce, ^{155}Eu, ^{125}Sb, ^{106}Ru, ^{239}Pu, and U in γ-ray and α-ray spectra of the passed solution were detected except ^{137}Cs.

3.4. Removal condition for ^{106}Ru with zinc-charcoal column

In order to investigate the effects of zinc to charcoal ratio, flow rate of feed solution, and pH on removal efficiency for ^{106}Ru, the following experiments were carried out. For these experiments the pretreated medium-level and high-level liquid waste-I were used as sample solutions, since the object of removal was chemical species of ^{106}Ru whose removal were difficult.

3.4.1. Effect of zinc to charcoal ratio

After adjusting pH to 4.9, 30mL of the pretreated high-level liquid waste-I was passed through columns packed with a mixture of 0~1g of zinc and 1g of charcoal. The results obtained are shown in Fig.2. Decontamination factor of ^{106}Ru increased with zinc to charcoal ratio, indicated 55 at 40% ratio and increased about twice to 10^2 at 80%, and at more than that decontamination factor approached saturation. Passing 30mL of the pretreated medium-level liquid waste through columns packed with 1g of 10~85 wt.% zinc-electrodeposited

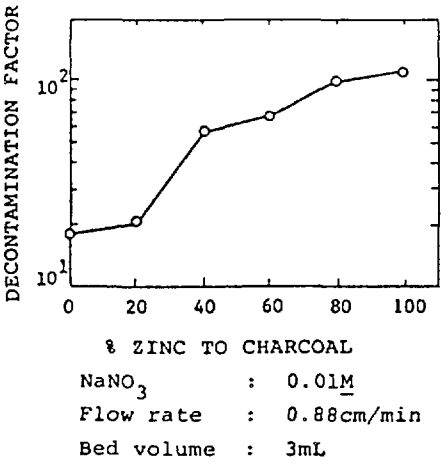

Fig.2 Effect of zinc/charcoal ratio on decontamination factor of ^{106}Ru

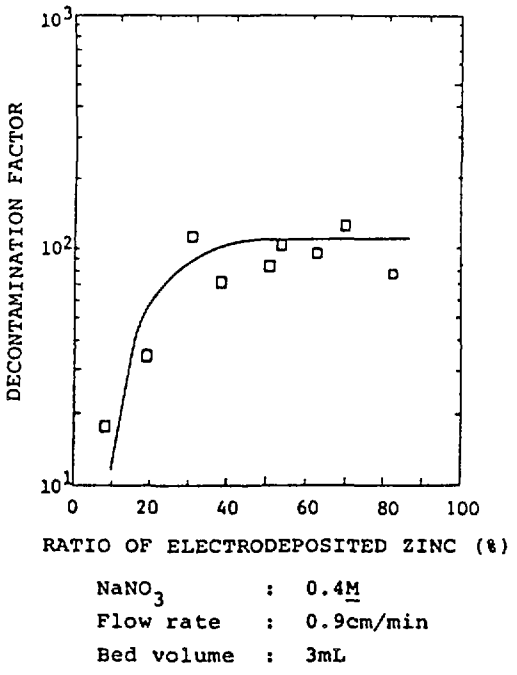

Fig.3 Effect of the ratio of electrodeposited zinc to charcoal on decontamination factor of ^{106}Ru

charcoal, which was developed to improve the mixing condition of zinc and charcoal, relation between electrodeposition ratio of zinc to charcoal and decontamination factor of ^{106}Ru was studied. The results are shown in Fig.3. Decontamination factor of ^{106}Ru increased with the electrodeposition ratio of zinc and approached saturation at more than 30%. From this result it is recognized that a charcoal which has the electrodeposition ratio of more than 30% zinc could be utilized effectively. Decontamination factor attained saturation at more than 60% of zinc in the case of a mixture of zinc and charcoal. It appears that zinc-electrodeposited charcoal reached saturation at low mixture ratio, because of small particle size and uniform dispersion of particles.

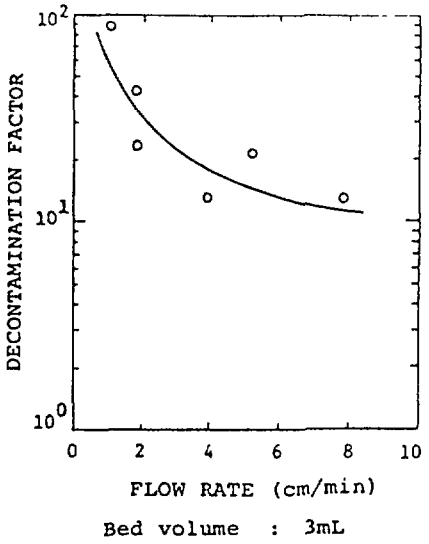

Fig.4 Effect of flow rate of feed solution on decontamination factor of ^{106}Ru

3.4.2. Effect of flow rate

After adjusting pH to 5.2, 30mL of the pretreated high-level liquid waste-I was passed through columns packed with a mixture of 1g each of zinc and charcoal at various flow rate. Figure 4 shows experimental results. Decontamination factor decreased with increasing flow rate, being ~60 at 1cm/min, ~30 at 2cm/min, and 10~20 at more than 4cm/min.

3.4.3. Effect of pH

After adjusting pH to 2.7~7.2, 30mL of the pretreated high level liquid waste-I was passed through columns packed with a mixture of 1g each of zinc and charcoal. The results are shown in Fig.5. Decontamination factor of ^{106}Ru was affected with concentration of nitric acid and became 40 at pH6, ~80 at pH 2~3, and it approached saturation when pH was lower than 4. Similar results were obtained in the experiments using the pretreated medium-level liquid waste.

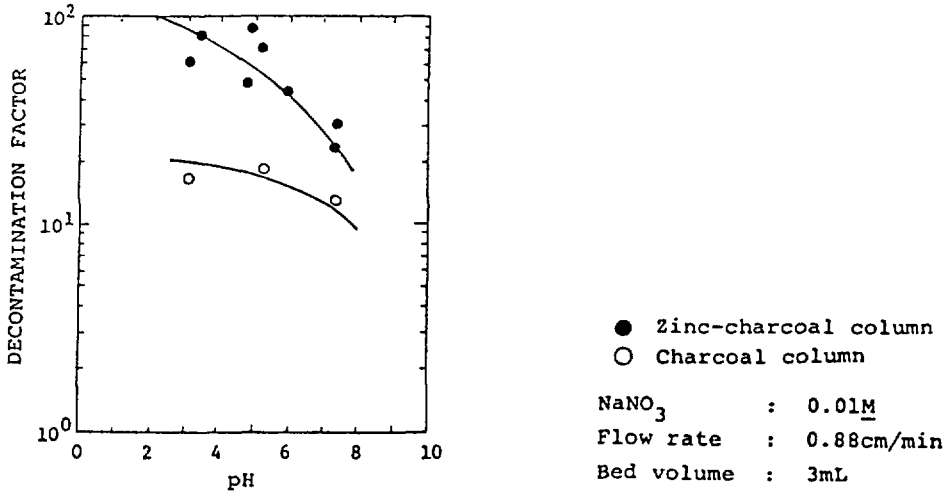

Fig.5 Effect of pH of feed solution of decontamination factor of ^{106}Ru

3.4.4. Effect of differences in volume of feed solution

The optimum condition for ^{106}Ru removal obtained from experimental results was as follows:

Ratio of zinc to charcoal = >1:1

pH of feed solution = ~3

In this condition relation between volume of feed solution and decontamination factor of ^{106}Ru was studied by passing 2.2L of the pretreated medium-level liquid waste, pH of which was adjusted to 3.1, through a column packed with a mixture of 30g each of zinc and charcoal. The results are shown in Fig.6. Decontamination factors of ^{106}Ru were $>10^3$ at 0.4L feed and $\sim10^2$ at 1.2L feed. The removal efficiency of this column was expected to attain to $\sim10^2$ provided that the volume of feed solution was confined within the range of 40mL per 1g of charcoal. Similar results were obtained by the experiments using the pretreated high-level liquid waste-I.

3.4.5. Recovery effect by washing columns

The zinc-charcoal column method required a large quantity of adsorbent for treatment of a large amount of waste, since decontamination factor decreased as the volume of feed solution increased. With the condition above, 15kg (45L of apparent volume) of adsorbent was necessary for the treatment of total amount of medium-level liquid waste, 600L. The volume reduction ratio should, therefore, be about 13, since no effective process was known to concentrate ^{106}Ru adsorbed in zinc-charcoal column.

In order to reduce the volume of solid waste arising from the treatment, possibility of recovery of efficiency of adsorbents and of repeat use of the column were examined using pretreated medium-level liquid waste. Immediately after passing 100mL of the waste solution through a column packed with a

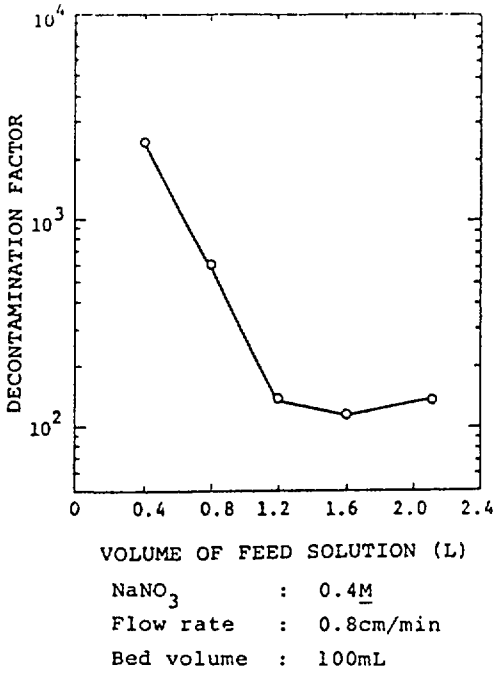

Fig.6 Effect of the difference in volume of feed solution on decontamination factor of ^{106}Ru

mixture of 4.5g each of zinc and charcoal, the column was washed repeatedly with water or nitric acid solution and change of the removal efficiency was observed. It was found that although the column efficiency could be completely recovered by washing immediately after use with water or dilute nitric acid, washing with dilute nitric acid of pH3 was preferable because no elution of ^{106}Ru was observed. The amount of washing solution necessary for the recovery of column efficiency was approximately equal to the volume of the column.

The recovery of column efficiency by washing and repeat use of the column made it possible to increase the amount of liquid waste to be treated by the column and accordingly to decrease the volume of the resulting solid waste as demonstrated on the treatment of actual waste below.

3.5. Removal of ^{106}Ru from actual liquid wastes [19,20]

For chemical species of ruthenium which were difficult to be removed in the medium-level liquid waste, zinc-charcoal columns and zinc-electrodeposited charcoal column were used after treatment first by electrolytic flocculation, then with zeolite column, and finally with titanic acid column. For the treatment of the high-level liquid waste, after dilution, neutralization, coprecipitation with nickel ferrocyanide, and adsorption with a slurry of ortho titanic acid, the solution was passed through the zinc-charcoal column.

A column with a diameter of 149mm and 5L of volume packed with a mixture of 2.5kg of 60~80 mesh zinc powder and 1.5kg of 60~300 mesh charcoal was prepared for treatment of the actual medium- and high-level liquid wastes. The liquid waste diluted with equal volume of water to 30L was passed through the column and then washed repeatedly with 5L of washing solution of pH2~3. Relations between the volume of feed solution and decontamination factor of ^{106}Ru in the treatment of the medium-level liquid wastes were shown in Fig.7.

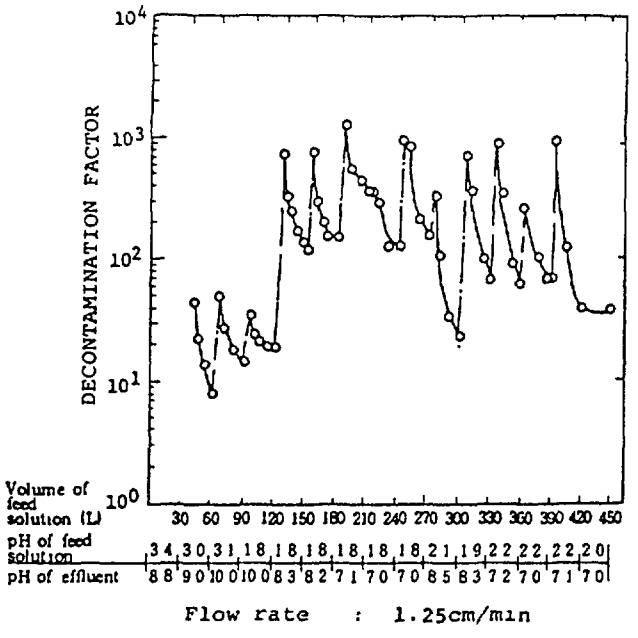

Fig.7 Removal of ^{106}Ru from medium-level liquid waste with zinc-charcoal column

The treatment of 450L of the medium-level liquid waste by repeat use of a single column resulted in decontamination factor of 10~20 at pH3, and 10^2 at pH2. Similar results were obtained using 31% zinc-electrodeposited charcoal as adsorbent. In the treatment of 280L of the high-level liquid waste decontamination factor of 10^2 with a feed solution of pH2 was obtained by washing with dilute nitric acid.

4. Conclusion

The conclusions based on the experimental results and interpretation of the data are as follows:

(1) Column packed with a mixture of metal powder and charcoal, especially zinc-charcoal mixture, and zinc-electrodeposited charcoal showed high efficiency of removal for all chemical species of ^{106}Ru, in particular for the species that were difficult to be removed by the conventional methods such as coprecipitation, aggregation and ion exchange, with high decontamination factor.

(2) Besides for ^{106}Ru, column packed with zinc-charcoal mixture was also highly efficient adsorbent for the removal of ^{239}Pu, U, ^{144}Ce, ^{155}Eu, and ^{125}Sb.

(3) Zinc-electrodeposited charcoal was preferably used for the preparation of packed column because the particles of metal were dispersed uniformly.

(4) The optimum condition of removal of ^{106}Ru by the present method was to use zinc-charcoal column or zinc-electro-deposited charcoal column of 30~80% of zinc content for the treatment of liquid waste within the acidic region of pH<3, at the flow rate of ~2cm/min.

(5) The efficiency of ^{106}Ru removal with zinc-charcoal column could be recovered by washing with water or dilute nitric acid after use. The column could, therefore, repeatedly be used for the treatment of a large amount of waste.

Although the usefulness of zinc-charcoal column for the waste management in the field of nuclear fuel cycle was demonstrated above, several problems are left to be solved by further research as follows:

(1) Improvement of the efficiency of the procedure for removal of ^{106}Ru and other radioactive elements.

(2) Extension or modification of the present technique to be applicable for treatment by batch system.

(3) Elucidation of the mechanism of radioactive ruthenium removal.

Studies concerning these problems are now in progress and the results will be soon published elsewhere.

Acknowledgements

The authors are grateful to Mr. T. Sato, Dr. H. Nakamura, Mr. Y. Kawakami, Mr. K. Suzuki, and Mr. T. Abe of the Japan Atomic Energy Research Institute for their useful suggestions and discussions given to us.

References

[1] FLETCHER J. M., et al., J. Inorg. Nucl. Chem., 1 (1955) 378.

[2] ZVYAGINTSEV O. E., et al., Peaceful Uses of Atomic Energy (Proc. 2nd Int. Conf. Geneva, 1958) Vol.17, UN, New York (1958) 130.

[3] Brown P. G. M., et al., Peaceful Uses of Atomic Energy (Proc. wnd Int. Conf, Geneva, 1958) Vol.17, UN, New York (1958) 118.
[4] FLETCHER J. M., et al., J. Inorg. Nucl. Chem., 12 (1959) 154.
[5] KOYAMA M., Nippon Kagaku Zasshi, 82 (1961) 1182.
[6] SUGIMOTO S., Radioisotopes, 28 (1979) 429.
[7] AKATSU E., Rep. JAERI-M 9159, JAERI, Tokyo (1980).
[8] KRIEGER H. L., et al., Rep. ORNL-1966, Oak Ridge National Lab., TN (1955).
[9] FEBER R. C., Process Chem., 2 (1958) 247.
[10] GARDNER E. R., BROWN P. G. M., UKAEA Rep. AERE-R 3551 (1960).
[11] ISHIYAMA T., et al., Radioisotopes 15 (1966) 181.
[12] LYNCH R. W., et al., Rep. SAND-75-5907, Sandia Lab., NM (1975).
[13] KENNA B. T., Rep. SAND-78-2019, Sandia Lab., NM (1978).
[14] SUGIMOTO S., SAKAKI T., Radioisotopes 28 (1979) 361.
[15] KANNO T., et al., J. At. Energy Soc. Jpn., 21 (1979) 737.
[16] NAKAMURA H., et al., JAPAN PATENT SH057-50698 (1982).
[17] NAKAMURA H., MOTOKI R., et al., IAEA/WMRA/13-81/11 JP04 (1982).
[18] SEGAWA T., J. At. Energy Soc. Jpn., 12 (1970) 599.
[19] IZUMO M., MOTOKI R., et al., Rep. JAERI-M 83-197, JAERI, Tokyo (1983).
[20] MOTOKI R., IZUMO M., et al., Rep. JAERI-M 84-015, JAERI, Tokyo (1984).

ION EXCHANGE CHARACTERISTICS OF HYDROUS OXIDES AND THEIR USE IN THE SEPARATION OF URANIUM AND THORIUM

N.Z. MISAK, H.N. SALAMA, E.M. MIKHAIL, I.M. EL-NAGGAR,
N. PETRO, H.F. GHONEIMY, S.S. SHAFIK
Nuclear Chemistry Department,
Nuclear Research Centre,
Atomic Energy Establishment,
Cairo, Egypt

Abstract

The ion exchange characteristics of several hydrous oxides have been studied. The kinetic studies done with zirconia and ceria have shown that the increase of the charge of cations has a minor effect on their mobility in the exchangers while the increase of charge or complexing ability of the anions decreases their mobility. A dehydration of the cations is deduced. The mobility of cations and anions decreases in the presence of alcohols.

For alkali cation exchange, it was deduced from thermodynamic data on hydrous zirconia and ceria that the Eisenman model is qualitatively, and sometimes quantitatively, applicable, and that it can be used for obtaining successful predictions of the trends in the thermodynamic functions. This is not the case with anion exchange. The thermodynamic studies on hydrous zirconia in methanolic solutions show that the cation and anion exchange selectivity constants can be, at least in certain cases, predicted from the values in the aqueous media by considering ion-solvent interactions. However, even in these cases large changes occur in the solid phase.

The physicochemical properties (acidity, capacity and porous texture) of hydrous oxides have a profound effect on their ion exchange behaviour. Besides, water structure effects seem to be of great importance in the case of alumina. The decrease of porosity and pore size seems to lead to the increase of hydrous oxide selectivity.

Sorption studies of uranium and thorium from aqueous solutions on hydrous ceria and from both aqueous and mixed-solvent media on hydrous tin oxide point to the possibility of the use of hydrous oxides for the separation of uranium and thorium from each other and from other elements.

INTRODUCTION

Hydrous oxides are an important class of inorganic ion exchangers. Fields of their potential application are: chemical seprations and purification, in particular for radioactive materials, ion exchange catalysis at high temperatures, treatment of high-temperature water, and purification of moderator and coolant water of nuclear reactors (1,2). Of course, a rational use of hydrous oxides in the various fields necessitates a good knowledge of their general and sorption properties and in particular their ion exchange selectivity behaviour. For this purpose, many hydrous oxides were prepared and studied in this laboratory. This paper reviews the work done.

EXPERIMENTAL

All the samples prepared were initially dried at 50°C and stored in a nitrogen atmosphere over saturated ammonium chloride. Some of the samples were heated at different temperatures and the surface characteristics were measured by nitrogen adsorption isotherms. Most of the samples were subjected to X-ray, thermal and IR analyses. When different samples of the same hydrous oxide are involved, they are referred to by the symbol of the metal atom of the oxide followed by a Roman number.

Hydrous ceria : Ce-I and Ce-II were prepared as previously mentioned (3,4). Ce-I (3) is amorphous and its DTA curve shows a large endothermic peak (only endothermic peaks indicative of loss of water or hydroyl groups will be mentioned) at about 125°C. Ce-II (4) is slightly crystalline. Its DTA curve has a large endothermic peak at a bout 130°C, a very small one at about 100°C and a small one at about 240°C. The IR spectra show that in both samples, the peaks due to water and due to both water and hydroxyl groups decrease continously with increase of temperature.

Hydrous zirconia : Zr-I is a Bio-Rad HZO-1 hydrous zirconium oxide (5), whereas Zr-II was prepared as given before (6). Zr-II is amorphous.

Hydrated alumina (or aluminium hydroxide) : Al-I, Al-II, Al-IV and Al-V were prepared according to the methods given before (4). Al-III is a ready JUDEX chemical designated as $Al(OH)_3$. All the alumina hydrates prepared are semicrystallins and their degree of crystallinity remains almost the same up to the heating temperature 250°C. All the samples give endothermic peaks at 270-280°C. Besides, very small endothermic peaks around 100°C are present in the DTA curves of Al-III and Al-IV. X-ray, DT and IR analyses (4) show that the aluminas are generally composed of one or more of the trihydrxides (gibbsite, bayerite, nordstrandite) with varying amounts of an amorphous oxyhydroxide. No significant changes occur in the samples up to 250°C. At 350°C, they are transformed to alumina which sorbs water from the atmosphere, partly as hydroxyl groups.

Ferric oxide gel : The methods of preparation of Fe-I, Fe-II and Fe-III are given in reference 4. Fe-I and Fe-II are virtually amorphous while Fe-III is semicrystalline (4). The crystallinity of all the samples increases with the increase of the heating temperature. The DTA curves show small endothermic peaks around 100°C in all the samples, large endothermic peaks in Fe-I and Fe-II at about 250°C, and two small endothermic peaks at about 250 and 300°C in Fe-III. From IR analysis, it was deduced that the gels begin to lose OH groups at temperatures $\geq$ 150°C. At 400°C, the samples still contain OH groups. Besides, molecular water is present, which is probably sorbed from the atmosphere.

Hydrous tin oxide : Hydrous tin oxide (β-stannic acid) was prepared as mentioned previously (7). β-stannic acid (4) is slightly crystalline. Its DTA curve shows a large endothermic peak at about 135°C. The IR spectra show that up to the temperature 400°C, the water lost is regained by sorption from the atmosphere.

RESULTS AND DISCUSSIONS

1-Review of Previous Kinetic and Equilibria Studies on Zr-I, Zr-II and Ce-I

Britz and Nancollas (5) have shown that Zr-I displays the selectivity pattern: Li > Na > K, i.e., the cation of the smaller bare radius is preferred. These authors suggested that the alkali cations are retained in the exchanger in a substantially dehydrated form. The kinetic studies done later by Misak et al. (8,9) on Zr-II showed that the increase of the charge of cations has a generally little effect on their mobility inside zirconia. The mobility of the alkali and earth alkali cations in zirconia decreases inthe order: Cs > K > Ca ~ Sr ~ Ba > Li > Na. This order supports a dehydration of the cations sorbed.

Kinetic studies on Ce-I (3) have shown that the mobility of some alkali and earth alkali cations decreases in the order: Ca ~ Na > K > Ba. This shows also that the cations are sorbed inside Ce-I in a dehydrated state. For mono- and bivalent anions, the mobility in Zr-II (9) and Ce-I (3) was found to decrease with the increase of the ability of the anion for complexing with the metal atom of the hydrous oxide. In the presence of alcohols, the internal diffusion coefficients of the Na/H and Cl/OH systems decrease due to a stronger interaction of the counter ions with the exchange sites (6).

According to Eisenman (10), the selectivity for alkali ions of solids containing fixed charges depends on two factors: ion hydration and electrostatic ion binding. When ion hydration is the dominant factor,

the selectivity pattern is: Cs > K > Na > Li, i.e., a preference for the alkali ion with a larger bare radius or lesser hydration energy is displayed. The completely reversed sequence results when electrostatic binding is the dominat factor. Partial reversals result in the intermediate conditions. The Eisenman model considers the sorption of ions in a completely dehydrated state. Besides, it takes into consideration only coulombic electrostatic interactions, and the changes in the entropy of the solid on replacing one ion in it by another are completely neglected. Nevertheless, this extremely simple model has been qualitatively successfully applied to organic resins by Reicheberg (11) and to zeolites by Sherry (12). Sherry (12) found that the neglected entropy changes often reinforce the selectivity patterns predicted by Eisenman.

We have tried to test the applicability of this model to hydrous oxides. When applying this model to cation exchange in hydrous oxides, reversed sequences may be expected to be favoured by the increase of capacity and pH at which selectivity is measured, and by the decrease of the acidity of the oxide which increases the field strength of the anionic O^- sites. All these factors increase the role of electrostatic interactions. Increase of crystallinity may lead to this by increasing the lattice energy providing for ion dehydration (5).

Equilibria measurements were done for many cations and anions on Ce-I (3). The results for alkali cations and for many anions on ceria and other hydrous oxides were subjected to a preliminary comparison. Regardless of the fact that the comparison often involved equilibrium distribution coefficients and that these coefficients may pertain only to a certain set of experimental conditions, the following observations seemed to be of a general nature. The sequence of preference of the ion of a lesser hydration energy is observed only with the more acidic oxides: silica (13), alumina (14), titania (15) and hydrous manganese dioxide (16,17). On the other hand, partially or completely reversed sequences are observed on less acidic oxides: zirconia (5,8), ceria (3) and thoria (15). For the anions, the results with the majority of the hydrous oxides (5,8,18-22) show a preference to the ion of a higher complexing ability with the metal atom of the oxide, which means a dominant role of electrostatic interactions.

This comparison has urged us to make detailed and thermodynamic studies on several hydrous oxides with the aim of testing the validity of the Eisenman model and examining the effect of the various factors such as acidity, capacity (or site density), porous texture and crystallinity on their exchange behaviour, and in particular the selectivity. The ultimate goal is to obtain a clear general picture for ion exchange on hydrous oxides.

The first studies involved the thermodynamics of alkali cation exchange and anion exchange in Ce-I (23,24). These studies involved the determination of the ΔG°, ΔH°, ΔS° of the exchanges and the comparison of the obtained data with similar studies on Zr-I (5) and Zr-II (25). These thermodynamic functions were resolved into two components: one pertaining to the solution phase and involves the thermodynamic hydration functions, ΔG^h, ΔH^h, ΔS^h, obtained from Rossainsky's data (26), and the other pertaining to the solid phase, $\overline{\Delta G^e}$, $\overline{\Delta H^e}$, $\overline{\Delta S^e}$, and is obtained from the relations: $\Delta G^\circ = G^h + \overline{\Delta G^e}$, $\overline{\Delta H^\circ} = \Delta H^h + \overline{\Delta H^e}$, and $\Delta S^\circ = \Delta S^h + \overline{\Delta S^e}$.

The Eisenman model considers only the free energy change (ΔG) of the exchange, and this was the only parameter considered in the application of the model to resins (11) and zeolites (12). We have tried to apply the ideas in the model also to the enthalpy changes (ΔH). The different data for the replacement of Li in the oxide by other alkali ions for Ce-I (23), Zr-I (5) and Zr-II (25) are given in Table I.

Zr-I has a considerably less water content than Zr-II in the various cationic forms (23). Hence Zr-I is apparently more dense and has probably a higher site density due to a less average spatial separation of the exchange sites. The capacities of the oxides are very close and the ions seem to be substantially dehydrated in them since the water contents of the different ionic forms are rather similar. Ceria is expected to be of lower acidity and hence to have a stronger field strength of its exchange sites.

Table I

Thermodynamic data for alkali cation exchange at 25°C on Ce-I[x], Zr-I[xx] and Zr-II[xxx]

Exchange	Exchange reaction	ΔG° kJ mol^{-1}	ΔH° kJ mol^{-1}	ΔS° J mol^{-1}K^{-1}	ΔG^h	ΔH^h	ΔS^L	$\overline{\Delta G}^e$	$\overline{\Delta H}^e$	$\overline{\Delta S}^e$
Ce-I	Li/Na	5.69	0.00	-19.1	-100.0	-109.2	-30.9	105.7	109.2	11.7
	Li/Cs	9.08	6.07	-10.1	-227.3	-251.5	-81.2	236.4	257.6	71.1
Zr-I	Li/Na	2.39	-0.71	-10.4	-100.0	-109.2	-30.9	102.4	108.5	20.5
Zr-II	Li/Na	2.05	-9.60	-39.1	-100.0	-109.2	-30.9	102.1	99.6	-8.4
	Li/Cs	-0.02	-23.46	-78.7	-227.3	-251.5	-81.2	227.3	228.0	2.4

x from Reference 23.

xx from reference 5.

xxx from reference 25.

Cosidering the above-mentioned facts and remarks, one may expect that a preference for the ion of a smaller bare radius would be more pronounced for the less acidic ceria (if porosity is of secondary imper-tancerelative to acidity), and for Zr-I relative to Zr-II. Besides, the contribution of $\overline{\Delta H}^e$ is expected to be higher for ceria than for zircon-ia and for Zr-I than for Zr-II. Since $\overline{\Delta H}^e$ is positive for the given ex-changes (Table I), ΔH° is expected to be less negative or more positive for ceria compared to zirconia, and for Zr-I compared to Zr-II. Table I shows that all these expectations are fulfilled for the given systems, which shows that the Eisenman model is qualitatively applicable to these systems. Table I shows that $\overline{\Delta S}^e$ is very small in the case of the Li/Cs exchange on Zr-II, which shows the quantitative applicability of the model in this case.

The study of the thermodynamics of NO_3^-/Cl^-, NO_3^-/Br^- and NO_3^-/SCN^- exchanges on Ce-I and the comparison of the results obtained with those for Zr-I (27), Zr-II (25) and another zirconia sample studied by Ruva-rac and Trtanj (28) have shown the inapplicability of the Eisenman model in the case of anion exchange. This was deduced (24) to be due to solid entropy changes and noncoulombic electrstatic interactions that hamper the applicability of the model in this case.

The study of the thermodynamics of Li/Na and Li/Cs exchanges on Zr-II in 30% and 50% methanol (29) has shown that the values of ΔH° and ΔS°, given in Table I, increase progressively on addition of metha-nol whereas the reverse occurs with ΔG°. Thus, the selectivity constant increases due to the entropy term. Using the data on the thermodynamics of transfer of the alkali ions from aqueous to methanolic solutions, the values of the changes in ΔG°, ΔH° and ΔS° due to ion-solvent in-teractions on addition of methanol were calculated. From these values, the changes in these functions due to changes in the solid phase were also calculated. The latter changes were found to be considerable. How-ever, for the Li/Na exchange in 30% methanol, ΔG° calculated theore-tically on the basis of ion-solvent interactions alone was found to be very close to the experimental value. It seems therefore that the solid phase changes lead to contributions to ΔH° and ΔS° that largely cancel each other. The thermodynamics of halide ion/ nitrate ion ex-change on the same exchanger in the same medium (30) revealed similar trends. However, for the nitrate ion/ bromide ion exchange in 60% me-thanol, ΔG° changed due to the enthalpy term.

2-Recent Studies on the Effect of the Physicochemical Properties of Hydrous Oxides on their Ion Exchange Behaviour

a-Kinetics of exchange

The values of the diffusion coefficients of Cs^+ (trace ion) in Al-IV and Al-V (Na-form) from a 0.1M NaOH medium are given in Table II at different heating temperatures of the exchangers. This table contains also the data of the calculated mean poe radii of the samples.

Table II

Diffusion coefficients at 25°C of Cs in Al-IV and Al-V heated at different temperatures.

Exchanger	Heating temp., °C	Mean pore radius, Å	$Dx10^8$ cm^2/sec
Al-IV	50	44	861
	250	27	67
	350	22	6.9
Al-V	50	77	398
	250	69	43.3
	350	17	9.4

Table II shows that for one and the same sample, D decreases with the decrease of the mean pore radius. Since D does not depend only on pore dimensions but also on the capacity of the exchanger, the strength of interaction with the exchange sites and the degree of dehydration(31) of the diffusing species, the above-mentioned fact may show that the pore width is the main factor governing the rate of ion diffusion in the exchangers.

It must be mentioned here that the mean pore radius may not be well representative of the actual width of the pores in which diffusion occurs. This is so because of differences in the geometries of pores and because the exchange sites may be restricted to pores of certain dimensions. These factors may be a reason of failure of comparison of diffusion rates in samples of different preparations on the basis of the mean pore radius, even if the above-mentioned other factors are taken into consideration.

Other data on ferric oxide gels (4) show also the major effect of pore size on the internal diffusion kinetics.

b-Selectivity behaviour

Before giving and discussing the data of the selectivity behaviour of alumina and ferric oxide, it is important to show here the 'anomalous' behaviour of Al-I heated at 350°C in respect of the variation of sorption of Na^+ with pH. Figure 1 shows the variation of sorption of sodium from 0.1M solutions (NaCl+NaOH) with pH on Al-I heated at different temperatures. Up to 250°C, the sorption increases with pH, as would be expected for an ion exchange process. For Al-I heated at 350°C, the sorption first decreases sharply and then increases with increase of pH.

It has been proved that the sorption of Na on Al-I heated at 350°C is an ion exchange process at all pH values. At 350°C, the exchange sites are presumably OH groups resulting from water sorption by the aluminium oxide fromed at this temperature. The first sharp decrease of sorption with increase of pH is therefore surprising. A plausible explanation of this situation may be related with water structure effects and the porous texture of the sample. At 350°C, Al-I is mainly compo-

sed of narrow pores (4). Water structure is expected to be enhanced at the oxide/water interface and water structure effects may be more pronounced in the narrower pores and may increase with increase of pH, resulting in a more ionization of the surface protons that are water-structure makers. Therefore, at the relatively low pH values, Na ions will be excluded from the narrower pores. As the pH increases, exclusion from the narrower pores increases and a decrease of sorption with the increase of pH may occur when this exclusion outweighs the normally expected increase of sorption with increase of pH. Another explanation may be the formation of a double layer, whose potential increases with increase of pH , at the mouths of pores. This double layer may constitute a barrier hindering the penetration of ions in the pores.

For saving space, selectivity data will be given here only for Al-I and Al-IV. The selectivity coefficients were measured at different loadings of the exchangers and the values given represent the selectivity coefficient at 50% loading of the Na-form of the exchanger with the entering alkali ion. This coefficient, designated here as $K_{0.5}$, may be equal to or quite close to the selectivity constant (11) and is anticipated to be a good representative of the overall selectivity displayed. The values of $K_{0.5}$ for the different alkali ion/ alkali ion exchanges in different media are given in Table III for Al-I heated at different temperatures and Al-IV dried at 50°C.

Table III shows that with the exception of the selectivity pattern displayed in 0.01M hydroxide solutions on Al-IV dried at 50°C, alumina shows a selectivity to Na over all the other alkali ions. For the other aluminas, a selectivity to Na over the other alkali ions is also displayed in all cases (4). The selectivity to Na over K and Cs may be attributed to the large effect of the latter ions in breaking the water structure and probably also to a stronger electrostatic interaction of Na with the exchange sites. The selectivity to Na over Li may be mainly due to the much higher hydration energy and hydration need of Li.

Table III

$K_{0.5}$ for alkali ion exchange at 25°C on Al-I and Al-IV under different conditions.

(M=alkali ion, the ion in the superscript is the entering ion).

Exchanger	Heating temp.	Equilibration solution	Capacity meq/g.	K^{Li}_{Na}	K^{K}_{Na}	K^{Cs}_{Na}	K^{K}_{Li}	K^{Cs}_{K}	K^{Cs}_{Li}
Al-I	50°C	0.01M MOH	0.024	0.17	0.16	0.15	0.94	0.94	0.88
	50°C	0.10M MOH	0.240	0.18	0.13	0.08	0.72	0.61	0.44
	250°C	0.01M MOH	0.025	0.16	0.17	0.15	1.06	0.88	0.94
	250°C	0.10M MOH	0.250	0.19	0.19	0.12	1.00	0.63	0.63
	50°C	0.10M MCl (pH=8.3)	0.029	0.028	0.032	0.048	1.14	1.50	1.70
	250°C	0.10M MCl (pH=8.3)	0.045	0.014	0.018	0.028	1.29	1.56	2.00
	350°C	0.10M MCl (pH=8.3)	0.150	0.10	0.08	0.18	0.80	2.75	1.80
	350°C	0.10M MOH	1.01	0.35	0.29	0.32	0.83	1.10	0.91
Al-IV	50°C	0.01M MOH	0.085	0.62	1.03	1.26	1.66	1.22	2.03
		0.10M MOH	0.342	0.17	0.19	0.25	1.12	1.32	1.47
		0.01M MCl	0.029	0.37	0.50	0.57	1.35	1.14	1.54
		0.10M MCl	0.117	0.09	0.12	0.13	1.28	1.08	1.44

In the chloride solutions, the affinity and selectivity to Na is much higher than in the hydroxide solutions. This seems to be due to a less ion exclusion from narrower pores in the former solutions. In the narrower pores, the selectivity to Na over K and Cs increases due to more profound water strucure effects, and that over Li increases due to a more role of ion hydration.

With Al-I heated at 50 and 250°C, the increase of site density generally increases the affinity or selectivity to the ion of a smaller crystallographic radius. This may be taken to indicate small differences in the hyiration degrees (large dehydration) of the alkali ions inside Al-I. This does not seem to be the case with Al-IV.

The increase of the heating temperature of Al-I from 50 to 250°C leads to the increase of surface area from 27 to 190 m^2/g, the increase of total pore volume (porosity) from 0.08 to 0.34 c.c./g, and the decrease of the mean pore radius from 57 to 36 Å. At 350°C, the surface area and porosity continue to increase to 437 m^2/g and 0.87 c.c./g, while the mean pore radius remains almost at the same value of 40 Å.

In the hydroxide solutions, the site density is the same at 50 and 250°C. The increase of heating temperature from 50 to 250°C leads to generally lower selectivity in the case of 0.1M hydroxide solutions and to almost no change in the case of 0.01M solutions. In the former case, this may be due to the effect of an increasing porosity, outweighing the effect of decreasing pore size. In the latter case, the two effects balance each other probably because narrower pores that become too narrow at 250°C are involved in the exchange. For the sample heated at 350°C, the selectivity is in general lowest, which is presumably due to the much higher porosity of this sample, outweighing the effects of a higher site density (Table III) and acidity (Fig.1). In the chloride medium, the selectivity seems to increase with increase of heating temperature from 50 to 250°C. This is probably due to the decrease of pore size, which may be dominant due to the involvement of much narrower pores in this medium. With Al-II and Al-III, the results (4) indicate that in the conditions favourable for comparison, the decrease of pore size increases the selectivity.

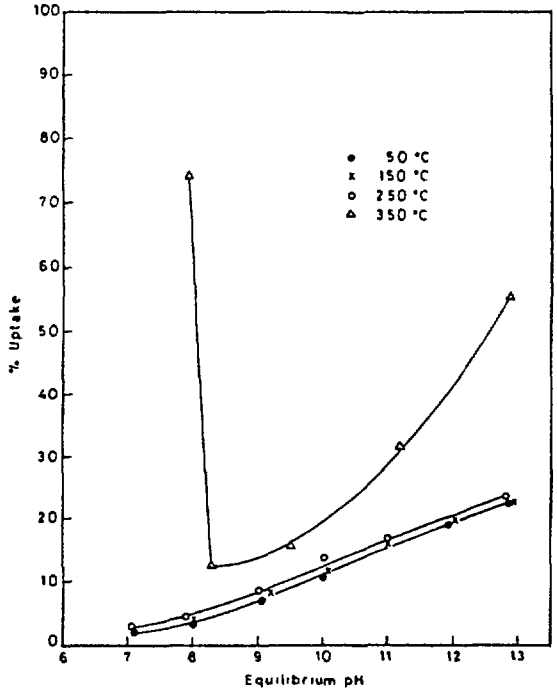

Fig.(1):Variation with pH of % uptake of Na^+ from 0.1M Na^+ solutions on Al-I heated at different temperatures (V/m = 10ml/g)

The capacity-pH curves (not given here for the sake of brevity) show that the acidity of the samples decreases in the order: Al-IV > Al-III > Al-I > Al-II. Table III shows that the selectivity to Na is considerably higher in Al-I than in Al-IV. Comparisons for other alu-

minas (4) show also that this selectivity is higher in the samples of lower acidity. Thus, the selectivity of alumina to Na increases not only with the decrease of pore size but also with the decrease of site acidity.

Fe-I and Fe-II have shown the same kinetic and sorption behaviour, in agreement with their similar X-ray, IR, DTA and porous texture data (4). The selectivity data on Fe-II and Fe-III under different conditions are given in Table IV.

Table IV

$K_{0.5}$ for alkali ion exchange at 25°C on Fe-II and Fe-III under different conditions.

(M=alkali ion, the ion in the superscript is the entering ion).

Exchanger	Heating temp. °C	Equilibration solution	Capacity, meq/g.	K^{Li}_{Na}	K^{K}_{Na}	K^{Cs}_{Na}	K^{K}_{Li}	K^{Cs}_{K}	K^{Cs}_{Li}
Fe-II	50°C	0.01M MOH	0.110	4.40	6.80	9.30	1.55	1.37	2.11
	50°C	0.10M MOH	0.310	8.60	5.80	3.40	0.67	0.59	0.40
	200°C	0.01M MOH	0.091	1.20	1.40	1.90	1.17	1.36	1.58
	200°C	0.10M MOH	0.220	1.48	0.63	0.49	0.43	0.78	0.33
	400°C	0.01M MOH	0.058	1.60	2.80	4.10	1.75	1.46	2.56
	400°C	0.10M MOH	0.190	1.68	0.48	0.38	0.29	0.79	0.23
Fe-III	50°C	0.01M MOH	0.104	3.80	7.90	10.10	2.10	1.28	2.66
	50°C	0.10M MOH	0.410	7.00	6.30	4.10	0.90	0.65	0.59
	200°C	0.01M MOH	0.090	1.70	2.20	2.70	1.29	1.23	1.59
	200°C	0.10M MOH	0.32	1.40	1.00	0.62	0.71	0.62	0.44
	400°C	0.01M MOH	0.056	3.90	3.80	4.70	0.97	1.24	1.21
	400°C	0.10M MOH	0.170	2.84	1.40	1.19	0.49	0.85	0.42

Table IV shows that at all heating temperatures, the increase of site density for both Fe-II and Fe-III leads to a large increase of the affinity or selectivity to the ion of a smaller bare radius. This probably shows that the alkali ions are largely dehydrated. Selectivity reversals occur, whereby the ion of a smaller bare radius becomes preferred at the higher site density. This is probably due to the fact that more weakly acidic sites are involved at the higher site density.

Before comparing the selectivity sequences, it must be mentioned that Fe-II has a porosity of 0.14, 0.36 and 0.24 c.c./g and mean pore radius of 23, 68 and 69 Å at the heating temperatures 50, 200 and 400°C, respectively. For Fe-III, these values are 0.29, 0.53 and 0.19 c.c./g and 40, 65 and 80 Å, respectively. The acidity of Fe-III is higher than that of Fe-II at all heating temperatures. At 200°C, the acidity of both samples is almost the same as that at 50°C up to a capacity of about 0.1 meq/g. At higher capacities, the average acidity is appreciably less at 200°C. At 400°C, the acidity decreases considerably for both samples.

In 0.01M solutions, the site density of Fe-II and Fe-III dried at 50°C is almost the same. In these conditions, the selectivity displayed for the ion of larger bare radius is generally somewhat higher for Fe-III. Since both the porosity and pore size are higher for

Fe-III, this may be dye to the higher acidity of this sample. For both samples heated at 200°C, The capacity in the 0.01M solutions differs little from that at 50°C. Besides, the acidity is, as mentioned above, the same. Table IV shows that in these solutions, the selectivity of both samples becomes much lower at 200°C. This is clearly due to the larger porosity and pore size at this heating temperature. In 0.1M solutions, the site density and acidity at 200°C are considerably lower than those at 50°C for both samples. In these solutions, the selectivity sequences are largely different at these two heating temperatures and with the exception of the Li/Na exchange they show a generally much higher affinity to the ion of the smaller bare radius at the higher heating temperature, which is presumably due to stronger electrostatic interactions as a result of the lower acidity. However, the lower site density and higher porosity and pore size at 200°C reveal themselves mainly in the much lower selectivity for Li over Na.

The selectivity pattern displayed in 0.1M solutions by Fe-II heated at 200°C is: Li > Na > K > Cs. This sequence is reinforced in the same solution at the heating temperature 400°C where, compared to the temperature 200°C, the acidity and porosity are lower whereas the site density and pore size are almost the same. The decrease of acidity reinforces this pattern, showing a preference for the ion of a smaller crystallographic radius, by increasing the role of electrostativ interactions, whereas the decrease of porosity reinforces it by increasing the selectivity.

3-Sorption of Uranium and Thorium by Hydrous Tin Oxide and Ce-II

Uranium and thorium are sorbed on hydrous tin oxide from acidic solutions (7,32). At a pH of 2 and 0.01M uranyl and thorium salt solutions, the capacity of this oxide is 0.36 and 0.44 meq/g for uranium from the aqueous nitrate and sulphate media, respectively, and 0.26 and 1.1 meq/g, respectively, for thorium. In the aqueous medium, the U/Th separation factors are rather poor. However, these factors can become very high in the mixed solvents. Thus, for example, for 0.001M nitrate solutions in 80% acetone and 0.01M nitric acid, K_d for uranium is about 600 and for thorium it is about 25 (V/m=25 ml/g). For 0.001M sulfate solutions in 20% acetone and 0.1N sulphuric acid, K_d for uranium is about 320 while for thorium it is about 1 (V/m = 25 ml/g). Schemes for U/Th separation have been suggested (7,32) on the basis of these and other results.

Relatively large uranium and thorium sorption capacities are also displayed by Ce-II. At pH 3, the thorium capacity from 0.01M nitrate solution is 0.9 meq/g, and at pH 3.2, the uranium capacity from the same solution is 0.44 meq/g. However, while uranium and thorium seem to be sorbed by hydrous tin oxide by an ion exchange mechanism, the sorption mechanism in ceria seems to be quite complex. Besides the rate of attainment of equilibrium is very slow in ceria, requiring more than a month. Nevertheless, the majority of exchange takes place in the first hour.

Experience shows that many hydrous oxides do not sorb any significant amounts of alkali, earth alkali or rare earth ions from acidic solutions. It is therefore anticipated that hydrous oxides can be used of uranium and thorium separation from many other elements.

ACKNOWLEDGEMENT - The authors wish to thank deeply the International Atomic Energy Agency for financial supprt under the Research Contract No. 2716/RB, 2716/R1/RB, 2716/R2/RB.

REFERENCES

1.AMPHLETT,C.B.,"Inorganic Ion Exchangers, McGraw-Hill, New York(1964).
2.RUVARAC,A.,"Inorganic Ion Exchange Materials",Editor: CLEARFIELD,A., Chap.5, CRC,Florida(1982).
3.MISAK,N.Z.,MIKHAIL,E.M.,J.appl.Chem.Biotechnol.28(1978)499.
4.MISAK.N.Z.,et al.,Progress reports submitted to IAEA,Research Contract No. 2716/RB,2716/R1/RB ,2716/R2/RB(1981-1984).
5.BRITZ,D.,NANCOLLAS,G.H.,J.inorg.nucl.Chem.31(1969)3861.
6.MISAK,N.Z.,GHONEIMY,H.F.,J.Chem.Tech.Biotechnol.32(1982)709.
7.MISAK,N.Z.,SALAMA,H.N.,EL-NAGGAR,I.M.,Chemica Scripta 22(1983)74.

8.HALLABA,E.,MISAK,N.Z.,SALAMA,H.N.,Indian J. Chem.11(1973)580.
9.MISAK,N.Z .,SALAMA,H .N.,Inorg.Nucl.Chem.Letters11(1975)559.
10.EISENMAN,G.,Biophys. J.2(1962)259.
11.REICHENBERG,G.,"Ion Exchange",Editor:MARINSKY,J.,Marcel Dekker, New York(1966)227.
12.SHERRY,H.S.,"Ion Exchange",Editor:MARINSKY,J.,Marcel Dekker,New York (1969)89.
13.TIEN,H .T.,J.Phys.Chem.69(1963)350.
14.CHURMS,S.C.,J.S. Afr.Chem.Inst.19(1966) 98.
15.HEITNER-WIRGUIN,C.,ALBU-YARON,A.,J.inorg.nucl.Chem.28(1966)2379.
16.GEREVINI,T.,SMOGLIANA,R.,Energia Nucl. Milano 6(1959)339.
17.LEONT'EVA,G.V.,VOL'KHIN,V.V.,Izv.Akad.Nauk SSSR,Neorg.Mater.4 (1968)728).
18.FLOOD,H.,Discussions Faraday Soc.7(1949)180.
19.TUSTANOWSKI,S.,J.Chroatog.31(1967)268.
20.TUSTANOWSKI,S.,J.Chromatog.31(1967)270.
21.AHRLAND,S.,CARLESON,G.,J.inorg.nucl.Chem.33(1971)2229.
22.DONALDSON,J.D.,FULLER,M.J.,J.inorg.nucl.Chem.32(1970)1703.
23.MISAK,N.Z., MIKHAIL,E.M.,J.inorg.nucl.Chem.43(1981)1663.
24.MISAK,N.Z.,MIKHAIL,E.M.,J.inorg.nucl.Chem.42(1981)1903.
25.GHONEIMY,H.F., M.Sc., Ain-Shams University, Cairo(1978).
26.ROSSEINSKY,D.R.,Chem.Rev.65(1965)467.
27.NANCOLLAS,G.H.,REID,D.S.,J.inorg.nucl.Chem.31(1969)213.
28.RUVARAC,A.,TRTANJ,M.,J.inorg.nucl.Chem.34(1972)3893).
29.MISAK,N.Z., GHONEIMY,H.F.,Colloids and Surfaces 7(1983)89.
30.MISAK,N.Z., GHONEIMY,H.F.,J.Chem.Tech.Biotechnol.32(1982)893.
31.HELFFERICH,F.,"Ion Exchange",McGraw-Hill,New York(1962).
32.MISAK,N.Z.,SALAMA,H.N.,EL-NAGGAR,I.M.,Chemica Scripta (in press).

INORGANIC SORBENTS IN SPENT RESIN INCINERATION – THE ATOS PROCESS

C. AIROLA, Å. HULTGREN
Studsvik Energiteknik AB,
Nyköping, Sweden

Abstract

The spent resins from the operation of nuclear power plants form a dominating waste category, by activity contents and by volume. Volume reduction by incineration is technically feasible but introduces problems by activity release in the off-gas and in ash solidification.

By a chemical pretreatment that transfers radioactive nuclides to inorganic sorbents a considerable improvement is obtained in the incineration route. The paper summarizes efforts at STUDSVIK on development work along this line over the last years, resulting in the ATOS process. Included are results from wet activity transfer experiments, incineration of pretreated resins, and ash immobilization. The overall conclusion is that the ATOS process offers clear advantages as to clean off-gases, significant volume reduction and stable products.

1. INTRODUCTION

Spent ion exchange resins from power reactor operation contain more than 95 % of the total radioactivity of wet reactor wastes. Cementation and bituminization are the two methods applied in Sweden up to now for the immobilization of these resins, both methods leading to final waste volumes by far exceeding the volume of the original resins.

The reactor wastes in Sweden will be disposed in a rock cavern under the sea bottom of the Baltic, 1 km from the shore. In order to minimize disposal costs it is desirable to reduce the volume of the wastes before disposal /1/.

One process developed and discussed in Sweden for volume reduction of spent resins is the PILO process /2/. In the PILO process the resins are eluted and the eluted activity (99.9 % of Cs-Sr) is sorbed in an inorganic material, such as zeolite. The eluted resin may then be incinerated or, possibly, disposed without further treatment.

In the ATOS process a chemical pretreatment enables that the resins are incinerated with the activity retained in the ashes as well as most of the sulphur from the cation resin.

2. THE ATOS CONCEPT

ATOS is an acronym for Activity Transfer from Organic resins to inorganic Stable solids.

Process flowsheets for ATOS and PILO are shown in Figure 1.

In the ATOS process the spent resins, beads or powder, are mixed simultaneously with an eluting agent and an inorganic sorbent. The slurry is dried and incinerated/calcined under controlled conditions.

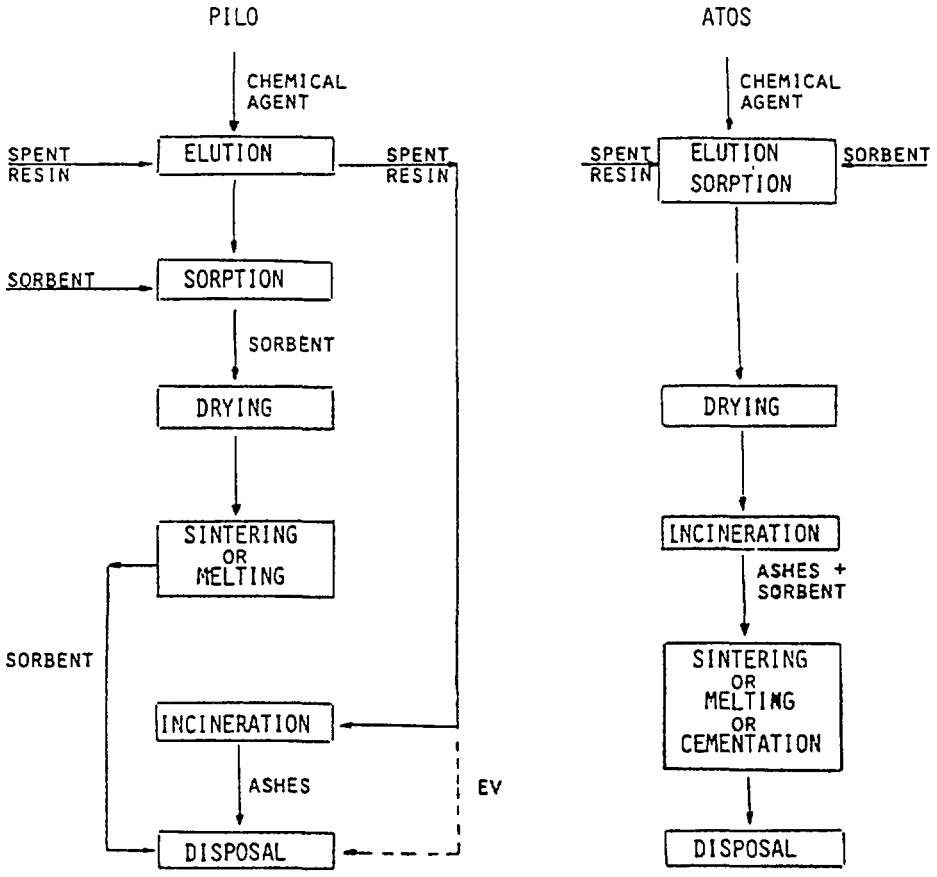

FIG. 1 Process flowsheets for PILO and ATOS

The incineration residue, a mixture of ash, inorganic sorbent and metal sulphates, may be immobilized in different ways. It may be sintered or melted with additives to a stable end product, or solidified by cementation, depending on local conditions at the site where ATOS will be applied.

The main objectives of the ATOS process are the following:

- transfer of cesium and other radioactive elements from the organic resins to an inorganic sorbent by a pretreatment process
- significant volume reduction of the waste by incineration of the pretreated resins
- easy adaptation to already existing processes for incineration and/or solidification
- simplified cleanup of off-gases
- a minimum generation of secondary waste.

The treatment stages to reach these objectives include a simple transfer of resin-water slurries from spent resin storage tanks to a mixing vessel, the addition of pretreatment chemicals, removal of excess water after treatment, transfer of the dewatered resin to a dryer/incinerator, incineration under controlled redox conditions thereby ensuring retainment of volatile activity, mainly cesium, and containment of most of the sulphur as metal sulphates.

3. PROCESS DEVELOPMENT /3-13/

3.1 Pretreatment

One main problem of the combustion of radioactive spent resins is the release of the volatile activity, principally Cs-compounds.

Studies were thus initiated at STUDSVIK assessing different ways by which Cs-compounds could be retained in the incineration residue during combustion where different additives such as zeolites and other inorganic sorbents were tried. In the drying-calcination process cesium is trapped in the structure of Na-Al-silicate systems, which gives a good retention of cesium during this stage of the process. Studies of the thermodynamic stability of various Cs-compounds under typical redox conditions encountered in a furnace were also conducted.

Bench scale tests with different eluting agents such as oxalic acid, Na-oxalate, tartaric acid, Na-tartrate, citric acid, Na-citrate, phosphoric acid, various phosphates and various formates showed that amounts of 2-4 meq's of the eluting agent per ml of resin is an optimal amount leading to almost exhaustive activity elution from the organic resin.

The different sorbents tested include Na-titanate, bentonite clay, mordenite, Ca-phosphate, Zr-oxide, Zr-phosphate as well as specially tailored sorbents like OXTI, PHOZIR A, PHOMIX A, POLYAN M, PERTITANIC and FE-CO-K (Applied Research Sprl, Belgium).

The performance of the above mentioned sorbents showed the PERTITANIC to be the best but also the most expensive one. Second choice is Na-titanate and bentonite clay and mixtures/blends of these. As Na-titanate is a good sorbent for Co-60 and bentonite clay for Cs-137 a standard sorbent consisting of 80 % Na-titanate and 20 % bentonite clay was used as a reference. The retention coefficient K_d of this mixture was for Cs, K_d=200 and for Co, K_d=600 ($K_d = C_{sorbent} : C_{solution}$, in ml/g).

The result of these studies led to the development of a process for the conditioning of spent resins prior to combustion. A simplified process flowsheet is shown in Figure 2.

The spent resins are transferred batchwise to a mixing vessel. From each batch a sample is withdrawn

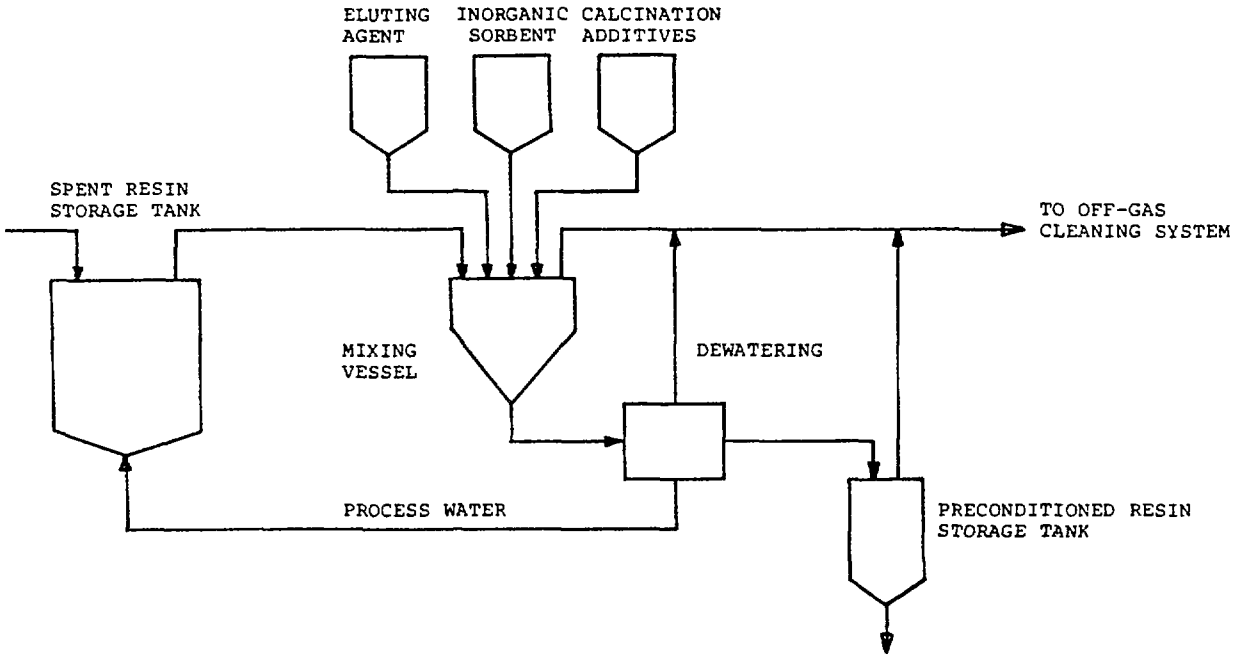

Simplified flowsheet for the ATOS pretreatment process

FIG. 2

and analyzed. Based upon this analysis eluting agent, inorganic sorbent and calcination additives/sulphur retainers are added. After treatment the conditioned resin is transferred to a storage tank. From this tank the resin is fed to the incinerator.

3.2 Incineration

A market survey made in late 1980 showed that at that time no proven commercial incineration system for resins was available. The development of such a system has been in progress in the USA, where e.g. the Aerojet company has demonstrated pilot plant scale incineration of ion exchange resins /11/.

At STUDSVIK incineration tests were performed, at first in laboratory scale to evaluate and optimize the pretreatment process. Later a prototype resin incinerator was built and tested on the kg/h scale.

Studies of the incineration process by thermal analysis showed that:

- untreated resins decompose in air at temperatures up to 300 °C . In pure oxygen the gases ignite explosively at about 300 °C if dried resins are used
- if wet untreated resins are used volatile decomposition products are distilled with the water. Ignition in oxygen now takes place at about 400 °C
- wet pretreated resins ignite explosively in oxygen at about 260-280 °C and are fully combusted at about 500 °C

- unloaded and untreated resins do not ignite even in oxygen, but decompose slowly up to about 700 °C.

Bench scale furnace tests were then made to verify the above mentioned observations, and results from these are shown in Table 1. In this table results from combustion in normal air and in oxygen are compared. The reason for using an oxygen atmosphere was to get a clean and complete incineration. Cesium may also be retained as Cs_2SO_4 which is formed in the presence of sulphur under oxidizing conditions.

From the table it can be seen that during combustion of untreated resins in oxygen some 7 % of the activity are emitted and that this figure can be lowered to about 0.1 % by preconditioning of the resin.

TABLE I Activity measurements from incineration tests

Resin treatment	Activity measured	Emission % of initial activity	
		Oxygen atm.	Air atm.
Untreated	Total	6.6	0.02
	Cs-137	5.5	0.04
	Cs-60	6.8	0.02
Untreated + inorganic sorbent	Total	1.6	0.004
	Cs-137	3.3	0.004
	Co-60	1.3	0.006
Pretreated	Total	0.4	0.02
	Cs-137	0.6	0.05
	Co-60	0.4	0.02
Pretreated + inorganic sorbent	Total	0.04	0.06
	Cs-137	0.08	0.02
	Co-60	0.2	0.1

Combustion in air showed a variation of the emission of activity between 0.02-0.06 %. These levels are so low that the accuracy of measurement of the low amounts of activity used are somewhat uncertain.

The tests also showed that good combustion characteristics with a high combustion efficiency indeed was obtained in an oxygen atmosphere whereas the amount of unburned resin was appreciable after combustion in plain air.

A prototype pilot plant resin incinerator with a capacity of about 1 kg/h (dry weight basis) was designed and built on the experiences obtained through the bench scale tests. The pilot plant incinerator is shown in Figure 3.

The resin is fed to the incinerator either through a screw feeder (powdered resins) or through a funnel feeder (bead resins). Incineration takes place on a heated turnable grating in an oxygen enriched atmosphere. The off-gases pass through an afterburner to a condenser and from there through a HEPA filter and activity monitoring to the laboratory stack.

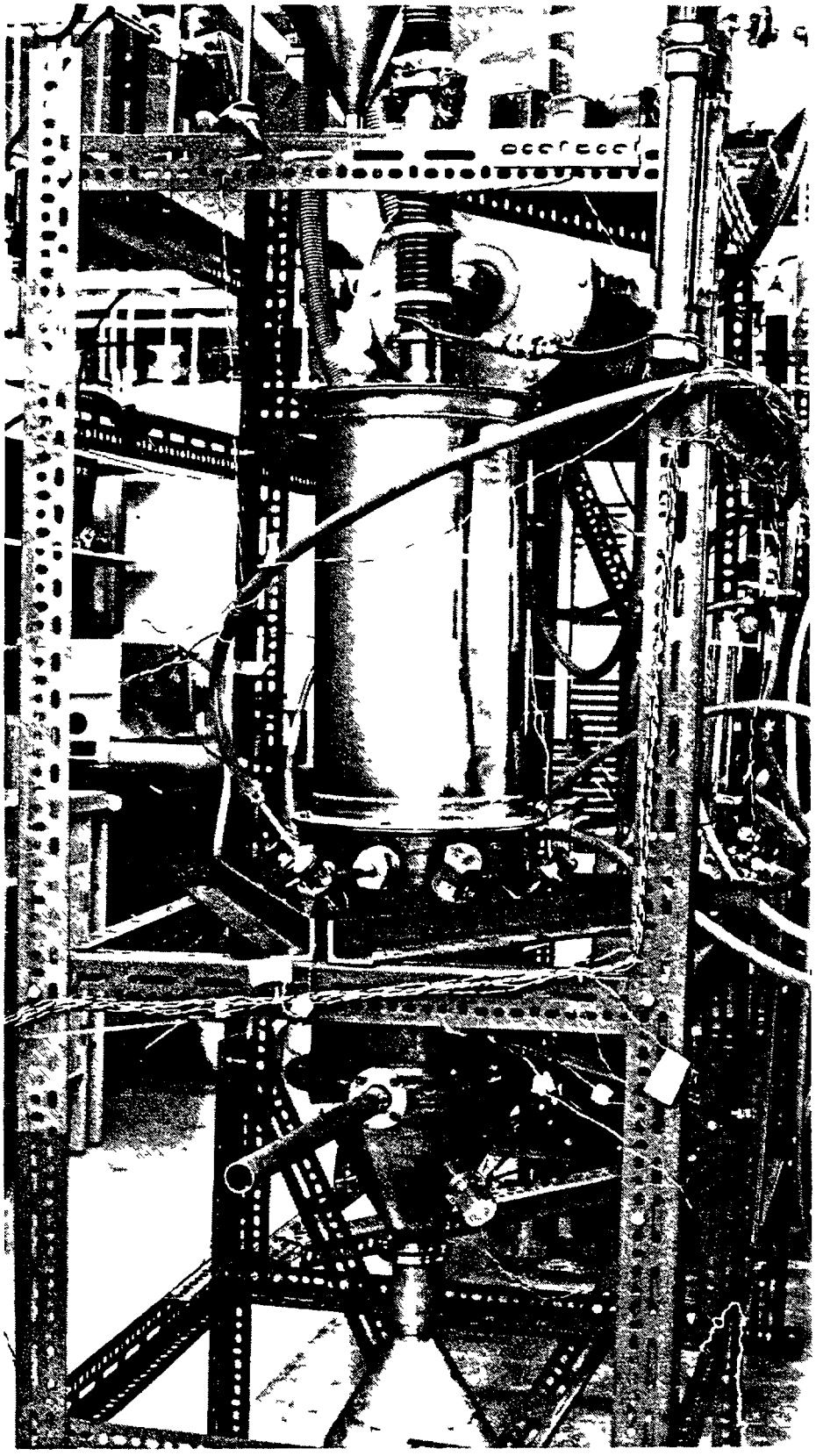

FIG. 3 Pilot plant incinerator

The results from a first series of inactive tests are summarized in Table II.

From this table it is seen that a considerable volume reduction factor may be achieved. The off-gases contain normally about 3500 ppm SO_2. This is of the same order of magnitude as reported by Aerojet. By adding suitable calcining additives preliminary tests indicate that the SO_2 content can be reduced to below 100 ppm. Further optimization of the incineration process is required, but the results so far are quite promising.

TABLE II A summary of the inactive test runs

	Range	Average
Resin feed kg/h	0.4 - 0.7	0.5
Incineration temp/ °C	700 - 850	800
Incineration time/min	50 - 170	80
Incineration residue/ml	80 - 250	150
residue/g	40 - 170	85
Volume reduction factor by vol	4 - 19	11
by weight	5 - 21	14
Offgas comp. oxygen/%	7 - 28	17
SO_2 /ppm	1000 -5000	3400 *
NO_x /ppm	100 -2500	750

* By addition of appropriate calcination additives the SO_2 content of the off-gases decreased to below 100 ppm

After modification of the pilot plant a series of active test runs will be performed.

A preliminary test to incinerate radioactive resins pretreated according to the ATOS process was made in the full scale waste incineration facility at STUDSVIK. 25 kg of spent resin containing 20 mCi Cs-137 and 5 mCi Co-60 were mixed with medical radioactive waste and incinerated. Activity emissions measured showed that only 0.6 ppm Cs and 2 ppm Co were emitted.

Traces of unburned resin were found in the ash which stresses the point that the combustion air should be enriched in oxygen.

3.3 Ash solidification

The ashes from resin incineration have to be solidified for transport and disposal. One of the methods used in Sweden today for the solidification

of various wastes including spent resins is cementation. This method is proven and accepted by the authorities. A main drawback of this method is the waste volume increase by a factor of at least two.

In order to maintain the volume reduction advantage achieved by incineration of the resins, the residue should be solidified with a minimum volume increase in the solidification stage. In Figure 4 the changes of volume due to different treatments are shown. From this figure it is seen that cementation of the incineration residue still provides an overall reduction of volume by a factor of about 5, compared to the initial volume.

Screening tests made at STUDSVIK show that the resin ashes may be solidified by sintering at temperatures about 1100-1200 °C. The adding of suitable sintering aids may somewhat reduce this temperature.

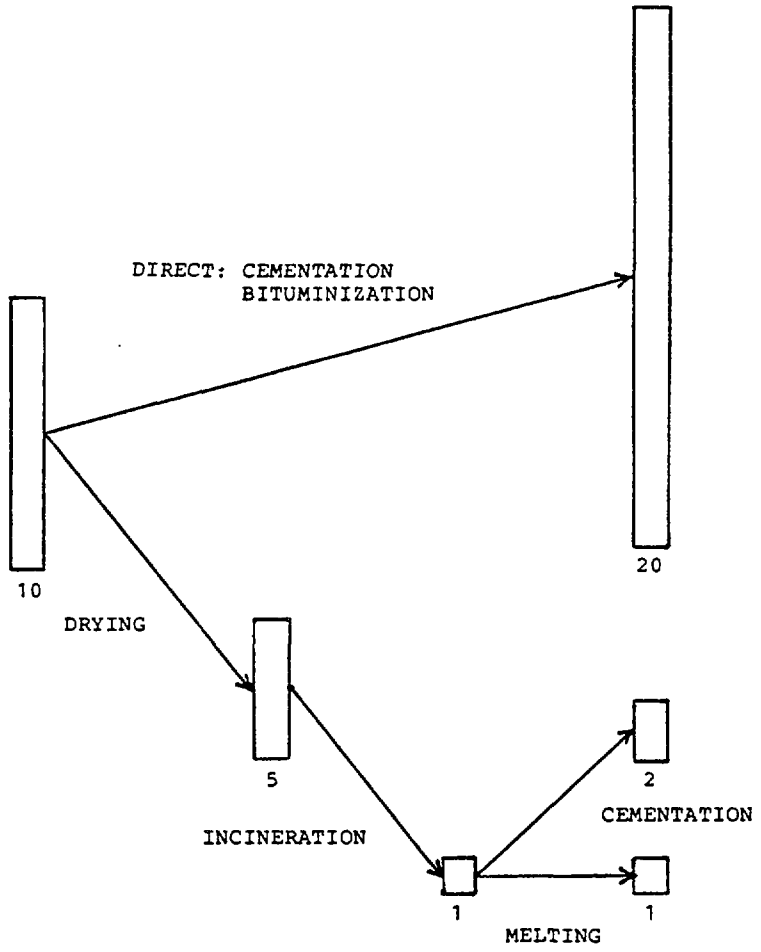

FIG. 4 Volume changes in different treatments of spent resins

The tests conducted at 1200 °C showed a Cs-emission of about 5 % and a volume reduction factor of about two. Lowering the sintering temperature to 1100 °C showed that the Cs-emission decreases to about 0.5 % but the additives required prohibit further volume reduction.

Tests have also been made to solidify the ash by cementation. The results so far show that a comparatively good solid can be obtained with an ash content of about 35 weight %. The compressive strength of this solid was 12 MPa and the volume increase factor only 1.3 in the cementation stage.

There are two problems encountered when cementing the ash: the metal sulphates and the carbon content. The former can be solved by using sulphate resistent cements or special cements like the US Gypsum cement. The second problem should be solved by an optimization of the incineration process, with a sufficiently long residence time under oxidizing conditions.

Work is now in progress at STUDSVIK to optimize solidification of the incineration residue by cementation. Results are expected during the fall, 1984.

4. CONCLUSIONS

A review of the results of the STUDSVIK studies supports the conclusion that incineration of resins pretreated as in the ATOS process is a feasible means to achieve a considerable volume reduction of the spent resins, while at the same time minimizing secondary waste generation and activity emission.

The use of appropriate inorganic sorbents in the pretreatment process ensures a complete combustion and minimized activity emission in the subsequent incineration step, provided that oxidizing combustion conditions are maintained. This means that the off-gas cleaning system can be relatively simple, thus reducing process and operating costs.

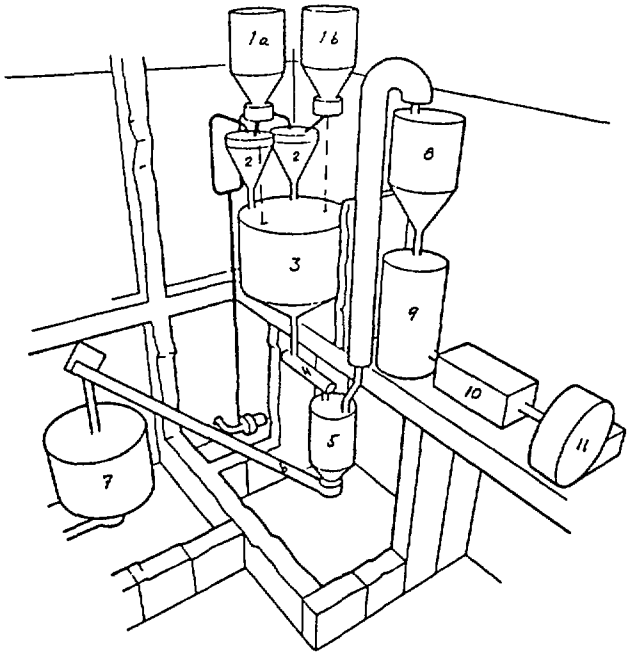

1a Eluting agent
1b Sorbent
2 Mixer-dryer
3 Buffer tank
4 Metering screw
5 Furnace
6 Ash conveyor
7 Ash storage tank
8 Afterburner
9 Scrubber
10 HEPA-filter
11 Fan

FIG. 5 Layout of an ATOS pilot plant

As to secondary waste generation promising results have been obtained by the addition of sulphur retainers to the incinerator/calciner. SO_2 emission is below 100 ppm, but more work is needed in order to bring this figure further down. As the overall volume reduction capability decreases with efficient sulphur retention a compromise has to be found between volume reduction and sulphur retention.

Pilot plant studies of a complete ATOS facility have also been made and a layout of such a facility is shown in Figure 5. The cost of such a plant has been estimated to about 10 MSEK at a capacity of about 10 m^3/year of spent resins.

REFERENCES

/1/ HULTGREN, Å., "Treatment of spent ion exchange resins - practices and developments in Sweden", Studsvik Technical Report NW-83/428 (1983) Contribution to the IAEA Third Research Coordination Meeting, Cairo, Egypt, 28 Feb-4 March, 1983.

/2/ HULTGREN, Å., AIROLA, C., FORBERG, S., FÄLTH, L., "Preparation of Titanates and Zeolites and Their Uses in Radioactive Waste Management, particularly in the Treatment of Spent Resins", Studsvik Technical Report NW-83/475, KBS TR 83-23, May 1983.

/3/ AIROLA, C., HULTGREN, Å., "Final treatment of spent resins with the ATOS process - a study of principles" (in Swedish), Studsvik Technical Report NW-82/237 (1982).

/4/ RINGBERG, H., Unpublished results.

/5/ RINGBERG, H., "Incineration experiments in air and oxygen with spent resins under various conditions" (in Swedish), Studsvik Technical Report NW-82/312 (1982).

/6/ RINGBERG, H., "Trial incineration of ATOS pre-treated resins in the STUDSVIK incineration plant" (in Swedish), Studsvik Technical Report NW-82/383 (1982).

/7/ OLLINEN, M., AIROLA, C., "Solidification experiments with ashes from the ATOS process" (in Swedish), Studsvik Technical Report NW-83/524 (1983).

/8/ BRODÉN, K., NIRSCHL, N., "Results from trials with incinerated resin ashes solidified in concrete" (in Swedish), Studsvik Technical Report NW-83/539 (1983).

/9/ AIROLA, C., "ATOS-AMOS plant, technical description" (in Swedish), Studsvik Technical Report NW-83/488 (1983).

/10/ HULTGREN, Å., "Development of ATOS technique. Status report September 1983" (in Swedish), Studsvik Technical Report NW-83/545 (1983).

/11/ LINDGREN, E., "Incineration of resins in the ATOS pilot plant. Results from trials performed during summer 1983" (in Swedish), Studsvik Technical Report NW-83/547 (1983).

/12/ MICHLINK, D.L., MARCHALL, R.W., TURNER, V.L., SMITH, K.R., VANDERWALL, E.M., "The Feasibility of Spent Resins Incineration at Nuclear Power Plants", Waste Management '83, Tucson, Arizona, 1983.

/13/ PATEK, P.R.M., TSYPLENKOV, V.S., HULTGREN, Å., POTTIER, P.E., "Treatment of Spent Ion Exchange Resins". International Conference on Radioactive Waste Management, Seattle, WA, USA, May 16-20, 1983. IAEA-CN-43/455.

PRECIPITATED MAGNETITE IN ALPHA EFFLUENT TREATMENT

K. HARDING
Atomic Energy Establishment Winfrith, UKAEA,
Dorchester, Dorset,
United Kingdom

Abstract

Iron present as a fortuitous component of most nuclear plant effluents can be precipitated as magnetite after suitable chemical treatment. The spinel crystal lattice of the magnetite is able to incorporate a wide range of foreign ions which includes many important radioactive species.

Provided the operating conditions are well chosen the precipitated magnetite provides an excellent scavenger for many radionuclides and gives a denser more granular solid product to be separated from the effluent than the more visual scavenging agent ferric hydroxide.

The conditions under which magnetite can be formed by precipitation and its properties are presented and compared with those of ferric hydroxide. Because magnetite has a high magnetic susceptibility its separation by high gradient magnetic separation becomes a possibility and data relevant to this is presented.

1. INTRODUCTION

Nuclear plant effluents frequently contain traces of iron typically at concentrations in the region of 10-200 g m^{-3} in association with radionuclide contaminants which vary from plant to plant. In reactors these are mainly activated circuit corrosion products ^{60}Co, ^{59}Fe, ^{54}Mn and ^{65}Zn with only minor amounts of fission products and alpha active nuclides. In fuel reprocessing plants they are reversed, fission products particularly ^{90}Sr, ^{137}Cs, ^{106}Ru predominate and significant amounts of alpha active nuclides, ie Pu and Am may be present.

On pH adjustment these effluents form a precipitate of ferric hydroxide which also carries with it many of the trace radioactive species as co-precipitates or by adsorption. Because these incorporation mechanisms are pH dependent, the efficiency of removal for the various active species varies widely and also for any given species consistent results are not easy to achieve. However satisfactory removal of this ferric floc can produce significant decontamination factors (DF) for such effluents. Unfortunately ferric floc is notoriously difficult to handle on mechanical filters being gelatinous, thin films quickly give rise to high pressure drops on conventional filters resulting in low capacity and causing problems with back washing. Because of this effect settling only is often resorted to, the plant then becoming large and expensive and can often give rise to variable DFs because of small particle carry over.

In an effort to improve the overall efficiency of effluent decontamination with particular emphasis on reducing costs the application of High Gradient Magnetic Separation (HGMS) to ferric floc filtration was investigated [1]. This work concluded that although HGMS would give process improvements it was not economically viable because the magnet system needed would be relatively large. What was required was a precipitate which had a higher magnetic susceptibility than ferric hydroxide and so reduce the size of the magnet, provided it was at least as effective as ferric hydroxide at removing activity from solution.

The obvious choice was to precipitate magnetite from solution instead of ferric hydroxide. That magnetite can be produced from cold solutions of ferric ferrous iron has been demonstrated by other workers [2, 3]. The results showed that the precipitated magnetite was strongly influenced by the presence of other ions in solution, some like sulphate being beneficial other like silica preventing its formation all together except at high temperatures.

However, the potential value for effluent clean up of precipitating a dense and strongly magnetic solid from an iron containing waste stream was considered to be worth detailed investigation. This paper reviews the progress made so far with the identification of the boundaries within which magnetite can be formed from cold solutions, its properties and potential for effluent clean up operations.

2. MAGNETITE - METHODS OF PRODUCTION

Magnetite is ferrous ferric oxide, having the chemical formula $FeO.Fe_2O_3$, and is the simplest of a large family of mixed oxides having the same structure of cubic close packing known as the spinel structure. The generic term for these mixed oxides is the ferrites. Many examples exist in minerals in which the divalent ion is nickel, copper, cobalt or zinc and the trivalent ion is aluminium or chromium. It is rare for these minerals to be fully stoichiometric, ie all the ferrous iron to be replaced by nickel or copper and consequently these minerals present a bewildering range of compositions and properties.

Many ferrites have interesting and useful electrical and magnetic properties and are now prepared commercially on a large scale. These include compounds not found in nature.

In general these synthetic ferrites are prepared by precipitation of mixed metal hydroxides by the addition of alkali to carefully formulated mixed salt solutions, followed by careful calcining and finally sintering to produce regular sized crystallites with the required mixed cation array.

In our application we require to produce a similar ordered array of ferrous and ferric ions with relatively small proportions of both the ferrous and ferric ions being replaced by the radioactive species also present in the effluent stream. Provided the size of these ions is within the acceptable range for the spinel structure they will be locked into the crystal

lattice and can only be removed if the precipitate is fully dissolved, unlike the situation with ferric hydroxide where such cations are often held by adsorption and are released by relatively small changes in solution composition.

Reports of the successful removal of very large ions such as cadmium lead and mercury by incorporation into ferrite precipitates [4, 5] indicates that a very wide range of radioactive species could well be held in this form. More recently work at Rocky Flats [6] has demonstrated that plutonium and americium ferrites can be prepared under appropriate conditions.

There are three methods whereby a solution can be made to yield a mixed oxide precipitate which is capable of conversion to a ferrite structure in which the predominant material is iron.

(a) Iron in the ferrous state and ferrous hydroxide is precipitated followed by partial oxidation usually with air.

(b) With iron in either the ferric or ferrous state an appropriate amount of the counter valance state iron is added to give the necessary stoichiometry for magnetite production, followed by pH adjustment.

(c) With iron in the ferric state partial reduction is carried out followed by pH adjustment to yield a mixed oxide precipitate.

A survey of the effluents to which this process could be applicable showed that the iron was predominantly present in the ferric state and therefore method (b) or (c) would be applicable. Method (b) involves the addition of further iron to the system thereby increasing the volume of solid waste to be handled and since this is highly undesirable, this method has not been investigated. Our work is being concentrated on method (c), ie the reduction of part of the iron present to yield a ferrous to ferric ratio of 0.5 ± 0.1.

Reduction of ferric ions to ferrous can be accomplished by a number of reagents and also electrolytically. However, any process designed to treat effluents needs to be both simple and economical and therefore only sulphite and hydrazine have been studied in detail so far in the programme. However dithionite (sodium hydrosulphite) is an interesting reagent suggested by Streeter et al [7] because in addition to its use for reduction in solution it can under some conditions convert ferric hydroxide to magnetite direct in a process analogous to the oxidation of ferrous hydroxide.

3. EXPERIMENTAL

3.1 Effects of Iron Concentration and Dissolved Oxygen

A reducing agent suitable for this process should be strong enough to reduce Fe^{+++} to Fe^{++} at an acceptable rate for an efficient process, but not strong enough to react with other

oxidising agents particularly nitrate which is always likely to be present in typical effluents. The presence of dissolved oxygen is a complicating factor in any likely process since there are no known reagents which can reduce Fe^{+++} to Fe^{++} in the presence of oxygen and therefore it must be removed by a prior deoxygenation operation, ie nitrogen sparging or reduced along with part of the iron.

At high iron concentrations, ie above 350 g m^{-3} the amount of sulphite needed to react with the dissolved oxygen is relatively small, approximately one third of the total needed, and does not seriously interfere with the control of the iron reduction reaction. However, as the iron concentration is reduced below 100 g m^{-3} the reduction of oxygen becomes the major sulphite consumer and control of the ferrous reduction reaction becomes more difficult. Also as the concentration of iron in solution is reduced the reaction with sulphite becomes slower and consequently the position where the optimum Fe^{++}/Fe^{+++} ratio is reached is more difficult to determine. Clearly some lower concentration of ferric iron will be reached where satisfactory formation of magnetite is not practicable. To examine this aspect the formation of magnetite has been examined over a range of concentrations in the presence and absence of oxygen all at ambient temperature (20-25°C).

A stock solution containing 1000 g m^{-3} iron as ferric nitrate with excess nitric acid to give a pH of 1.5-2.0 was used to prepare by dilution a series of test solutions containing a range of iron concentrations. The solutions were either purged with nitrogen to remove dissolved oxygen followed by the addition of sufficient sodium sulphite solution to reduce one third of the iron to the ferrous state, or sufficient sodium sulphite was added to react with the dissolved oxygen and also reduce one third of the iron. After stirring to ensure the reduction reaction was substantially complete the pH was adjusted to 10.0. On standing the properties of the precipitate formed were assessed visually and with a magnet.

Tables 1 and 2 show typical results from these experiments.

Because of the small scale of the experiments, problems were encountered with the exclusion of atmospheric oxygen and some variation in results was obtained. The data presented represents average resuts. From these results it can be seen that in the absence of oxygen a magnetic, low volume product is produced at iron concentrations as low as 30 g m^{-3} but the process is impractical below that. The presence of oxygen inhibits magnetite production; a good quality product only being formed at iron concentrations of 100 g m^{-3} or above.

3.2 Effect of Ferrous/Ferric Ratio on Magnetite Formation

The essential step in the reaction to form magnetite is the development of the optimum ratio of Fe^{++} to Fe^{+++} ions in the solution prior to precipitation. From the composition of magnetite $FeO.Fe_2O_3$ it is clear that this ratio should be close to 0.5. However precise control of this ratio on a plant scale will not be simple and therefore if this process is to be considered for industrial applications it will be necessary to

Table 1

Formation of Magnetite from Ferric Nitrate Solution Free from Dissolved Oxygen

Iron Concentration ppm Fe^{3+}	Mixing Time (mins) before alkali addition	Final pH	Observations
150	5	10.8	Immediate heavy ppt - dense black/brown - magnetic
100	7	10.4	Immediate granular, colour - black - magnetic
80	10	10.5	Immediate granular, colour - black - magnetic
70	10	10.6	Immediate ppt, not as granular as before - magnetic
50	10	10.2	Instant fine - black precipitate - magnetic
30	15	10.2	Fine ppt, black/brown - formed after 1 minute - magnetic
15	15	10.2	Initial dark green solution formed a very fine suspension after 1 minute, which did not start to settle until after 3 minutes, black/brown - less strongly magnetic

Table 2

Formation of Magnetite from Ferric Nitrate Solution With the Presence of Dissolved Oxygen

Iron Concentration ppm Fe^{3+}	2% Na_2So_2 Added cm^3	Mixing* Time (mins)+	Final pH	Observations
150	10	5	10.6	Dense brown/black ppt formed immediately - magnetic
100	8	7	10.5	Black granular precipitate - magnetic
80	6	10	10.7	Dark brown floc quick to form - weakly magnetic
70	5	15	10.8	Brown floc, becoming denser on standing - weakly magnetic
50	4	15	11.2	Light brown floc faintly magnetic
30	3	15	11.2	Yellow/brown floc, non-magnetic

*Mixing time considered just sufficient for reaction to be complete.

+Before alkali addition

demonstrate that some degree of freedom can be allowed in the adjustment of the Fe^{++}/Fe^{+++} ratio and still produce a satisfactory product.

Table 3 shows the results of a series of experiments to determine the effect of varying this ratio on the production of a magnetic produce over a range of iron concentrations. All solutions were purged free from oxygen.

Table 3

Magnetite Formation from Cold Aqueous Solutions

Ferrous/Ferric Ratio	Total Iron Concentration				
	50	100	150	300	600
0.2	Brown NM	Brown NM	Brown NM	Brown NM	Brown NM
0.3	Dark Brown WM	Dark Brown WM	Dark Brown WM	Dark Brown WM	Dark Brown WM
0.4	Dense Black SM	Dense Black SM	Dense Black SM	Dense Black SM	Dense Black SM
0.5	Dense Black SM	Dense Black SM	Dense Black SM	Dense Black SM	Dense Black SM
0.6	"	"	"	"	"
0.7	Brown WM	Dark Brown SM	Dense Black SM	Dense Black SM	Dense Black SM
0.8	Green NM	Brown WM	Green/Black WM	Green/Black WM	Dark Brown SM
1.0	Green NM	Green NM	Green NM	Green NM	Green NM

Note: NM - Non-magnetic
WM - Weakly magnetic
SM - Strongly magnetic

At low ferrous concentrations the formation of a magnetic precipitate shows no iron concentration dependence. However at Fe^{++}/Fe^{+++} ratios beyond 0.6 the formation of a magnetic product is dependent on iron concentration. At high iron concentrations (600 g m^{-3}) even at ratios as high as 0.8 a magnetic product is readily produced.

These results were encouraging for the development of a possible industrial scale process and the scope of these tests were widened to study possible plant control systems.

In a solution containing both oxidised and reduced forms of an ionic species the potential taken up by an inert electrode has a constant value under standard conditions of species

concentration known as the redox potential of the system. This effect can easily be used to determine when an oxidisation or reduction reaction has been taken to completion because a sharp change in the solution potential is obtained as the last fraction of one species is converted to the other. The situation is not as clearly defined when one requires to take a reduction reaction to an intermediate position.

Experiments were carried out in which the redox potential of a deoxygenated ferric nitrate solution was followed as it was titrated with sodium sulphite solution; samples of solution being withdrawn periodically and the Fe^{++}/Fe^{+++} ratio being determined colorimetrically. Figure 1 shows the changes in redox potential against sulphite addition, the region where the Fe^{++}/Fe^{+++} ratio was between 0.4 and 0.6 (ie magnetite is produced) is seen to lie between 400 and 350 mV. This graph clearly shows how the control of conditions needed for magnetite production is easier at higher iron concentrations. Another feature of interest shown in this graph is that the amount of sulphite required to reduce one third of the iron is greater than the theoretical amount.

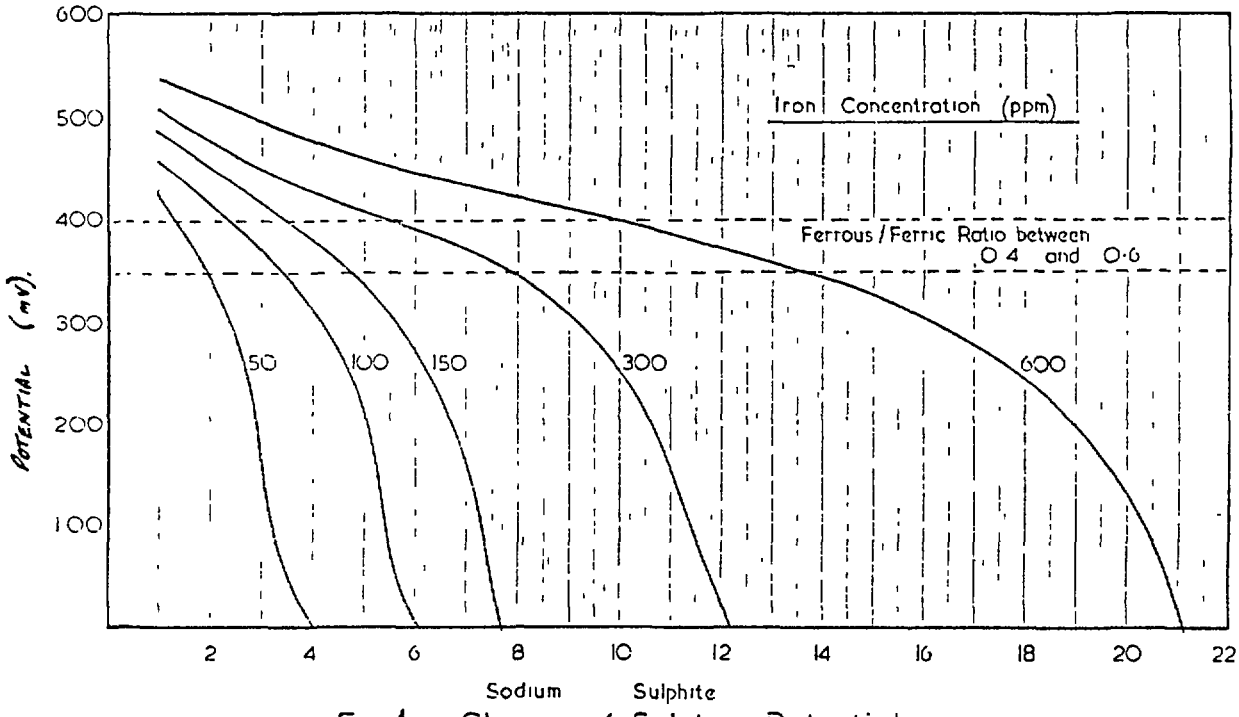

Fig 1 :- Change of Solution Potential as Ferrous / Ferric Ratio Changes.

It should also be noted that the presence of nitrate ion changes the position of the solution potential band within which magnetite is formed but not the overall width or general shape of the titration curves.

3.3 Effect of some Interfering Ions on Magnetite Precipitation

The most comprehensive work on the precipitation of magnetite from ambient temperature solutions has been carried out for the treatment of mineral waters [2]. More recently reference [8] has also addressed this problem.

Table 4

Effect of Magnesium on Magnetite Formation

Stirring Time Mins	Fe(III) Conc ppm	Mg(II) Conc ppm	Mg/Fe Ratio	2% Sodium Sulphate Added cm^3	Initial pH	Final pH	Observations
10	15	5	0.33	0.75	2.1	10.7	Very fine black ppt - 5 mins to settle around magnet - magnetic
10	15	10	0.66	0.75	2.2	10.5	15 minutes for any settling to occur around magnet, most settled within 30 minutes.
10	15	15	1	0.75	2.2	10.7	Fine suspension visible after 15 mins. 1 hr to settle completely. Formed overnight - weakly magnetic
10	15	20	1.33	0.75	2.2	11	Fine suspension visible after 20 mins. Yellow solution after 30 mins. Light brown floc after 1½ hrs. Non-magnetic
10	15	25	1.67	0.75	2.2	11	Non-magnetic floc after 15 mins
7	30	5	0.167	1.5	1.9	10.7	Immediate formation of black ppt - magnetic
7	30	10	0.33	1.5	1.9	10.7	Fine suspension at first, precipitation on magnet after 4 minutes - magnetic.
7	30	20	0.66	1.5	1.9	11.0	Floc-like suspension, settled as magnetite in 20 mins - magnetic
7	30	25	0.833	1.5	1.9	10.6	Very fine immediate suspension. Fine ppt around magnet after 20 mins. Full settling after 40 minutes - weakly magnetic.
7	30	30	1	1.5	1.8	10.6	Greenish-brown ppt after 20 min - weakly magnetic. Dark brown magnetic ppt after 30 min. Floc-like mixture of magnetic/non-magnetic ppt formed overnight
7	30	35	1.167	1.5	1.9	10.8	Green floc-like ppt formed in < 1 hr. Formed a floc-like mixture, as above, overnight.
7	30	40	1.33	1.5	2.0	11	Fine floc suspension - formed overnight, non-magnetic
7	30	50	1.667	1.5	2.2	11	Fine green floc, forming brown floc. Non-magnetic

These workers report results from systems where the iron concentrations and those of the interfering ions are much higher than is likely to be the case with typical nuclear industry effluents. However, the main ions which suppress magnetite formation are identified as magnesium, aluminium and soluble silicate whereas sulphate enhances its production.

Table 5

Effect of Aluminium on Magnetite Formation

Stirring Time Mins	Fe(III) Conc ppm	Al(III) Conc ppm	Al/Fe Ratio	Initial pH	Final pH	Observations
7	15	0	0	2.2	10.9	Fine ppt of magnetite immediately - solution test.
7	15	1	0.066	2.2	10.5	Instant ppt of magnetite.
7	15	2	0.133	2.2	10.8	Fine suspension showing after 3 mins - settled in 10 mins.
7	15	3	0.2	2.2	10.8	Magnetic ppt settled in 30 mins - brown/black
7	15	5	0.33	2.2	10.95	Fine suspension slo to form, settled as brown floc - not magnetic
7	15	10	0.66	2.3	10.9	Floc-like brown ppt, not magnetic
5	30	2	0.066	1.9	10.9	Fine black ppt, settled after 3 mins - magnetic
5	30	3	0.1	1.9	10.7	Fine suspension visible in 5 mins. Settled as faint ppt after 30 mins - magnetic
5	30	5	0.167	1.9	10.4	Fine suspension visible in 5 mins. Settled as faint ppt in 20 mins - became denser after 2 hr - magnetic
5	30	10	0.33	1.9	10.5	Fine suspension slow to form, settled as dark brown floc, non-magnetic

To assess the effects of these ions on the formation of magnetite at relatively low iron concentrations and where the ferrous ions are produced by in situ reduction a series of tests have been carried out in the presence of varying concentrations of magnesium, aluminium and soluble silicate. Again all solutions were deoxygenated by nitrogen purging prior to the test.

Tables 4, 5 and 6 present the results obtained from which the following conclusions can be drawn.

(a) Magnesium interferes least strongly, with solutions containing Mg/Fe ratios up to one able to form a magnetic ppt even at low iron concentrations. As the iron concentration increases the proportion of magnesium which can be tolerated also increases.

(b) Aluminium interference is more serious than that of magnesium. At low iron concentrations magnetite formation starts to be suppressed at Al/Fe ratios of 0.2 but, as with magnesium, as the iron concentration increases a higher Al/Fe ratio can be tolerated.

Table 6

Effect of Silicate on Magnetite Formation

Stirring Time Mins	Fe(III) Conc ppm	Silicate Conc ppm	Si/Fe Ratio	Initial pH	Final pH	Observations
5	30	1	0.033	1.9	11	Instant black ppt of magnetite - strongly magnetic
5	30	2	0.066	1.9	10.8	Paramagnetic green floc instantly formed - darkened slowly - magnetic
5	30	3	0.1	1.9	10.8	Green floc - darkened slowly - became magnetic after 20 mins
5	30	5	0.167	1.9	11	Dark brown floc - not magnetic even on standing
5	30	10	0.33	1.9	10.3	Light brown floc - not magnetic on standing.
7	15	0	0	2.1	10.5	Fine black ppt immediately - solution blank test
7	15	1	0.66	2.0	10.1	Faint black ppt after 10 mins - magnetic
7	15	2	0.133	2.0	10.2	Fine suspension does not settle after 30 mins. Non-magnetic
7	15	5	0.33	2.0	10.4	Yellow solution - ferric floc ppt very slow to settle. Non-magnetic
7	15	10	0.66	2.1	10.7	Yellow solution, ferric floc slow to settle as before.

(c) Soluble silicate prevents the formation of magnetite at mole ratios above 0.1. However, unlike aluminium, increasing the iron concentration does not lead to a greater toleration for silicate.

3.4 Activity Uptake by Magnetite

Following the identification of a wide region of solution conditions where magnetite can be precipitated from solution the capability of this material to remove trace activity from solution was compared with that of ferric floc under similar conditions.

A stock solution of 300 g m^{-3} iron as ferric nitrate containing traces of typical radionuclide contaminants was used. Its composition is given in Table 7.

Aliquots of this stock solution were taken and either treated directly with ammonia to precipitate ferric floc (pH 10.5) or dissolved oxygen was removed by purging with nitrogen followed by sulphite addition to produce a Fe^{++}/Fe^{+++} ratio

Table 7

Analysis of Active Stock Solution

Solution Component		Concentration
Iron	mg/litre	300
Magnesium	"	10
Plutonium (238, 240, 241)	µCi/litre	15
Americium 241	"	1.4
Cobalt 60	"	2.1
Caesium 137	"	2.9
Cerium 144	"	1.4
Europium 154	"	8.0
Ruthenium 106	"	4.2
Strontium 90	"	69

Table 8

Comparison of Radio Nuclide Uptake by Ferric Floc and Precipitated Magnetite

Radio Isotope	DF							
	Ferric Floc				Magnetite			
Plutonium	100	150	200	150	800	150	1000	1000
Americium	150	250	100	150	500	800	700	600
Co 60	10	15	10	15	100	80	100	150
Cs 137	NIL	NIL	NIL	NIL	NIL	NIL	NIL	NIL
Ce 144	50	40	12	20	50	90	100	80
Eu 154	20	20	15	10	100	80	100	100
Ru 106	10	6	10	8	50	100	40	60
Sr 90	2	2	1.5	1.8	10	20	15	10

of 0.5 before making alkaline with ammonia to pH 10.5. After allowing both precipitates to settle overnight the supernatent liquid was decanted off, filtered through a 0.45 micron millipore filter and this clear liquor was analysed for radionuclides. The results from 4 pairs of experiments are given in Table 8.

These results confirm the expectation that precipitated magnetite should be a more effective getter for trace active species than ferric floc. For alpha active species this improvement is only marginal since ferric floc is an effective getter for the transuranic elements. The main advantage seen to be obtained from the use of magnetite is the more consistent DF for alpha coupled with a significant improvement in performance for the beta emitters ^{90}Sr and ^{106}Ru.

4. PROPERTIES OF PRECIPITATED MAGNETITE COMPARED WITH FERRIC FLOC

4.1 Settling Rates and Densities

Although magnetite has been shown to give improved DFs for a number of radionuclides it is its high magnetic susceptibility with the attendant possibility of efficient solids separation using HGMS which originally prompted this work. In much of the scoping tests directed at finding the boundaries within which magnetite could be formed the fact that the precipitate was black and attracted by a magnet was taken as sufficient evidence that magnetite was being produced.

Having established the operational conditions necessary to produce a "magnetite" precipitate, experimental work was directed towards the characterisation of this material and the comparison of its separation properties with those of ferric floc precipitated from the same solution composition. The composition of the solution used was 300 g m^{-3} of iron as ferric nitrate with nitric acid to pH 1.5. Treatment used was as before. The settling rates of the two precipitates were measured and are plotted in Figure 2. The magnetite settles significantly faster than the ferric floc despite the fact that the magnetite particles are a good deal smaller than those of the ferric floc (see Figures 3 and 4). Scanning electron photo micrographs (SEM) pictures of the two types of particles indicate a possible explanation for this behaviour, the ferric floc particles having a sponge-like appearance whereas the magnetite particles were smooth but "stringy".

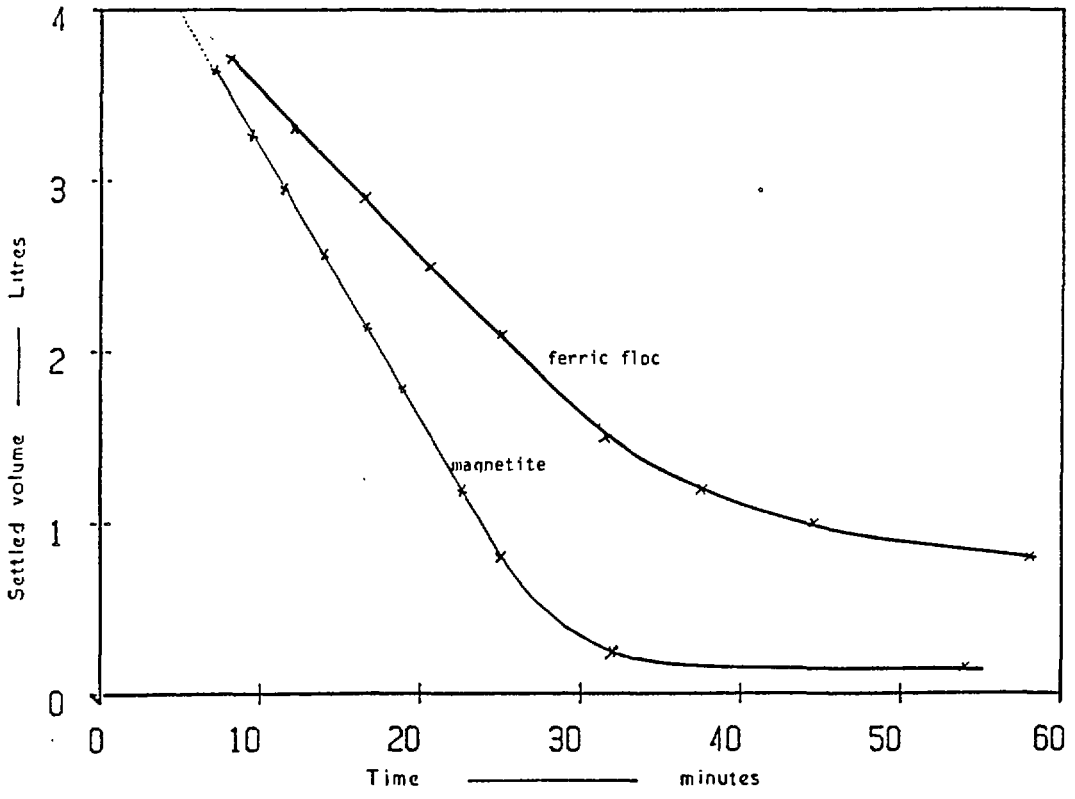

Fig 2:- SETTLING CURVES FOR THE FIRST HOUR.

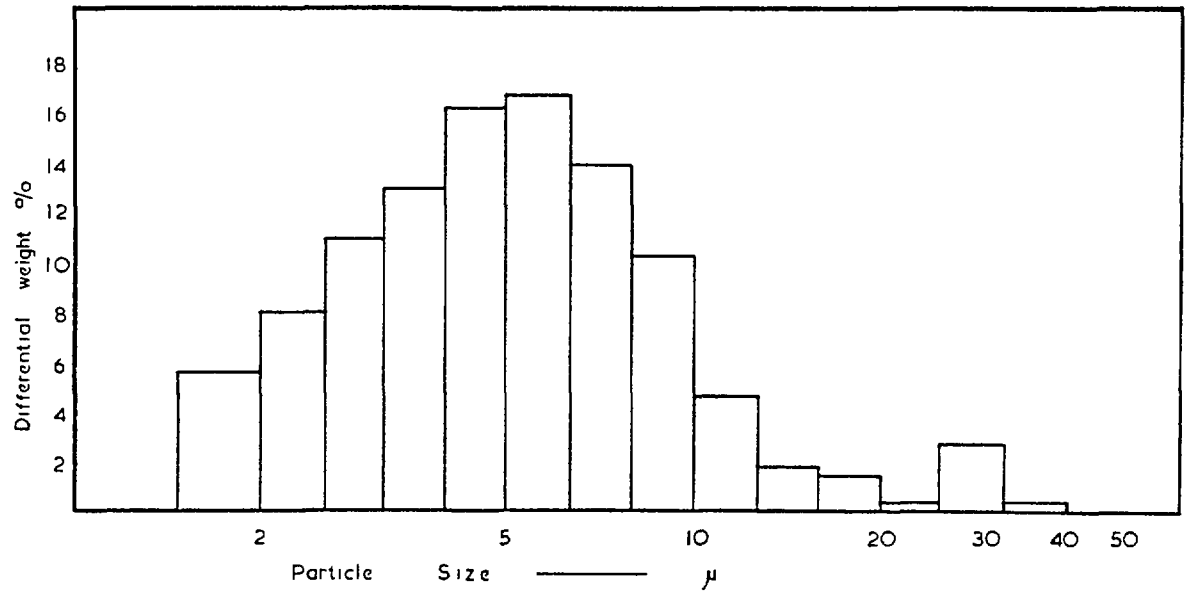

Fig 3:- PARTICLE SIZE DISTRIBUTION FOR MAGNETITE.

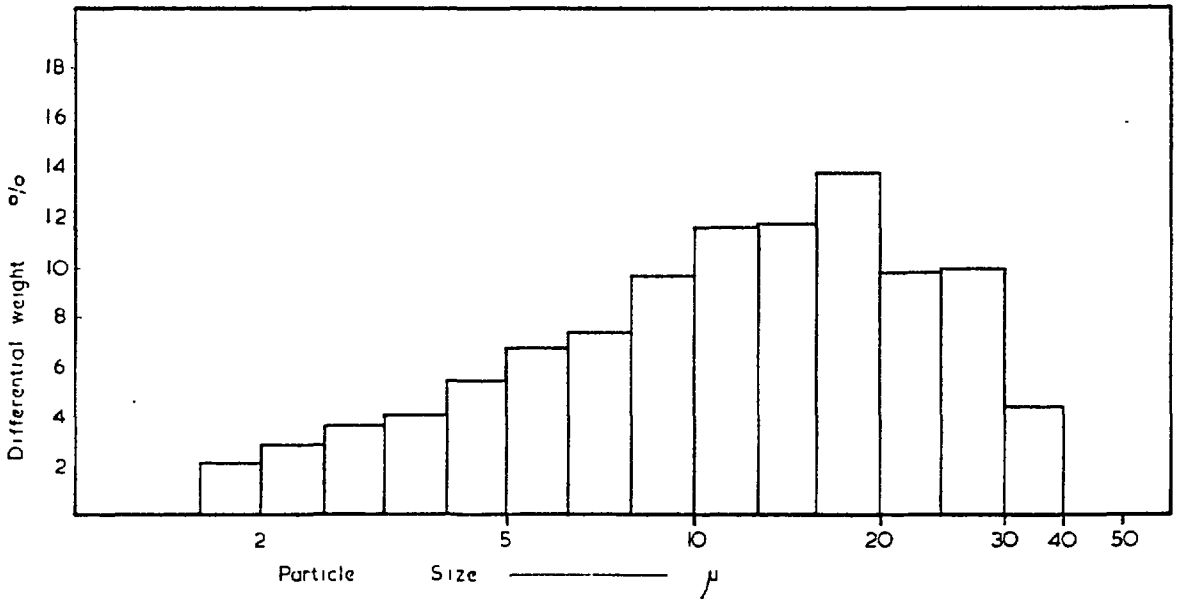

Fig 4 :- PARTICLE SIZE DISTRIBUTION FOR FERRIC FLOC.

The settled densities of the two precipitates varied with time. At 30 minutes the settled magnetite had five times the density of the ferric floc, at 20 hours it was only twice as dense and by 200 hours it was only 20% greater at 8.5% total solids. This relatively low final settled density is disappointing and clearly more work is needed to develop the conditions for the production of a more crystalline form of magnetite.

4.2 Magnetic Susceptibility

As indicated in the scoping test results given in Table 4 the formation of magnetite or at least the development of strong magnetic properties is not instantaneous on precipitation.

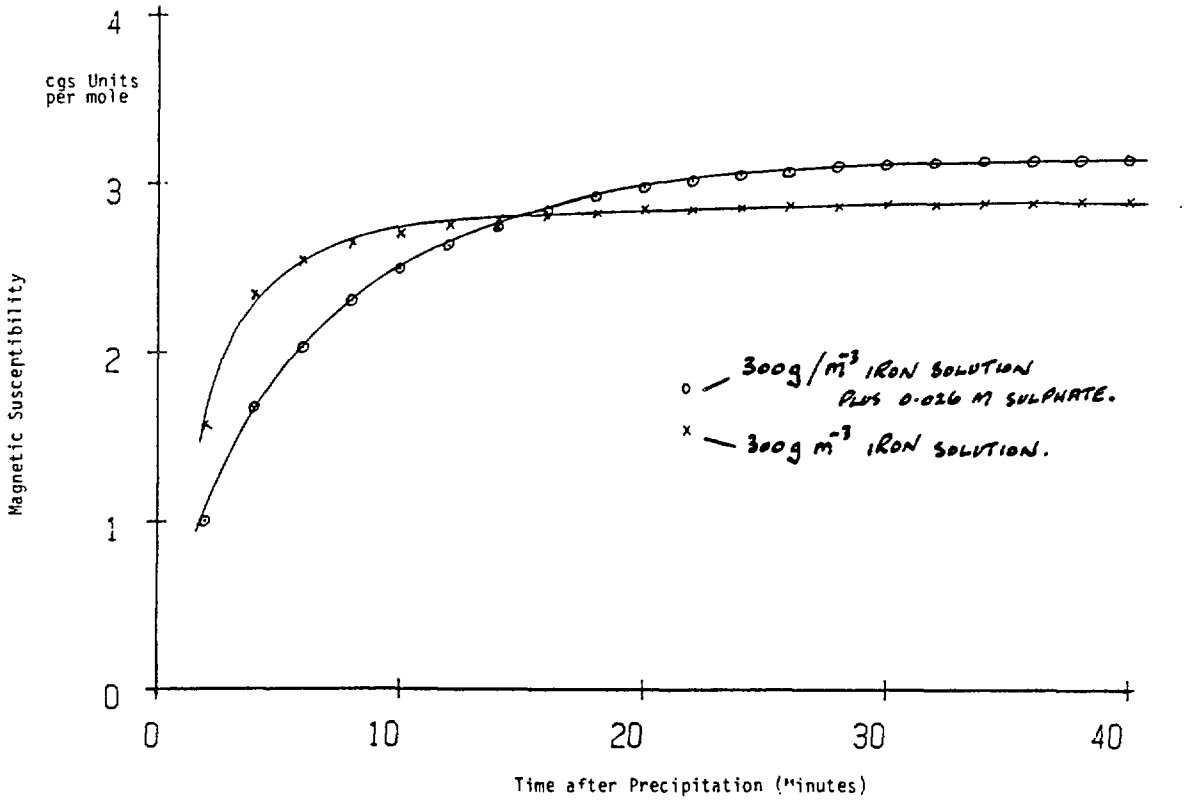

Magnetic Susceptibility of Magnetite Directly after Precipitation

Figure 5:

Figure 5 shows the change of magnetic susceptibility of two magnetite precipitates with time. Both develop strong magnetic properties of the same value as mineral magnetite at 2.6 and 3.0 CGS units per mole (ground mineral magnetite had a magnetic susceptibility of 2.7 CGS units per mole). The presence of sulphate ion retards the development of magnetic properties initially but results in higher values being developed ultimately. This material was also more crystalline as shown in electron micrographs of the particles. These values can be compared with a value of 0.01 CGS units per mole for ferric floc.

5. CONCLUSIONS AND POTENTIAL APPLICATIONS

5.1 Precipitation of Magnetite

It has been demonstrated that a magnetite-like solid can be produced from effluents containing iron on suitable treatment of the effluent and that this solid:

(a) has high collecting power for radionuclides

(b) settles rapidly but its ultimate settled density requires to be increased

(c) has a high magnetic susceptibility.

It is not possible to precipitate magnetite directly from all solution compositions, in that there are a number of common ions which suppress its formation direct from ambient temperature solution. However, the addition of more iron to that naturally present will in the great majority of such cases enable the interference to be overcome.

The use of the cheap reducing agent sulphite to produce the necessary conditions for magnetite precipitation without adding to the bulk of waste produced when sufficient iron is naturally present in the effluent has distinct advantages for subsequent waste disposal [9].

5.2 Applications

(a) Gravity Settling - the increased density of magnetite gives rise to faster settling of this material than with ferric floc enabling smaller settlers to be used for a given throughput. However, the smaller particle size gives rise to some problems with carryover.

(b) HGMS - the very high magnetic susceptibility of this material provides a potential application for solids separation using a magnetic filter directly in place of a settler. Alternatively, a gravity settler to handle the bulk of the solids followed by an HGMS unit to polish the last traces of solids appears to be attractive if maximum DFs are needed.

(c) Magnetic Assisted Gravity Settling - again because of the strong magnetic properties of the precipitate a relatively weak magnetic gradient which will both flocculate and attract the magnetite particles has been shown to produce high rates of settling and higher settled solids densities of up to 14%.

REFERENCES

[1] HARDING, K., BAXTER, W., "Application of HGMS to Ferric Hydroxide Filtration" paper 14-4, Intermag, Grenoble (1981).

[2] "US Environmental Protection Agency Water Quality Office Studies on Densification of Coal Mine Drainage Sludge", Report 14618 MJT (August 1971).

[3] OKUDA, T., SUGANO, I., SUJI, T. T., "Removal of Heavy Metals from Waste Water by Ferrite Co-precipitation Technique", Filtration and Separation Journal (January/ February 1976).

[4] TAKADA, T., "Removal of Heavy Metal Ions from Waste Water by Ferritisation", Kago to Taisaki 13, 37 (1977), RFP translation 281.

[5] IGUCHI, T., KAMURA, T., INOUE, M., "Ferrite Process for Treatment of Waste Water Containing Hevy Metals", PPM 10, 49 (1979), RFP translation 284.

[6] BOYD, T. E., KOCHEN, R. L., PRICE, M. Y., "Ferrite Treatment of Actinide Waste Solutions", RFP 3299 (July 1982).

[7] STREETER, R. C., McLEAN, D. C., LOVELL, H. L., "Reduction of Hydrous Ferric Oxide to a Magnetic Form with Sodium Dithinite; Implications for Coal Mining Drainage Treatment", Am. Chem. Soc. (September 1971).

[8] VAINSHTEIN, V. I., et al., "Influence of Salt Composition on the Kinetics of Magnetite Formation, Its Magnetic Susceptibility and Mechanical Dehydration", Zhumal Prikladnoi Khinii, 55 1 (1982) 133-138.

[9] HARDING, K., WILLIAMS, R., Provisional UK Patent 2091135 A (1981)

THE APPLICATION OF INORGANIC ION EXCHANGERS TO THE TREATMENT OF ALPHA-BEARING WASTE STREAMS

E.W. HOOPER
Chemical Technology Division,
Atomic Energy Research Establishment, UKAEA,
Harwell, United Kingdom

Abstract

The Department of the Environment is funding a generic programme of work at AERE, Harwell to examine the application of inorganic ion exchangers to the removal of radionuclides from aqueous waste streams.

A literature survey has identified six exchangers of potential use, they are:- Titanium Phosphate, Zirconium Phosphate, Manganese Dioxide, Polyantimonic Acid, Hydrous Titanium Oxide and Copper Hexacyanoferrate.

A programme of batch contact experiments using spiked solutions and solutions of irradiated fuel has examined the extent and rate of absorption of radionuclides from solutions 1 Molar in nitrate ion and with hydrogen ion concentrations between 1 Molar and pH = 10; 2M and 4M nitric acid solutions have also been examined.

This paper presents the data obtained so far on the absorption of plutonium, americium and neptunium from spiked solutions and of total α-activity removal from solutions of irradiated fuel.

1. Introduction

In 1982 the UK Department of the Environment initiated at AERE Harwell a programme of work with the objective of developing processes which would provide efficient and safe concentration of the radioactive constituents of waste streams into solid materials which can be consolidated into forms suitable for storage or disposal.

A search of the literature showed that a considerable volume of information is available on the use of inorganic absorbers for the decontamination of waste streams but the reported data are often of limited use in selecting an absorber for a particular

waste stream since the candidate material has generally been examined only for a few or individual nuclides over a small range of operating conditions. Also the information available on α-decontamination is considerably less than that for βγ removal.

An assessment exercise[1], based on the literature search, identified six ion exchangers with a known affinity for actinides and/or fission products and an experimental programme of work is now in progress to obtain a comprehensive knowledge of the capabilities of these exchangers. The absorbers selected for this study are:- Titanium Phosphate, Zirconium Phosphate, Manganese Dioxide, Polyantimonic Acid, Hydrous Titanium Oxide and Sodium Copper Hexacyanoferrate.

This paper presents the data obtained so far on the absorption of plutonium, americium and neptunium from spiked solutions and of total α-activity removal from solutions of irradiated fuel.

2. Experimental

2.1 Absorbers

Hydrous Titanium Oxide (HTiO) was prepared by precipitation from titanium tetrachloride solution by addition of sodium hydroxide solution. The precipitate was washed and then dried to a glassy gel.

Manganese Dioxide (MANOX A,MnO_2), Titanium Phosphate (PHOTI D,TiP), Zirconium Phosphate (PHOZIR A, ZrP), Polyantimonic Acid (POLYAN S, SbA) and Copper Ferrocyanide (FeCu) were obtained from Applied Research SPRL, Belgium.

Polyantimonic Acid and Titanium Phosphate absorbers have also been prepared at Harwell.

All absorbers were sieved to provide material with the particle size range 212-425μm.

2.2 Waste Simulates

Simulates of salt-free acid wastes were prepared by spiking 1-4M nitric acid solutions with radionuclides. Simulates of salt bearing wastes were prepared from 1M sodium nitrate solution.

Solutions of Am-241 in 3M HNO_3, Pu-239 in 4M HNO_3, Np-237 in 4M HNO_3 and irradiated fuel in HNO_3 (~ 3M) were used as sources of radionuclides.

The pH of the waste simulate was adjusted to the required value by addition of HNO_3 or NaOH.

2.3 Conditioning of Absorbers

Conditioning is necessary in order to maintain a constant solution pH during the course of a kinetic run. Absorbers were washed in order to remove adherent fines then contacted with water for several days at a pH maintained at the required value by the addition of either HNO_3 or NaOH solution from an autotitrator. The conditioned absorbers were washed with distilled water and, with the exception of HTiO, allowed to air dry for several days. It was observed that HTiO undergoes dissolution at a solution pH < 1.0, and that MnO_2 had to be conditioned in the presence of $NaNO_3$ since, in solutions of low ionic strength, it tended to break down.

2.4 Kinetics of Absorption

The rate of absorption of radio-ions was followed by batch contact experiments. 0.25 to 1g of conditioned absorber was added to 50 mL of waste simulate which had been adjusted to the required pH. The flasks were then shaken at a fixed rate for 24 hours, samples being removed periodically for analysis.

The percentage removal of an isotope as a function of time was calculated from the following equation:

$$\% \text{ removal} = \left(\frac{A_o - A_t}{A_o}\right) 100$$

where,

A_o = initial activity in (unit volume of) solution

A_t = activity at time t in (unit volume of) solution

2.5 Distribution Coefficient Measurements

A 50 mL aliquot of waste simulate solution was added to an accurately weighed amount of ion-exchanger. The solution was then allowed to stand at 25°C, with intermittent shaking, for periods of up to two weeks.

Distribution coefficients (K_D) were calculated from the following:

$$K_D = \frac{A_o - A_\infty}{A_\infty} \frac{V}{w} \quad (mL\ g^{-1})$$

where,

V = total solution volume (mL)

w = weight of exchanger (g)

3. Results

3.1 Plutonium Absorption

The absorption kinetics of Pu(IV) (28 μM) on a variety of exchangers under different solution conditions are shown in figures 1 to 4 inclusive. Initial rates were fairly rapid but equilibrium was only achieved after several days contact, and possibly particle diffusion may be rate controlling. In going from pH 1.0 to 2.0, the hydrolysis of Pu(IV) produces species with less positive charge[2], which could account for the observed decrease in uptake kinetics (figures 1 and 2). There should also be a decrease in competition for exchange sites by H^+ ions, which, in the case of MnO_2, appears to more than compensate for any change in charge of the Pu species present in solution.

Figure 1
Kinetics of Pu (iv) removal by inorganic ion exchange.

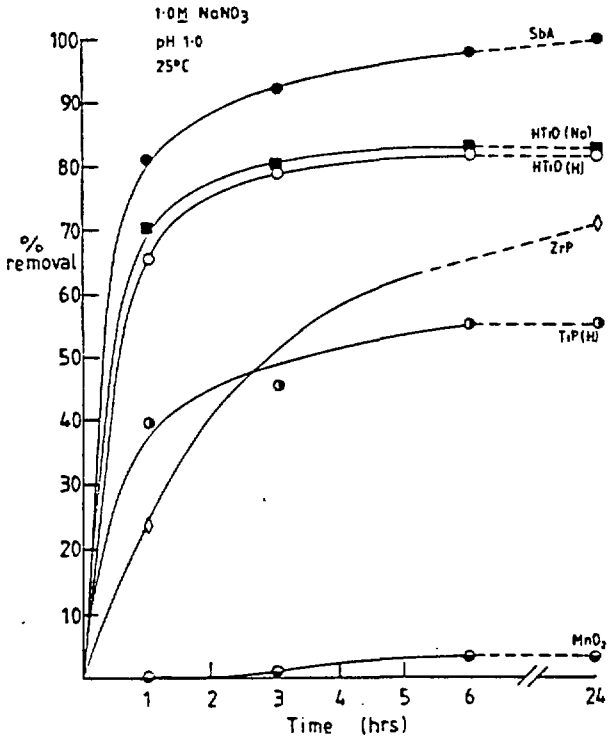

Figure 2
Kinetics of Pu (iv) removal by inorganic ion exchangers.

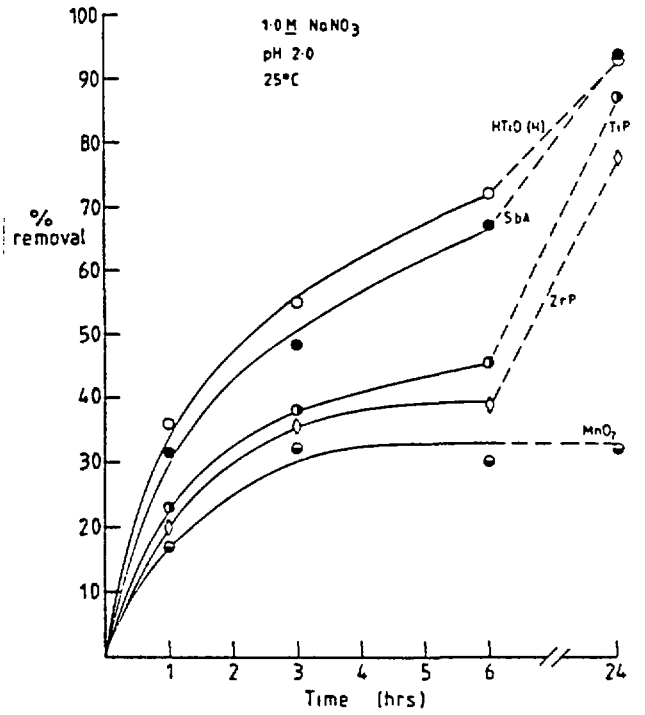

Figure 3
Kinetics of Pu(iv) uptake by SbA

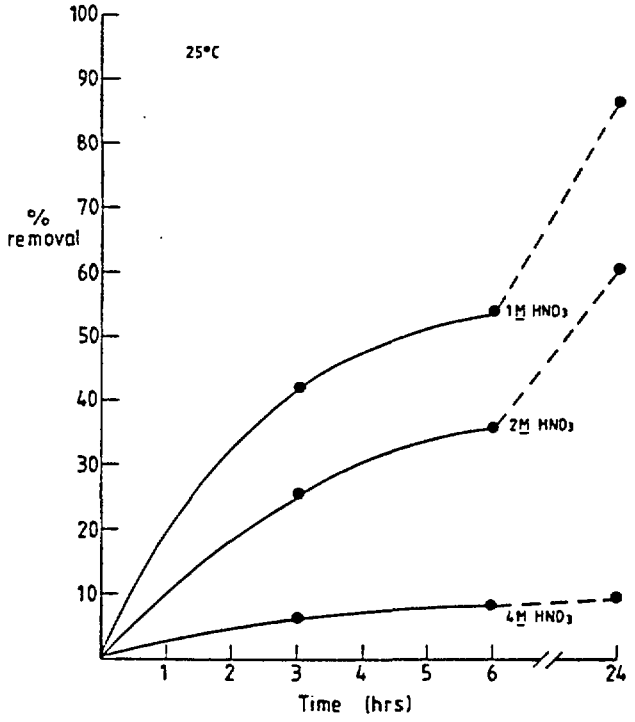

Figure 4
Kinetics of Pu (iv) removal by TiP

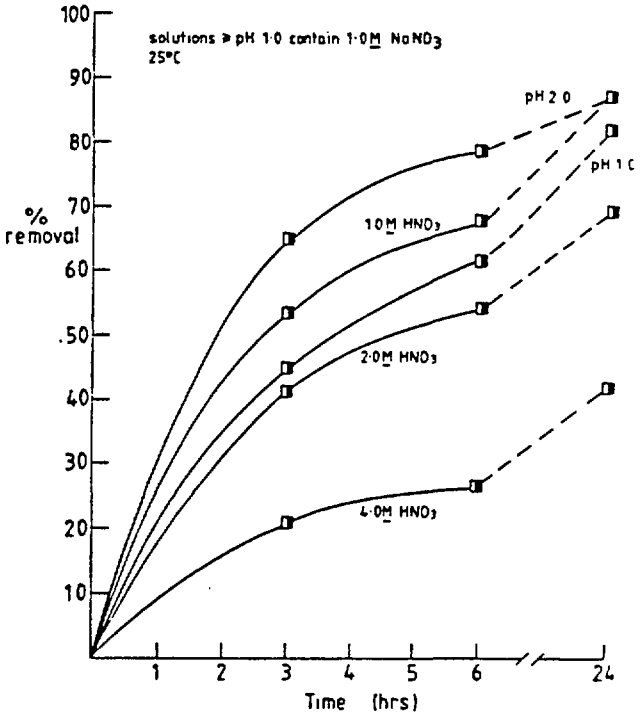

Figure 5 pH profile for Pu(IV) removal by SbA 25 μM Pu; 25°C

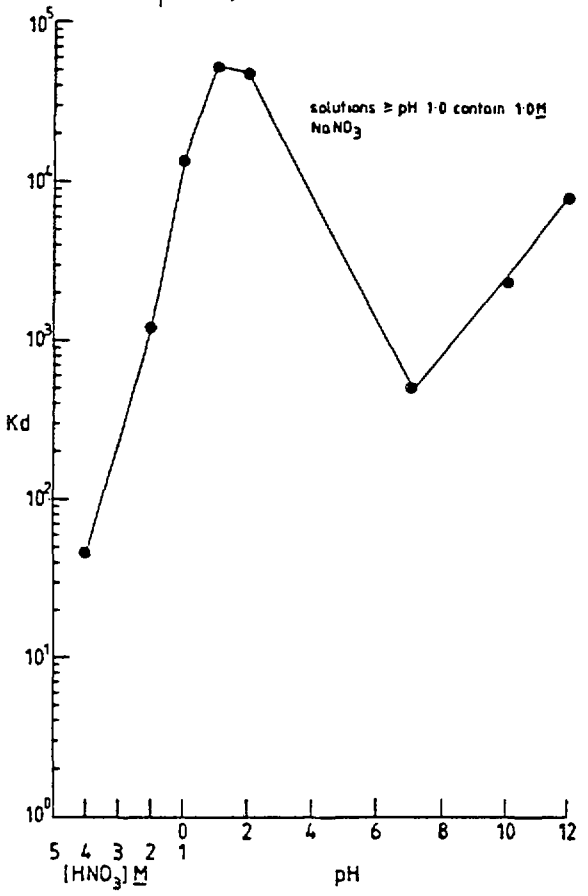

Figure 6 pH profile for Pu(IV) removal by inorganic ion exchangers. 25 μM Pu; 25°C

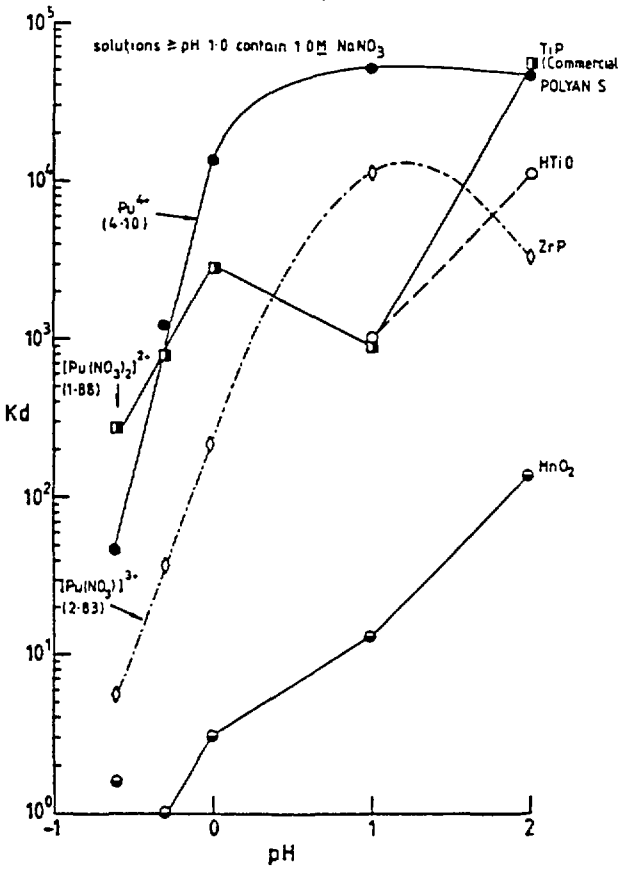

K_D values for Pu(IV) are listed in Table I. Plots of log K_D vs pH are shown in figures 5 and 6. Over the range of nitric acid concentrations from 4M to 1M the graph is expected to be a linear function of pH with a slope equal to the charge on the species being absorbed. The limited data in Fig. 6 suggest that Pu(IV) may be absorbed as Pu^{4+}, $[Pu(NO_3)]^{3+}$ and $[Pu(NO)_3)_2]^{2+}$ from acid media by different absorbers. With the exception of ZrP, Na^+ ions have little effect on the uptake of Pu. Above pH 1 colloidal Pu interferes with absorption, both ZrP and SbA producing a maximum in the K_D value at pH ~ 1. This inflection point can be calculated from the expression for the solubility product[2]:

$$K_{sp} = [Pu^{4+}] [OH^-]^4$$

$$K_{sp} = 7 \times 10^{-56}, [Pu^{4+}] = 2.8 \times 10^{-6} \text{ M}$$

hence, the pH at which the $[OH^-]$ is sufficient to reach K_{sp} is approximately 1.35.

TABLE I

K_D values for Pu(IV)

Acidity/ pH	ABSORBERS				
	CSbA	ZrP	MnO_2	TiP	HTiO
4 M	4.660×10^1	5.720×10^0	1.610×10^0	2.740×10^2	n.m.
2 M	1.220×10^3	3.830×10^1	1.000×10^0	7.720×10^2	n.m.
1 M	1.340×10^4	2.160×10^2	3.100×10^0	2.890×10^3	n.m.
pH 1	5.160×10^4	1.150×10^4	1.300×10^1	8.970×10^2	1.020×10^3
pH 2	4.740×10^4	3.420×10^3	1.400×10^2	5.620×10^4	1.160×10^4
pH 7	5.130×10^2	n.m.	n.m.	n.m.	n.m.
pH 10	2.370×10^3	n.m.	n.m.	n.m.	n.m.
pH 12	7.890×10^3	n.m.	n.m.	n.m.	n.m.

All solutions with pH > 1.0 contained 1.0 M $NaNO_3$

n.m. = not measured

25°C

The increase in K_D with increasing pH observed for TiP, HTiO and MnO_2 can be interpreted as being due to the decrease in competition by H^+ which out-weighs the effects of colloid formation.

3.2 Americium Absorption

The exchange kinetics for Am(III) are shown in figures 7 to 9 inclusive. Exchange is fairly rapid for solution with pH > 1 and shows a dependence on solution pH. These data can be interpreted in terms of the formation of hydrolysis products of Am[3]. Decrease in competition by H^+ for exchange sites account for rate increases whereas rate decreases are attributed to the formation of hydrolysis products of Am with reduced or zero charge.

K_D values for Am(III) are listed in Table II. The variation in $\log_{10} K_D$ for Am(III) with solution pH is shown in figures 10 and 11. The general trend is for K_D to increase with solution pH, due to reduced competition by H^+. There is little

Figure 7

Kinetics of Am removal by POLYAN S

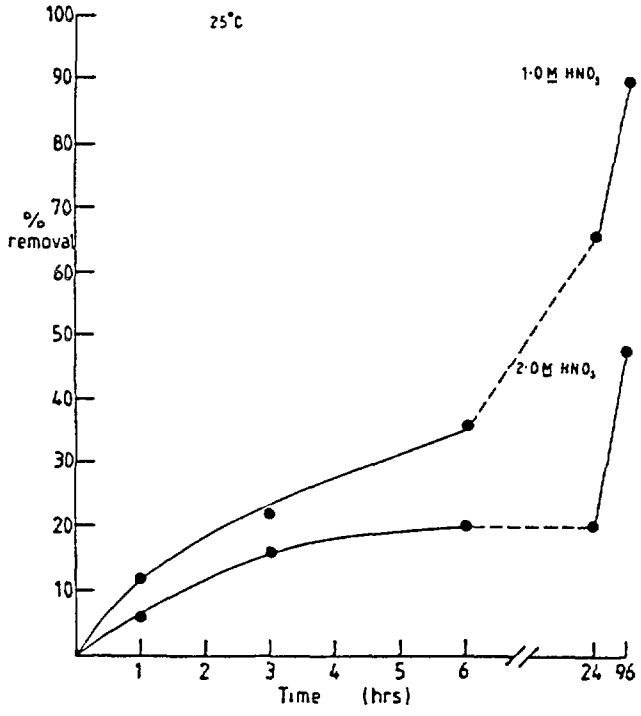

Figure 8

Kinetics of Am (III) removal by inorganic ion exchangers.

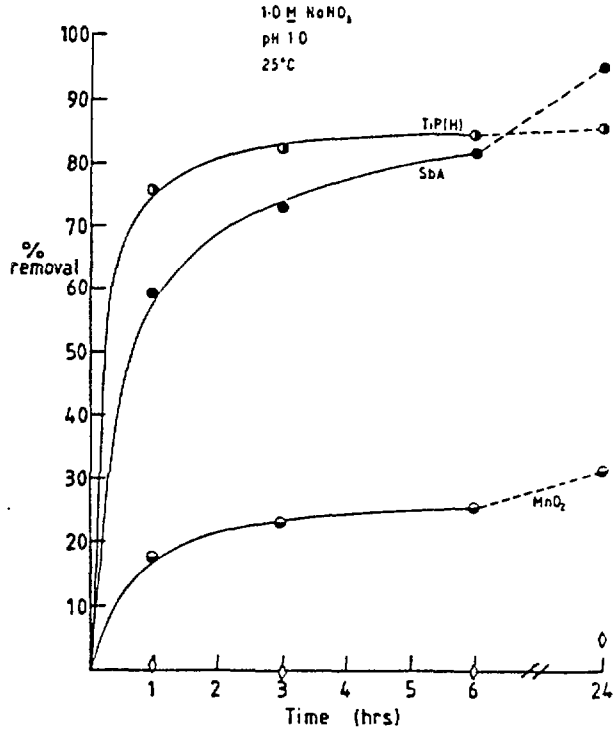

Figure 9

Kinetics of Am(III) removal by inorganic ion exchangers

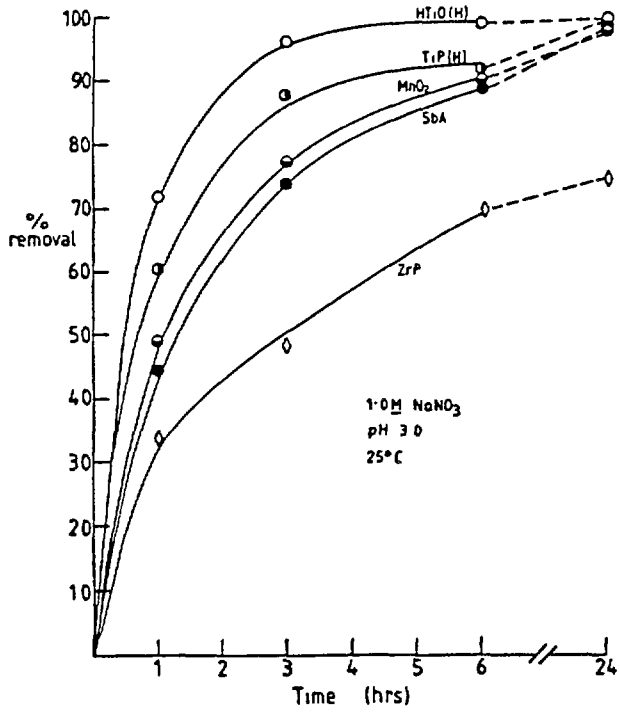

TABLE II

K_D values for Am(III)

Acidity/ pH	ABSORBERS				
	Polyan S	ZrP	MnO_2	TiP	HTiO
4 M	2.320×10^1	8.930×10^0	1.180×10^1	1.010×10^1	n.m.
2 M	1.370×10^2	2.170×10^1	1.150×10^1	1.780×10^{-1}	n.m.
1 M	2.800×10^3	2.710×10^1	7.900×10^0	1.060×10^1	n.m.
pH 1	5.590×10^3	2.360×10^1	4.400×10^1	7.900×10^1	2.150×10^1
pH 3	2.720×10^5	1.910×10^3	6.130×10^4	2.230×10^4	1.470×10^5
pH 8.8	9.280×10^4	n.m.	n.m.	n.m.	n.m.
pH 10	1.430×10^5	n.m.	n.m.	n.m.	n.m.
pH 12	1.330×10^4	n.m.	n.m.	n.m.	n.m.

All solutions with pH > 1.0 contained 1.0 M $NaNO_3$

n.m. = not measured

25°C

Figure 10 pH profile for Am(III) removal by inorganic ion exchangers. 0.76 μM Am; 25°C

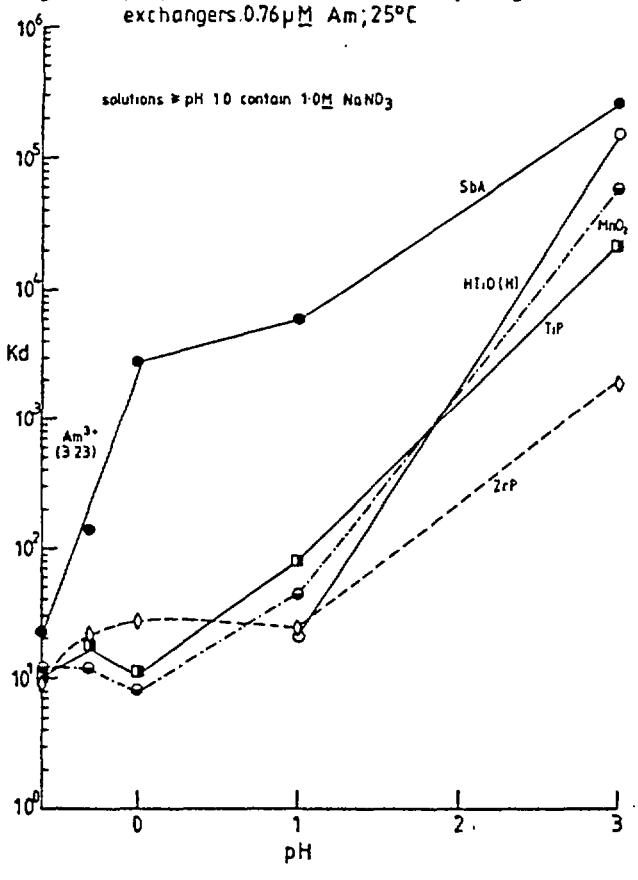

Figure 11 . pH profile for Am(III) removal by POLYAN S and HTiO 0.76 μM Am; 25°C

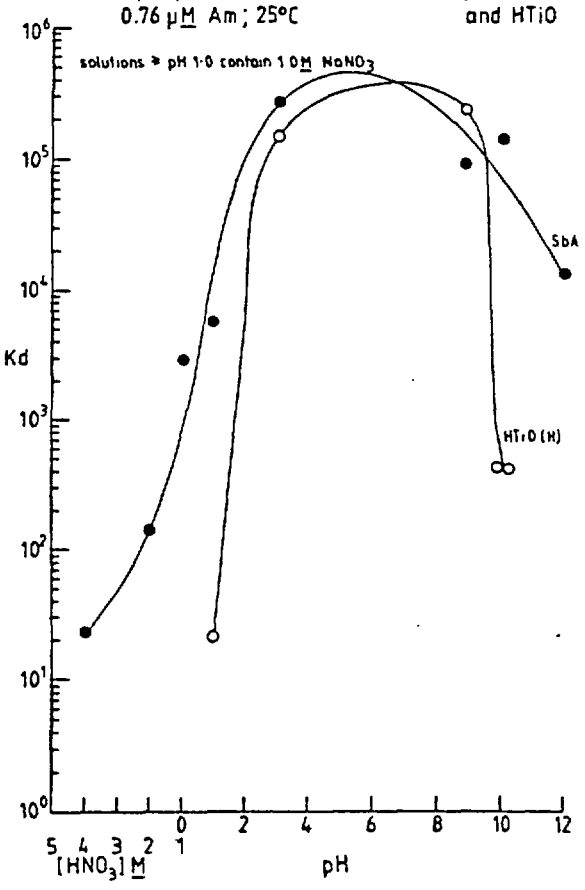

interference from competing Na^+ ions for solution pH up to 3-4 but figure 11 shows a decrease in Am absorption above pH 6 which may be due to Am hydrolysis or increased Na^+ absorption.

The slope of the graph for SbA over the HNO_3 concentration range 4M to 1M (figure 10) is about 3.2, which corresponds to the uptake of a tripositive Am species.

3.3 Neptunium Absorption

Np(V) is the most stable oxidation state of neptunium and it is usually present in solution at NpO_2^+ but disproportionates at high acid concentrations[4].

$$2\ NpO_2^+ + 4H^+ \rightleftharpoons Np^{4+} + NpO_2^{2+}$$

The exchange kinetics of Np(V) (0.42 mM in 1M $NaNO_3$) on various exchangers are shown in figures 12 and 13. Rates increase with increase in pH, which is interpreted as being due to decreasing competition from H^+. In general, uptake is slow, presumably due to the absorbed species having a relatively large radius and bearing only a single positive charge; particle diffusion is probably rate determining.

Figure 12
Kinetics of Np(v) removal by inorganic ion exchangers.

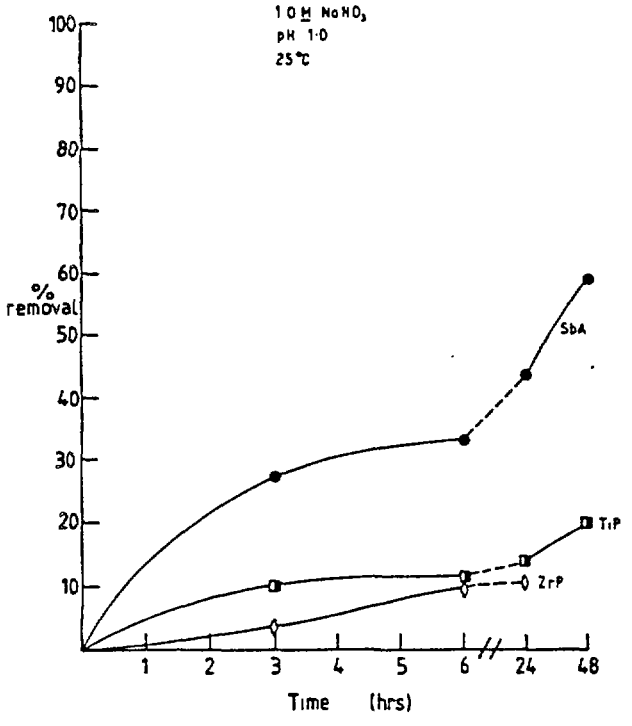

Figure 13
Kinetics of Np (v) removal by inorganic ion exchangers.

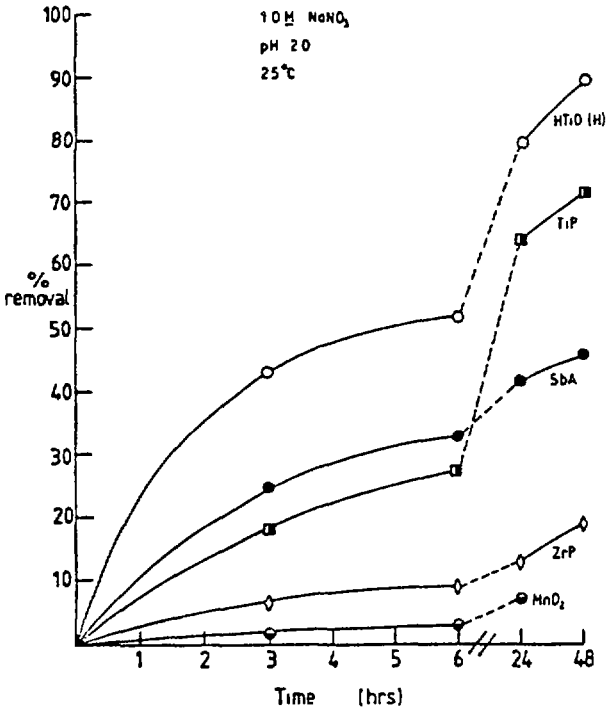

Measured K_D values for Np(V) in acid and 1.0 M $NaNO_3$ solutions are listed in Table III. The variation of K_D for Np(V) with solution pH is shown in figure 14. It should be noted that solutions with pH > 1 are 1.0 M in $NaNO_3$. Above pH = 0 there is a general increase in K_D with increase in solution pH because of decreasing competition for exchange sites by H^+. Below pH = 0, the disproportionation of NpO_2^+ to species with higher charge produces an increase in K_D. The net effect is a minima in the K_D-pH curve.

TABLE III

K_D values for Np(V) as NpO_2^+

Acidity/ pH	ABSORBERS				
	CSbA	ZrP	MnO_2	TiP	HTiO
4 M	4.380×10^1	1.530×10^1	1.110×10^1	7.060×10^0	n.m.
2 M	1.980×10^1	1.030×10^1	6.850×10^0	4.700×10^0	n.m.
1 M	2.920×10^1	1.170×10^1	7.800×10^{-1}	~ 0	n.m.
pH 1	1.540×10^2	8.450×10^0	1.130×10^1	5.470×10^1	5.940×10^0
pH 2	1.800×10^2	5.065×10^1	1.740×10^1	5.310×10^2	1.980×10^3

All solutions with pH > 1.0 contained 1.0 M $NaNO_3$

n.m. = not measured

25°C

Figure 14 . pH profile for Np (v) removal by inorganic ion exchangers

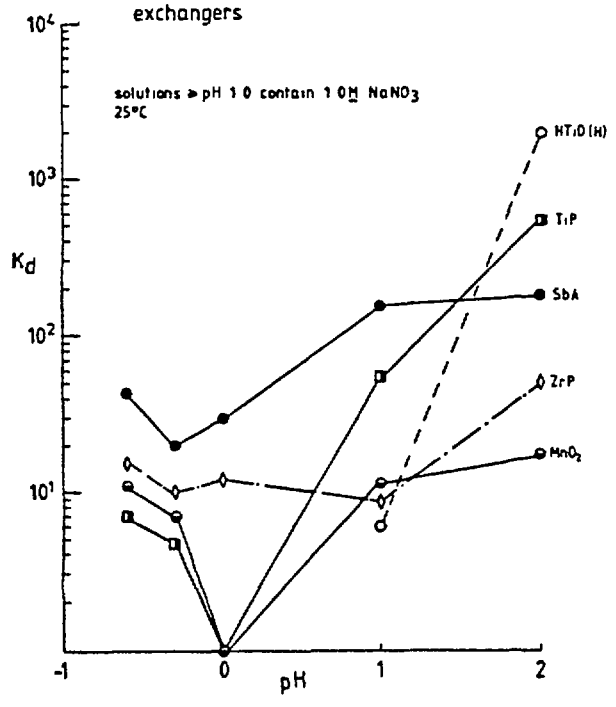

3.4 Total α Absorption

Figure 15 illustrates the extent of α-activity removal by different absorbers from solutions of irradiated fuel dissolved in nitric acid and then adjusted to various pH values. The experimental data on which these graphs are based is listed in Table IV.

Figure 15

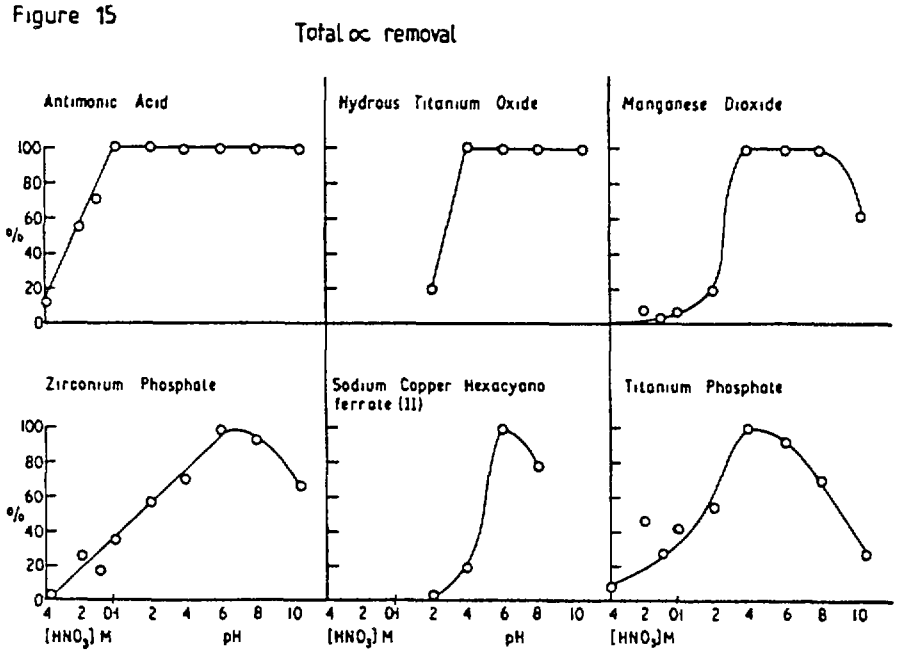

TABLE IV

α - emitters Removal

Percentage Recovery

pH / molarity	Time (hrs)	Manganese Dioxide	Antimonic Acid	Zirconum Phosphate	Titanium Phosphate	Copper Hexacyano ferrate(II)	Hydrous Titanium Oxide
4 M	49.33	0	12.36	0	6.43	/	/
2 M	47.50	7.51	54.45	25.95	45.42	/	/
1 M	47.75	1.83	70.17	16.09	26.56	/	/
0.1 M	91.08	6.23	99.10	35.08	40.85	/	/
pH 2	90.00	18.82	99.21	55.90	53.64	3.56	18.91
pH 3.8	48.83	99.00	97.75	69.53	99.61	18.86	/
pH 6	89.50	99.61	99.80	98.18	90.44	98.08	98.84
pH 8	92.42	99.74	98.32	92.54	68.39	77.69	98.06
pH 10 -11	1.50	61.26	98.37	65.80	26.54	/	98.13

It is apparent from figure 15 that SbA is a very effective absorber for α-emitters over a wide range of solution H^+ concentration. HTiO and MnO_2 also exhibit a strong affinity for actinides at solution pH values between4-10 and 4-8 respectively.

ZrP, TiP and Copper Hexacyanoferrate show good affinity for α-emitters at solution pH of 5-6 but the absorption of actinides falls off rapidly at higher or lower pH values.

3.5 The Effect of Interfering Ions

Some waste streams contain inactive salts of elements such as Fe^{3+}, Al^{3+} and Mg^{2+} which arise from magnox or stainless steel cladding treatments or are introduced as process reagents such as ferrous sulphamate for Pu reduction or Al^{3+} for complexing F^- ions. These ions may be present at high concentrations and could seriously interfere with the absorption of radionculides by ion exchangers.

Exchange kinetics for the uptake of Pu(IV) from 1.0M $NaNO_3$ solutions containing 0.28 g L^{-1} Al^{3+}, 40 g L^{-1} Mg^{2+} or 7 g L^{-1} Fe^{3+} are shown in Figures 16, 17 and 18 respectively. With the

Figure 16
Kinetics of Pu(iv) removal by inorganic ion exchangers

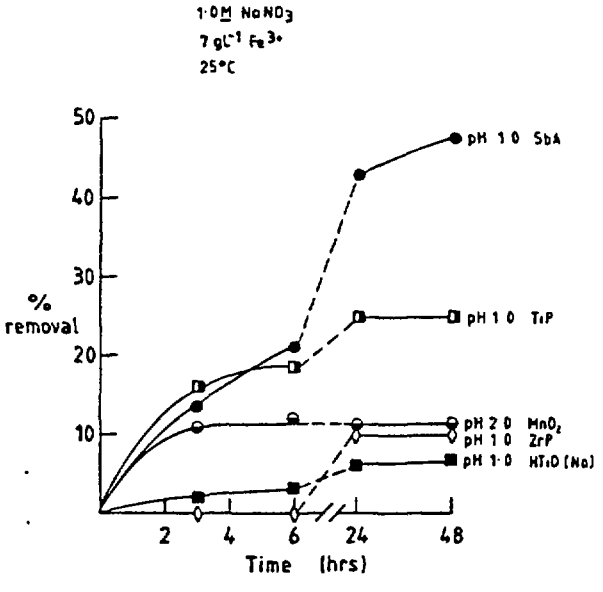

Figure 17
Kinetics of Pu (iv) removal by inorganic ion exchangers.

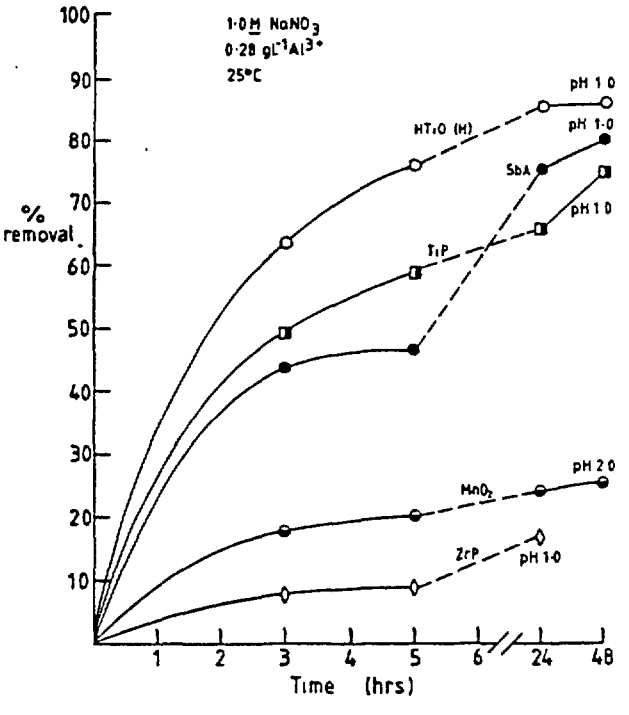

Figure 18
Kinetics of Pu (iv) removal by inorganic ion exchangers.

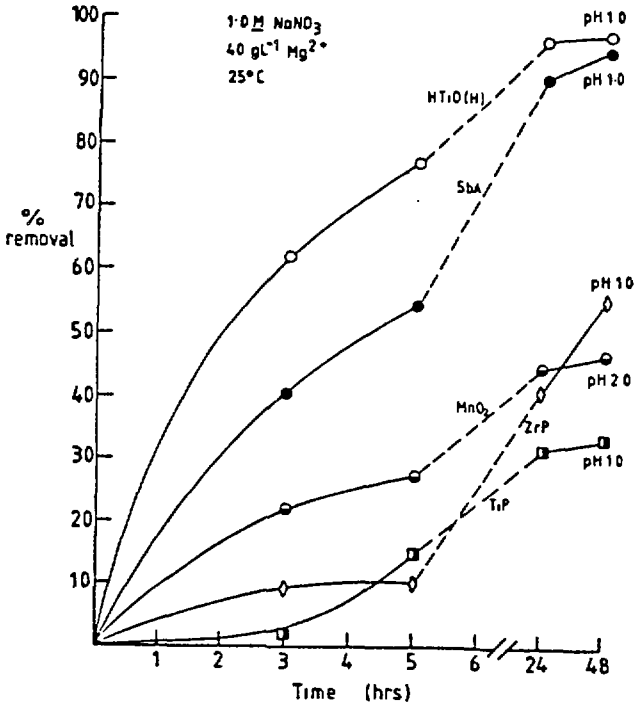

exception of MnO_2 (pH 2.0), solution pH had been adjusted to 1.0. It should be noted that degradation of HTiO interfered with kinetic measurements and therefore these results are not completely reliable because of change in absorber particle size during the experiment.

The presence of Fe^{3+} markedly reduces the rate of absorption and the effective capacity of the absorber for Pu. The effect of Al^{3+} at much lower concentration than in the experiments with Fe^{3+}, is to lower the absorption rate and the effective capacity to some extent. When Mg^{+} is present at 40 g/L (1.66M) the rate of absorption is reduced but generally there is little effect on absorber capacity for Pu.

Pu K_D measurements in the presence of Fe^{2+}, Fe^{3+}, Al^{3+} and Mg^{2+} are listed in Table V. Because of the reduction of Pu(IV) by Fe^{2+}, Pu K_D measurements are for the Pu(III) oxidation state. Fe^{2+} has very little effect on Pu uptake, presumably because of its lower charge, which suggests that Pu decontamination of Fe^{3+} bearing waste streams may be improved by pretreatment with a reducing agent.

TABLE V

K_D values for Pu(IV) - (interfering ions)

Ion	pH	ABSORBERS				
		Polyan S	ZrP	MnO_2	TiP	HTiO
Fe^{3+}	0	8.330×10^2	3.750×10^1	1.730×10^1	6.410×10^1	n.m.
	1	1.580×10^3	3.490×10^1	2.460×10^1	1.765×10^2	3.290×10^1
	2	1.990×10^3	3.100×10^1	3.130×10^1	1.030×10^2	1.440×10^3
* Fe^{2+}	2	4.300×10^4	1.953×10^3	~ 0	2.352×10^3	1.853×10^4
Al^{3+}	0	1.465×10^4	1.950×10^2	1.690×10^1	5.430×10^2	n.m.
	1	5.230×10^3	4.970×10^2	8.900×10^0	8.455×10^2	9.130×10^1
	2	9.930×10^4	4.420×10^2	1.070×10^2	4.130×10^2	1.500×10^3
Mg^{2+}	0	6.240×10^2	6.970×10^1	2.760×10^1	1.200×10^3	n.m.
	1	6.280×10^3	5.580×10^2	1.840×10^1	2.080×10^3	2.910×10^4
	2	1.940×10^4	1.230×10^3	1.380×10^3	4.570×10^2	1.590×10^3

[Fe] = 7 gL^{-1}
[Al] = 0.28 gL^{-1}
[Mg] = 40 gL^{-1}

All solutions with pH > 1.0 contained 1.0 M $NaNO_3$
n.m. = not measured
25°C
* Pu as Pu(III)

Am(III) exchange kinetics at pH 3 from solutions containing either Al^{3+} (0.28 g L^{-1}), or Mg^{2+} (40 g L^{-1}) are shown in figures 19 and 20 respectively. Experiments with Fe^{3+} were carried out at pH 2.0, in order to prevent the formation of $Fe(OH)_3$; Fe^{3+} completely interfered with the uptake of Am and therefore no results can be shown.

There is a decrease in the uptake kinetics on all exchange materials, ZrP and TiP being the most affected.

K_D values for Am(III) in the presence of the interfering ions Fe^{3+}, Fe^{2+}, Al^{3+} and Mg^{2+} are listed in Table VI. Whereas Fe^{3+} is absorbed in preference to Am^{3+}, Fe^{2+} is not. It should be

Figure 19

Kinetics of Am (III) removal by inorganic ion exchangers

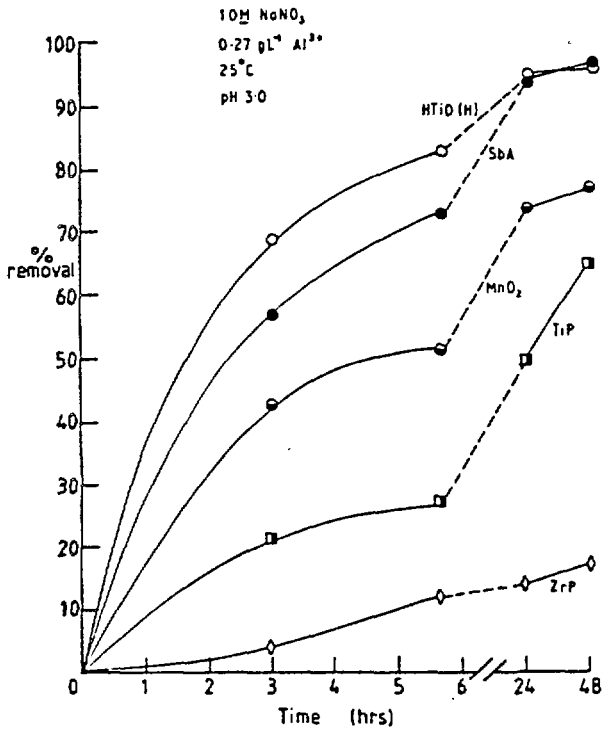

Figure 20

Kinetics of Am(III) removal by inorganic ion exchanger

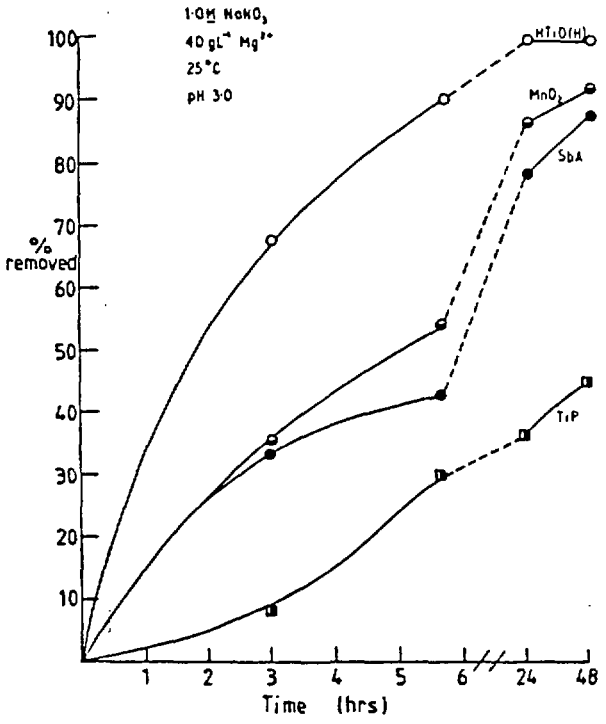

TABLE VI

K_D values for Am(III) - (interfering ions)

Ion	pH	ABSORBERS				
		Polyan S	ZrP	MnO_2	TiP	HTiO
Fe^{3+}	0	2.170×10^{1}	5.580×10^{0}	~ 0	~ 0	n.m.
	1	1.460×10^{1}	~ 0	~ 0	~ 0	1.400×10^{0}
	2	~ 0	~ 0	~ 0	~ 0	~ 0
Fe^{2+}	2	3.426×10^{2}	2.350×10^{1}	~ 0	3.970×10^{1}	4.810×10^{1}
Al^{3+}	0	2.100×10^{3}	8.450×10^{0}	2.000×10^{1}	6.810×10^{0}	n.m.
	1	1.570×10^{3}	5.050×10^{1}	5.480×10^{1}	6.700×10^{1}	5.470×10^{1}
	3	6.200×10^{4}	5.750×10^{1}	3.100×10^{3}	1.110×10^{3}	7.070×10^{3}
Mg^{2+}	0	3.780×10^{1}	1.960×10^{1}	1.490×10^{1}	~ 0	n.m.
	1	9.720×10^{2}	6.140×10^{0}	7.520×10^{1}	3.780×10^{1}	1.020×10^{3}
	3	5.180×10^{3}	3.380×10^{1}	1.380×10^{5}	2.400×10^{2}	2.940×10^{5}

All solutions with pH > 1.0 contained 1.0 M $NaNO_3$

n.m. = not measured

25°C

[Fe] = 7 gL^{-1}

[Al] = 0.28 gL^{-1}

[Mg] = 40 gL^{-1}

noted, however, that the solution pH at which these Fe measurements were carried out, was not optimum for Am^{3+} uptake. In contrast to this, Al^{3+} and Mg^{2+} have very little effect on Am removal over the solution pH range 0-1 but as the pH is increased above 1, the effect of Al and Mg on K_D for Am is different for different absorbers. Mg^{2+} has little effect on the Am K_D values for MnO_2 and HTiO and may enhance them slightly.

K_D measurements for Np(V) uptake from solutions containing Fe^{3+} (7 gL^{-1}), Al^{3+} (9.28 g L^{-1}) or Mg^{2+} (40 g L^{-1}) are listed in Table VII. The presence of these ions in the waste simulates reduces the value of K_D for Np(V) because of competition for exchange sites. The affinity of these exchangers for NpO_2^+ is greater than that for Na^+ since, due to its larger ionic size, its hydration sphere is held less firmly than that of Na^+ and hence its coordination H_2O molecules are displaced more readily.

TABLE VII

K_D values for Np(V) as NpO_2^+ - (interfering ions)

Ion	pH	ABSORBERS				
		CSbA	ZrP	MnO_2	TiP	HTiO
Fe^{3+}	0	~ 0	~ 0	~ 0	~ 0	n.m.
	1	4.850×10^{1}	4.320×10^{0}	8.940×10^{0}	2.970×10^{0}	1.02×10^{0}
	2	4.070×10^{1}	~ 0	1.680×10^{1}	~ 0	2.270×10^{1}
Al^{3+}	0	2.980×10^{1}	9.640×10^{0}	1.990×10^{1}	7.400×10^{0}	n.m.
	1	1.120×10^{2}	8.130×10^{0}	4.820×10^{0}	6.060×10^{1}	7.500×10^{0}
	2	1.730×10^{2}	1.250×10^{1}	1.340×10^{0}	1.170×10^{2}	6.180×10^{2}
Mg^{2+}	0	2.210×10^{1}	1.900×10^{1}	7.820×10^{0}	1.460×10^{1}	n.m.
	1	2.350×10^{2}	4.990×10^{1}	3.370×10^{1}	5.430×10^{2}	3.330×10^{3}
	2	1.640×10^{2}	1.180×10^{1}	2.860×10^{1}	1.400×10^{2}	8.670×10^{1}

[Fe] = 7 gL^{-1}

[Al] = 0.28 gL^{-1}

[Mg] = 40 $gl^{-}L$

All solutions with pH > 1.0 contained 1.0 M $NaNO_3$

n.m. = not measured

25°C

With exception of MnO_2, the extent of competition at pH1 (and in 1.0 M $NaNO_3$) decreases in the sequence

$$Fe^{3+} > Al^{3+} > Mg^{2+}$$

at the concentrations examined.

These data may be rationalized in terms of the ionic charges and radii of the competing ions. The smaller charge on Mg^{2+} compared with that for both Fe^{3+} and Al^{3+} is reflected in its smallest interfering effect. Fe^{3+} and Al^{3+} possess ionic radii of 0.64 and 0.51Å respectively, and as such, the hydration sphere around Al^{3+} is more firmly bound than that for Fe^{3+}. It is therefore easier for Fe^{3+} to lose its water molecules and enter the ion exchange structure.

4. Summary

The experimental data collected so far in this study of exchangers is showing that there are several inorganic ion exchangers that can provide high distribution coefficients for actinide ions. In general, the value of K_D is greater for Pu(IV) than for Am(III) and is lowest for Np(V). This behaviour might be expected because of the different charges on the actinide ions i.e. Pu^{4+}, Am^{3+} and NpO_2^+. The presence of di- and tri- valent metal ions, such as Fe^{3+}, Al^{3+} and Mg^{2+} in the solution, reduces the value of K_D for the actinides because of competition for exchange sites.

The performance of these selected absorbers under flow conditions is now being examined together with a study of recovery of absorbed radionuclides by elution and absorber recycle.

5. Acknowledgments

The experimental data presented in this paper was obtained by B.A. Phillips, S.P. Dagnall and N.P. Monckton of Separation Processes Group, Chemical Technology Division, AERE, Harwell. Their help in the preparation of this paper is also gratefully acknowledged.

This work was commissioned by the UK Department of the Environment as part of its radioactive waste management research programme. The results will be used in the formulation of Government policy but at this stage they do not necessarily represent Government policy.

References

[1] Hooper, E.W.; Phillips, B.A; Dagnall, S.P; Monckton, N.P. DoE Report No DoE/RW/83.171, Harwell Report No. AERE-R11088

[2] Coleman, G.H. The Radiochemistry of Plutonium, Atomic Energy Commission.

[3] Schulz, W.W., The Chemistry of Americium, Technical Information Center, ERDA(1976).

[4] Burney, G.A; Harbour, R.H., Radiochemistry of Neptunium. NAS-NS-3060, U.S.A.E.C. Washington (1974).

SEPARATION AND PURIFICATION OF FISSION PRODUCTS FROM PROCESS STREAMS OF IRRADIATED NUCLEAR FUEL

S.A. ALI, H.J. ACHE
Institut für Radiochemie,
Kernforschungszentrum Karlsruhe,
Karlsruhe, Federal Republic of Germany

Abstract

New results are presented of studies of the application of inorganic exchangers in the following fields:

- Concentration and removal of fission product molybdenum from solutions of irradiated, short-cooled fuel element targets by attachment to water-containing metal oxides and subsequent thermal desorption of MoO_3 from the stationary phase. The volatilization yields were clearly improved by the addition of water vapor to the mobile gas phase.

- Chromatographic removal of cesium from the aqueous medium-active waste streams of nuclear fuel reprocessing plants on ammonium molybdatophosphate, ammonium hexacyanocobalt ferrate and zirconium phosphate. In this case, stationary phases of ammonium molybdatophosphate were found to be by far the most efficient exchangers among those studied.

Inorganic exchangers, because of their stability against oxidizing and reducing media and their resistance to radiation, have found extensive application in radiochemical separation techniques and as stationary phases in the radionuclide generators used worldwide, especially in nuclear medicine [1]. Another interesting application has been indicated by more recent studies of cesium removal from the concentrates of medium-level waste and directly from the cesium-bearing partial streams acidified with nitric acid, respectively, in nuclear fuel reprocessing plants. Cesium removal from these solutions would clearly reduce the required additional thicknesses of so-called "lost concrete shields" and thus generate considerable savings in the costs of final waste conditioning.

Metal oxides, because of their extensive use in generator applications, are among the best proven inorganic fission product adsorbers.

The generator used most frequently by far is the technetium-99m generator. Technetium, because of its low gamma energy of approx. 140 keV and its halflife of 6 hours, has optimal characteristics for organ functioning tests. The worldwide success of Tc-99m generators began only after suitable exchangers had been found for the parent nuclide, molybdenum-99, which is increasingly being isolated from short-cooled fuel element targets irradiated specifically for this purpose, because of the extremely high specific activities produced by this technique. The most successful stationary phase used in technetium generators has been acid aluminum oxide. It can immobilize molybdate anions with high retention coefficients from weakly acidified solutions, while the technetium passes through the column. Several development studies have been conducted in order to utilize the favorable properties of aluminum oxide in fission product molybdenum removal and concentration. The results achieved to date have led to inorganic exchanger columns having become established parts in most fission product molybdenum removal processes. Normally, molybdenum decontaminated to a high degree from solutions of low acidity is immobilized on Al_2O_3 columns and then eluted by ammonia after the completion of the washing processes [2]. In some production plants all organic impurities are removed in a time consuming process in which the molybdenum containing solution is evaporated to dryness and molybdenum is sublimed as molybdenum trioxide at 1000 °C. In these studies [3] it has been attempted for the first time to streamline the process by combining the immobilization of molybdenum to hydrated metal oxides and the subsequent direct sublimation of the molybdenum from the adsorber matrix. If this modification can be realized, it would clearly reduce the expenditures in terms of manpower and time of the respective production campaigns and would decrease the amount of radioactive waste solutions accumulating without entailing any losses of quality of the final product.

In order for the desired development to be applicable to full-scale production processes, volatilization should be feasible at the lowest possible temperatures. A major reduction in the sublimation temperature of molybdenum in volatilization from the exchanger matrix can be achieved by making use of the increased vapor pressure of molybdenum oxohydroxide, $MoO_2(OH)_2$; this is a gaseous compound observed in the pure MoO_3-water vapor system at temperatures around 650 °C [4].

In the first few experiments the steady-state exchanger behavior of molybdenum was studied in media acidified with nitric acid and containing the respective inorganic exchangers, Al_2O_3, SnO_2, MnO_2, and Sb_2O_5. Fig. 1 is a plot of the molybdenum retention

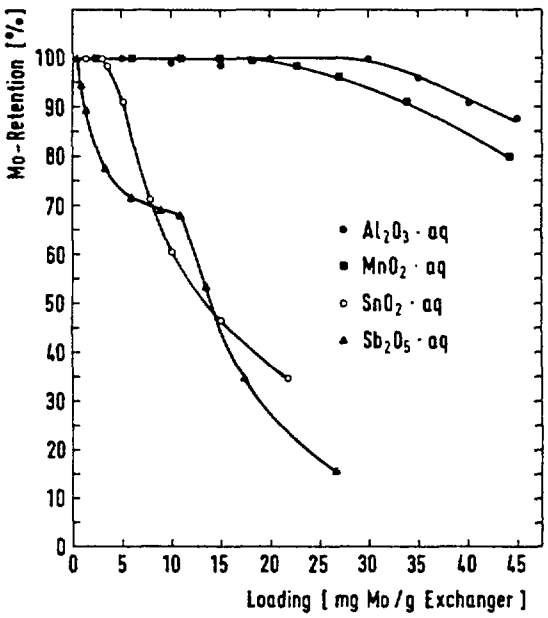

Figure 1: Retention of Mo [%] on the oxides vs. Mo-loading in 0.02 M HNO_3.

of water-bearing metal oxides in an 0.02 M HNO_3 medium as a function of feed loading. The feed load is the ratio of the amount of molybdenum in the solution to the amount fed into the exchanger. As the diagram shows, aluminum oxide at this pH has the highest retention coefficients with 30 mg of Mo/g of exchanger. The comparatively high retention of Al_2O_3 in this pH range can be explained by its high porosity. Exchanger experiments at higher concentrations of nitric acid produced mainly decreasing Mo retention capacities in all exchangers.

In view of the intended use under hot conditions numerous experiments were conducted in the exchanger systems mentioned above to define their kinetic and wear behavior. Aluminum oxide and tin dioxide exhibited the most advantageous preconditions. Antimony pentoxide, because of its slow exchange kinetics, and manganese dioxide, because of its pronounced wear sensitivity, were excluded from further study.

To optimize the retention of molybdenum, the influence of the pH on sorption to Al_2O_3 and SnO_2 was studied over a wide range at constant molybdenum feed loads (3 mg Mo/g of exchanger) and a molybdenum concentration of 2×10^{-3} mole/l. Fig. 2 is a plot of the amounts of molybdenum immobilized on the SnO_2 and Al_2O_3 exchangers, respectively, as a function of pH after 20 hours of contact time. Al_2O_3 acts as an anion exchanger already from a pH of 9 onward, completely immobilizing 3 mg of Mo/g of exchanger from a pH of 8.5 on. When the pH is reduced, complete retention is maintained up to pH 1, but afterwards

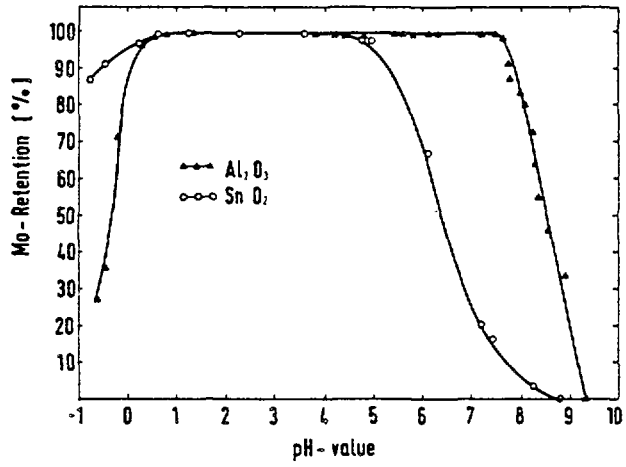

Figure 2: Retention of Mo [%] on the oxides vs. pH

there is a steep decline in capacity. SnO_2 shows a similar behavior in principle, but the entire curve is shifted more to the acid region. Above pH 8 it acts as an anion exchanger, and at pH 5 it achieves complete retention of molybdenum, which is maintained up to a pH of 0. This is followed by a slight decline much less pronounced, however, than in the case of Al_2O_3. The reason for the shift in the SnO_2 anion exchange towards lower pH levels is the lower basicity of the $-\overset{|}{\underset{|}{Sn}}O^-$-group compared with Al_2O_3. The electron density of oxygen is deformed strongly to the positive metal ion by the tetravalent oxidation level of tin, which binds more firmly the OH^--group to be exchanged and allows anion exchange to take place only at higher H^+-concentrations than in the case of Al_2O_3.

After optimization of the exchange conditions it was possible to start the volatilization experiments. It was important to elucidate the dependence of the MoO_3 desorption yield on the loading of the stationary phase; for this purpose, Al_2O_3 with different loads was predried at 100 °C and subsequently subjected to a 30-minute thermal treatment at temperatures up to 1200 °C.

Fig. 3 is a plot of the sublimed MoO_3 fraction over the exchanger loads. It indicates that, for high volatilization yields to be attained under these conditions, Al_2O_3 must be loaded with the molybdenum carrier almost to the limit of capacity (dashed line). At lower loads, the volatilization yields decline drastically to levels below 10%. This is one major disadvantage of Al_2O_3, for large quantities of inactive molybdenum carrier would entail low specific activities of the product.

Another reason for avoiding high loads is the marked decline in the exchange rate. Clear advantages

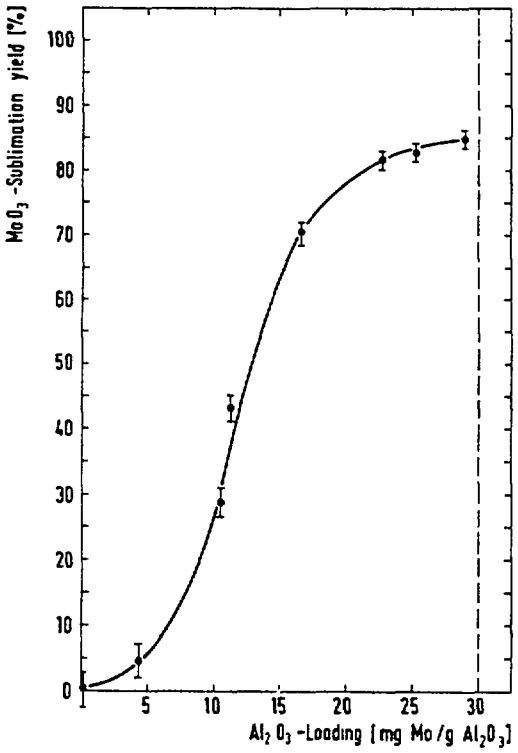

Figure 3: Yield of the sublimation of MoO_3 [%] vs. Mo-loading.
Temperature = 1200 °C.

in this respect were found in SnO_2. In a number of series of experiments the influence on molybdenum sublimation yields of volatilization temperatures, the duration of thermal treatment, and of water vapor in the mobile phase passing through the molybdenum-loaded adsorbers was studied.

Fig. 4 shows the comparable thermal molybdenum desorption yields from systems containing Al_2O_3 and SnO_2 in the presence of water vapor plotted vs. sublimation time. One characteristic of the development of sublimation in tin oxide is the steep initial rise in MoO_3 sublimation yields which then gradually declines with the decrease of MoO_3 on the exchanger surface. The reason is the drop of the concentration gradient, which is the prime mover. The much flatter rise in the sublimation yield in Al_2O_3, however, is indicative of volatilization being determined by the slow diffusion step through the pores in the surface.

In another program of specific technological orientation conducted within the framework of the Reprocessing and Waste Treatment Project, chromatographic techniques are developed mainly for the specific decontamination of individual medium-active waste streams arising in the reprocessing of nuclear fuels and in fuel element fabrication [5]. The underlying concept is based on the fact that these solutions contain largely similar chemical species of the

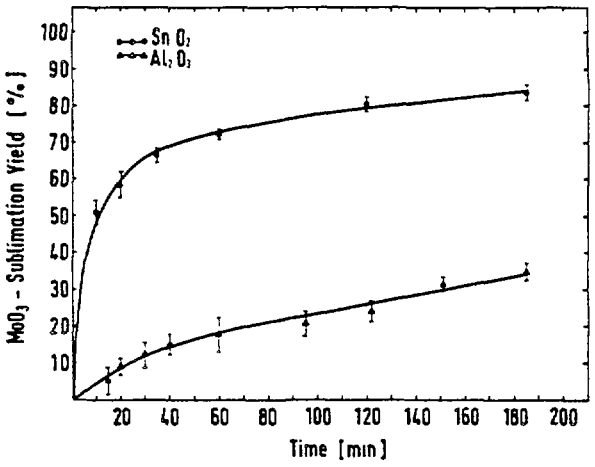

Figure 4: Yield of the sublimation of MoO_3 [%] vs. time of sublimation at a loading of 4 [mg Mo/g oxide].
Temperature of sublimation = 1050 °C in the presence of H_2O vapor.

carriers of activity. Their removal by a directly connected specific decontamination step would be much simpler and more effective than the procedure devised so far in which first nearly all aqueous process wastes consisting mainly of nitric acid and sodium carbonate solution are co-evaporated. Decontaminating the concentrate of the carriers of activity is to be achieved by cumbersome procedures comprising essentially a series of precipitation steps.

At the Institute of Radiochemistry (IRCH) modern, simple and effective decontamination procedures by extraction chromatography have been developed within the Reprocessing and Waste Treatment Project for such important partial process streams as the basic carbonate stream [6, 7], the solvent wash in reprocessing, and the oxalate bearing mother liquords of Pu oxalate precipitation in nuclear fuel fabrication.

The activities in this field are at present being concentrated on studies of cesium removal from the aqueous medium active solutions of nuclear fuel reprocessing plants. If this project were to be implemented, it would offer a possibility for removal of the longer-lived Cs-137 source of activity, which would entail clear savings in shielding costs of the waste after final treatment.

The process to be developed should permit rather wide variations in the composition of the solutions from which cesium is to be removed, thus obviating the need for additional expenditures to set optimum process conditions, such as the salinity and acidity of the solution. It is known from experience that the cesium distribution is limited to the process

streams acidified with nitric acid and enters the evaporator concentrate in this way; a powerful method therefore would have to be able under all conditions to allow high cesium decontamination levels to be achieved in nitrate-bearing solutions strongly acidified with nitric acid.

In steady-state and dynamic experiments the distribution and retention behavior, respectively, of cesium from aqueous solutions of various acidities and basicities, respectively, and various sodium nitrate contents on the inorganic exchangers ammonium molybdatophosphate (AMP-1) made by Bio-Rad and ammonium hexacyanocobalt ferrate (NCFC), hydrated antimony pentoxide (HAP), and zirconium phosphate (ZPH) made by the Carlo Erba company was studied [8]. The data determined so far underline the clear superiority of AMP-1 under almost all experimental conditions. Fig. 5 is a plot of the cesium retention percentage determined dynamically as a function of the loading of AMP-1 in systems of different pH levels.

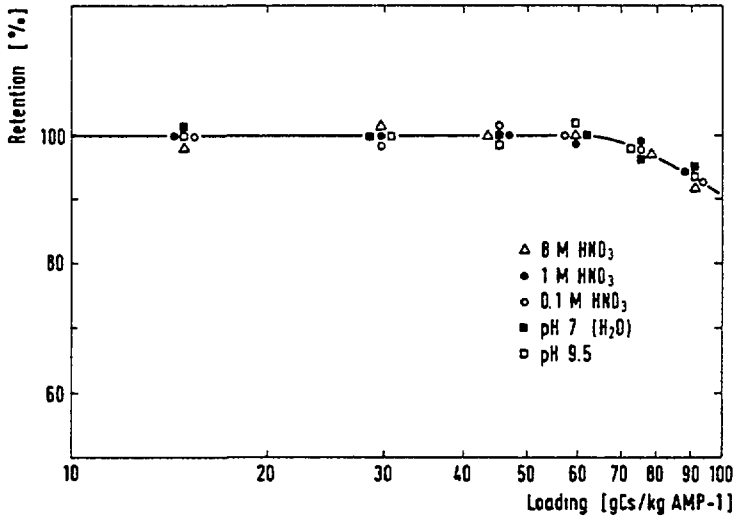

Figure 5: Retention of cesium on AMP-1 vs. loading for various H^+-concentrations.

The diagram shows that cesium is retained > 99% by AMP-1 in solutions ranging between higher HNO_3-concentrations and weakly basic solutions with a capacity of > 60 g/kg of exchanger. The uncommon versatility of this exchanger is demonstrated by the comparison below of data determined under steady-state conditions in systems whose stationary phases in each case were the NCFC and ZPH exchangers. Fig. 6 is a plot of the cesium retention percentage determined under dynamic conditions from aqueous phases of various acidity and basicity levels, respectively, on the ammonium hexacyanocobalt ferrate (NCFC) inorganic exchanger as a function of the loading of the solid phase.

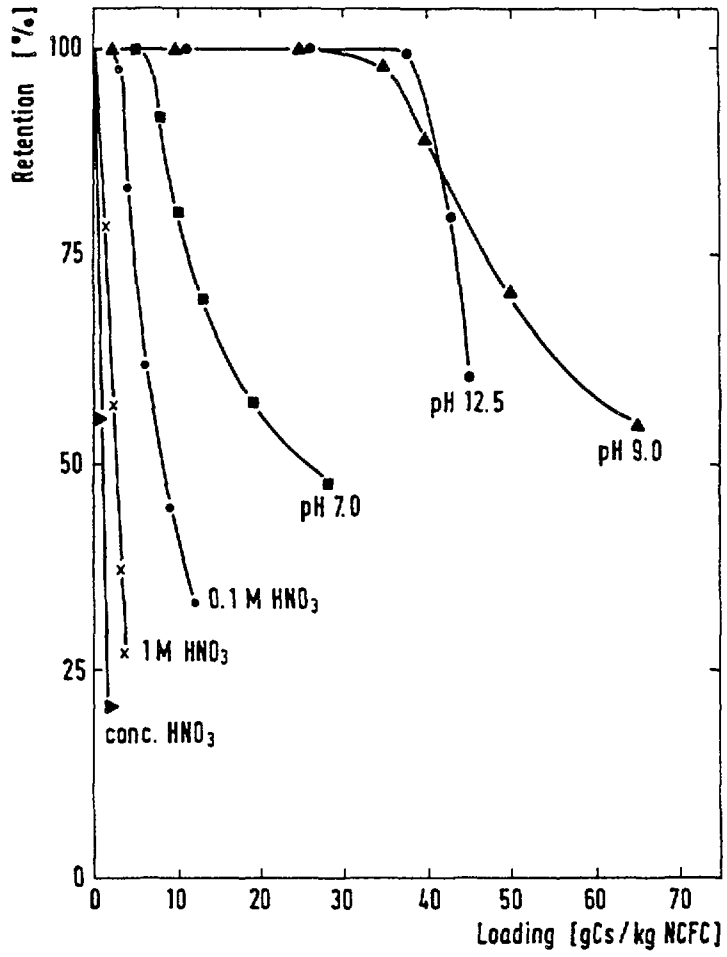

Figure 6: Retention of cesium on NCFC vs. loading for various H^+-concentrations.

The diagram shows the very low retention levels in acid media; even in neutral solutions the use of this exchanger cannot be recommended. Acceptable values can be achieved only above a pH of 9.

Comparable data take a clearly different turn if zirconium phosphate is used as the stationary phase (Fig. 7). In neutral systems zirconium phosphate is found to be particularly powerful. Under these conditions, approx. 100 g of cesium can be immobilized quantitatively on 1 kg of exchanger. However, the high retention decreases rapidly with increasing shifts both in the acid and in the basic directions; already at a pH of 1 only some 8 g of cesium/kg of exchanger can be retained. In basic systems the losses of capacity are also intolerably high. A comparison of the retention levels attainable in NCFC and ZPH systems with those of AMP-1 indicates the clear discrepancy in the range of applicability. It is possible with AMP-1 columns to retain cesium quantitatively from highly acidified, neutral and basic systems without any pH adjustment.

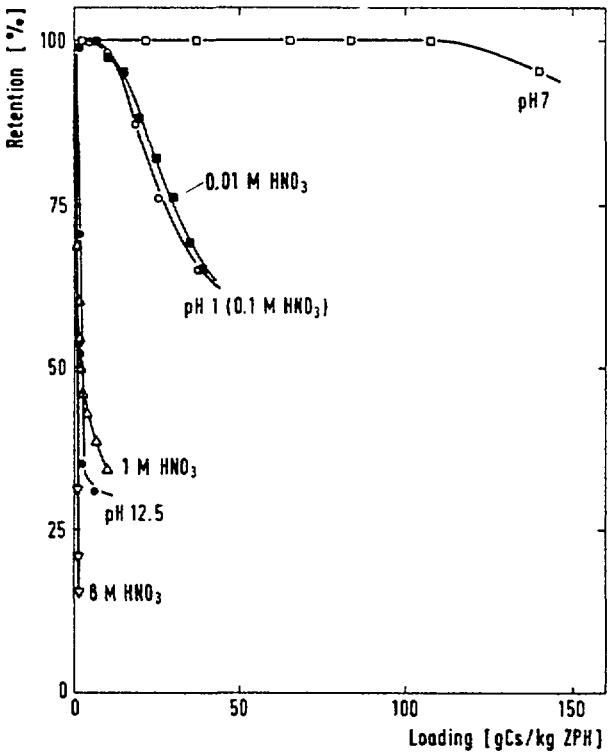

Figure 7: Retention of cesium on ZPH vs. loading for various H^+-concentrations.

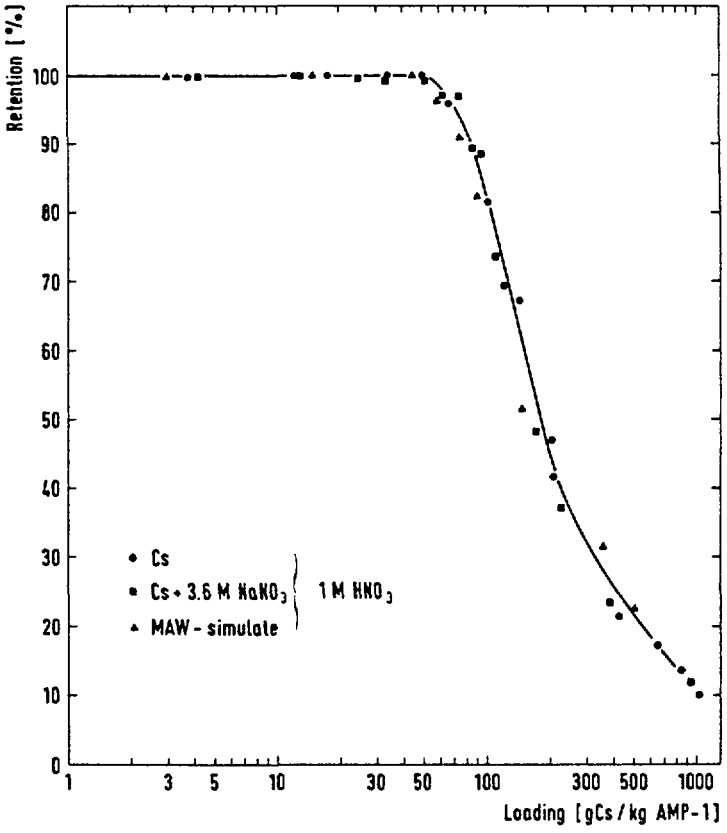

Figure 8: Retention of cesium on AMP-1 vs. loading in 1 M HNO_3 for Cs in (a) pure, (b) $NaNO_3$-contaminated, (c) simulated MLW solutions.

Another important criterion of the practical applicability of an exchanger is its behavior in the presence of higher nitrate concentrations, such as those which occur in an MLW concentrate.

Fig. 8 shows the cesium retention levels obtainable as a function of exchanger loading from 1 M HNO_3, 1 M HNO_3 + 3.6 M $NaNO_3$, and 1 M HNO_3 + MAW simulate. While hardly any negative effect could be observed in the AMP-1 system, the retention capacities of all the other exchangers broke down even under their most favorable exchange conditions.

References

[1] "Radioisotope Production and Quality Control", IAEA, Vienna (1971), Technical Report Series No. 128, pp 659-743

[2] Sameh A. Ali, H.J. Ache, Fourth Intern. Symposium on Radiopharmaceutical Chemistry (Abstracts), Jülich (1982) 168

[3] J. Bürck, Sameh A. Ali, H.J. Ache, KfK-3754 (1984)

[4] O. Glemser, R.V. Haeseler, Zeitschrift für anorganische und allgemeine Chemie, Band 316 (1962) 168-181

[5] W. Faubel, P.-M. Menzler, Sameh A. Ali, KfK-3617 (1984)

[6] J. Haag, Sameh A. Ali, KfK-3015 (1981)

[7] J. Haag KfK-3460 (1983)

[8] W. Faubel, P.-M. Menzler, Sameh A. Ali, KfK-3742 (1984)

EFFICACY OF ARGILLACEOUS MINERALS USED AS A MIGRATION BARRIER IN A GEOLOGICAL WASTE REPOSITORY

E.R. MERZ
Institute of Chemical Technology,
Kernforschungsanlage Jülich,
Jülich, Federal Republic of Germany

Abstract

The current strategy for isolating nuclear wastes in an underground geological repository relies on a series of multiple barriers to restrict the release of radionuclides to the biosphere. Waste form and canister as well as the backfill material used to fill the space between the waste canister and the host rock, provide engineered barriers, whereas the repository itself and the overlying geologic medium represent natural barriers.

A suitable backfill material, preferentially argillaceous minerals, exhibits the potential for providing a multifunctional role in the overall performance of the waste package, significantly retarding radionuclide migration via solution flow. The backfill barrier will serve both as a physical barrier, preventing convective solution flow and allowing radionuclide penetration only by diffusion, and as a chemical barrier capable of chemically interacting with the radionuclides via sorption, ion exchange or precipitation.

The paper presents measurements of the hydraulic properties and the diffusion and sorption abilities of various bentonites and clays. They include investigations dealing with the sorption and retardation behaviour of the two most important fission product radionuclides strontium and cesium. The K_d-values determined by batch distribution measurements show a strong dependence from the salt concentration in the solutions. Brine solutions bring about a displacement action upon sorbed ions. In highly compacted bentonites the transport of radionuclides through the backfill may be dominated by diffusion through the interstitial water. The rate of diffusion will thus depend on normal diffusion and on the sorption properties of the clay minerals.

Introduction

The general strategy in isolating nuclear waste is to impose a series of barriers between the radioactive material and the biosphere. The different barriers

considered are in their order of proximity to the biosphere:

- geological repository including overlying strata,
- backfill and sealing material in the repository,
- canister including overpack,
- waste form.

It is possible that either one of the first three barriers, if appropriately choosen, could by themselves provide the necessary isolation of wastes, irrespective of the quality of the waste form. Thus, the main function of the waste form would be to contain and safely isolate the radioactive materials during handling and transportation procedures until proper deposition in the geological repository. However, it is common understanding that the waste form should be made as chemical resistant as reasonable achievable to provide the maximum possible protection within an acceptable cost range.

In this contribution the attention is directed towards the usefulness and efficacy of backfill materials on the basis of argillaceous minerals. Emphasis is put only on salt evaporites as the geological host media since salt domes are the favorite choice for a high-level waste repository in the Federal Republic of Germany [1].

Function of backfill materials

Various backfill materials are considered to be used in a geological repository to fill the space between the waste canisters and the host rock. Suitable backfill materials may also be used to fill the mine drifts and shafts when the repository is sealed. Proper selection of backfill- and displacement materials, respectively, and methods of emplacement creates an additional barrier between the radioactive waste and the biosphere in case an aqueous solution is present as the transport medium in the repository.

A comprehensive review related to backfill performance of various materials has been prepared by WHEELWRIGHT et al [2]. Most promising materials are argillaceous minerals, preferably expanding clays like sodium or calcium bentonites.

The backfill has the potential for providing a multifunctional role in the overall performance of the waste package, significantly retarding or minimizing waste package degradation and subsequent radionculides release. The primary function is threefold:

- to retard or exclude the migration of ground water or salt brine between the host geology and the waste canister;

- to buffer the pH value and chemical composition of the aqueous solution and the canister surface in order to suppress corrosive attack;

- to retard the migration of selected chemical species from the waste matrix into the ground water after breaching of the canister has started.

In addition, supportive functions are the self-sealing of cracks in the backfill or interfacing host geology, the provision of resistance to applied mechanical forces and a good heat conductibility from the canister to the host rock system.

Experimental Information

The objective of the investigations was focused on two items:

- the hydraulic and
- the sorptive as well as migration retardation

properties of selected backfill materials.

Only expanding clays with a high content of bentonite and montmorillonite, respectively, have been considered as potential candidates, since they combine the two most important required properties, namely, of solution convection suppressing and ion sorption capabilities. They include natural as well as activated bentonites and different salt clays with high contents of alcaline or alcaline earth bentonites.

The ability of these materials to reduce significantly or to stop the flow of brine and ground water between the host rock and the waste canisters is of primary importance, because it inhibits the single viable mechanism for transporting radionuclides from the repository to the biosphere. Migration tests include studies of the ability of the clay materials to retard the outward migration of radionuclides leached from the waste form after the structural canister barriers are breached, and secondarly, to slow down the inward migration of chemical species that may enhance corrosion of the canister.

Experimental Results

Materials

The materials used are:

1. Natural bentonite (NB), Kärlicher Ton- und Schamottewerke,
2. Activated bentonite I, II, III (AB), Kärlicher Ton- und Schamottewerke,

3. Grey salt clay (T3), Werk Niedersachsen-Riedel,
   500 m level,
4. Red salt clay, brown fraction (T4B), Werk Niedersachsen-Riedel,
   1305 m level,
5. Red salt clay, red fraction (T4R), Werk Niedersachsen-Riedel,
   1305 m level,
6. Brick clay (ZT), clay pit Altwarmbüchen near Hannover.

The composition of the various materials determined by chemical analysis [3] are depicted in table I.

The solutions used and their composition are listed in table II.

Table I: Composition of materials used

Component	Mass Fraction in %							
	NB	AB I	AB II	AB III	T3	T4B	T4R	ZT
SiO_2	60.1	58,6	56.0	52.5	46.1	47.7	45.9	58.1
TiO_2	0.88	0.51	0.3	0.7	0.68	0.29	0.43	0.83
Al_2O_3	17.3	17,6	20.6	16.9	14.4	8.1	12.9	19,4
Fe_2O_3	9.5	5.1	4.7	8.8	1.5	1.9	3.0	5.2
MgO	1.8	4.1	3.4	1.9	17.1	9.3	11.9	2.5
CaO	1.4	3.0	2.0	1.3	1.0	19.0	3.1	3.0
SrO	<0.009	<0.007	–	–	0.043	0.11	0.069	<0.006
Na_2O	0.21	1.9	3.0	8.4	0.46	0.75	9.9	1.4
K_2O	2.1	1.8	1.4	1.5	2.0	1.3	2.2	3.1
Cs_2O	0.0008	0.0006	–	–	0.0005	0.0004	0.0007	0.0006
H_2O (total)	7.1	7.8	7.5	7.6	14.6	3.1	3.4	1.8

Table II: Composition of solutions used

Component	Destilled	Quinere Brine (Quil 1) [g/l]	Quarternere Brine (Qual) [g/l]	Saturated NaCl-Brine [g/l]
Na^+	–	44,3	44,3	14,5
K^+	–	31,8	31,8	–
Mg^{2+}	–	43,4	42,2	–
Cl^-	–	220,4	220,4	21,3
SO_4^{2-}	–	4,7	–	–
$Density_4^{20}$ [g/cm³]	1,00	1,233	1,226	1,197

Hydration Rate

The rate of water intake was measured for several bentonite species at room temperature applying a method originally proposed by ENSLIN [4].

The samples were compacted to a density of approximately 2,0 g/cm^3. The water intake velocity as well as the value for water saturation show a dependence on the sodium content of the bentonite samples. The higher their share, the greater their water intake capability [5]. The results obtained are illustrated in figure 1.

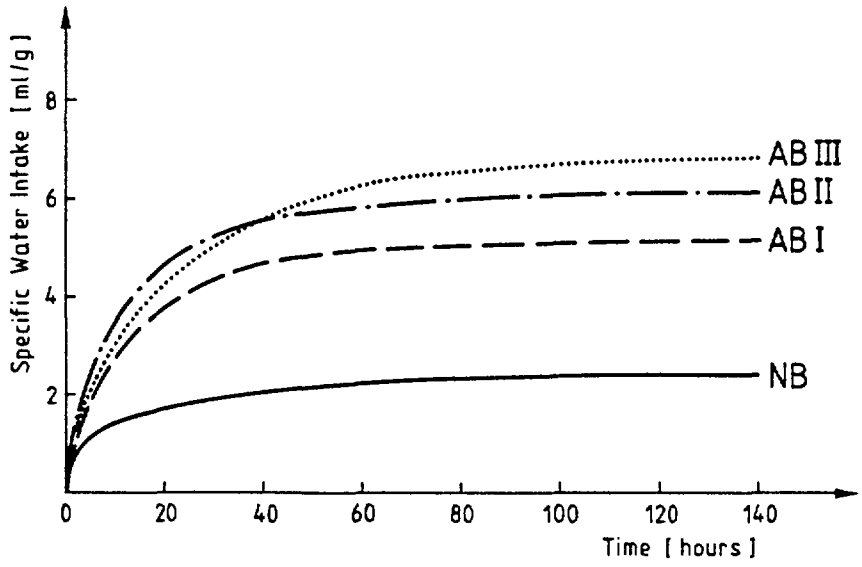

FIG. 1: Temporal progress of water intake of various bentonite specimen

Swelling Pressure

If a compacted bentonite body has access to external water and is confined so that its total volume remains constant, a swelling pressure is built up. The mechanism of this phenomena is fairly well understood [6]. It is known that the swelling pressure of smectite clays is a function of their initial compaction density.

The swelling pressure of compacted high-density bentonite samples (ρ = 2.0 - 2.1 g/cm^3) was measured in an apparatus shown in figure 2.

It allows the determination of the swelling pressure by measuring the force applied on a load cell by a water exposed sample, restrained to a constant colume [5].

The results obtained applying two different large areas exposed to water access are illustrated in figure 3. In the lower curve by far no saturation has been achieved due to the fact that only about one fifth of

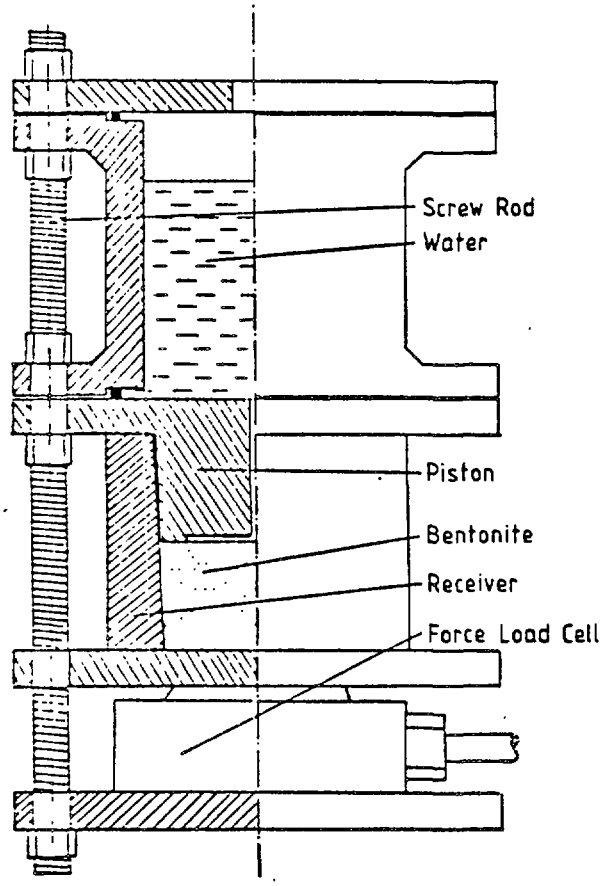

FIG. 2: Schematic view of the swelling pressure measuring device

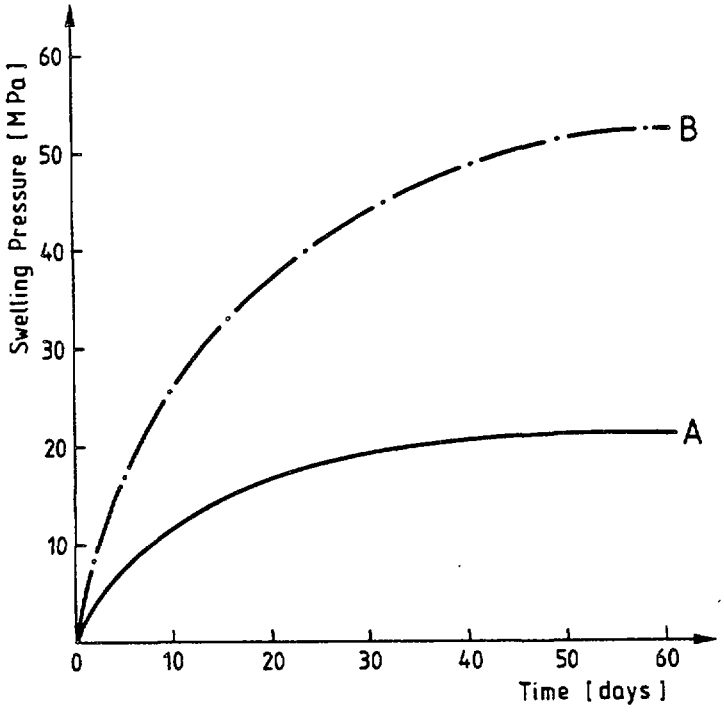

FIG. 3: Swelling pressure of highly compacted sodium bentonite

Curve A: water exposed surface area 200 mm^2; water content after 60 days exposure approx. 4 %

Curve B: water exposed surface area 1000 mm^2; water content after 60 days exposure approx. 16 %

the sample surface has been exposed to water access. The upper curve represents a more realistic picture. But even in this case no complete saturation of water intake has been reached after 60 days of exposure.

Permeability

Some material transport will take place towards the canister wall and vice versa from the eventually breached canister backwards through the backfill material. The predictive theory which describes the flow of brine or ground water, respectively, in a porous material is DARCY's law; the directly derived parameter is the hydraulic conductivity.

$$Q = -K \cdot i \cdot A$$

Q = discharge rate [cm^3/s]
K = hydraulic conductivity [cm/s]
i = hydraulic gradient [cm/cm]
A = cross sectional area [cm^2]

In the formalism of DARCY's law, the hydraulic conductivity, K is a constant relating discharge to the hydraulic gradient. It is a function of both the solid material and the fluid as indicated by the relationship

$$K = \frac{k \cdot \rho \cdot g}{\eta}$$

k = permeability (intrinsic) [cm^2]
ρ = fluid density [g/cm^3]
η = fluid viscosity [$g/cm \cdot s^2$]
g = gravitational acceleration [cm/s^2]

The permeability k is a function of the solid media and depends upon variables such as grain size, grain shape, porosity and path tortuosity. The density and viscosity factors depend entirely upon the fluid phase; and the dependence on viscosity clearly indicates that hydraulic conductivities vary strongly with temperature.

After saturation of the backfill, chemical species may be transported through the backfill either by movement of liquid, or if the backfill performs as expected, by diffusion through the interstitial water. In either case, the ability of the backfill to retard the migration by sorption, precipitation, or any other mechanism is one of the more important attributes of the backfill.

The hydraulic conductivity of brine through compacted bentonite (density 2.1 g/cm^3) has been measured at room temperature in a constant-volume flow cell. The backfill material is confined triaxially between porous stone plates, and liquid brine is pumped through

the material at a constant hydraulic head pressure until saturation is achieved. The time elapsed until saturation yields the materials hydration rate; the flow rate after saturation yields the materials liquid permeability in units of [Darcies], or, equivalently, the hydraulic conductivity in units of [m/s].

The hydraulic conductivity dropped rapidly with time before stabilizing at a much lower value than at the beginning (about 1/4 of its original value).

TableIII summarizes the measured data.

The high permeability coefficients observed give rise to make the backfill material practically impervious to brine percolation. However, radionuclide transport is still possible - though at a very low rate - by another mechanism, namely diffusion. Sufficient quantitative data of radioisotope diffusivity are still lacking [7,8].

Table III: Permeability measurements of activated Na-bentonite samples. Depicted values after stabilisation (time span elapsed ~ 500 h)

Material Activated Na-bentonite	Density [g/cm³]	Hydraulic Head Pressure [MPa]	Hydraulic Gradient	Hydraulic Conductivity [cm/s]
AB I	2.11	15	$1.3 \cdot 10^5$	$4.8 \cdot 10^{-13}$
AB II	2.10	15	$1.5 \cdot 10^5$	$4.0 \cdot 10^{-13}$
AB III	2.09	15	$1.6 \cdot 10^5$	$5.4 \cdot 10^{-13}$

Diffusion Measurements

In a series of experiments the apparent diffusitivity of cesium, sodium and chlorine ions have been measured using a stack of highly compacted bentonite disks forming a diffusion cell and applying radio-tracers of Na-22, Cl-36 and Cs-134 in a saturated NaCl brine. The bentonite was compacted to a density of 1.9 g/cm^3. After a period of 2 months the cell was dismounted, and the individual disks measured separately with regard to their radioactivity; the γ-radioactivity with a Ge(Li)detector and the β-emitters applying liquid scintillation counting.

The diffusitivity (D) for one-dimensional diffusion is given by the equation

$$\frac{dc}{dt} = \frac{d}{dx}(D \frac{dc}{dx})$$

which has to be solved by applying appropriate initial and boundary conditions [9].

With a plane source containing a limited amount of substance which is diffusing in a cylinder of infinite length and assuming a concentration independent D, the solution is

$$\frac{c}{M} = \frac{1}{2(\pi \cdot Dt)^{1/2}} e^{-x^2/4Dt}$$

c = concentration [mMol/cm^3]
M = total amount of diffusing species [mMol/cm^2]
x = distance from source [cm]
D = diffusitivity [cm^2/s]
t = time [s]

The diffusitivity obtained applying this equation to measured concentration profiles yields an apparent diffusitivity (D_a), including the effect of sorption on the solid [10]. The relation between the apparent diffusitivity, D_a, and the diffusitivity not affected by sorption, D, is

$$D = D_a(1 + K_D\rho)$$

ρ = density of the solid [g/cm^3]

With the few data available as yet, shown in table IV, it is impossible to draw any meaningful conclusion. More elaborate measurements are needed.

Table IV: Measured diffusivities

Element	D_a (best estimates) [cm^2/s]
Cs	$2 \cdot 10^{-9}$
Na	$8 \cdot 10^{-7}$
Cl	$5 \cdot 10^{-8}$

Nuclide Migration

The physico-chemical mechanismns underlying radionuclide migration through argillaceous clays are rather complex. In most cases several effects may be superimposed in attaining fixation of the released radionuclides to the solid backfill. Important are

- adsorption and exchange phenomena,
- complex formation and hydrolysis,
- precipitation and surface reactions,
- mixed crystal formation and recrystallisation,
- filtration effects if suspended particles are present in the liquid media.

In order to determine the retardation capabilities of candidate backfill materials, batch distribution measurements of K_d values for strontium and cesium have been performed with 6 different argillaceous clays and bentonites using the various solutions listed in table II [3]. Samples of each (10 and 20 g) were contacted with 50 ml solution for sufficient time (between 1 and 20 hours). The quinere brine was applied only in the Cs system but not in the Sr system in order to avoid precipitation of $SrSO_4$.

Variables have been the equilibrium concentrations of Sr- and Cs-ions in the respective solutions, temperature (25° and 100°C), and pressure (1 and 100 bar).

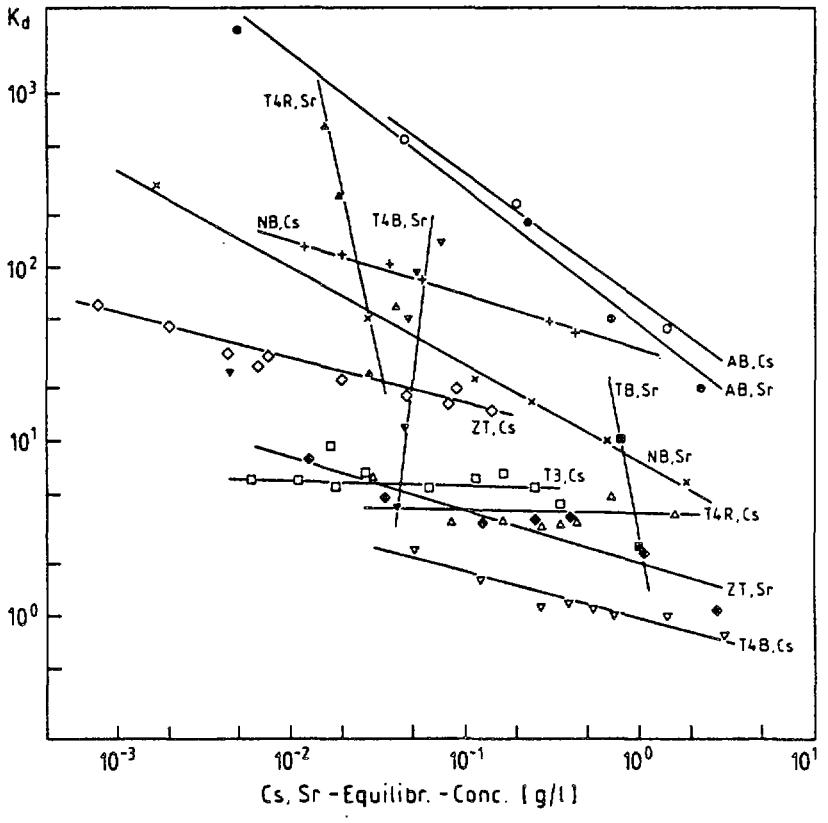

FIG. 4: Batch distribution K_d-values as a function of equilibrium concentrations for Sr and Cs in aqueous solution at 1 bar and 25°C for different argillaceous clays

The contents of Sr and Cs were determined applying X-ray fluorescence analysis. The results are shown in figures 4 to 8.

The results show that strontium and cesium are retained by the bentonites and clays. The substance which diffuses through the backfill material will be retarded in transport owing to sorption until equilibrium is established. Only then the substance will migrate further. Retardation increases as the values of K_d increases.

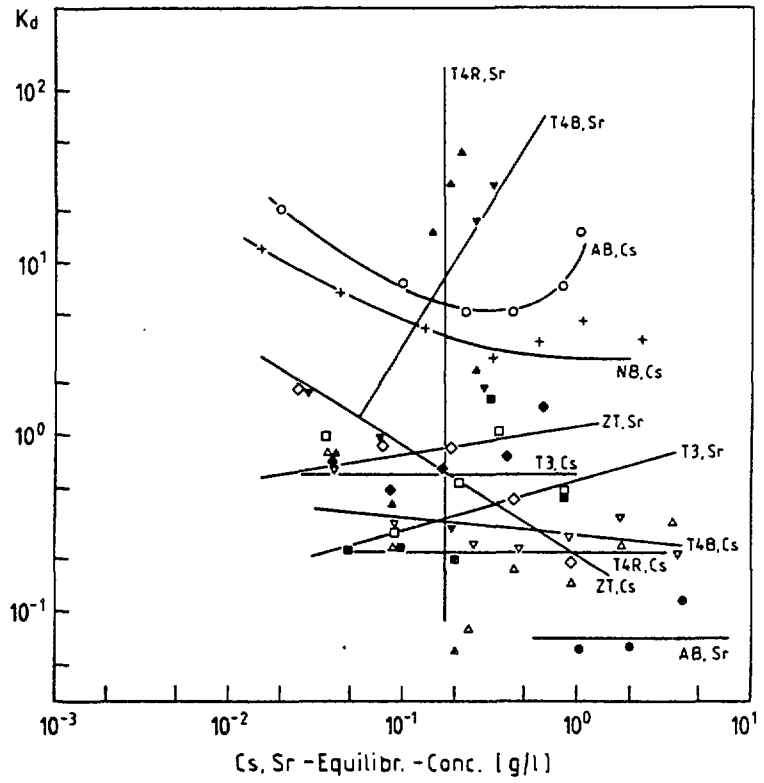

FIG. 5: Batch distribution K_d-values as a function of equilibrium concentrations for Sr and Cs in salt brine, quinere and quarternere brines at 1 bar and 25°C for different argillaceous clays

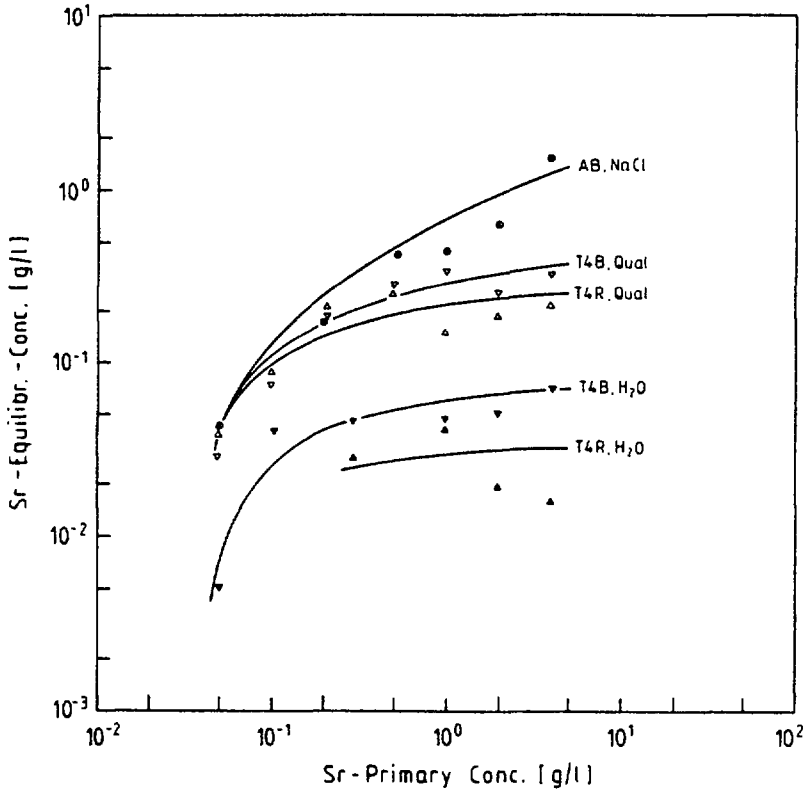

FIG. 6: Adsorption isothermes of Sr at 1 bar, 25°C

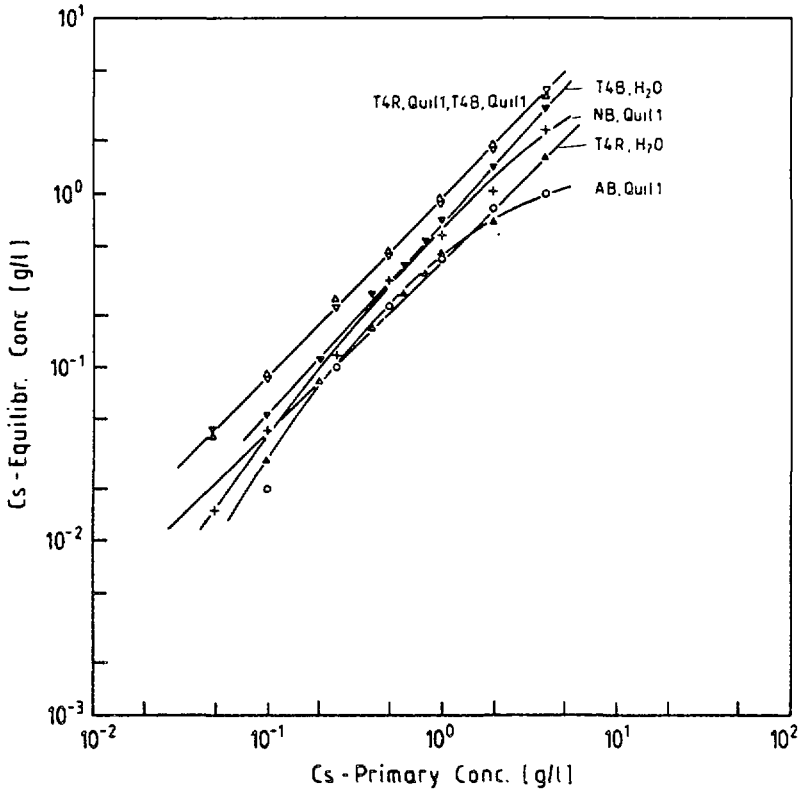

FIG. 7: Adsorption isothermes of Cs at 1 bar, 25°C

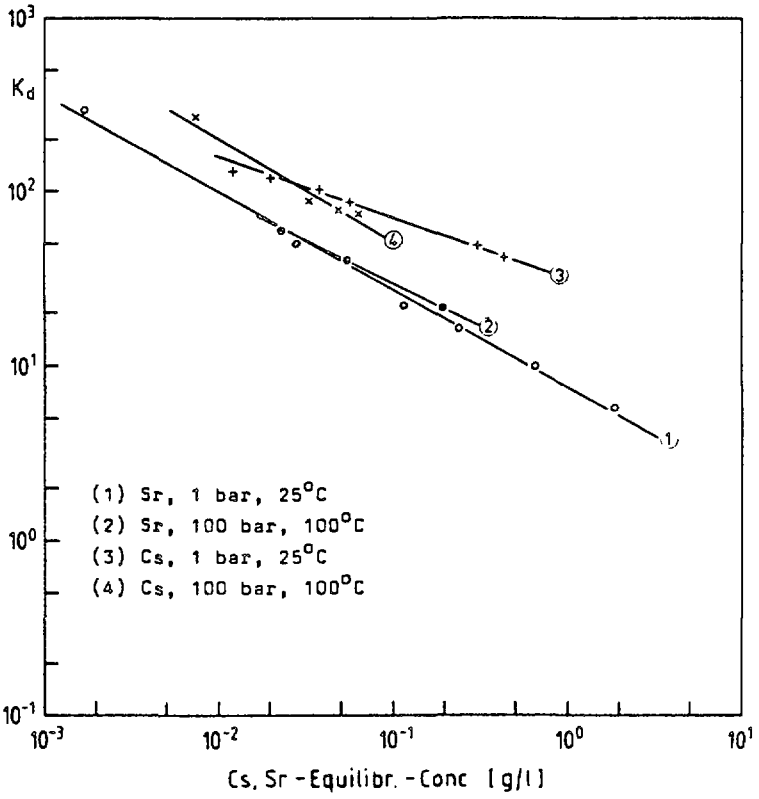

FIG. 8: K_d-values as a function of equilibrium concentrations for Sr and Cs in aqueous solutions at different pressures and temperatures

However, the sorptive capacity decreases strongly with increasing salinity of the solutions. The cations in the brine give rise to a strong displacement action. An influence of increased temperature and hydrostatic pressure is measurable but comparably small and only of minor importance. An interesting behaviour has been found for the strontium retardation, which is abnormally high under certain circumstances. Obviously, it is due to a precipitation of $SrSO_4$, originating from a small content of Sr ions in the clay minerals.

The rate of diffusion through the backfill is controlled by normal diffusion processes and on the sorption properties of the backfill materials. The migration of various ions exhibits a different pattern depending on the sodium content of the bentonite. It seems highly probable that, over the long term, transport of solution through the backfill will be so slow that diffusion will be the main mechanism of radionuclide transport and release. In addition to sorption and ion exchange, precipitation as well as remineralisation may play an important role in the retention of radionuclides.

References

[1] HERRMANN, A.G., Geowissenschaftliche Probleme bei der Endlagerung radioaktiver Substanzen in Salzdiapiren Norddeutschlands.
Z. dt. geol. Ges. 131 (1980) 433-459

[2] WHEELWRIGHT, E.J., et al., Development of Backfill Material as an Engineered Barrier in the Waste Package System.
Report PNL-3873 (1981) 105 p.

[3] BRODDA, B.G., MERZ, E., Zur Wirksamkeit von Tonmineralien als Rückhaltebarriere bei der Endlagerung radioaktiver Abfälle in Salzgesteinen.
Z. dt. geol. Ges. 134 (1983) 453-466

[4] ENSLIN, O., Die chemische Fabrik 13 (1933)

[5] MIRSCHINKA, V., Eigenschaften von Behälterwerkstoffen und Verfüllmaterialien für die Endlagerung hochradioaktiver Spaltprodukte.
Report JÜL-Spez-226 (1984) 100 S.

[6] PUSCH, R., Highly Compacted Sodium Bentonite for Isolating Rock-Deposited Radioactive Waste Products.
Nuclear Technology 45 (1979) 153-157

[7] NOWAK, E.J., Diffusion of Cs(I) and Sr(II) in Liquid-Saturated Beds of Backfill Materials.
Report SAND-82-6750 (1982) 52 p.

[8] PUSCH, R., ERIKSEN, T., JACOBSSON, A., Ion/Water Migration Phenomena in Dense Bentonites. Scientific Basis for Radioactive Waste Management V, Vol. 11, Elsevier Science Publishing Co., Amsterdam-New York (1982) 649-658

[9] CRANK, J., The Mathematics of Diffusion. Oxford University Press, London (1956)

[10] TORSTENFELT, H., et al., Transport of Actinides through a Bentonite Backfill. Scientific Basis for Radioactive Waste Management V, Vol. 11, Elsevier Science Publishing Co., Amsterdam-New York (1982) 649-658

TEN YEARS OF EXPERIENCE IN EXTRACTION CHROMATOGRAPHIC PROCESSES FOR THE RECOVERY, SEPARATION AND PURIFICATION OF ACTINIDE ELEMENTS

C. MADIC, J. BOURGES, G. KOEHLY
Section des transuraniens,
Institut de recherche technologique et de développement industriel,
Centre d'études nucléaires,
Commissariat à l'énergie atomique,
Fontenay-aux-Roses, France

Abstract

An extraction chromatographic process has been developed for the recovery of actinide elements (^{242}Cm, ^{241}Am, ^{238}Pu, ^{237}Np, ^{234}U and others) from irradiated targets, from alpha liquid wastes and from aged actinide stocks. An inorganic adsorbent can be used as a stable, inert support for an inorganic extractant, e.g., TBP- impregnated silica. Due to the large variety of organic extractants available, this technique can be applied successfully to solve difficult actinide separations in quantities ranging from micrograms to kilograms. A comparison of extraction chromatography is also made with resin chromatography and liquid-liquid extraction.

I INTRODUCTION

Since about fifteen years the French Atomic Energy Commission has developed a program for the production of isotopes of actinides elements for french and international uses. An overview of the isotopes produced, the accumulated amounts since the beginning of the program and the method of preparation is presented Table I. Basically there is two types of programs.

I.1. Major programs

(i) Involving the preparation of special targets, their irradiation by neutrons in nuclear reactors and the chemical treatment of the irradiated targets
- production of ^{233}U by irradiation and treatment of $^{232}ThO_2$ targets
- production of ^{238}Pu by irradiation and treatment of $^{237}Np/Al$ or $^{237}NpO_2/MgO$ targets
- production of ^{242}Pu, ^{243}Am, ^{244}Cm by irradiation and treatment of $^{239}Pu/Al$ targets or $^{242}PuO_2$ targets.

(ii) Involving the milking of large amounts of parent material : production of ^{241}Am by chemical treatment of kilogram amounts of PuO_2 or Pu metal stocks rich in ^{241}Pu.

(iii) Involving the chemical treatment of large volumes of alpha active liquid wastes : recovery of ^{241}Am.

I.2. Minor programs

Which correspond to productions of special isotopes either by milking of stocks of aged parent (^{228}Th, ^{229}Th, ^{234}U, ^{237}U, ^{239}Np, ^{240}Pu, ^{248}Cm) or by chemical treatment of small irradiated targets (^{242}Cm).

TABLE I

ISOTOPES PRODUCED OR RECOVERED

ELEMENT	ISOTOPE	METHOD OF PRODUCTION	Scale of production since the beginning of the program
THORIUM	^{228}Th	$^{232}U \xrightarrow{\alpha} {}^{228}Th$ milking of large amounts of aged ^{233}U rich in ^{232}U	10 µg
	^{229}Th	$^{233}U \xrightarrow{\alpha} {}^{229}Th$ milking of large amounts of aged ^{233}U	mg
URANIUM	^{233}U	Irradiation of ^{232}Th by neutrons Chemical treatment of irradiated $^{232}ThO_2$ targets	hundreds of grams
	^{234}U	$^{238}Pu \xrightarrow{\alpha} {}^{234}U$ milking of large amounts of aged $^{238}PuO_2$	grams
	^{237}U	$^{241}Pu \xrightarrow{\alpha} {}^{237}U$ milking of aged plutonium rich in ^{241}Pu isotope	µCi
NEPTUNIUM	^{237}Np	Recovered in special campains in the reprocessing plant devoted to treatment of irradiated nuclear fuels	10 kg
	^{239}Np	$^{243}Am \xrightarrow{\alpha} {}^{239}Np$ milking of aged $^{243}AmO_2$	µg
PLUTONIUM	^{238}Pu	Irradiation of $^{237}Np/n$ Chemical treatment of irradiated Np/Al or NpO_2/MgO targets	kg
	^{240}Pu	$^{244}Cm \xrightarrow{\alpha} {}^{240}Pu$ milking of aged $^{244}CmO_2$	10 of mg
	^{242}Pu	Irradiation of ^{239}Pu targets/n chemical treatment of irradiated Pu-Al targets	hundreds
AMERICIUM	^{241}Am	$^{241}Pu \xrightarrow{\beta^-} {}^{241}Am$ Milking of aged PuO_2 or Pu metal stocks - Chemical treatment of alpha active liquid wastes	kilogram
	^{243}Am	Irradiation of ^{239}Pu or ^{242}Pu by neutrons Chemical treatment of Pu-Al or PuO_2 irradiated targets	100 g
CURIUM	^{242}Cm	Irradiation of ^{241}Am by neutrons Chemical treatment of irradiated AmO_2 targets	10 mg
	^{244}Cm	Irradiation of ^{239}Pu or ^{242}Pu by neutrons - Chemical treatment of irradiated Pu-Al or PuO_2 targets	100 g
	^{248}Cm	$^{252}Cf \xrightarrow{\alpha} {}^{248}Cm$ Milking of aged ^{252}Cf stock	10 of µg

For the production and purification of all these isotopes chemical separations must be achieved ; in few cases these separations are easy to be performed due to the large difference in chemical properties of the two elements in presence, this is the case for the production of ^{239}Np ($^{239}Np(IV)$)/($^{243}Am(III)$) separation or ^{240}Pu ($^{240}Pu(IV)$)/$^{244}Cm(III)$) separation ; for the other isotopes produced difficult separations are needed :

- recovery of traces of $^{233}U(VI)$ in large amounts of $^{232}Th(IV)$
- recovery of traces of ^{228}, $^{229}Th(IV)$ in large amounts of $^{233}U(VI)$ (containing ^{232}U)
- separation $^{238}Pu/^{237}Np$
- separation $^{243}Am/^{244}Cm$.

At the beginning of the programs these separations were realized using liquid-liquid extraction (L.L.E.) techniques operated in mixer-settlers but ten years ago the extraction chromatographic technique was developed for preparative purposes and is now applied for all chemicals separations needed for the production of actinides isotopes. That technique appears to be simple and flexible. It can be used for the production of μg to kilogram amounts of actinide isotopes. This paper focuses on the experience gained after ten years and describes some peculiar production of actinide isotopes solved by using extraction chromatographic techniques.

II EXTRACTION CHROMATOGRAPHY TECHNIQUE

More than ten years ago extraction chromatography technique was principally used in analytical laboratories for the separation of small amounts of metallic ions [1]. Its field of applications in now extended to process chemistry especially for nuclear applications [2] to [5]. The main advantages of extraction chromatography techniques can be compared with those of more conventional liquid-liquid extraction or ion exchange chromatography methods. Table II presents such a comparison ; in spite of a lower capacity than that possessed by ion exchange chromatography, extraction chromatography seems preferable due to the large versatility of extracting functions available and the simple method which can be used for the recovery of actinide trapped in the extracting material. The main advantage of extraction chromatography vs liquid-liquid extraction lies in the simplicity of the device used to perform the separations. Of course the small exchange capacities of the columns used in extraction chromatography make that technique only ideal for the production of μgrams to kilograms amounts of actinides. For the production of tons amounts of actinides, extraction chromatography cannot compete with liquid-liquid extraction.

METHOD / CHARACTERISTICS	EXTRACTION CHROMATOGRAPHY	ION EXCHANGE CHROMATOGRAPHY	LIQUID-LIQUID EXTRACTION
Versability of extracting functions	large	mean	very large
Exchange capacity	mean (adjustable)	large	mean (adjustable)
Extracting device	simple (1 column + 1 pump)	simple (1 column + 1 pump)	complex (mixer-settlers + pumps)
Number of plates	large	large	small
Sensitivity of performance to operating conditions	small	small	large
Recovery of the actinide trapped in the extracting material	simple A diluent washing of the column allows the recovery of the extractant and of the actinide	very difficult A possible method is to calcine the resin and to dissolve ashes in acid	simple Technique of solvent washing
Elimination of alpha contaminated material	easy (quasi solid waste)	easy (solid waste)	difficult (large volumes of alpha organic liquid wastes)

TABLE II Comparison of extraction chromatography, resin chromatography and liquid-liquid extraction techniques for actinides separations

II.1. Extracting molecules and their uses

The choice of an extracting molecule suitable for extraction chromatography application depends on several criteria :

- affinity for the actinide to be recovered
- simple conditions for loading and elution are needed
- impregnation conditions of the extracting molecule on the inert support
- lowest molecular weight possible allowing the highest exchange capacity of the columns
- low solubility in aqueous solutions.

N°	FORMULA	ABBREVIATION	STATE	MOLECULAR (weight)	TYPE OF APPLICATION
①	$(C_4H_9O)_3P{=}O$	TBP	liquid	266	$^{238}Pu(IV)/^{237}Np(V)$; $^{243}Am/^{244}Cm$
②	$(C_6H_{13})_2(C_7H_{15}\text{-}O\text{-}CH_2)P{=}O$	POX.11	liquid	346	$^{241}Am(III)$/transition elements
③	$(C_6H_{13}O)_2P(O)\text{-}CH_2\text{-}C(=O)\text{-}N(C_2H_5)_2$	DHDECMP	liquid	363	$^{241}Am(III)$/transition elements
④	$(C_6H_5)_2P(O)\text{-}CH_2\text{-}C(=O)\text{-}N(CH_4H_9)(C_4H_9)$	φφ	solid	371	$^{241}Am(III)$/transition elements
⑤	$(C_8H_{17})_3NH^+, NO_3^-$	$TOAHNO_3$	solid	416	$^{237}Np(IV)/^{238}Pu(III)$
⑥	$[(CH_3)_2\text{-}CH\text{-}CH_2]_2\text{-}CH\text{-}O)_2P(O)OH$	HD(DIBM)P	liquid	350	$^{241}Am(VI)$/Gd(III), Ln(III)
⑦	$(C_8H_{17}\text{-}O)_2P(S)SH$	D_2EHDTP	liquid	354	$^{234}U(VI)/^{238}Pu(IV)$

TABLE III Extracting molecules and their uses in actinide separations
① tri-n butylphosphate
② di-n-hexyloctoxymethylphosphine oxide
③ di-n-hexyl diethyl carbamoymethylene phosphonate
④ di phenyl di-n-butyl carbamoyl methylene phosphine oxide
⑤ tri-n-octylammonium nitrate
⑥ bis(2,6 dimethyl 4 heptyl)phosporic acid
⑦ di-2-ethyl hexyl phosphoro dithioic acid

Table III presents some characteristics of extracting molecules used in our laboratory meeting some or all the criteria described above.

The simplest molecule used is the TBP for which the behavior for the extraction of actinides ions is well known from liquid-liquid extraction (L.L.E.) data. The transposition of the knowledge from L.L.E. to L.L.C. is simple and easy. The high affinity of TBP for U(VI) and Pu(IV) present in acidic aqueous solutions makes L.L.E. technique using TBP extracting agent ideal for purification of uranium and plutonium. To obtain high distribution coefficients for trivalent actinides (Am(III) and Cm(III)) with TBP it is necessary to use highly salted aqueous solutions which induces liquid wastes difficult to manage, that is why a research of extracting molecules having a high affinity for trivalent actinides in acidic media was initiated. In a first step POX.11 (a phosphine oxide) whose properties are close to those of TOPO was studied. The use of POX.11 instead of TBP for the extraction of Am(III) allows a decrease of the concentration of the salting out reagent needed in aqueous solutions : 3.6. M instead of 7 to 8 M $LiNO_3$. The main advantage of POX.11 vs TOPO lies in its liquid nature

allowing simple method for loading the extracting molecule on the inert support. In a second step search for molecules able to extract Am(III) from nitric acid solutions without salting out reagent was pursued. For this application DHDECMP, an extracting molecule developped in the U.S.A. [6] [7] and $\varphi\varphi$ (a new molecule) were selected. At first the use of $\varphi\varphi$ in L.L.E. was considered difficult because of the solid nature of this compound involving difficulties for the homogeneous loading on the inert support, but it was found that the solvate between $\varphi\varphi$ and nitric acid is liquid and easy to impregnate on the stationary phase.

In the case of $TnOAHNO_3$, preparation of the loaded material is easy : first liquid TOA is loaded on the support and when the column is filled with this material, a flow of nitric acid through the column converts the amine in its salt. The high affinity of $TOAHNO_3$ for tetravalent actinides from nitric acid solutions makes this extracting agent suitable for the purification of Pu(IV) or Np(IV).

The use of HD(DIBM)P, a highly sterically hindered extractant is restricted to the separation between Am(VI) and trivalent actinides or lanthanides. The selectivity of the separation is very high. The special properties of di-2-ethylhexylphosphorodithioic acid able to extract U(VI) in a synergetic combination with TBP from acidic solutions and to reduce Pu(IV), allow a very special separation U(VI)/Pu(IV) without the need to reduce plutonium to Pu(III) in the feed.

II.2. Inert support

The properties needed for the inert support used in L.L.C. are :

- commercial availability
- low prices
- high specific area
- hydrophobic properties
- highest specific gravity possible.

Three different inert supports were used : Celite 545, Gas Chrom Q (Applied Science Lab) and hydrophobic silica (Merck). Celite 545 was made hydrophobic by treatment with dimethyl dichlorosilane. The particule size distribution of Celite 545 and Gas Chrom Q is 110 to 140 μ and their specific area $\simeq 1\ m^2.g^{-1}$. The highest specific gravity of the hydrophobic silica makes this product more attractive than the two others, this permit highest extracting capacities for the column per unit of volume.

II.3. Preparation and characteristics of the stationary phases

Impregnations of the stationary phase with the extracting molecule are carried out as follows : a certain mass of material is placed in contact with a solution of extractant in hexane or acetone, the solvent is then evaporated under reduced pressure by means of a Buchi Rotavapor rotary evaporator. Impregnation levels in mass in the final mixtures are respectively : TBP (27 %), POX 11 (30 %), DHDECMP (30 %), $\varphi\varphi$ (30 %), TOA (25 %), HD(DIBM)P (30 %), HD_2EHDTP + TBP (30 %). Batches of mixture can be prepared at the 3 kg scale. Table IV presents the exchange capacities of the different stationary phases used, for the extraction of actinide at different oxidation states from nitrate solutions.

II.4. Chromatographic equipment

The chromatograhic equipment includes :

- plexiglass columns packed with the stationary phase impregnated with the extractant
- Prominent proportioning pumps
- storage tanks for various solutions
- gauge for in-line detection at the outlet of the column.

STATIONARY PHASE		EXTRACTED COMPOUND	EXCHANGE CAPACITY m.mole.g^{-1}
TBP	(27 %)	$UO_2(NO_3)_2$. $(TBP)_2$ $Pu(NO_3)_4$. $(TBP)_2$ $Am(NO_3)_3$. $(TBP)_3$	0.507 0.507 0.338
POX.11	(30 %)	$UO_2(NO_3)_2$ $(POX.11)_2$ $Pu(NO_3)_4$ $(POX.11)_2$ $Am(NO_3)_3$ $(POX.11)_4$	0.433 0.433 0.216
DHDECMP	(30 %)	$Am(NO_3)_3$ $(DHDECMP)_3$	0.275
φφ	(30 %	$Am(NO_3)_3$ $(\phi\phi)_3$	0.269
TOA	(25 %)	$Np(NO_3)_6(TOAH)_2(TOAHNO_3)_2$	0.177
HD(DIBM)P	(30 %)	$AmO_2(D(DiBM)P))_2$ $(HD(DiBMP))_2$	0.214
D_2EHDTP (HA) TBP	(20 %) (10 %)	UO_2A_2-TBP	0.282

TABLE IV Exchange capacities of the different stationary phases used

The column is filled by successive additions and repeated packings of the dry stationary phase. Once the packing is completed and the top cover cemented, the column is placed in the glove-box or the hot cell, where it undergoes pre-equilibrium designed to produce the chemical conditions required for fixation and to expel the air.

Two kinds of gauges are used for in-line selection at the outlet of the column :

- small Geiger-Muller tube for detection of ^{241}Am (60 keV)
- cerium doped glass scintillator for alpha detection.

Depending on the amount of actinide to be extracted the size of column varies from 100 g to 9 kgof stationary phase contained. The most used columns contain 2.8 kg of stationary phase and possess a Ø : 82 mm and a height h : 700 mm, their void volume is about 1.5 liters. Degradation of the column can occur by washing or radiolytic damage of the extractant. The columns the most sensitive to these phenomena are those loaded with DHDECMP used for the extraction of americium 241. Columns loaded with D_2EHDTP are sensitive to oxydation by nitric acid media, thus it is necessary to add an anti-nitrite agent (NH_2SO_3H) in the feed. Used columns can be eliminated as alpha solid waste after removal of the solution contained.

III SEPARATION AND PURIFICATION OF ACTINIDES ISOTOPES BY EXTRACTION CHROMATOGRAPHY

Instead of an overall description of a special process for the production of an actinide isotope we will describe in the present chapter some peculiar points corresponding to different processes :

- treatment of irradiated targets
- recovery of actinides from alpha active wastes
- recovery of decay products from aged actinide stocks.

III.1. Treatment of irradiated targets

III.1.1. Neptunium 237 irradiated targets

This program was initiated in France in 1969 in order to prepare plutonium 238 batteries suitable for nuclear pacemakers. That production of plutonium 238 was based on the irradiation of Np/Al or NpO_2/MgO targets in nuclear reactors, the chemical treatment of the irradiated targets after six months of cooling with a double aim : recovery of plutonium 238 and of neptunium 237 for recycling. The overall process was based on liquid-liquid extraction technique operated in mixer-settlers after the dissolution of the targets in nitric acid solutions [8]-[10].

In 1975 we started to test extraction chromatography as an alternative for the L.L.E. process. Here we will focus on two experiments concerning the difficult separation between plutonium and neptunium. Such a separation can be achieved by two systems based on :

- Valence adjustment, Pu(IV)/Np(V) then selective extraction of Pu(IV) by $TOAHNO_3$ columns
- Valence adjustment, Np(IV)/Pu(III) then selective extraction of Np(IV) by $TOAHNO_3$ columns.

(i) Pu(IV)/Np(V) separation on $TOAHNO_3$ column

In nitric acid media the most stable oxidation states for plutonium and neptunium are Pu(IV) and Np(V), it is thus possible to perform the separation by selective extraction of Pu(IV). Such a separation faces with a difficulty : the Np(V) trend to disproportionate according to

$$2\,NpO_2^{+} + 4\,H^{+} \rightleftharpoons Np^{4+} + NpO_2^{2+} + 2\,H_2O \qquad (1)$$

If in nitric acid of moderate concentration reaction (1) is shifted to the left, in the presence of an extracting agent having affinities for Np^{4+}, NpO_2^{2+} or for both, reaction (1) is shifted to the right, thus the neptunium is coextracted with the plutonium(IV).

To minimize this phenomenon and thus the efficiency of the Pu(IV)/Np(V) separation the feed must be adjusted to a low nitric acidity (1 M) compatible with hydrolytic properties of Pu(IV). A dissolution liquor of an NpO_2/MgO irradiated target of total volume = 23 l : Np(V) = 11 $g.l^{-1}$, Pu(IV) = 0.6 $g.l^{-1}$ was adjusted to HNO_3 = 1 M and then injected on a $TOAHNO_3$/Gas chrom Q column containing 1015 g of stationary phase ($\emptyset$ = 60 mm, H = 700 mm) with a flow rate equal to 2.5 $l.h^{-1}$. After washing the column with HNO_3 = 2 N at 2.5 $l.h^{-1}$, plutonium 238 was eluted with a solution of following composition : H_2SO_4 = 1 M, HNO_3 = 0.2 M.

Forteen grams of ^{238}Pu were recovered in one cycle, ^{237}Np was free of ^{238}Pu, decontamination factor F.D. Pu(Np) was only moderate $\simeq$ 20 but acceptable for a first cycle of Pu/Np separation, decontamination of ^{238}Pu from fission products was high.

(ii) Np(IV)/Pu(III) separation on $TOAHNO_3$ column

Separation between neptunium 237 and plutonium 238 can be achieved after reduction to Np(IV) and Pu(III) by selective extraction of Np(IV). Such a separation is difficult to perform with high concentration of plutonium 238 in solution because of the intense radiolysis leading to the destruction of the excess of reductor used and thus to the oxidation of plutonium to Pu(IV). Such a process can be used for final purification of neptunium 237 contaminated with traces of plutonium 238. Recently the purification of 300 grams of neptunium 237 contaminated with 17.5 ppm of plutonium 238 (due to the large difference in the half lives of these isotopes the alpha contribution of plutonium 238 was 30 %) was realized using the following procedure.

Feed The concentration of neptunium in the feed was 100 $g.l^{-1}$ in 6 M HNO_3, the reduction of neptunium to Np(IV) and plutonium to Pu(III) was done by addition of $N_2H_5NO_3$ to 1.5 M and a warming of the solution to 80°C during two hours. Thus after cooling the solution was adjusted to 0.1 M in ferrous sulfamate ($Fe(NH_2SO_3)_2$) freshly prepared under nitrogen by dissolution of iron in sulfamic acid. The presence of ferrous sulfamate in the feed allows the maintenance of plutonium as Pu(III). The presence of small amount of iron(III) in the feed, induces a small oxidation of plutonium to Pu(IV) and thus a decrease in the performance of the separation.

The feed is then injected on a $TOAHNO_3$ column containing few percent of octanol 2 in order to decrease a little the distribution coefficient of tetravalent actinide and thus improve the quality of the separation.

Washing The column loaded with Np(IV) was washed by HNO_3 = 3 M to remove plutonium and iron ions present in the void volume.

Elution The elution of Np(IV) was performed with a solution : HNO_3 = 0.1 M ; H_2SO_4 = 0.75 M due to the complexing properties of SO_4^{--} ions. In the purified neptunium the concentration of plutonium was 0.24 ppm. The decontamination factor for the entire process was $F.D._{Np(Pu)}$ = 73 which is a good performance for this low level of ^{238}Pu contamination.

III.1.2. Plutonium 239 irradiated targets [11], [12]

This program was initiated for the production of americium 243 and curium 244 isotopes. The Pu/Al targets containing initially 400 g of fissile material were irradiated with an integrated flux of 11.28 $n.kb^{-1}$. Chemical treatment started after three years of cooling time.

The overall process is operated by L.L.C. after dissolution of the targets in nitric acid which is realized using 88 liters. The highly radioactive solutions contain 350 $Ci.l^{-1}$ of β,γ emitters and 44 g of ^{242}Pu ; 8.35 g of ^{243}Am and 7.44 g of ^{244}Cm.

The first step of the process lies in the recovery and purification of the plutonium 242, which is realized by extraction chromatography using a $TOAHNO_3$ column or a TBP column. To prevent clogging of these columns by fission products precipitates, the feed is filtrated through a small column containing a bed of silica. After washing of the column with nitric acid solution the elution of the plutonium 242 is realized with a sulfonitric solution ($TOAHNO_3$ column) or a hydroxylammonium nitrate reducing solution (TBP column).

The largest difficulty associated with that treatment lies :

- In the separation of trivalent actinides (^{243}Am, ^{244}Cm) from trivalent lanthanides present in the solution in large quantities ($\simeq$140 g).
- In the separation Am/Cm. The difficulties have been solved by L.L.C. using a TALSPEAK like system, where TBP extractant was used instead of HDEHP. Thus in this system the selectivity of the separation is only due to the DTPA present in aqueous solution.

All the lanthanides possess a higher affinity than Am(III) and Cm(III) for TBP column from $LiNO_3$ = 8 M, HNO_3 = 0 $\pm$ 0.05 M, DTPA = 0.1 M, pH = 1.2 solution, the separation factor $\alpha = D_{Ln^{3+}}.D_{Am^{3+}}^{-1}$ is large for the light lanthanides and is close to 1.4 for Tb and heavier Ln(III). To achieve a good separation (Am, Cm) from Ln, it is necessary to perform several cycles.

Separation between americium 243 and curium 244 is based for the first step on the same procedure. Figure 1 presents the separation between 1.51 g of curium 244 and 1.75 g of americum 243 using a TBP column and a Talspeak like system.

Final purification of americium 243 is performed by selective extraction of Am(VI) on a HD(DiBM)P column using a process identical with that described below for the purification of americium 241. That process appears very simple and flexible, easy to operate in the difficult conditions found in hot cells. Until now about 100 g of americium 243 and $\simeq$90 g of curium 244 of high purities have been successfully produced.

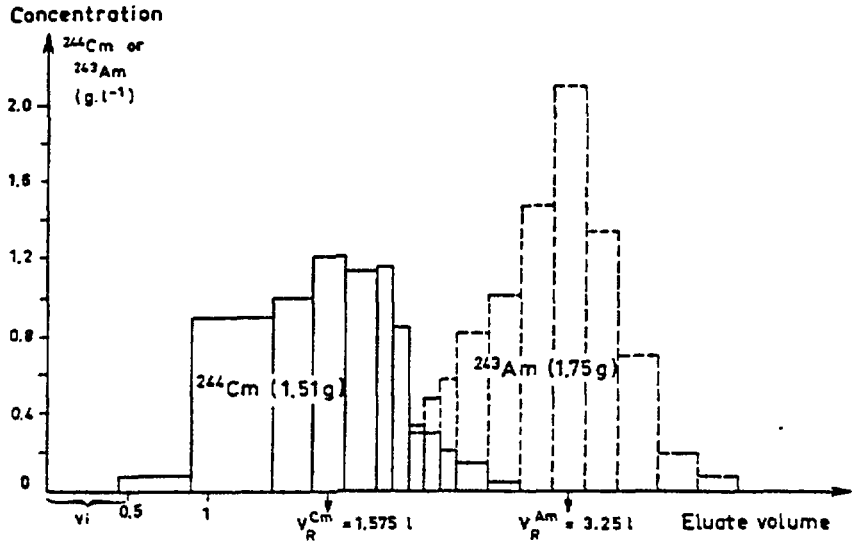

Figure 1 Separation $^{243}Am/^{244}Cm$ by extraction chromatography on a TBP/Gas Chrom Q column

FEED = DTPA = 0.1 M, Al^{3+} = 0.5 M, $LiNO_3$ 7 M
SCRUB = $LiNO_3$ 8 M
ELUTION = $LiNO_3$ 8 M DTPA 0.1 M, pH 1.20

Column TBP (25 %) Gas Chrom Q, m = 500 g, L = 64 cm, Ø 4,2 cm
Flow rate = 1.2 $l.h^{-1}$

III.2. Recovery of actinides from alpha aqueous wastes

In 1978 a program was initiated with the goal of producing large amounts of americium 241 used to prepare neutron sources (americium 241-beryllium or americium-lithium) for oil industry. The first source of americium 241 found in the C.E.A. consisted in alpha aqueous liquid wastes :

- "Masurca" waste resulting from the reprocessing of certain irradiated fuels and from criticallity analyses. Cadmium was added to the solution for safety reasons and then its initial volume of about 400 m^3 was reduced to 4 m^3 by distillation
- Waste coming from the reprocessing of fabrication scrap from fabricating $(U, Pu)O_2$ fuels intended for fast breeder reactors. The annual volume of this waste solution amounts to some tens of m^3.

The americium 241 contents of these wastes were respectively 108 $mg.l^{-1}$ and 28 $mg.l^{-1}$. As the uranium content of the "Masurca" waste was high (12 $g.l^{-1}$) it appears that L.L.C. wasn't suitable for its recovery prior to recovery of higher actinides. Thus conventional L.L.E. using TBP organic solution in mixer-settlers was used. The neptunium 237 and plutonium 239 were recovered by ion exchange chromatography using an anionic resin (IRA 400) prior to the recovery of americium 241 by extraction chromatography. In order to decrease the concentration of the salting out reagent necessary to obtain high distribution coefficient of Am(III), dinhexyloctoxymethylphosphine oxide (POX.11) [13] was selected as extracting agent. A moderate concentration of $LiNO_3$ = 3.6 M was found sufficient to obtain high K_DAm(III) ($\simeq 5.10^3 ml.g^{-1}$) for a nitric acid concentration of 0.1 M. The POX.11 nevertheless has the disadvantage of extracting Fe(III) with rather slow kinetics, which in the case of the "Masurca" waste gives rise to a sharp drop in K_DAm(III). The addition of EDTA to aqueous solution in equal concentration to Fe(III) (0.2 M) helps to avoid its extraction and to restore all the extractive properties of the POX.11 for Am(III). This is due to the selective formation of the complex FeY^- (with YH_4 = EDTA) whose formation constant $\log(FeY^-)$ = 25.1 [14] is much higher than that of the americium(III) complex = $\log(AmY^-)$ = 18.0 [15]).

Experiments were realized to determine the exchange capacity of POX.11 vs Am^{3+}, simulations of Am^{3+} by Nd^{3+} was also used in order to decrease the irradiation of the chemist working in a glove-box. Figure 2, presents studies of saturation of a POX.11 column by Am(III) or by Nd(III) nitrates. In each case the breakthrough is obtained for a stoichiometric ratio POX.11/M(III) close to 4 indicating that the extracted complex possesses the following formula : $M(NO_3)_3$ $(POX.11)_4$. That result was confirmed either by the study of POX.11 (30 %)/SiO_2 mixture saturation in test tubes or by the saturation of a POX.11 dodecane solution. Such a stoichiometry is very unusual because for trioctylphosphine oxide (TOPO) trivalent actinides or lanthanides are extracted as $M(NO_3)_3.(TOPO)_3$. The POX.11 possesses a high affinity for U(VI) and Pu(IV), for these ions stoichiometries are similar to those obtained with TOPO = $UO_2(NO_3)_2$ $(POX.11)_2$ and $Pu(NO_3)_4$ $(POX.11)_2$.

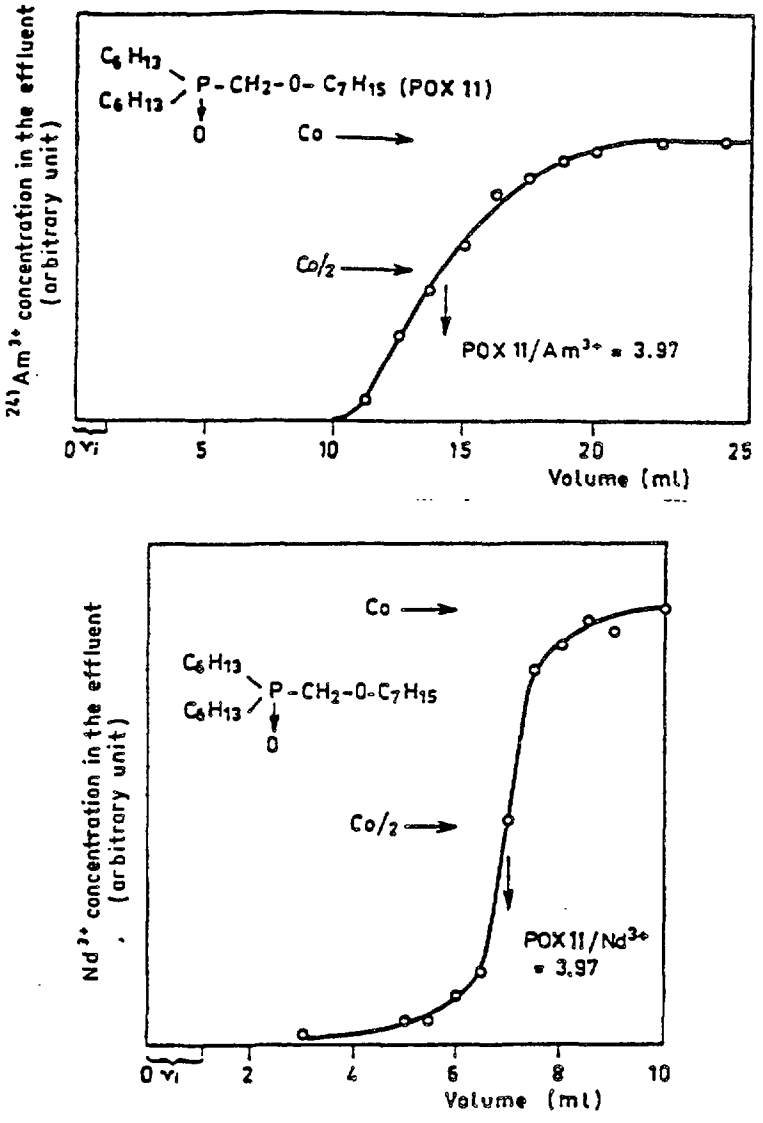

Figure 2 Saturation of POX.11/SiO_2 column with ^{241}Am and Nd

Columns = 1 g POX.11 (29,7 %)/SiO_2 Ø = 5 mm, H = 80 mm,
Void volume = 1.37 ml (Am^{3+}), 1,1 ml (Nd^{3+})

Aqueous phase =

[$LiNO_3$] = 3.6 M, [HNO_3] = 0.1 M, [Am^{3+}] = 3.81 $g.l^{-1}$ or [Nd^{3+}] = 5 $g.l^{-1}$

Flow rates = 15.1 $ml.h^{-1}$ (Am^{3+}), 1.25 $ml.h^{-1}$ (Nd^{3+})

During the chemical treatment of the "Masurca" waste rather large POX.11 column was used containing 9 kilograms of POX.11 (30 %)/SiO_2 stationary phase. A feed of 685 liters of total volume was treated, the decontamination factor of the effluent in americium 241 was 250 ; americium 241 (17 g) was recovered by elution with 20 liters of nitric acid (concentration factor = 34) with 89 % yield and its decontamination vs Cd^{2+} and Fe^{3+} was close to 130 [16].

The major drawbacks encountered in the use of POX.11 process for the recovery of americium 241 from alpha liquid wastes lies in the rather complicated feed adjustment :presence of $LiNO_3$ 3.6 M as salting-out reagent and of EDTA to complex Fe(III) present in the feed. That is why new molecules able to extract trivalent americium from nitric acid media without need of salt and possessing high affinity and selectivity for trivalent actinides were considered. The first molecule investigated is di-n-hexyldiethylcarbamoyl-methylenephosphonate (DHDECMP) well studied for L.L.E. in the U.S.A. [5].

Distribution coefficient of Am(III) between nitric acid solutions and DHDECMP (30 %)/SiO_2 stationary phase were measured at low nitric acid concentration K_DAm^{3+} = 0.9 $ml.g^{-1}$ (HNO_3 = 0.1 M) and K_DAm^{3+} maximum = 26 $ml.g^{-1}$ is obtained for HNO_3 = 6 M. It is thus possible to extract trivalent americium from moderate volumes of 5 to 6 M HNO_3 (due to the relatively low value of K_DAm^{3+} maximum) and to perform the elution with water.

Figure 3 presents an experiment related to the separation of americium 241 from fission products ^{134}, ^{137}Cs and ^{106}Ru and from inactive contaminants contained in a real waste. During the loading step

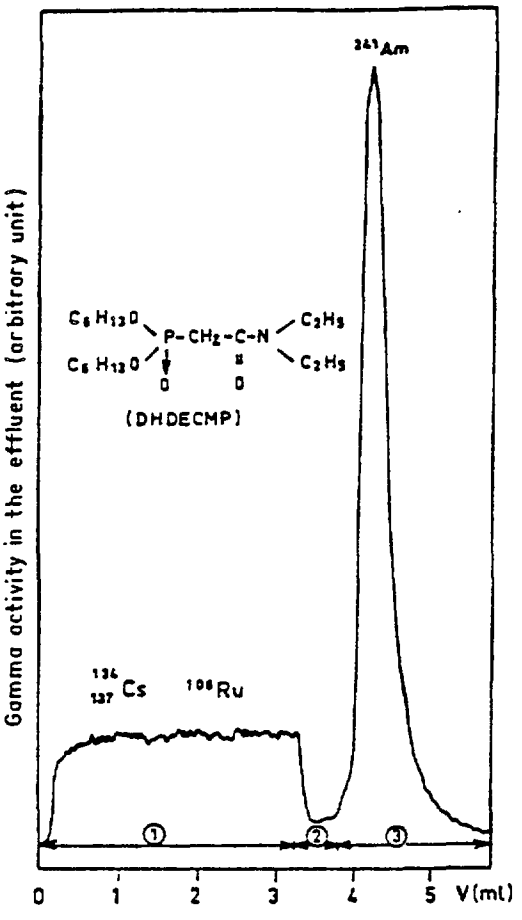

Figure 3 Purification of americium 241 from an industrial waste by extraction chromatography using a DHDECMP/SiO_2 column

Column = 1 g DHDECMP (30 %)/SiO_2, Ø = 5 mm, H = 80 mm

Aqueous Phases
- ① alpha active waste free from U and Pu (HNO_3 = 5 N)
- ② HNO_3 = 5 M
- ③ H_2O flow rate 2 $ml.h^{-1}$

fission products and inactive contaminants escaped from the column. After the washing of the column by a small volume of HNO_3 = 5 M, the americium 241 is eluted with three void volumes of the column. Americium 241 was recovered with a yield of 98 % and after conversion to AmO_2, its purity was found 85 % which is a very good performance for only one cycle. Adaptation of DHDECMP process to the purification of large amounts of americium 241 (50 grams) was realized but the lives of the columns were found to be limited because of the washing and radiolytic damage of the DHDECMP.

Another molecule able to extract trivalent americium from nitric acid solution was studied : the diphenyl di-n-butyl carbamoyl methylene phosphine oxide (ϕϕ). High distribution coefficients of Am^{3+} were obtained from nitric acid solutions with a maximum for HNO_3 = 2.5 M. The extraction reaction is :

$$Am^{3+}, 3NO_3^- + 3\overline{\varphi\varphi} \rightleftharpoons \overline{Am(NO_3)_3(\varphi\varphi)_3} \qquad (2)$$

The usefullness of that molecule for the recovery of americium 241 from nitric acid solutions by L.L.C. was demonstrated in an experiment where a nitric acid solution (HNO_3 = 2 M) containing 13,4 $mg.l^{-1}$ ^{241}Am was loaded on a small column containing 1 g of ϕϕ (30 %)/SiO_2 stationary phase. Four hundreds voids volume of the column were decontaminated with F.D. (Am^{3+}) = 388. Americium 241 can be eluted from the ϕϕSiO_2 column, after washing by water, with a K_2CO_3 solution.

III.3. Recovery of decay products from aged actinide stocks

III.3.1. Recovery of americium 241 from aged plutonium metal or PuO_2 stocks

The recovery of americium 241 from alpha active wastes is a rather complicated method due to the large volumes involved and their low concentration in americium. A more attractive way to produce hundreds of grams amounts of americium 241 is to treat aged stocks of plutonium metal or plutonium dioxide initially rich in ^{241}Pu. The first step of the process consists in the dissolution of the starting material on 300 g scale in nitric medium (containing F^- ion) under reflux conditions in a tantalum dissolver. After filtration the solution is injected on a TBP column for Pu(IV) extraction, americium 241 escapes from the column.

After washing of the column with 5 M nitric acid, the plutonium is eluted as Pu(III) with a hydroxylamine nitrate solution and then converted in PuO_2. The raffinate containing the ^{241}Am is then adjusted to the following conditions : H^+ = 0 ± 0.05, Al(III) = 1.8 M, DTPA = 0.1 M and loaded on a TBP column in order to decontaminate americium 241 from impurities (Pu, inactive metallic ions) and to reduce the volume of the americiated solution. After a washing of the TBP column with 8 M $LiNO_3$ solution, americium is eluted with 2 M nitric acid. Final purification of americium 241 is performed with a method described in Figure 4. The first step consists in the precipitation of $Am(OH)_3$, which is redissolved after filtration, in concentrated K_2CO_3 solution.

The addition of $K_2S_2O_8$ allows the precipitation of americium(V), potassium double carbonate. After precipitation, the precipitate is taken up with an oxidizing acidic solution containing $K_2S_2O_8$ and Ag ions acting as catalyst in the oxidation of Am(V) to Am(VI) by $S_2O_8^{--}$ions. After warming to 50°C americium is totally converted to Am(VI) (a spectrometric measurement is performed prior loading the solution into the L.L.C. column). The adjusted Am(VI) feed is then injected on a bis (2,6 dimethyl 4-heptyl)phosphoric (HDDiBMP) acid column previously treated by an oxidizing solution ($S_2O_8^{--}$ and Ag(II) ions) until persistance of the dark color

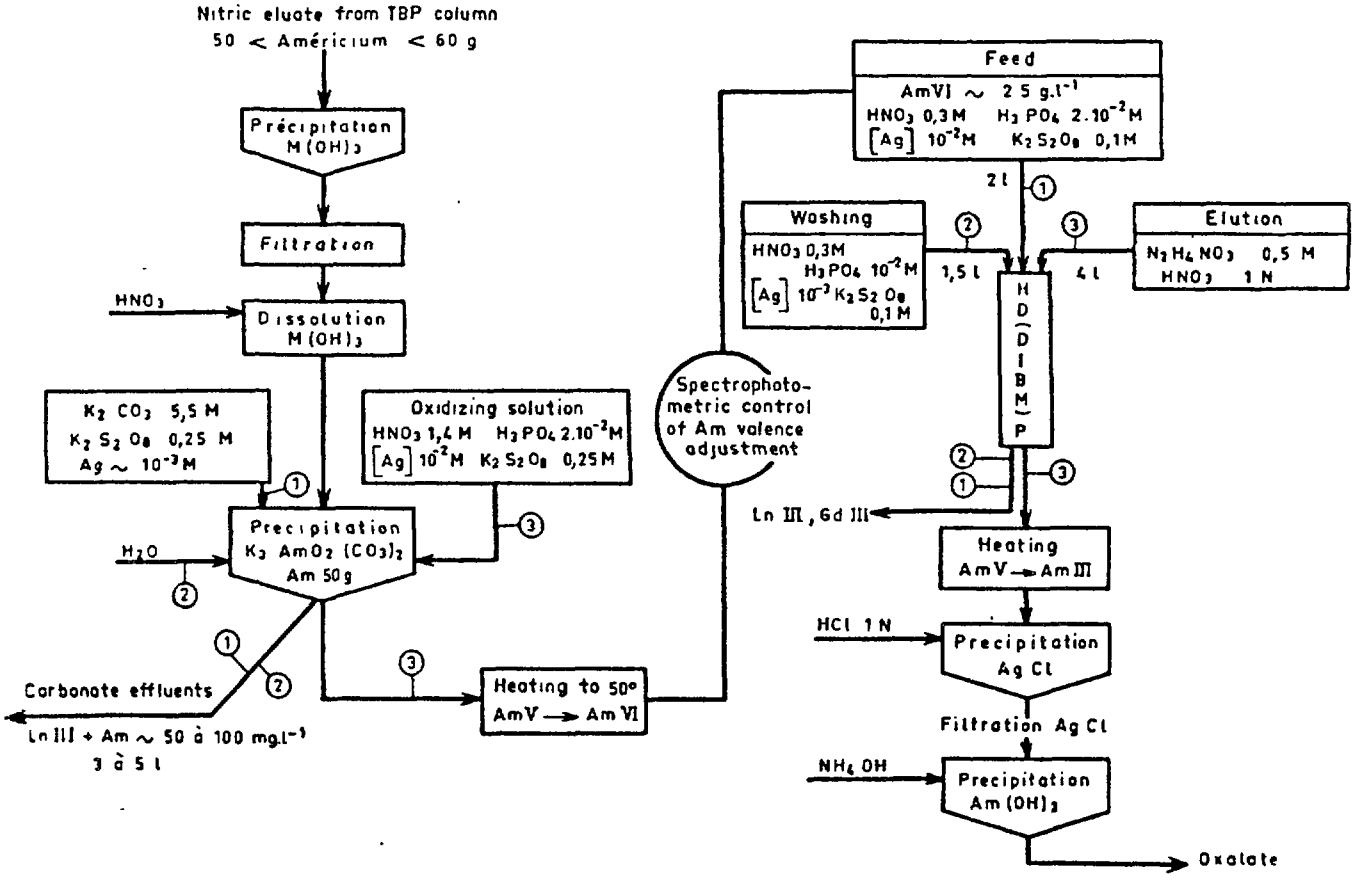

Figure 4 Recovery of americium 241 from aged plutonium stocks
Final purification process for americium 241

of Ag(II) ions in the effluent. Extraction of Am(VI) is apparent on the column by a greenish band. After washing of the column by an oxidizing solution americium is eluted with a reducing solution ($N_2H_5NO_3$ = 0.5 M, HNO_3 = 1 M).

Such a process is applied successfully on a 50 to 60 g. of ^{241}Am scale. The yield of the purification lies on the range 85 to 97 % for routine experiment. Americium 241 purity of 98.5 % was measured by calorimetry after transformation into AmO_2.

Laboratory experiments were performed in order to determine the stoichiometry of the extracted americium(VI) compound and thus the exchange capacity of the HD(DIBM)P columns. Figure 5 presents the curve obtained on the study of the saturation of a small HD(DIBM)P column with Am(VI), the concentration of ^{241}Am in the effluent is measured in line with a small Geiger-Muller detector. The break through is obtained for an HD(DIBM)P/Am(VI) ratio equal to 4, thus if HA stands for HD(DiBM)P the formula of the extracted americium(VI) compound is = $AmO_2A_2(HA)_2$. The same stoichiometry was found for U(VI) extracted complex.

Using this process, about 500 g. of high purity ^{241}Am have been produced.

III.3.2. Recovery of uranium 234 from aged plutonium 238 stocks

In aged plutonium 238 dioxide, uranium 234 accumulates. Due to the very different half lives of these isotopes ($t\ \frac{1}{2}$ = 87,7 years for plutonium 238 and $2.44.10^5$ years for uranium 234) the recovery of high nuclear purity uranium 234 necessitates very efficient separation process.

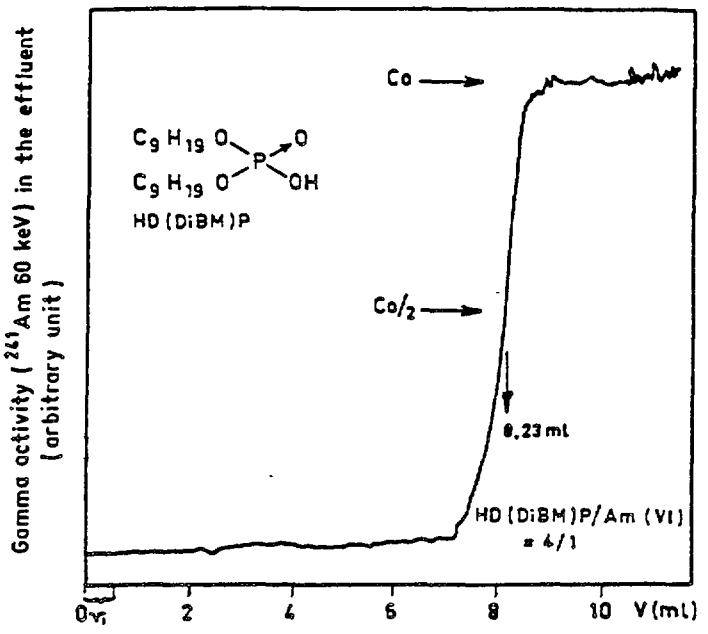

Figure 5 Saturation of HD(DIBM)P/SiO_2 column with ^{241}Am(VI)

Column = stationary phase = 0.500 g of HD(DIBM)P (29,56 %)SiO_2

Aqueous Phase [$NaNO_3$] = 2 M, [HNO_3] = 0.1 M, [$K_2S_2O_8$] = 0.2 M, [Ag] = 2.10^{-2}M, [Am(VI)] = 3.27 $g.l^{-1}$

Flow rate = 6 $ml.h^{-1}$

60 keV ^{241}Am detection by in-line Geiger Muller gauge

Ten grams of plutonium 238 on the dioxide form were processed for uranium 234 recovery according to the following scheme :

(i) Dissolution of PuO_2 in HNO_3 acid with F^- ion acting as catalyst.

(ii) Precipitation of the bulk of plutonium 238 as oxalate, ^{234}U(VI) remains in the mother liquor.

(iii) Change of medium by Pu(IV), U(VI) coextraction with TBP and back extraction with the addition of alpha bromocapric acid to the organic phase towards HNO_3 = 1 N aqueous solution.

(iv) Extraction chromatography on HD_2EHDTP (20 %), TBP (10 %)/Gas Chrom Q column.

The extraction chromatographic separations between ^{238}Pu and ^{234}U were performed using a column containing 20 g of stationary phase. During the loading step of the feed, extraction of ^{234}U(VI) is realized by the synergetic mixture : di 2 ethyl hexyl phosphorodithioic acid (HA)/tributyl phosphate. The extracted complex which formula is : UO_2A_2.TBP possesses an intense yellow color [17]. The di 2 ethyl hexyl phosphorodithioic acid possesses reductive properties vs Pu(IV) thus plutonium 238 escapes from the column as blue Pu(III). A fraction of the column (at the top) is destroyed by this reaction.

After washing of the column with a solution of composition HNO_3 = 1 N, NH_2SO_3H = 0.1 M, ^{234}U(VI) is eluted with a 0.4 M $(NH_4)_2C_2O_4$ solution. Forty six milligrams of uranium 234 were recovered and after two cycles of extraction chromatographic separations the alpha contribution of plutonium 238 in the purified uranium 234 was only 1.27 %.

Decontamination factors for extraction chromatographic separations were respectively : cycle 1 F.D. U(Pu) = 517 ; cycle 2 F.D. U(Pu) = 452. For the entire process F.D. U(Pu) = $4.5.10^7$ was obtained and the uranium 234 recovery yield was 75 %.

IV CONCLUSIONS

Extraction chromatography technique was developped in the last ten years for actinides recovery, separations and purifications. Due to the large variety of organic extracting ligands available, that technique can be applied successfully to solve difficult actinides separations. The processes developped for the recovery and purification of microgram to kilogram amounts of actinides isotopes are easy to operate either in glove boxes or in hot cells. Nevertheless there is still some difficulties to solve : especially the extraction of trivalent americium from nitric acid solutions for which if some opportunities exist : uses of DHDECMP or $\varphi\varphi$, their performances are not really ideal. More research is needed in this area.

REFERENCES

1 BRAUN, T., GHERSINI, G. Extraction Chromatography, Elsevier, Amsterdam (1975)
2 BUIJS, K, MULLER, W., REUL, J., TOUSSAINT, J.C., EUR 504e, (1973)
3 ESCHRICH, H., OCHSENFELD, W. Separation Science and Technology 15 4 (1980) 697.
4 WENZEL, U., MERZ, E., RITTER, G. Separation Science and Technology 15 4 (1980) 733.
5 MARTELLA, L.L., NAVRATIL, J.D., SABA, M.T. "Actinide Recovery from Waste and low grade Sources" Harwood Academic Publishers, Chur, London, New-York (1982) 27.
6 Mc ISAAC, L.D., BAKER, J.D., KRUPA, J.F., MEIKRANTZ, D.H., SCHROEDER, N.C. A.C.S. Symposium Series 117, (1980) 395.
7 KNIGHTON, J.B., HAGAN, P.G., NAVRATIL, J.D., THOMPSON, G.H. A.C.S. Symposium Series 161 (1981), 53.
8 KOEHLY, G., MADIC, C., BERGER, R. Proceedings of the International Solvent extraction Conference, The Hague. Society of Chemical Industry, London (1971) 768.
9 for the entire program of production of ^{238}Pu see : B.I.S.T. 218, (1976).
10 SONTAG, R., KOEHLY, G. B.I.S.T. 218 (1976) 23.
11 BOURGES, J., MADIC, C., KOEHLY, G. A.C.S. Symposium Series 117, (1980) 33.
12 KOEHLY, G., BOURGES, J., MADIC, C., SONTAG, R., KERTESZ, C. A.C.S. Symposium Series 161, (1981) 19.
13 GUILLAUME, B. Personal communication.
14 GUSTAFSON, R.L., MARTELL, A.E. J. Phys. Chem. 67 (1963) 576.
15 MOSKVIN, A.I., KHALTURIN, G.V. GEL'MAN, A.D., Radiokhimiya 1 (1959) 141.
16 MADIC, C., KERTESZ, C., SONTAG, R., KOEHLY, G., Separation Science and Technology 15 4 (1980) 745.
17 FITOUSSI, R., Ph D Thesis (1980) CEA-R-5152 (1981)

SYNTHETIC INORGANIC ION EXCHANGERS AND THEIR POTENTIAL USE IN THE NUCLEAR FUEL CYCLE

A. CLEARFIELD
College Station,
Texas A and M University,
Texas, United States of America

Abstract

This paper describes the structure and principal ion exchange characteristics of acid salts of polyvalent metals and hydrous oxides. The acid salts can be prepared in crystalline (layered) form, as amorphous gels and in intermediate stages of crystallinity. Ion exchange behavior is then related to the crystallinity of the exchanger. Separations of importance to nuclear technology are also described. The acid salts can be classified into five types based upon structure. The hydrous oxides are considered to fall into two main types. Those such as ZrO_2, TiO_2 and SnO_2 consist of small particles of oxide with hydrated surfaces and interparticle water. The nature of the surface is described and related to the ion exchange properties of the hydrous oxide. Other hydrous oxides such as Sb_2O_5 and MnO_2 are described in terms of the pyrochlore and spinel structures, respectively. It is suggested that the properties of these exchangers can be controlled to greater specificities through synthetic procedures.

1. Introduction

The phenomenon of ion exchange in inorganic compounds is now known to be very widespread. Among the major classes of compounds we may cite

1. clays
2. zeolites
3. hydrous oxides
4. acid salts of polyvalent metals
5. heteropoly acid salts
6. synthetic apatites
7. insoluble ferrocyanides
8. insoluble sulfides and sulfates
9. condensed phosphates and titanates

In addition a large range of miscellaneous exchangers is known so that a systematization based on structural principles and

exchange behavior is highly desirable. In this paper we shall confine ourselves to the acid salts of polyvalent cations and to a lesser extent to certain hydrous oxides. Even here a bewildering array of crystalline and amorphous phases are known. Attempts at systematization and new directions for synthesis of exchangers with greater specificities will be described.

The original discovery and subsequent exploitation of acid salts of polyvalent cations grew out of the need for ion exchangers with greater stability to elevated temperatures and the effects of radiation damage [1,2]. These compounds were initially prepared as amorphous gels and an extensive literature on these gels developed [3,4]. In 1964 gelatinous zirconium phosphate was crystallized and its layered nature demonstrated [5]. This compound, $Zr(HPO_4)_2 \cdot H_2O$, has now been designated as α-ZrP. Shortly thereafter a second variety of zirconium phosphate, $Zr(HPO_4)_2 \cdot 2H_2O$, was crystallized [8]. It has an interlayer distance of 12.2Å compared to 7.6Å for α-ZrP and is very likely a different layer type. It will be referred to as γ-ZrP.

In the intervening time period, a large number of layered inorganic ion exchangers have been prepared [7] so that it is useful to classify them by structure type. In this we follow the scheme proposed by Alberti [8]: (1) Exchangers with α-layered structure; (2) Exchangers with γ-type layered structure; (3) Exchangers with fibrous structure; (4) Compounds with a three-dimensional structure; and (5) Acid salts of unknown structure.

2. Exchangers of the α-Layered Type

2.1 Preparation

A listing of some of the compounds with α-layered structures is given in Table 1 [8]. They are prepared from their respective gels by refluxing in strong phosphoric or arsenic acid. The crystallization is gradual and the degree of crystallinity of the products depends upon the concentration of acid used and the reflux time [5,9]. This is shown in Fig. 1. To achieve an average crystallite size of 1-2μm for α-ZrP requires 14 days of refluxing in 12M H_3PO_4. The process may be greatly speeded up by autoclaving in 14M acid at 200-250°C. Large crystals can be prepared by dissolving a titanium or zirconium salt in HF and adding H_3PO_4, followed by slow evaporation at 60°C [10-12]. For most purposes small crystallites, such as are obtained in 1-2 hr of refluxing may be used.

Table 1. Some important acid salts of tetravalent metals with layered structure of the α-type.

Compound	Formula	Inter-layer distance (Å)	Ion-exchange capacity meq/g
Titanium phosphate	$Ti(HPO_4)_2 \cdot H_2O$	7.56	7.76
Zirconium phosphate	$Zr(HPO_4)_2 \cdot H_2O$	7.56	6.64
Hafnium phosphate	$Hf(HPO_4)_2 \cdot H_2O$	7.56	4.17
Germanium(IV) phosphate	$Ge(HPO_4)_2 \cdot H_2O$	7.6	7.08
Tin(IV) phosphate	$Sn(HPO_4)_2 \cdot H_2O$	7.76	6.08
Lead(IV) phosphate	$Pb(HPO_4)_2 \cdot H_2O$	7.8	4.79
Titanium arsenate	$Ti(HAsO_4)_2 \cdot H_2O$	7.77	5.78
Zirconium arsenate	$Zr(HAsO_4)_2 \cdot H_2O$	7.78	5.14
Tin(IV) arsenate	$Sn(HAsO_4)_2 \cdot H_2O$	7.8	4.80

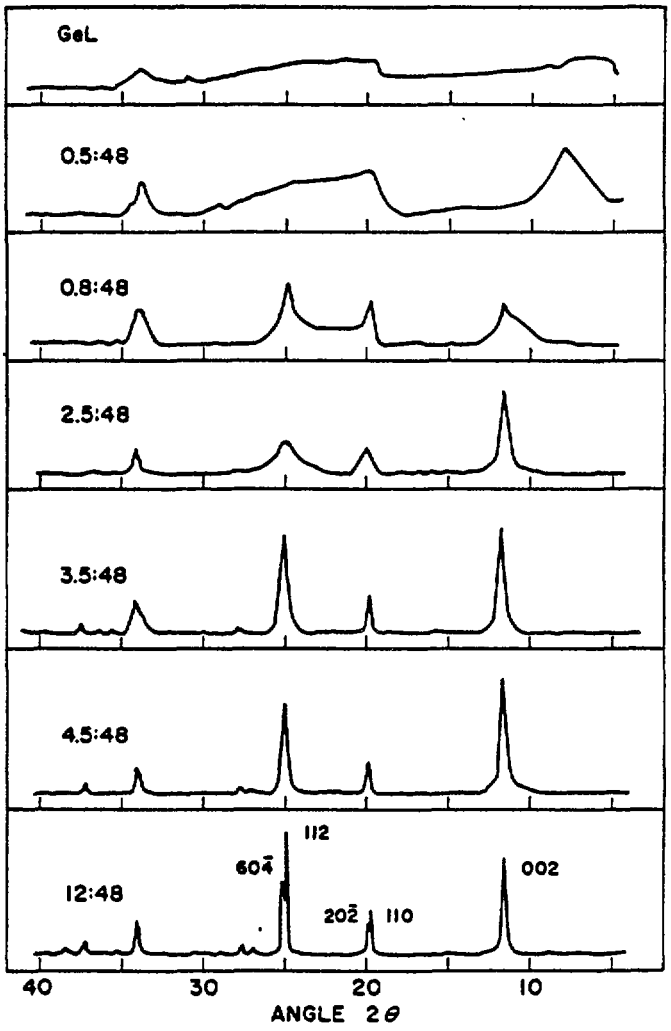

X-ray powder patterns of α-zirconium phosphates of different degrees of crystallinity. Numbers above each pattern indicate concentration of H_3PO_4 and time of reflux.
(From Ref. 9, with permission.)

Fig. 1.

Amorphous gels are prepared by rapid addition of a soluble salt of the cation to the acid. Even if the acid is present in excess, the ratio of phosphate or arsenate to M(IV) is less than two [4]. Stirring for several hours or heating is required to obtain a stoichiometric product. The non-stoichiometric solids can be represented as $M(IV)(OH)_z(HXO_4)_{2-z/2}\cdot YH_2O$ where X = P, As and $0 \leq Z \leq 2$. The ion exchange behavior and other properties of these acid salts depend upon the composition and degree of crystallinity. This will be discussed in more detail following a discussion of the α-structure.

2.2 Structure of the α-layered compounds

The crystal structure of both α-zirconium phosphate [13,14] and arsenate [15] have been determined. The layers consist of metal atoms which very nearly lie in a plane (±0.25Å from the plane) and are bridged by phosphate (arsenate) groups. These are situated alternately above and below the metal atom plane. Three oxygen atoms of each phosphate group are bonded to three different zirconium atoms which form a distorted equilateral triangle. The coordination of the metal atoms is therefore six-fold. The adjacent layers are arranged so as to form six sided cavities as shown in Fig. 2. Each of the oxygen atoms not bonded to a metal atom bears a proton and forms part of the cavity walls. The P-OH groups hydrogen bond to the water molecules which reside in the center of the cavities [16]. There is just one mole of cavities per formula weight and the free volume into the cavities is that of an unhydrated K^+.

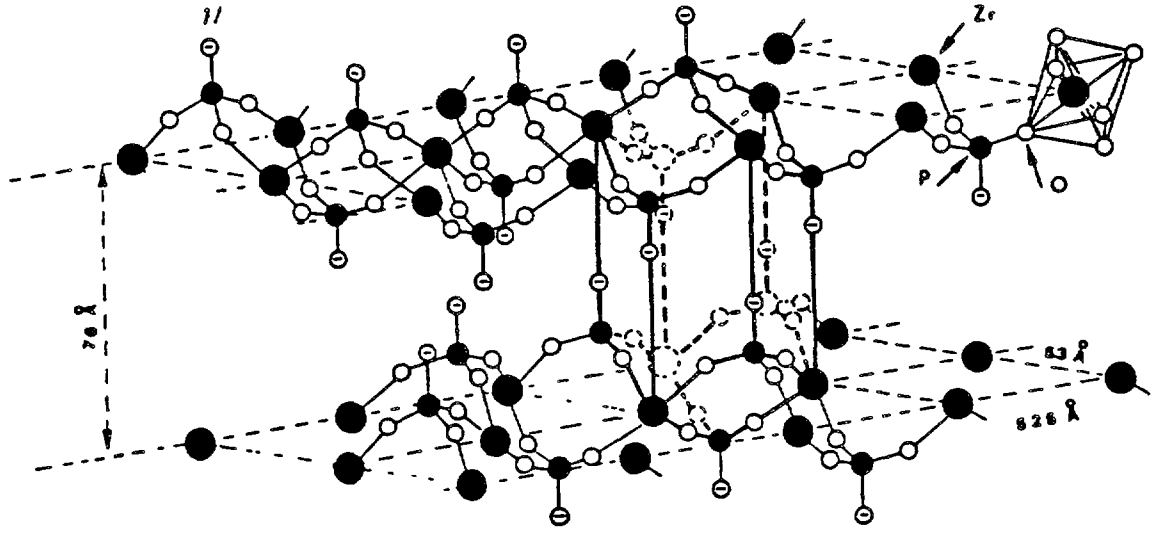

Fig. 2. Idealized structure of α-ZrP showing one of the zeolite like cavities created by the layer arrangement. (From Alberti, G. in "Study Week on Membranes," Passino, R., Ed., Pontificiae Academie Scientarum Scripta Varia, Rome, 1976, 629, with permission.)

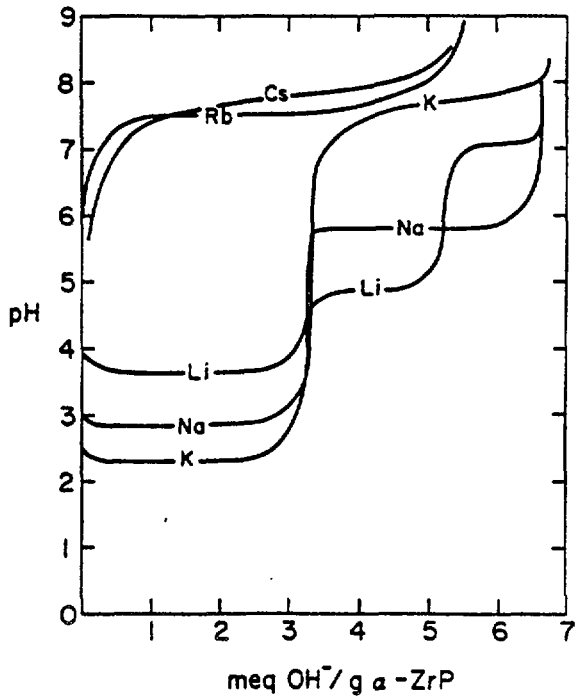

Fig. 3. Potentiometric titration curves for alkali metal ions on α-ZrP (12:336). The Cs^+ curve was obtained on a less crystalline exchanger. (From Ref. 17, with permission.)

2.3 Ion Exchange Behavior of Crystals

The ion exchange behavior of α-ZrP crystals is conditioned by the tight binding of the layers and the small entranceways into the interlayer cavities. This is illustrated by the ion exchange titration curves of Fig. 3 [7,17]. Li^+, Na^+ and K^+ are exchanged in acid solution to form half-exchanged phases of the type $ZrMH(PO_4)_2 \cdot XH_2O$. The ions take up positions in the interlayer spaces which requires diffusion of unhydrated ions into the crystal lattice. Thus, the selectivity favors the more weakly hydrated cation viz. $K^+ > Na^+ > Li^+$. Rb^+ and Cs^+ do not exchange in acid solution since, even in the unhydrated condition, they are too large to diffuse in between the layers. However on addition of base, it is thought that OH^- removes protons from the lattice causing the layers to open somewhat and permit diffusion of the larger ions. In alkaline medium a 3/4 phase $ZrM_{1.5}H_{0.5}(PO_4) \cdot XH_2O$ is formed rather than the half-exchanged type [17].

Exchange of ions into the crystalline layered group(IV) phosphates results in discontinuous changes in the interlayer distances. The interlayer distance depends upon the type of phase, i.e., half, three-quarter or fully exchanged, the size of the entering cation and the amount of water taken up [7,18]. Thus, the half-exchanged sodium phase has 5 waters of hydration and an interlayer distance of 11.8A while the fully exchanged phase,

$Zr(NaPO_4)_2 \cdot 3H_2O$ has an interlayer spacing of 9.8A [19]. The hydrated sodium ion is too large to enter between the α-ZrP layers and therefore must shed some of its waters of hydration to diffuse into the layers. Rehydration of the Na^+ with expansion of the layers then occurs for the pentahydrate. Diffusion begins at the edges and works toward the center so that at intermediate stages of exchange both the unexchanged or proton form and the exchanged phase are present in the same crystal [18]. This mechanism results in irreversible exchange behavior in the forward versus the backward directions [7,18].

The differences in ion exchange behavior of crystalline group(IV) phosphates which have an α-layered structure arise from the different sizes of their unit cell dimensions. The smaller these dimensions, the smaller the dimensions of the openings into the cavities, and the greater the steric hindrance to cations. Furthermore, as the product of the cell dimensions within the layers (a x b) decreases, the density of fixed charges (i.e. phosphate groups) increases creating a greater barrier to ion diffusion. Therefore, higher pH values are required for exchange to occur, i.e. to spread the layers apart. In the salt forms of the exchanger the forces holding the layers together are essentially coulombic. Thus, it is likely that these forces become greater as the density of fixed charges increases. The stronger the forces holding the layers together, the more rigid they become and the more likely are the exchangers to exhibit ion-sieve effects [8].

From the foregoing it is evident that cation exchange on the α-layered acids will not occur in highly acid solutions. Under milder conditions where exchange takes place, the exchange behavior becomes complicated because of the formation of a second phase. This is usually a half-exchanged cation phase which has a larger interlayer spacing than the original α-phase. Thus if a third cation is present, it may interact with the half-exchanged phase to give complicated phase relationships. A number of studies have been carried out to elucidate these phase relationships as a necessary prelude to chromatographic separations [20,21]. Other approaches to utilizing the crystalline phases in chromatographic procedures involve expanding the layers prior to exchanging cations. These procedures will be discussed subsequently.

2.4 Ion Exchange Behavior of Gels

Amorphous gels of zirconium phosphate behave very differently from the crystals. In the early literature very little attention

was paid to preparative methods and to proper characterization of the gels. This led to irreproducible behavior. The reasons for this are now well understood [4,22]. If during preparation the mol ratio of phosphate to zirconium is less than two, precipitation still occurs; but the product is a hydroxyphosphate, $Zr(OH)_x(HPO_4)_{2-x/2}$. In such gels the ion exchange behavior of the hydroxyl groups must be considered as well as those of the monohydrogen phosphate groups. Even when the ratio of phosphate to zirconium exceeds two in the reactant mix, the precipitate which first forms may have a ratio lower than two [22]. However on aging the precipitate in the mother liquor, its phosphate content increases and in the limit P/Zr = 2. Ratios higher than this indicate sorbed phosphate [4]. Greater resistance to hydrolysis and more reproducible behavior result if the gel is refluxed in about 0.5M H_3PO_4 for 10 hours or more [9]. When dried thoroughly over P_2O_5 the refluxed gels have the same composition as the crystals, but they swell in water taking up an additional 4 moles of H_2O. This property of the gels allows them to exchange rather large cations as the interlayer distances are greatly increased by the swelling.

A typical Cs^+ titration curve for a gel that has been refluxed in 0.5M H_3PO_4 for 48h is shown in Fig. 4. In contrast to the crystals where the pH remains relatively constant at ca. 7.5 - 8 with ion uptake, each increment of Cs^+ exchanged results in an increase in pH. There are no breaks or endpoints in the curve and the process is reversible [9]. This is similar to results obtained with weak acid organic resin ion exchangers except that the effect is much more marked. It indicates that the cation is uniformly distributed in the gel to form a solid solution rather than clustering in adjacent cavities to form a new phase as in the crystals

The gel behaves as a weak field exchanger in the sense of Eisenman's theory [23] and the selectivity is $Cs^+ > Rb^+ > K^+ > Na^+ > Li^+$ [24]. As the cation content increases, the selectivities change gradually in the way predicted by Eisenman's theory, that is, to the strong field situation with $Li^+ > Na^+ > K^+ > Rb^+ > Cs^+$. The interlayer distance attains a maximum at relatively low cation uptake and then decreases with further loading [9]. Thus the cations are brought closer and closer to the negative sites of the layers with consequent increase in field strength.

2.5 Semi-crystalline Exchangers

By refluxing a gel in phosphoric acid of different concentrations and for different lengths of time, it is possible to build in any desired amount of crystallinity [5,9]. The particle

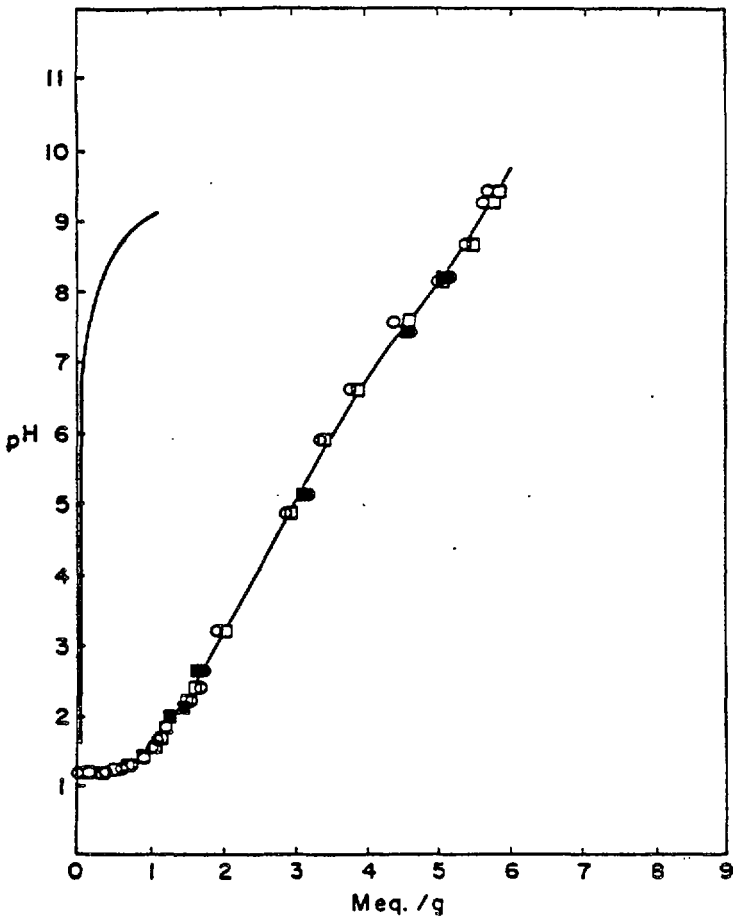

Fig. 4. Potentiometric titration curve for Cs^+ uptake (Titrant 0.1N CsCl+CsOH) on amorphous zirconium phosphate (0.5:48). Solid line at left is phosphate release to the solution. (From Clearfield, A., Oskarsson, A. Ion Exchange and Membranes, 1, (1974) 205, with permission.)

size of the refluxed product increases with increase in crystallinity, and the titration curves change in a continuous fashion from the gel type to that exhibited by the crystals [4,9,25]. This is shown in Fig. 5. As the crystallinity increases the solid solution range decreases for each of the phases formed. For example, with a gel that had been refluxed in 4.5M H_3PO_4 for 48 hours, Na^+ is initially taken up with no phase change. At a loading of 0.25 meq/g the half-exchanged phase appears and increases in amount relative to the sodium containing α-phase until at 3 meq/g load it is the only phase present. The composition range for the half-exchanged phase is approximately 3-3.45 meq/g. This may sound like a contradiction in terms, but by the half-exchanged phase for a semi-crystalline preparation we mean, a solid whose X-ray pattern resembles that of the true half exchanged phase, $ZrM^+H(PO_4)_2 \cdot XH_2O$, but with broadened reflections.

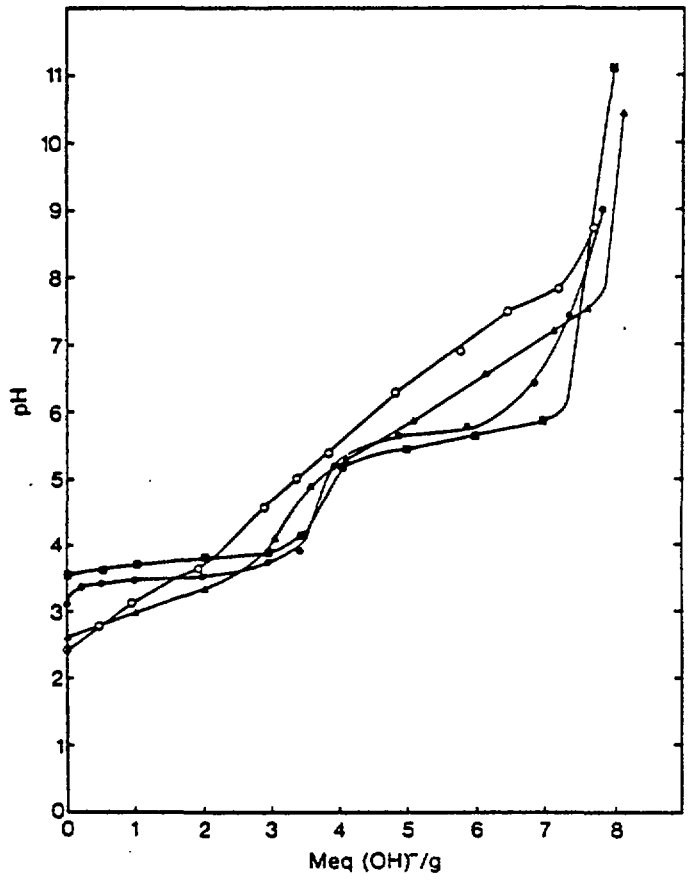

Fig. 5. Titration curves for α-ZrP of low and intermediate crystallinity: 0.8:48 -○, 2.5:48 -▲, 4.5:48 -●, 12:48 -■. (From Ref. 9, with permission.)

2.6 Cation Separations

As a guide to carrying out cation separations several comprehensive determinations of distribution coefficients for amorphous zirconium phosphate have been published [26,27]. Similiar values for amorphous zirconium tungstate and molybdate were included [27]. The trouble with this data is that the exchangers were poorly characterized so that the results serve only as a rough guide. The effect of crystallinity of the exchanger on measured distribution coefficients of divalent ions was measured by Tuhtar [28]. His results are shown in Fig. 6. A dramatic decrease in K_d as a function of increasing crystallinity is observed due largely to the exclusion of highly hydrated cations by the small passageways between the layers. The same trend is exhibited by tri- and tetravalent cations [28].

A rather complete summary of possible cation separations by group(IV) phosphate gels has recently been published [29]. In this paper we shall confine ourselves to those separations related to nuclear processes. ^{137}Cs has been separated from nuclear reprocessing solutions [30,31]. Distribution coefficients and some

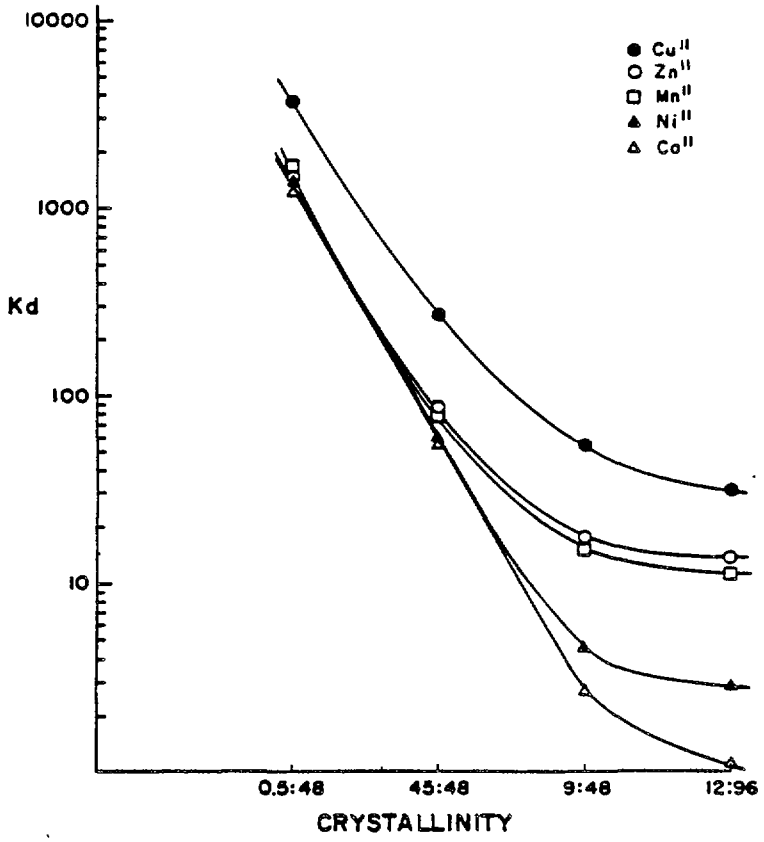

Fig. 6. Variation of distribution coefficient (at almost zero load) with increasing crystallinity of α-ZrP.

chromatographic data for recovery of Cs^+ and Sr^{2+} from reprocessing solutions has also been given [32,33]. Separation of Ba^{2+} from other divalent cations [34] and Cs^+ [35] has been reported.

Amorphous zirconium phosphate has received a great deal of attention for separation of radioactive ions because of its resistance to ionizing radiation, oxidizing media and strong acid solutions [36]. The sorption of tracer concentrations of Am(III), Cm(III), Bk(IV), Cf(III), Ce(III), Eu(III) and U(VI) on ZrP with P/Zr = 1.34 was investigated at 75°C [37]. It was found that separation factors for ions with the same charge are low, whereas those for ions with different oxidation states were large. It was suggested that Bk(IV) could be separated from the trivalent ions. A good separation of americium from curium had also been reported [38].

A number of procedures are based upon the fact that better separations are effected on zirconium phosphate if the cations differ in oxidation state. For example, Am(III) is separated from Cm(III) by first oxidizing it to Am(V). The Cm(III) is preferentially retained on the column [38-40].

This general procedure has also been applied to neptunium-plutonium separations [44], Np(V) - Pu(IV) - Pr(III) [42] and

Ce(IV) - Pr(III) - Cm(III) separations [43]. It has been found that separations which take advantage of different oxidation states may be further enhanced by use of non-aqueous solvents [44]. The sharp decline in K_d for the lower valent state contrasts with the increase to a maximum for the higher valent state as the alcohol content goes to 50%. These differences are attributed to the relative stabilities of the chloro-complexes formed by the two ions in the changing solvent composition. In fact it has led to a method of determining the stability constants of these and related uranium complexes as well as improved separations [45,46]. Distribution coefficients for Th, Pa, U, Np and Pu were also measured and procedures for their separation outlined [47]. Separation of uranyl ion from several di- and trivalent cations has also been described [48].

2.7. Nuclear Waste Processing and Water Purification.

The original search for new inorganic ion exchangers was instigated by the desire for materials stable in intense radiation fields and at high temperatures. Early efforts in this direction have already been mentioned [1-3,35]. Zirconium phosphate has indeed been found to be stable to radiation [49,50], but exhibits increased hydrolysis at elevated temperatures. Resistance to hydrolysis is increased by use of semicrystalline zirconium phosphate as shown by Ahrland and Carleson [51]. Even so, a mixed hydrous zirconia-zirconium phosphate column was used to prevent phosphate bleeding during purification of dilute solutions containing transition metal ions.

A method for separating ^{137}Cs from fission products has been used by the French Atomic Energy Commission which utilizes a mixed bed of ZrP and ammonium phosphotungstate [52]. We have already mentioned the separation of uranium from plutonium on amorphous zirconium phosphate with P/Zr = 1.34. The effect of added fission products was also assessed.

Other interesting applications of zirconium phosphate include the removal of ^{106}Ru and ^{95}Zr from purex solvent [53] and separation of parent-daughter radioisotopes such as ^{115}Cd - ^{115m}In, ^{144}Ce - ^{144}Pr and ^{210}Pb - ^{210}Bi [54].

2.8 Ion Exchange with Expanded Layer Zirconium Phosphates

From the earlier discussion on crystalline α-ZrP it is evident that its usefulness for separations is severely limited. However, it turns out that it is relatively easy to increase the interlayer distance of α-ZrP by a number of processes. In the expanded layer forms the barrier to diffusion of large cations is drastically

reduced. Therefore, exchange processes can take place without the use of added base. The half-exchanged sodium form, $ZrNaH(PO_4)_2 \cdot 5H_2O$ has an interlayer distance of 11.8Å [19]. It behaves as a monofunctional exchanger with a capacity of 2.53 meq/g [55]. Kornyei and Szirtes have reported [56] the separation of strontium from radioactive wastewater on $ZrNaH(PO_4)_2 \cdot 5H_2O$.

If sufficient acid is added to remove the sodium ion from $ZrNaH(PO_4)_2 \cdot 5H_2O$, α-ZrP is not obtained but rather a higher hydrate containing 5-6 moles of H_2O and named θ-ZrP [19,57]. This exchanger has an interlayer spacing of 10.4Å so that it accepts large cations more readily than α-ZrP. This is shown in Fig. 7 where potentiometric titrations for alkaline earth cations on α-ZrP and θ-ZrP are compared [58]. As yet no cation separations have been carried out with θ-ZrP, but this would seem to be a fruitful area for investigation.

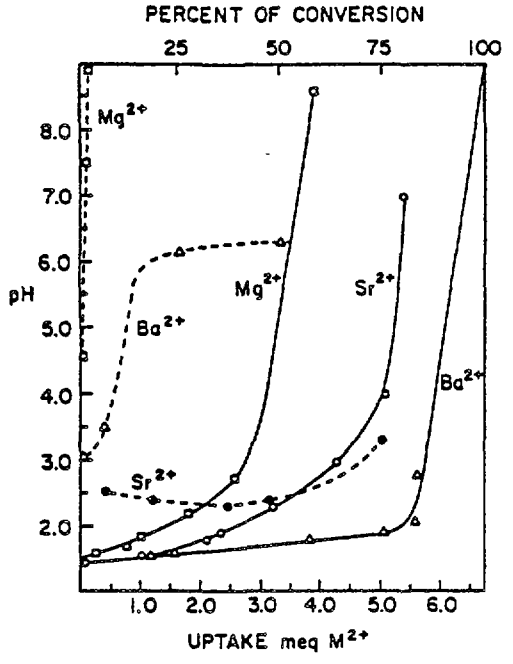

Fig. 7. Potentiometric titration curves for alkaline earth cations on θ-ZrP (solid lines) and α-ZrP (dashed lines).
(From Ref. 58, with permission.)

Another way of expanding the layers of α-ZrP is by amine intercalation [59]. For example, in the butylamine intercalate the interlayer spacing is 18.6Å and this is large enough to put complex ions in between the layers [60,61]. In this case the amine acts to keep the pH high so that no added base is required to load ions into the exchanger. Up to 4-5 meq/g of divalent ions may be exchanged and multiple ions can be loaded. Thus it would seem that this could be the basis for many cation separation techniques.

3. Exchangers of the γ-Layered Type

Only two members of this series are known; γ-ZrP [6] and γ-TiP [62]. These compounds are not merely more highly hydrated forms of α-compounds but have different, as yet unknown, types of layers [63,64]. Because the interlayer distances of these two compounds are large, 12.2Å and 11.6Å, respectively, they are able to exchange large cations and complexes [65,66]. However due to the closeness of the fixed charges, hydrolysis becomes severe at high levels of exchange. A highly crystalline form has recently been prepared [67] which may be less susceptible to hydrolysis. The selectivity sequence at low to moderate loadings as obtained from titration data is $K^+ > Rb^+ > Cs^+ > Na^+ > Li^+$ [65]. I view of this sequence, it is surprising that an extremely high affinity for Cs^+ by γ-ZrP has been reported [68], high enough to recommend its use in reactor water cleanup.

4. Acid Salts With Fibrous Structure

Members of this group include cerium(IV) phosphate (CeP_f) [69] thorium phosphate (ThP_f) [70] and titanium phosphate and arsenate [8,71]. These fibrous compounds have been used to prepare inorganic ion-exchange papers, or thin layers, suitable for fast separations of cations [72]. The fibers are prepared by adding dropwise 0.05M $Ce(SO_4)_2 \cdot 4H_2O$ in 0.5M H_2SO_4 to a well stirred solution of 6M H_3PO_4 previously heated to 95°C. Flexible sheets can be obtained by dispersing the fibrous precipitate in a large volume of water, then filtering the slurry in a large Buchner funnel. The formula of CeP_f is probably $Ce(HPO_4)_2 \cdot H_2O$, but its structure is unknown.

5. Acid Salts with Three-Dimensional Structure

This class includes compounds with the general formula $AM_2(IV)(XO_4)_3$ [(M(IV) = Ti, Zr, Th, Ge; X = P, As and A = any univalent cation]. We have prepared these compounds by thermal decomposition of exchanged forms of α-ZrP [7,19] and by hydrothermal means [73,74]. $HZr_2(PO_4)_3$ may be prepared by treating $LiZr_2(PO_4)_3$ with acid [8] or thermal decomposition of $NH_4Zr_2(PO_4)_3$ [74]. The structure of these triphosphates is shown in Fig. 8 [75]. It is built up of Zr bridged to Zr through 3 phosphate groups. This arrangement produces M(IV) octahedra linked by corners to the tetrahedra the whole forming a three dimensional network containing cavities which are of two types.

There are four cavities per formula, one of which is occupied by Na^+. Silicate can replace part or all of the PO_4^{3-} and this requires additional Na^+ ions to progressively fill up the remaining cavities [76,77]. The silicate ions enlarge the cavities sufficiently to allow relatively free movement of the univalent

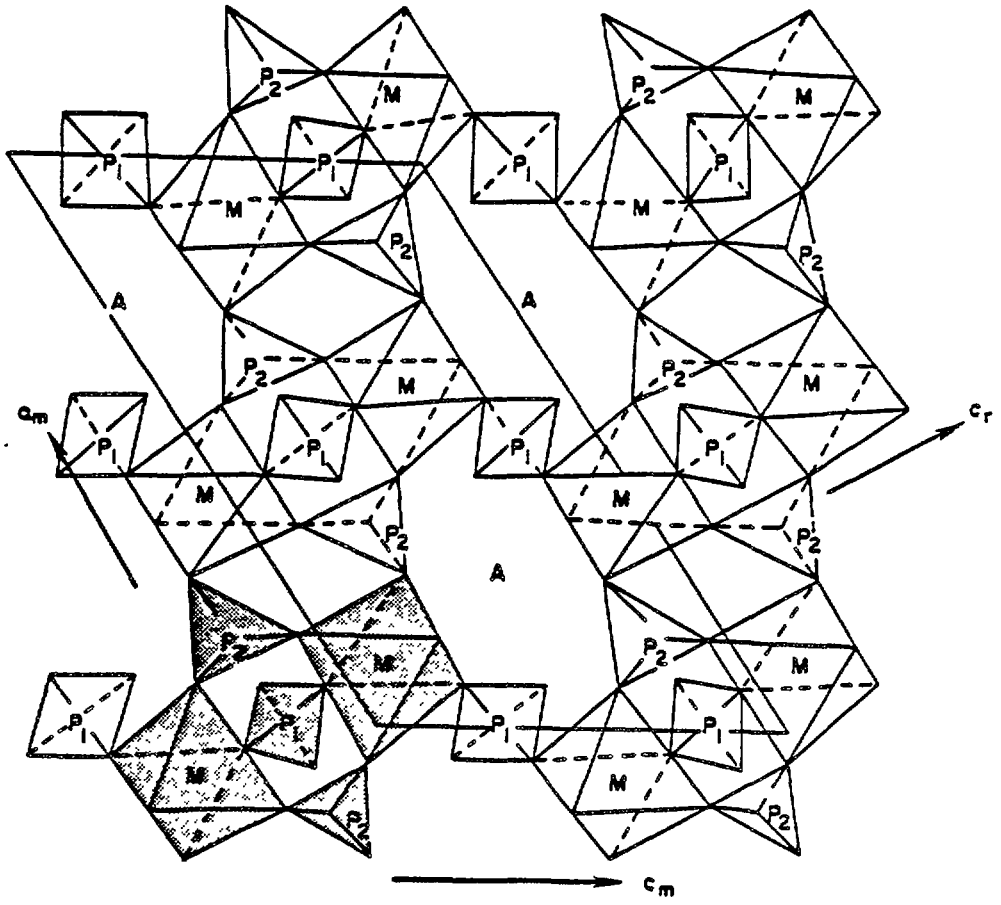

Fig. 8. Projection of half the unit cell of $NaZr_2(PO_4)_3$ onto the ac plane, showing the cavity built up by the $Zr_2(PO_4)_3^-$ groups. Numbers next to the atoms indicate height (in hundredths) above the zero level plane. (From Ref. 76, with permission.)

cations when about 2/3 of the phosphate groups are replaced. The Na^+ ions can now be exchanged by Li^+ or H^+. Similiar Li^+-H^+ exchange reactions are possible with $HZr(PO_4)_3$. Since the cavity and passageway sizes and exchange capacity can be modified over a broad range by choice of M^{4+}, the XO_4 anion and substitutions for M^{4+}, it should be possible to prepare exchangers in this system which are highly selective and stable to high temperature, radiation fields and a broad range of pH. This idea is extended to other systems in the next section.

6. Hydrous Oxides and other "Amorphous" Exchangers

A number of hydrous oxides including TiO_2, ZrO_2, MnO_2 and antimonic acid have been examined for use in nuclear processes. The exchange characteristics of these compounds has been summarized and reviewed in a recent book [7]. Hydrous titania readily sorbs uranium [78] and has been considered for extraction of uranium from sea water [79,80]. Hydrous oxides were also used in the purification and isolation of neptunium, plutonium [81,82] americium and berkelium [83].

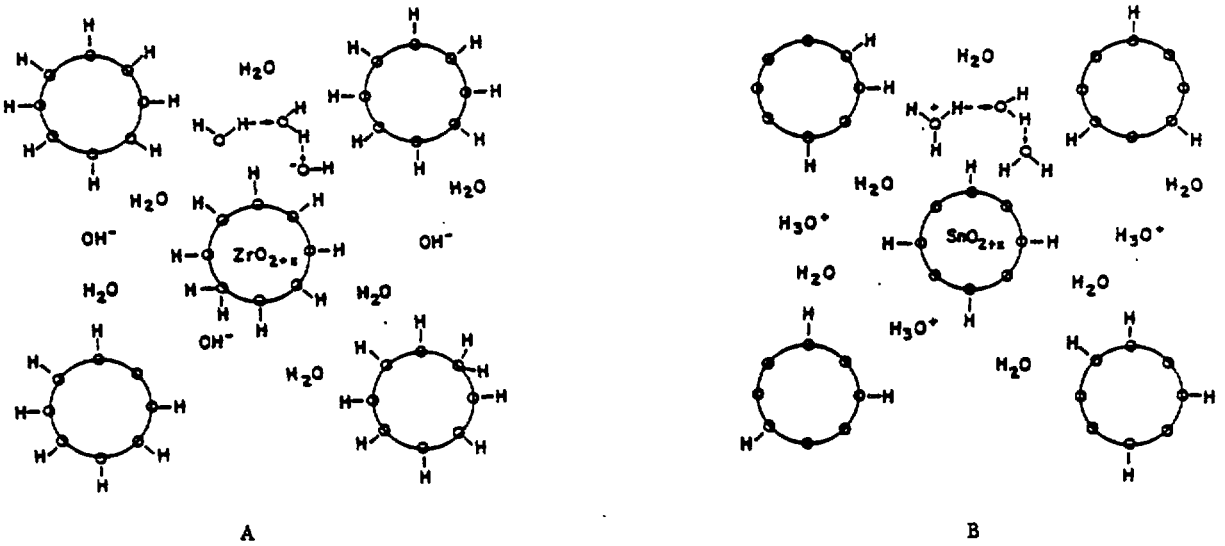

Fig. 9. Schematic representation of hydrous oxide particles. A. $ZrO_2 \cdot nH_2O$ with hydroxyl ion in the intercrystalline water neutralizing the positively charged particle surface; B. $SnO_2 \cdot nH_2O$ with H_3O^+ in the intercrystalline water neutralizing the negatively charged particle surface.

A simple structual model of hydrous oxides of the TiO_2, ZrO_2, SnO_2 type has recently been given [84]. The solid precipitated by ammonia consists of particles ca. 25-30A in diameter. In the interior of these particles the structure is that of a crystalline anhydrous oxide [85]. These small particles are joined together to form agglomerates containing large cracks and fissures. The full metal coordination is preserved at the surface by partial coordination of H_2O. The remaining water molecules form an interparticle solution, the acidity of which depends upon the degree of protonation of the surface oxygens. By aging or refluxing it is possible to obtain more crystalline forms of these oxides. A detailed description of how amorphous and crystalline hydrous zirconia are formed from solutions of the tetrameric zirconyl ion has been given by Clearfield [86]. The formula of these hydrous oxides is best represented [84] as $[MO_a(OH)_b(H_2O)_{R-a+b}]^{4-(2a+b)} + S$. On the assumption that all the metal atoms are fully coordinated, the oxygen-metal ratio, R, will be greater than 2. For the fluorite structure (ZrO_2) a 25A cubic particle will have R = 2.15. The extra oxygen atoms at the surface must be supplied by water molecules. The remaining water molecules, S, form the interparticle solution. Whether S is acidic (SnO_2) or basic (ZrO_2) depends on the degree of protonation of the oxygens at the particle surface. This is illustrated schematically in Fig. 9. In the basic limit, the surface oxygens are supplied by terminal H_2O and metal bridging OH^-; in the acidic limit the oxygens are bare O^{2-} ions making the particle charge negative with compensating H_3O^+ in the interparticle solution.

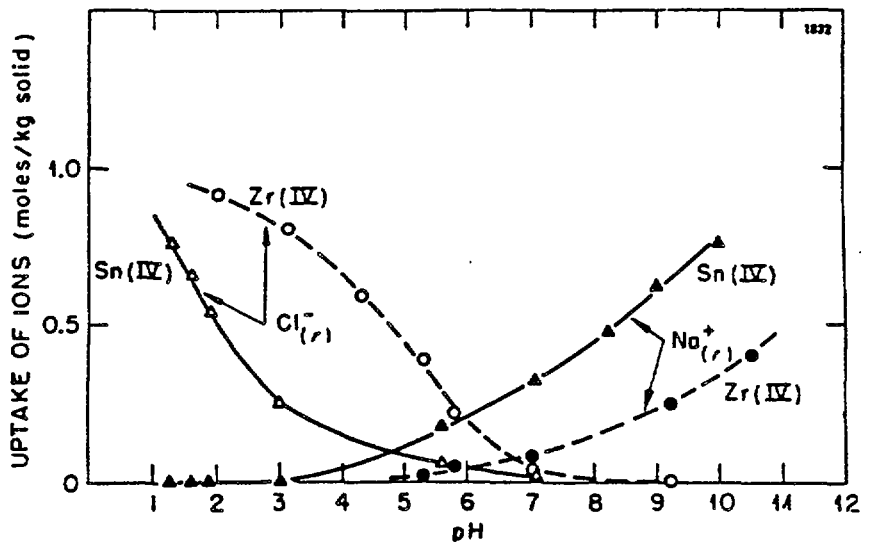

Fig. 10. Ion exchange capacity versus pH for hydrous tin and zirconium oxides.

Based on the foregoing picture of hydrous oxides, hydrous tin oxide should readily exchange cations in acid solution because H_3O^+ is present in the interparticle solution. A more basic oxide such as that of zirconium would require higher pH values to exchange cations because the OH^- in the interparticle water must be neutralized first before surface protons will detach from the surface oxygens. The opposite is then true for anion exchange. This is illustrated in Fig. 10 [35]. The exchange capacity for cations will increase with increasing pH but in the limit depends upon the total removable protons on the surface. The selectivity for a particular ion will not only depend upon these factors but also the complex formation constant of the surface-ion complex.

In contrast to the foregoing picture crystalline antimonic acid exchanges only cations and exhibits the anomalous selectivity sequence [87] $Na^+ > K^+ > Rb^+ > Cs^+ > Li^+$. This is attributed to the fact that antimonic acid has a pyrochlore structure with an $(Sb_2O_6)^{2-}$ framework with almost $3H_2O$ distributed over the A_2O' interpenetrating framework [84]. The water molecules would be expected to be in the 16d and 8b sites with two protons in the A^+ sites. Thus, the formula $Sb_2O_5 \cdot 3.9H_2O$ is structurally represented as $(H_3O)_2Sb_2O_6 \cdot 0.9H_2O$ in analogy with the $A_2B_2O_6$ pyrochlore representation. There is no interparticle water as it is all in the crystal lattice. The theoretical exchange capacity, 5.08 meq g^{-1}, matches the experimental one, 5.1 meq g^{-1}. Furthermore, antimonic acid behaves as a strong acid exchanger with a relatively constant exchange capacity over a large pH range.

Recently a layered form of $HSbO_3 \cdot XH_2O$ was prepared by ion exchange from the ilmenite form of $KSbO_3$ [88]. Similiar reactions were carried out to prepare $HNbO_3$ and $HTaO_3$. When the starting phases were the pyrochlore thallium salts, heating them in 3N HNO_3

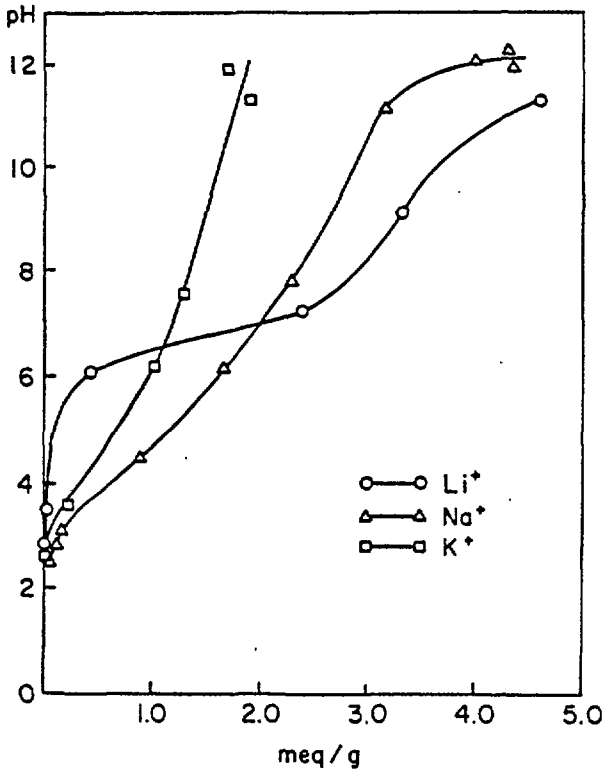

Fig. 11. Potentiometric titration of hydrous MnO_2 by the static method. Titrant 0.1M (MCl + MOH) with M = Li^+ - ○, Na^+ - △ and K^+ - □.

converted them to the corresponding acids $HNbO_3 \cdot XH_2O$ and $HTaO_3 \cdot XH_2O$ with retention of pyrochlore structure [88]. However if lithium niobate or tantalate were used as starting phases the acid products had a perovskite structure [89].

We have recently examined hydrous manganese dioxide prepared electrolytically [90]. The exchange capacity depends upon the temperature of preparation but for most samples is about 4.6 meq/g. The exchanger behaves in some respects as a hydrous oxide, its capacity changing with pH; but it also exhibits ion sieve behavior. This is shown in the titration curves in Fig. 11. The exchange capacity for K^+ is about 1/3 the theoretical capacity and much lower than that for either Na^+ or K^+. However in acid solution, the distribution coefficients indicate the selectivity sequence $K^+ > Na^+ > Li^+$. We interpret this data to indicate that the exchanger contains cavities with different sizes. The largest cavities, perhaps those on the surface prefer the largest unhydrated ion, K^+. A second group of intermediate sized cavities can accomodate Na^+ in acid solution and finally in basic solution Li^+ becomes the most preferred cation. However when the fully exchanged Li^+ form of hydrous manganese dioxide was heated at 500°C, it formed a weakly crystalline λ-MnO_2 and on washing out the Li^+ with acid showed a remarkably high selectivity for Li^+. This λ-MnO_2 is related to the spinel $LiMn_2O_4$ [91] and Thackeray, et al. have shown that Li^+ can be replaced by H^+ in this spinel [92]. All of this suggests possible routes to the synthesis of new inorganic ion exchangers

with high selectivities for individual ions and great temperature and radiation stability. We have mentioned that pyrochlores, spinels, illmenites, perovskites and triphosphates can all be converted to acid forms and that certain hydrous oxides can take on these crystalline structures. By synthesizing many of these phases hydrothermally, or from gels, in the presence of a particular ion it may be possible to alter the structure or size of the cavities or tunnels to be highly specific for ions which easily fit into the structure. A case in point is zirconium phosphosilicate. It is prepared by treating a zirconium silicate gel with H_3PO_4 [93]. This exchanger has been examined at length for sorption and separation of lanthanides [94] and for separation of neptunium from berkelium [96]. Decontamination factors of 3000 and 200 were obtained for the separation of Pu from ^{95}Zr + ^{95}Nb and ^{106}Ru, respectively [96]. The large change in distribution coefficients which this exchanger exhibits with pH change suggests its amorphous hydrous nature. However we have succeeded in converting such gels into crystalline triphosphate-like phases under mild conditions. The ion exchange behavior of these exchangers is under active investigation.

7. Acknowledgement

The work carried out in the author's research laboratory was supported by the National Science Foundation under grants numbered CHE81-14613 (Chemical Division) and DMR80-25184 (Division of Materials Research) for which grateful acknowledgement is made.

8. References

[1.] RUSSELL, E.R., ADAMSON, A.W., SHUBERT, J., BOYD, G.E., "Decontamination of product by adsorption on tailor-made inorganic adsorbents", U.S.A.E.C. Rep. CN-508 (1943).

[2.] KRAUS, K.A., PHILLIPS, H.O., J. Amer. Chem. Soc. 78 (1956) 644.

[3.] AMPHLETT, C.B., Inorganic Ion Exchangers, Elsevier, Amsterdam (1964).

[4.] AHRLAND, S., ALBERTSSON, J., JOHANSSON, L., NIHLGARD, B., NILSSON, L., Acta Chem. Scand. 18 (1964) 1346, 1357.

[5.] CLEARFIELD, A., STYNES, J.A., J. Inorg. Nucl. Chem. 26 (1964) 117.

[6.] CLEARFIELD, A., BLESSING, R.H., STYNES, J.A., J. Inorg. Nucl. Chem. 30 (1968) 2249.

[7.] CLEARFIELD, A., "Zirconium phosphates", Inorganic Ion Exchange Materials (Clearfield, A., Ed.) CRC Press, Boca Raton, Florida (1982).
[8.] ALBERTI, G., Ref 7, Ch. 2.
[9.] CLEARFIELD, A., OSKARSSON, A., OSKARSSON, C., Ion Exch. Membr. 1 (1972) 9.
[10.] ALBERTI, G., TORRACCA, E.J., Inorg. Nucl. Chem. 30 (1968) 317.
[11.] ALBERTI, G., COSTANTINO, U., GIULIETTI, R., J. Inorg. Nucl. Chem. 42 (1980) 1062.
[12.] INOUE, Y., YAMADA, Y., Bull. Chem. Soc. Jpn. 52 (1979) 3528.
[13.] CLEARFIELD, A., SMITH, G.D., Inorg. Chem. 8 (1969) 431.
[14.] TROUP, J.M., CLEARFIELD, A., Inorg. Chem. 16 (1977) 3311.
[15.] CLEARFIELD, A., DUAX, W.L., Acta Cryst. B25 (1969) 2658.
[16.] ALBERTSSON, J., OSKARSSON, A., TELLGREN, R., THOMAS, J.O., J. Phys. Chem., 81 (1977) 1574.
[17.] KULLBERG, L., CLEARFIELD, A., J. Phys. Chem. 85 (1981) 1585.
[18.] ALBERTI, G., Acc. Chem. Res., 11 (1978) 163.
[19.] CLEARFIELD, A., DUAX, W.L., MEDINA, A.S., SMITH, G.D., Thomas, J.R., J. Phys. Chem. 73 (1969) 3424.
[20.] KULLBERG, L., CLEARFIELD, A., J. Inorg. Nucl. Chem. 43 (1981) 2543.
[21.] KULLBERG, L., CLEARFIELD, A., Solvent Extraction and Ion Exchange 1 (1983) 77.
[22.] AHRLAND, S., ALBERTSSON, J., JOHANSSON, L., NIHLGARD, B., NILSSON, L., Acta Chem. Scand. 18 (1964) 707.
[23.] EISENMAN, G., Biophys. J. 2 (1962) 259.
[24.] KULLBERG, L., CLEARFIELD, A., J. Phys. Chem. 85 (1981) 1578.
[25.] CLEARFIELD, A., KULLBERG, L., OSKARSSON, A., J. Phys. Chem. 78 (1974) 1150.
[26.] AKATSU, E., ONO, R., TSUKUECHI, K., UCHIRYOMA, H., J. Nucl. Sci. Tech. 2 (1965) 141.
[27.] MAECK, W.J., KUSSY, M.E., REIM, J.E., Anal. Chem. 35 (1963) 2086.
[28.] TUHTAR, D., Ph.D. Thesis Ohio University Athens (1975).
[29.] CLEARFIELD, A., Sep. Sci., in press.
[30.] PROSPERT, J., "Some Properties of Zirconium Phosphate", Rappt. CEA-R 2835 Commissariat A L'Energie Atomique Paris (1966).
[31.] PROSPERT, J., LEFEVRE, J., RAGGENBASS, A., "Recovery of cesium-137 using a mineral ion exchanger", Communaute Eur. Energ. At. EURATOM EUR-4075 (1968).

[32.] BAETSLE, L.H., VAN DEYCK, D., HUYS, D., GUERY, A., "The use of inorganic ion exchangers in acid medium for the recovery of Cs and Sr from reprocessing solutions", AEC Accession No. 7613 Rept. No. BLG-267 (1964).

[33.] BAETSLE, L. HUYS, D., J. Inorg. Nucl. Chem. 21 (1961) 133.

[34.] NUNEZ-CORTES, M.P.M., SANCHEZ-BUTANERO, P., Afinidad 37 (1980) 451.

[35.] KRAUS, K.A., PHILLIPS, H.O., CARLSON, T.A., JOHNSON, J. S., "Ion exchange properties of hydrous oxides", 2nd UN Conference on Peaceful Uses of Atomic Energy, Geneva (1958) 1832.

[36.] GAL, I., RUVARAC, A., J. Chromatogr. 13 (1964) 549.

[37.] HOROWITZ, E.P., J. Inorg. Nucl. Chem. 28 (1966) 1469.

[38.] MOORE, F.L., Anal. Chem. 43 (1971) 487.

[39.] SHAFIEV, A.I., EFREMOV, Yu.V., NIKOLAEV, V.M., YAKOVLEV, G.N., Radiokhimiya 13 (1971) 129.

[40.] SHAFIEV, A.I., EFREMOV, Yu.V., ANDREEV, V.P., Radiokhimiya 15 (1973) 265.

[41.] CHERNORUKOV, N.G., KORSHUNOV, I.A., PROKOF'EVA, T.V., ZHUK, M.I., MOSKVICHEV, E.P., S'ezd Obshch. Prikl. Khim 1 (1975) 270.

[42.] SHAFIEV, A.I., EFREMOV, Yu.V., NIKOLAEV, V.M., YAKOVLEV, G.N., Radiokhhimiya 13 (1971) 126.

[43.] SHAFIEV, A.I., EFREMOV, Yu.V., Radiokhimiya 14 (1972) 771.

[44.] SOUKA, N., ABDEL-REHIM, F., J. Radioanal. Chem. 23 (1974) 43.

[45.] ALY, H.F., ABDEL-RASSOUL, A.A., ZAKAREIA, N., Z. Physik. Chem. Neue Folge. 94, (1975) 11.

[46.] ALY, H.F., MAREI, S., ZAKAREIA, N., Mikrochim. Acta 1 (1973).

[47.] SOUKA, N., ABDEL-GAWAD, A.S., SHABANA, R., FARAH, K., Radiochim. Acta 22, (1975) 180.

[48.] GAL, I., PERIC', N., Microchim. Acta 251 (1965) 251.

[49.] BORN, E., PAUL, G., Z. Kristallogr. 146 (1977) 19.

[50.] ZSINKA, L., SZIRTES, L., MINK, J., KALMAN, A., J. Inorg. Nucl. Chem. 36 (1974) 447.

[51.] AHRLAND, S., CARLESON, G., J. Inorg. Nucl. Chem. 33 (1971) 2229.

[52.] RAGGENBASS, A., COUROUBLE, J.M., LEFEBVRE, J., FRADIN, J., PEREBASKINE, C., "ELAN: Installation for the recovery and packaging cesium-137 in France", AEC Accession No. 39319, Rep. DP-1066, Vol. 2, Paris (1966).

[53.] TURCANU, C.N., RADU, D., Radiochem. Radioanal. Letters 43 (1980) 245.
[54.] BHATTACHARYYA, D.K., BASU, S., J. Radioanal. Chem. 47 (1978) 105.
[55.] ALBERTI, G., COSTANTINO, U., GUPTA, J.P., J. Inorg. Nucl. Chem. 36 (1974) 2103.
[56.] KORNYEI, J., SZIRTES, L., Izotoptechnika, 23 (1980) 243.
[57.] CLEARFIELD, A., LANDIS, A.L., MEDINA, A.S., TROUP, J.M., J. Inorg. Nucl. Chem. 35 (1973) 1099.
[58.] ALBERTI, G., COSTANTINO, U., GILL, J.S., J. Inorg. Nucl. Chem. 38 (1976) 1733.
[59.] COSTANTINO, U., "Intercalation behavior of group IV layered phosphates", Inorganic Ion Exchange Materials (Clearfield, A., Ed.) CRC Press, Boca Raton, Florida (1982) chap. 3.
[60.] CLEARFIELD, A., TINDWA, R.M., Inorg. Nucl. Chem. Letter. 15 (1979) 251.
[61.] QUAYLE, L.R., CLEARFIELD, A., Inorg. Chem. 21 (1982) 4197.
[62.] ALLULLI, S., FERRAGINA, C., LAGINESTRA, A., MASSUCCI, J.A., TOMMASSINI, N., J. Inorg. Nucl. Chem. 39 1977 1043.
[63.] YAMANAKA, S., TANAKA, M., J. Inorg. Nucl. Chem. 41 (1979) 45.
[64.] ALBERTI, G., COSTANTINO, U., GIOVAGNOTTI, M. L., J. Inorg. Nucl. Chem. 41 (1979) 643.
[65.] CLEARFIELD, A., GARCES, J.M., J. Inorg. Nucl. Chem. 41 (1979) 879.
[66.] CLEARFIELD, A., KALNINS, J.M., J. Inorg. Nucl. Chem 40 (1976) 1933.
[67.] YAMANAKA, S., Inorg. Chem. 15 (1976) 2811.
[68.] KOMARNENI, S., ROY, R., Nature 299 (1982) 707.
[69.] ALBERTI, G., COSTANTINO, U., DI GREGORIO, F., GALLI, P., TORRACCA, E., J. Inorg. Nucl. Chem. 30 (1968) 295.
[70.] ALBERTI, G., COSTANTINO, U., J. Chromatog. 50 (1970) 482.
[71.] ALBERTI, G., COSTANTINO, U., ALLULLI, S. TOMASSINI, N., J. Inorg. Nucl. Chem. 40 (1978) 1113.
[72.] ALBERTI, G., MASSUCCI, M.A., TORRACCA, E., J. Chromatog. 30 (1967) 579.
[73.] CLEARFIELD, A., JERUS, P., COTMAN, R.N., PACK, S.P., Mat. Res. Bull. 15 (1980) 1603.
[74.] CLEARFIELD, A., ROBERTS, B., SUBRAMANIAN, M.A., Mat. Res. Bull. 19 (1984) 219.
[75.] HAGMAN, L.O., KIERKEGAARD, P., Acta. Chem. Scand. 12 (1968) 1822.

[76.] HONG, H.Y-P. Mat. Res. Bull. 11 (1976) 173.
[77.] GOODENOUGH, J., HONG, H.Y-P., KAFALAS, J.A., Mat. Res. Bull. 11 (1976) 20.
[78.] YAMASHITA, H., NAKAJIMA, F., Bull. Chem. soc. Jpn. ISSN 0009-2676, 53 (1980) 1 and 53 (1980) 3050.
[79.] KANNO, M. "Extraction of uranium from seawater", Rep. IAEA-CN 36/161, Vienna (1977).
[80.] BETTINALI, C., PANTANETTI, F., "Uranium from seawater: possibilities of recovery exploiting slow coastal currents", Proc. Advis. Group Meet., 1975 IAEA, Vienna (1976).
[81.] KORSHUNOV, I.A., CHERNORUKOV, N.G., PROKOF'EVA, T.V., Radiochimya 18 (1976) 5.
[82.] KENNEDY, J., PECKETT, J.W., PERKINS, R., "The removal of plutonium and certain fission products from alkaline media by hydrated titanium dioxide", U.K. At. Ener. Auth. Res. Group At. Ener. Estab. Rep. AERE-R-4516 U.K. At. Energy Establishment, Harwell (1964).
[83.] MYASOEDOV, B.F.,Usp. Anal. Khim. 148 (1974).
[84.] ENGLAND, W.A., CROSS, M.G., HAMNETT, A., WISEMAN, P.J., GOODENOUGH, J.B., Solid State Ionics 1 (1980) 231.
[85.] CLEARFIELD, A., Inorg. Chem. 3 (1964) 146.
[86.] CLEARFIELD, A., Rev. Pure Appl. Chem. 14 (1964) 91.
[87.] ABE, M., J. Inorg. Nucl. Chem. 41 (1979) 85.
[88.] CHOWDHRY, U., BARKLEY, J.R., ENGLISH, A.D., SLEIGHT, A.W., Mat. Res. Bull. 17 (1982) 917.
[89.] RICE, C.E., JACKEL, J.L., J. Solid State Chem. 41 (1982) 308.
[90.] SHEN, X-M., CLEARFIELD, A., work in progress.
[91.] THACKERAY, M.M., JOHNSON, P.J., DE PICCIOTTA, L.A., BRUCE, P.G., GOODENOUGH, J.B., Mat. Res. Bull. 19 (1984) 179.
[92.] DAVID, W.I.F., THACKERAY, M.M., BRUCE, P.G., GOODENOUGH, J.B., Mat. Res. Bull. 19 (1984) 99.
[93.] NAUMANN, D., Kernenergie 6 (1963) 173.
[94.] MAREI, S.A., BOTROS, N., Talanta 27 (1980) 599.
[95.] OOMS, R., SCHONKEN, P., D'OLIESLAGER, W., BAETSLE, L., D'HONT, M., J. Inorg. Nucl. Chem. 36, (1974) 665.
[96.] MYASOEDOV, B.F., BARSUKOVA, K.V., RODIONAVA, G.N., Radiochem. Radioanal. Lett. 7 (1971) 269.
[97.] NAQUI, S.J., Nucleus 8 (1970 - published 1971) 76.

FUNDAMENTAL PROPERTIES OF ACID SALTS OF TETRAVALENT METALS AND SOME CONSIDERATIONS ON THE PERSPECTIVES OF THEIR APPLICATION IN NUCLEAR TECHNOLOGY

G. ALBERTI
Department of Chemistry,
Perugia University,
Perugia, Italy

Abstract

Beginning from 1964, acid salts of tetravalent metals started to be obtained as crystalline materials and research was essentially focused for many years in their syntheses and structures. Now that the chemistry of these inorganic ion-exchangers is well enough established, interest has turned to their uses in various technological fields. Among them, their employment in the nuclear fuel cycle as well as in the recovery, separation and purification of some radionuclides is very attractive.
After a brief survey in the syntheses and classification of the various acid salts and their derivatives and after a short review of the ion-exchange properties of zirconium phosphate and its salt forms with α and γ lamellar structures some properties such as hydrolysis and stability towards temperature and ionizing radiations, that are of fundamental importance for their use in nuclear technology, are reported and discussed.

1. Introduction

Acid salts of tetravalent metals have been known for a long time only as amorphous materials [1]. Because of their high ion-exchange capacity and for their good stability to acid and oxidizing solutions as well as to temperature and ionizing radiations, the potential uses of these materials were subject to intense investigations in the decade 1954 - 1964, especially in nuclear centers. The success was however very limited, essentially because of the great tendency of

the amorphous acid salts to hydrolyze in alkaline or even in neutral warm solutions.

Beginning from 1964, acid salts of tetravalent metals started to be obtained as crystalline materials and research was essentially focused for many years in their syntheses and structures, as well as in the determination of their fundamental properties.

To-day, after two decady of research carried out on these materials in various laboratories, a large number of crystalline acid salts with lamellar, fibrous and three dimensional structures has been obtained and their fundamental properties determined.

A vast literature has accumulated and it is currently well known that acid salts of tetravalent metals are members of a very wide class of inorganic compounds[2-5].

Now that the chemistry of these materials is well enough established, interest has again turned to their uses in various technological fields. Among them, their employment in the nuclear fuel cycle, in the recovery, separation and purification of some radionuclides as well as in the treatment of effluents from nuclear powder plants, is still very attractive. Furthermore the crystalline acid salts, contrary to the amorphous ones, have definite chemical compositions and structures. The study of their ion-exchange properties is therefore considerably facilitated by a knowledge of their crystalline structure, phase transitions during ion-exchange processes, thermal behaviour and so on.

Useful information can be obtained and even some predictions on their potential applications in nuclear technology can be made, if the presently known fundamental properties of these materials are taken into careful consideration.

For this reason, it is useful to divide the crystalline acid salts into various subclasses according to their composition and crystalline structure and to give a brief account

on the known fundamental properties of each subclass with particular attention to those useful for a better understanding of ion-exchange behaviour.

2. Classification of acid salts of tetravalent metals.

Acid salts of tetravalent metals can be considered as being constituted by macroanions carrying fixed negative charges which are neutralized by protons or other counterions.
A classification can therefore be made on the basis of the composition and structure of their macroanions.
To date, two different kinds of macroanions are known:

$$\left[M^{IV}(XO_4)_2\right]_n^{2n-} \quad \text{and} \quad \left[M^{IV}_2(XO_4)_3\right]_n^{n-}$$

where M^{IV} = Ti, Zr, Hf, Ge, Sn, Pb, Ce, Th while X is an element of the fifth group (usually P and As).
Table 1 reports such a type of classification. Note that the structure of the $\left[M^{IV}(XO_4)_2\right]_n^{2n-}$ macroanion may be either a fibrous or a lamellar one. In turn, two different lamellar structures, usually called α and γ lamellar structures are known at present [2-4].

Table 1

Classification of acid salts of tetravalent metals according to their composition and crystalline structure of the macroanion.

$\left[M^{(IV)}(XO_4)_2\right]_n^{2n-}$	Amorphous	
	linear (or fibrous structure)	
	bidimensional (or lamellar) structure	α-type / γ-type
$\left[M_2^{(IV)}(XO_4)_3\right]_n^{n-}$	amorphous	
	threedimensional structure	at least 2 different modification

M(IV) = Zr, Ti, Ge, Sn; Ce; Th..... X = P; As; Sb.

To give a complete picture of the classification of the acid salts of tetravalent metals it must also be remembered that lamellar compounds having the general formulae $\left[M^{IV}(RXO_3)_2\right]_n$; $\left[M^{IV}(R\text{-}OXO_3)_2\right]_n$ and $\left[M^{IV}(O_3XRXO_3)\right]_n$, where R is an organic radical, have recently been obtained [6,7].

These compounds are known as organic derivatives of acid salts. If the organic R group contains an acid group such as -COOH and $-SO_3H$, the organic derivative may be considered as an organic-inorganic ion-exchanger [8,9].

Because of their potential uses in nuclear technology, our attention will be essentially focused on lamellar zirconium phosphates and on the threedimensional acid salts with skeleton structure. It seems that the presently known fibrous acid salts are not very stable to hydrolysis and to high doses of ionizing radiations [10] while the organic derivatives are expected to exhibit less resistence to drastic working conditions than pure inorganic exchangers.

3. Acid salts with α-layered structure.

Some important acid salts with α-layered structure are listed in Table 2. Among them, the α-zirconium phosphate is

Table 2

Some important acid salts of tetravalent metals with layered structure of the α-type.

Compound	Formula	Interlayer distance (Å)	Ion exchange capacity meq/g
Titanium phosphate	$\left[Ti(PO_4)_2\right]H_2\cdot H_2O$	7.56	7.76
Zirconium phosphate	$\left[Zr(PO_4)_2\right]H_2\cdot H_2O$	7.56	6.64
Hafnium phosphate	$\left[Hf(PO_4)_2\right]H_2\cdot H_2O$	7.56	4.17
Germanium(IV) phosphate	$\left[Ge(PO_4)_2\right]H_2\cdot H_2O$	7.6	7.08
Tin(IV) phosphate	$\left[Sn(PO_4)_2\right]H_2\cdot H_2O$	7.76	6.08
Lead(IV) phosphate	$\left[Pb(PO_4)_2\right]H_2\cdot H_2O$	7.8	4.79
Titanium arsenate	$\left[Ti(AsO_4)_2\right]H_2\cdot H_2O$	7.8	5.78
Zirconium arsenate	$\left[Zr(AsO_4)_2\right]H_2\cdot H_2O$	7.78	5.14
Tin(IV) arsenate	$\left[Sn(AsO_4)_2\right]H_2\cdot H_2O$	7.8	4.80

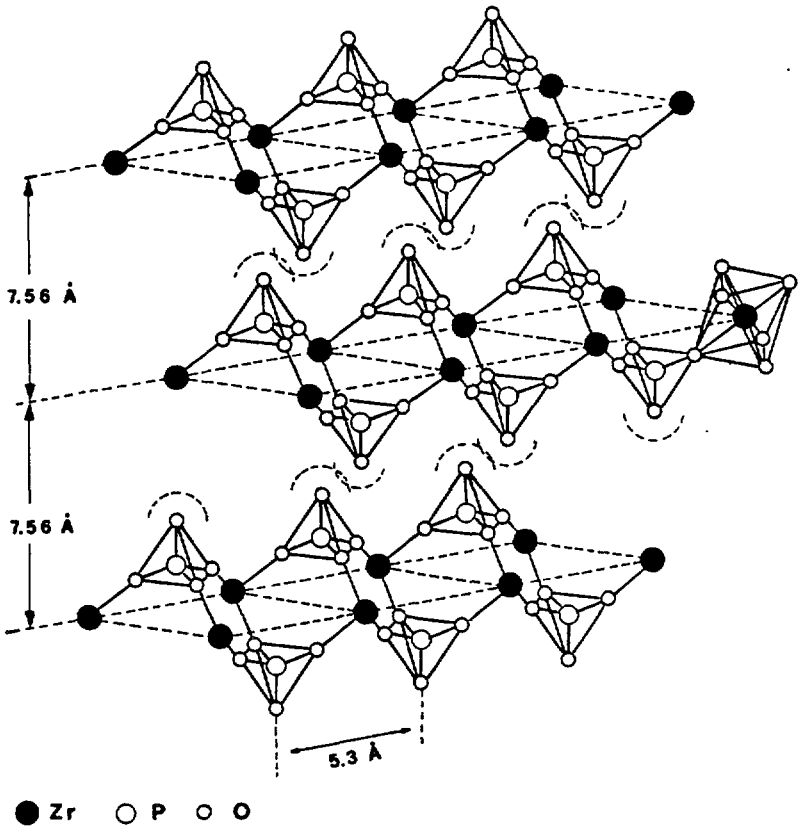

Fig. 1. Schematic structure of layered α-$\left[Zr(PO_4)_2\right]H_2 \cdot H_2O$ (protons and water are not shown in the figure).

certainly the fullest investigated and the most stable to hydrolysis. Our attention will therefore be focused on this compound. Its layered structure was first elucidated by Clearfield [11] . A schematic representation of the arrangement of three layers of α-$\left[Zr(PO_4)_2\right]_n^{2n-}$ planar macroanions is shown in Fig. 1. The distance between adjacent negative charges is 5.3 Å. The layered crystals may be regarded as packed macroanions with intercalated counterions. Consequently, the interlayer distance will depend on the arrangement, volume and solvation of the inter-lamellar counterions.

The packing of the layers creates cavities in the interlayer region (one for each zirconium atom) where there is room enough for accommodating one water molecule or large divalent cations such as Ba^{2+} [2].

Such cavities are interconnected by narrow windows whose dimensions depend on the interlayer distance.

In α-$[Zr(PO_4)_2]H_2 \cdot H_2O$ (d = 7.56 Å) there is a strong steric hindrance to the diffusion of counterions with ionic diameter larger than 2.6 Å. Thus, at acid pH values, only a small number of cations (e.g. Li^+, Na^+, Ag^+, Tl^+, Cu^+, Ca^{2+}) is able to exchange the protons of α-$[Zr(PO_4)_2]H_2 \cdot H_2O$.
Potassium and strontium give slow but appreciable ion-exchange rates while, in the case of large monovalent and divalent cations such as NH_4^+, Rb^+, Cs_2^+ and Ba^{2+} or highly hydrated divalent or trivalent cations such as Mg^{2+}, Co^{3+} etc., the protons in the inter-lamellar region cannot be appreciably exchanged even after several days of contact with aqueous solutions of these cations at room temperature. Thus, α-$[Zr(PO_4)_2]H_2 \cdot H_2O$ seems to be a poor exchanger. However, zirconium phosphate is not such a rigid exchanger as zeolites; as the interlayer distance is increased there is a correspondent increase in the dimensions of the windows connecting the cavities and cations of large size can be exchanged.
Various possibilities are currently known for obtaining considerable enlargement of the original interlayer distance. For example, a naked or partially hydrated Na^+ ion diffuses very easily in the interlayer region replacing one proton for each cavity [2,3]. Once inside the cavities it tends to rehydrate and water is forced to enter too.
Since there is no room in the original cavities for water accommodation, the interlayer distance increases until an equilibrium between hydration and expansion of the interlayer distance is reached. At room temperature this process can be summarized as follows:

$$\underset{(7.56\ \text{Å})}{\overline{H_2 \cdot H_2O}} + Na^+_{aq.} \longrightarrow \underset{(11.9\ \text{Å})}{\overline{HNa.5H_2O}} + H_3O^+$$

where barred species refer to the exchanger phase while numbers in brackets give the corresponding interlayer distances. Owing to its large interlayer distance, the

monosodium form is now able to exchange large cationic species such as Cs^+, Ba^{2+} as well as highly hydrated divalent or trivalent cations [12-14,2,3].

For example, the ion-exchange processes with Cs^+, Ba^{2+} and Cr^{3+} are as follows:

$$\overline{HNa\cdot 5H_2O} + Cs^+_{aq.} \longrightarrow \overline{HCs} + Na^+_{aq.}$$
(11.9 Å) (8.0 Å)

$$\overline{HNa\cdot 5H_2O} + 0.5\ Ba^{2+}_{aq.} \longrightarrow \overline{HBa_{0.5}\cdot 4H_2O} + Na^+_{aq.}$$
(11.9 Å) (10.0 Å)

$$\overline{HNa\cdot 5H_2O} + 0.5\ Cr^{3+} \longrightarrow \overline{H_{0.5}Cr_{0.5}\cdot 4H_2O} + 0.5H_3O^+ + Na^+_{aq.}$$
(11.9 Å) (11.6 Å)

It was found in our laboratory [15,16] that large cations can easily be exchanged even in the original α-$[Zr(PO_4)_2]H_2\cdot H_2O$ if small amounts of Na^+ are present in the external solution. The sodium ion acts as an ion-exchange catalyst in the sense that there is a considerable increase of the ion-exchange rate while, after the ion-exchange process, all the added Na^+ was found to be present in the aqueous solution. The mechanism of this catalytic behaviour can be understood by taking into account that the diffusion begins at the edges of the crystals and proceeds towards the inner part. As an example, Fig. 2 shows schematically the Ba^{2+} exchange in the presence of added Na^+. Initially only Na^+ ions are able to exchange the protons of the exchanger by enlarging the interlayer distance of the external part of the crystal to 11.8 Å.

This expansion permits the diffusion of the Ba^{2+} which exchanges the Na^+ ions within the enlarged cavities. The exchanged Na^+ ions go towards the inner part replacing other protons and enlarging another fraction of the crystals and so on. At the end of the process, when all the protons are exchanged Na^+

ion must come back to the aqueous solution since the selectivity of the exchanger for Ba^{2+} is much higher than for Na^{+}.
There exists another possiblity for the exchange of large cationic species in crystalline zirconium phosphate [3,17].

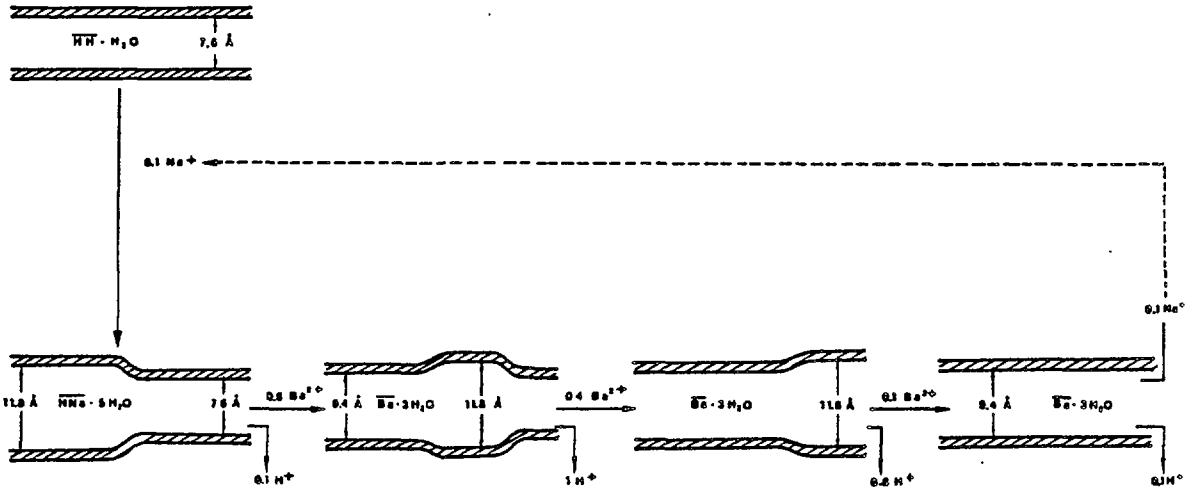

Fig. 2 – Catalytic effect of Na^{+} on the exchange of large cations on α-$[Zr(PO_4)_2]H_2 \cdot H_2O$ (schematic)

When the monosodium form is regenerated into the hydrogen form with dilute mineral acids, the original α-$[Zr(PO_4)_2]H_2 \cdot H_2O$ is no longer obtained but one has instead a pentahydrate form (usually called ϑ-zirconium phosphate) with an interlayer distance of 10.4 Å. The process is the following:

$$\overline{HNa \cdot 5H_2O} + H_3O^{+} \longrightarrow \overline{H_2 \cdot 5H_2O} + Na_{aq.}$$

(11.9 Å) (10.4 Å)

Also, the replacement of the Na^{+} ion with some alcohols in acid media (e.g. ethanol acidified with HCl) gives intercalates with a high interlayer distance. When these intercalates are put in contact with water, the alcohol is replaced by water and α-$[Zr(PO_4)_2]H_2 \cdot 5H_2O$ is obtained .
The zirconium phosphate pentahydrate is a very selective exchanger for large cations and deserves further attention.
When air-dried four molecules of water are lost with an irreversible conversion into α-$[Zr(PO_4)_2]H_2 \cdot H_2O$. Thus α-$[Zr(PO_4)_2]H_2$.

$5H_2O$ must be kept wet. We are presently studying its thermal stability in water and preliminary results seem to show that α-zirconium phosphate possesses a good stability up to 150°C. In conclusion, many possibilities are known to-day for obviating the steric hindrance to the diffusion of large cationic species in the interlayer region of α-zirconium phosphate. This exchanger can therefore be used for the exchange of the most part of monovalent, divalent and trivalent cations.
The problem is now the following: what is the chemical and thermal stability of zirconium phosphate for applications at high temperature? Its high thermal stability in air is well known [3,19,20]. At a temperature rate of 2°C/min, the thermal behaviours is the following:

$$\underset{(7.56\ \text{Å})}{\left[Zr(PO_4)_2\right]H_2\cdot H_2O} \xrightarrow[-H_2O]{110°C} \underset{(7.41\ \text{Å})}{\left[Zr(PO_4)_2\right]H_2} \xrightarrow{220°C} \underset{(6.80\ \text{Å})}{\left[Zr(PO_4)_2\right]H_2}$$

$$\xrightarrow{450°-650°C} \underset{(6.10\ \text{Å})}{\frac{1}{2}\,ZrP_2O_7} \xrightarrow{800°-1000°C} \underset{\text{(cubic pyrophosphate)}}{\frac{1}{2}\,ZrP_2O_7}$$

The loss of the hydration water is irreversible and rehydration does not occur even when $\left[Zr(PO_4)_2\right]H_2$ is dipped in cold water. The phase transition at 220°C is instead reversible. The condensation of ≡P-OH groups to lamellar pyrophosphate depends obviously on the experimental conditions of dehydration [21] (e.g. relative humidity, rate of temperature increase etc.) and on the degree of crystallinity. For crystalline samples the condensation does not occur until about 450°C while for its salt-forms condensation cannot occur and the thermal stability is even higher than 500°C.
In conclusion, α-zirconium phosphate may be considered a very stable exchanger in anhydrous conditions; but what happens at high temperature in the presence of water?

Since no data are available in the literature we have carried out some preliminary investigations on the stability of α-$\left[Zr(PO_4)_2\right]H_2 \cdot H_2O$ and its monosodium form.
It was found that α-$\left[Zr(PO_4)_2\right]H_2 \cdot H_2O$ is stable in water at least up to 300°C. Only a reversible dehydration at 200°-300°C was found.

$$\alpha\text{-}\left[Zr(PO_4)_2\right]H_2 \cdot H_2O \underset{}{\overset{200°\text{-}300°C}{\rightleftharpoons}} \alpha\text{-}\left[Zr(PO_4)_2\right]H_2 + H_2O$$

Hydrolysis is negligible and it seems to be limited to the external part of the microcrystals.
In the case of the monosodium form the following behaviour was found:

$$\alpha\text{-}\left[Zr(PO_4)_2\right]HNa \cdot 5H_2O \xrightarrow[-4H_2O]{50°\text{-}100°C} \alpha\text{-}\left[Zr(PO_4)_2\right]HNa \cdot H_2O$$

(11.9 Å) (7.9 Å)

$$\xrightarrow{210°\text{-}250°C} \frac{1}{2}\left[Zr_2(PO_4)_3\right]Na + \frac{1}{2}\,NaH_2PO_4$$

The decomposition into sodium dizirconium threephosphate is irreversible; therefore α-zirconium.phosphate cannot be used in an aqueous medium at temperature higher than 200°C if Na^+ ions are present. This temperature is however high enough for many practical uses.
Another inconvenience for the use of lamellar acid salts is that they are usually obtained as small platelets ($\sim 1\,\mu$)
Thus very compact chromatographic columns are usually obtained. The flows are therefore slow while some particles tend to be released into the external solution. The problem can be overcome by using larger particles. In our laboratory it is now possible to prepare crystals of zirconium phosphate having dimensions of some millimeters [22].
No inconvenience for the preparation of the columns is enountered with large crystals; however, it must be taken in consideration that the rate of exchange decreases when the size of the crystals is increased.

4. Acid salts with γ-layered structure.

Other than with the α-structure already discussed, lamellar acid salts of tetravalent metals have been obtained with a different structure usually known as γ-structure [3,23-25]. Until now single crystals large enough for X-ray structural determination have been not obtained, so present information on the structure of γ-acid salts is very limited. Investigations performed by Yamanaka and Tanaka [23] as well as studies carried out in our laboratory [25] indicate that the γ-structure, similar to α-acid salts, is built up by the packing of planar macroanions $\left[M^{IV}(XO_4)_2\right]_n^{2n-}$ whose negatives charges are neutralized by protons or other counterions. However the structure of the γ-macroanion is different from that of the α-one. The planar density of fixed charges is higher in γ than in α-macroanions (about 1.37 times). Counterions, water and other polar molecules can be arranged in the inter-lamellar region.

Owing to its large interlayer distance, steric hindrance to the diffusiono of large cations is much less than in α-acid salts. In particular, γ-$\left[Zr(PO_4)_2\right]H_2\cdot 2H_2O$ (d = 12.2 Å) seems to be very selective for Cs^+ and its use in nuclear technology has therefore been predicted [26].

5. Acid salts of tetravalent metals with fibrous structure.

The first fibrous acid salt of a tetravalent metal, cerium phosphate, was obtained in out laboratory in 1968 [27]. Subsequently, fibrous thorium phosphate was also obtained [28] and zirconium and titanium phosphates have also recently been prepared by hydrothermal methods [29].
Fibrous inorganic ion exchangers are interesting because they can be used to prepare ion-exchange papers and membranes. A photograph of a sample of $\left[Ce(PO_4)_2\right]H_2\cdot H_2O$ showing its fibrous structure is shown in Fig. 3.
Fibrous acid salts have not been widely investigated and no structures studies are presently available.

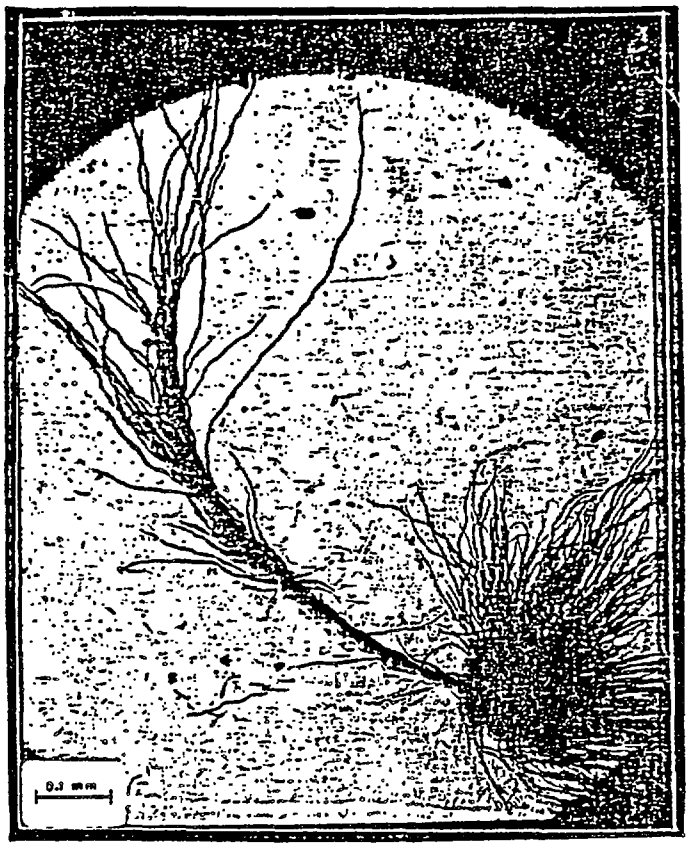

Fig. 3 - Photograph, taken at optical microscope, of a fragment of $Ce(HPO_4)_2 \cdot H_2O$.

Thermal and chemical stability of fibrous cerium phosphate seems to be lower than that of α-zirconium phosphate. Also the resistance to radiation, seems to be lower than that of α-zirconium phosphate [10]. However fibrous cerium phosphate exhibits some particular selectivity (i.e. towards lead) that could be utilized for the separation of radionuclides [7,30]. Furthermore, fibrous acid salts, contrary to the lamellar ones, are suitable materials for the preparation of chromatographic columns or for the preparation of very compact ion-exchange filters.

6. Acid salts of tetravalent metals with skeleton structures.

Compounds of the general formula $\left[M_2^{IV}(XO_4)_3\right]M^I$ have been known for a long time [31,32]. They have usually been prepared by solid state reactions at high temperature (1100°-1400°C).

Their structures may be described in terms of XO_4 tetrahedra and $M^{IV}O_6$ octahedra which are linked by corners to form a threedimensional network.

Although these compounds may be considered as salt forms of acid salts $\left[M^{IV}(XO_4)_3\right]H$, the replacement of M^{IV}_2 counterions with protons is very difficult. However, it was recently found that if the Li-form is prepared by decomposition of α-$\left[Zr(PO_4)_2\right]Li_2$ at 600°-800°C [33]

$$2\left[Zr(PO_4)_2\right]Li_2 \xrightarrow{600\text{-}800°C} \left[Zr_2(PO_4)_3\right]Li + Li_3PO_4$$

or by solid state synthesis at relatively low temperature [34] the replacement of the Li^+ with protons can easily be carried out by single contact with acid solutions. The dizirconium threephosphate in hydrogen form has been found to behave as a narrow ionic sieve. Only H^+, Li^+, Na^+ and Ag^+ can diffuse easily within the exchanger while large monovalent and all the polyvalent cations are not exchanged.

The acid salts of tetravalent metals with skeleton structure can therefore be used for the recovery of Li^+, Na^+ and Ag^+ or for the purification of cationic species, even in very concentrated solutions, from traces of Li^+, Na^+ and Ag^+.

7. Some concluding remarks.

Table 3 reports some important characteristics of some acid salts of tetravalent metals for use in nuclear technology. A great deal of experimental work is still needed to see if some of these materials are indeed useful fro some practical applications in nuclear technology.

Certainly crystalline acid salts exhibit in many cases a complete different behaviour from the corresponding amorphous materials.

Table 3

Important characteristics of some acid salts of tetravalent metals for use in nuclear technology.

Characteristics	Lamellar α-$[Zr(PO_4)_2]H_2 \cdot H_2O$	Lamellar γ-$[Zr(PO_4)_2]H_2 2H_2O$	Fibrous $[Ce(PO_4)_2]H_2H_2O$	Threedimensional $[Zr_2(PO_4)_3]H$
Ion-exchange capacity	Very good	Very good	Very good	Low
Resistance to ionizing radiations	" "	?	Bad	Very good (estimated)
Resistance to oxidizing solutions	" "	Very good	Very good	" " (")
Resistance to reducing solutions	" "	" "	Bad	" " (")
Resistance to acid solutions	" "	Good	Moderate	" " (")
Resistance to alkaline solutions	Bad	Bad	Very bad	Sufficient
Thermal stability in air	Very good up to 450°C	Good	Good	Very good up to 600°C
Thermal stability in water	Very good up to 300°C; bad over 210°C for its monosodium form.	?	?	Very good
Ion-exchange rate	Sufficiently good	Good	Sufficiently good	Sufficiently good
Selectivity	High for Cs^+ Sr^{2+} Ba^{2+} and trivalent cations if Na^+ traces are present.	High for Cs^+ and NH_4^+ ions	High for Pb^{2+}, Ba^{2+}, Cu^{2+} and K^+.	Highly selective for Li^+, Na^+ and Ag^+. Large monovalent cations and polyvalent cations are not exchanged.

Thus many negative results previously obtained with amorphous acid salts should be critically examined in order to see if some inconveniences may be overcome by using the new crystalline acid salts of tetravalent metals. In any case, the investigations on the chemistry of acid salts are continuing in several laboratories and new materials and new properties are continously being found. Referring only to new acid salts recently obtained in our laboratory, we can cite the preparation of pellicular α-zirconium phosphate, [35] the synthesis of α-zirconium phosphate-phosphite [36,37] with composition $[Zr(PO_4)_{0.66}(HPO_3)_{1.33}]H_{0.66}$ and several new organic derivatives of α-zirconium phosphate [38]. We are now studying the ion-exchange properties of these new materials. In particular it was found that zirconium phosphate-phosphite, for its structure (Fig. 4), is able to accommodate in the interlayer region large cationic and polar species.

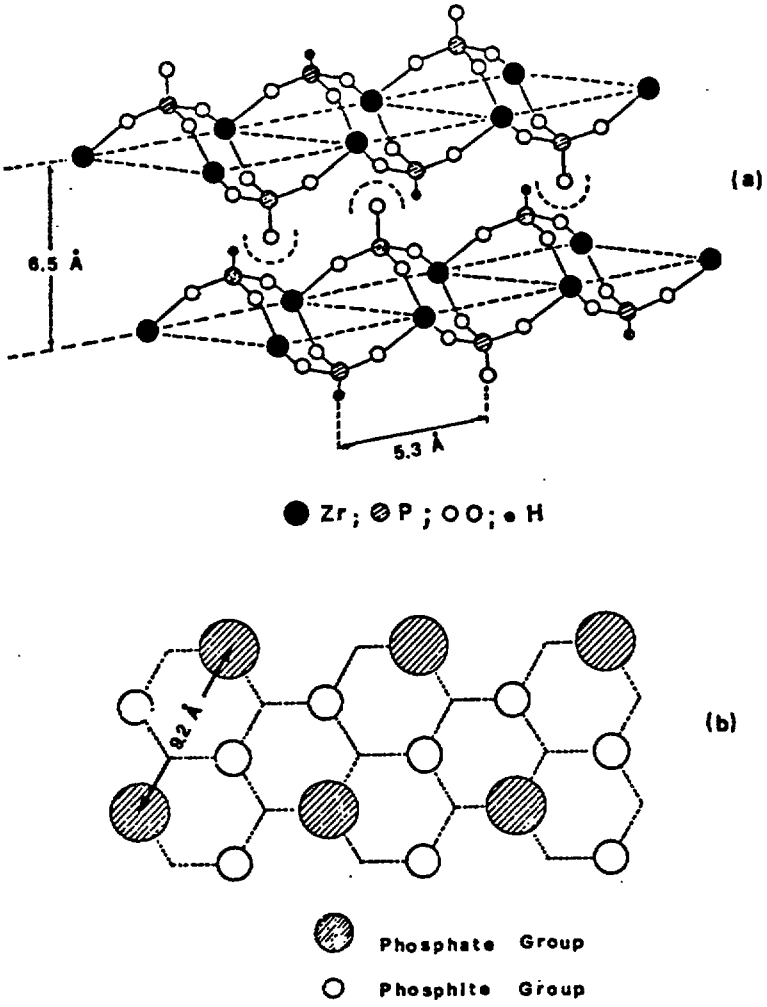

Fig. 4. a) Idealized structure of α-zirconium phosphate-phosphite of composition $\alpha\text{-}\left[Zr(PO_4)_{0.66}(HPO_3)_{1.34}\right]H_{0.66}$
b) Phosphate and phosphite groups on one side of a layer.

Acknowledgements

The work carried out in the author's laboratory was supported by Finalized Project of F.C.S.C. of C.N.R. and by M.P.I.. The author is indebted to his co-workers U. Costantino and M. Casciola for many discussions and the use of certain results in advance of full publications.

References

[1.] AMPHLETT, C.B., "Inorganic Ion Exchangers", Elsevier, Amsterdam (1964).

[2.] ALBERTI, G., Acc. Chem. Res., 11 (1978) 163.

[3.] CLEARFIELD, A., Chapter 1 of "Inorganic Ion Exchange Materials" (Clearfield, A., Ed.) CRC Press, Boca Raton, Florida (1982).

[4.] ALBERTI, G., Ref. 3, Chap. 2.

[5.] COSTANTINO, U., Ref. 3, Chap. 3.

[6.] ALBERTI, G., ALLULLI, S., COSTANTINO, U., TOMASSINI, N., J. Inorg. Nucl. Chem., 40 (1978) 1113.

[7.] DINES, M.B., DI GIACOMO, P.M., Inorg. Chem. 20 (1981) 92.

[8.] ALBERTI, G., COSTANTINO, U., LUCIANI GIOVAGNOTTI, M.L., J. Chromatog. 180 (1980) 45.

[9.] DINES, M.B., DI GIACOMO, P.M., Inorg. Chem. 20 (1981) 92.

[10.] ZSINKA, L., SZIRTES, L., MINK, J., KALMAN, K., J. Inorg. Nucl. Chem. 36 (1974) 1147.

[11.] CLEARFIELD, A., STYNES, J.A., J. Inorg. Nucl. Chem. 26 (1974) 117.

[12.] ALBERTI, G., COSTANTINO, U., GUPTA, J.P., J. Inorg. Nucl. Chem. 36 (1974) 2103.

[13.] ALBERTI, G., BERTRAMI, R., CASCIOLA, M., COSTANTINO, U., GUPTA, J.P., J. Inorg. Nucl. Chem 38 (1978) 843.

[14.] ALBERTI, G., BERNASCONI, M.G., COSTANTINO, U., GILL, J.S., J. Chromatog. 132 (1977) 477.

[15.] ALBERTI, G., COSTANTINO, U., GUPTA, J.P., J. Inorg. Nucl. Chem. 36 (1974) 2109.

[16.] ALBERTI, G., BERTRAMI, R., COSTANTINO, U., J. Inorg. Nucl. Chem. 38 (1976) 1729.

[17.] ALBERTI, G., COSTANTINO, U., GILL, J.S., J. Inorg. Nucl. Chem. 38 (1976) 1733.

[18.] COSTANTINO, U., J.C.S. Dalton (1979) 402.

[19.] LA GINESTRA, A., MASSUCCI, M.A., FERRAGINA, C., TOMASSINI, N., Thermal Analysis, Proc. 4th I.C.T.A. Budapest 1974, Vol. I, Heyden, London (1975) 631.

[20.] HORSLEY, S.E., NOWELL, D.V., Thermal Analysis, Proc. 3th I.C.T.A., Davos, Vol. 2, Birkhauser Verlag, Basel (1971) 611.

[21.] COSTANTINO, U., LA GINESTRA, A., Thermochim. Acta 58 (1982) 179.

[22.] ALBERTI, G., COSTANTINO, U., GIULIETTI, R., J. Inorg. Nucl. Chem. 42 (1980) 1062.

[23.] YAMANAKA, S., TANAKA, M., J. Inorg. Nucl. Chem. 41 (1979) 45.

[24.] ALLULLI, S., FERRAGINA, C., LA GINESTRA, A., MASSUCCI, M.A., TOMASSINI, N., J. Inorg. Nucl. Chem. 39 (1977) 1043.

[25.] ALBERTI, G., COSTANTINO, U., LUCIANI GIOVAGNOTTI, M.L., J. Inorg. Nucl. Chem. 41 (1979) 643.

[26.] KOMARMENI, S., ROY, R., Nature 299 (1982) 707.

[27.] ALBERTI, G., COSTANTINO, U., DI GREGORIO, F., GALLI, P., TORRACCA, E., J. Inorg. Nucl. Chem. 30 (1968) 295.

[28.] ALBERTI, G., COSTANTINO, U., J. Chromatog. 50 (1970) 482.

[29.] ALBERTI, G., COSTANTINO, U., LUCIANI GIOVAGNOTTI, M.L., to be published.

[30.] ALBERTI, G., MASSUCCI, M.A., TORRACCA, E., J. Chromatog. 30 (1967) 579.

[31.] HAGMAN, L.O., KIERKEGAARD, P., Acta Chem. Scand. 22 (1968) 1822.

[32.] SLJUKIC, M., MATKOVIC, B., PRODIC, B., SCAVNICAR, Croat. Chem. Acta 37 (1965) 115.

[33.] ALLULLI, S., MASSUCCI, M.A., TOMASSINI, N., Italian Patent no. 48852A/79, 26 april (1979).

[34.] ALBERTI, G., COSTANTINO, U., MASSUCCI, M.A., TOMASSINI, N., Italian Patent no. 49546A/83, 20 december (1983).

[35.] ALBERTI, G., COSTANTINO, U., Italian Patent no. 484387/A, 17 may (1982).

[36.] ALBERTI, G., BARTOLI, F., COSTANTINO, U., DI GREGORIO, F., Italian Patent no. 22365/A83, 1 august (1983).

[37.] ALBERTI, G., COSTANTINO, U., GIULIETTI, R., Gazz. Chim. Ital. 113 (1983) 547.

[38.] ALBERTI, G., COSTANTINO, U., KORNYEI, J., to be published.

RECOVERY OF CESIUM-137 FROM RADIOACTIVE WASTE SOLUTIONS WITH A NEW COMPLEX INORGANIC ION EXCHANGER

S. ZHAOXIANG, T. ZHIGANG, H. ZUN,
L. ZHENGHAO, W. HAOMIN, L. TAIHUA, L. BOLI
Beijing Normal University,
Beijing, China

Abstract

Recovery of ^{137}Cs from radioactive waste solution has been studied by using titanium phosphate - ammonium molybdophosphate. The complex ion-exchanger shows favorable performance for the adsorption and elution of Cs. The product ^{137}Cs has more than 99% radioactive purity and high decontamination factors for ^{103}Ru, ^{95}Zr, ^{22}Na, ^{90}Sr, ^{241}Am but less for ^{86}Rb and ^{144}Ce. A scheme for recovery process of ^{137}Cs from radioactive waste solution is suggested from the experimental results with this new complex ion-exchanger.

Introduction

Utilizion of high-level liquid waste from spent fuel reprocessing containing useful isotopes is a matter of great importance for their potential nuclear applications. Two isotopes that have received considerable attention are cesium-137 and strontium-90. Possible technique for recovery of cesium and strontium from radioactive waste solution(IAW) fall into three categories: precipitation, solvent extraction amd ion exchange. In general the precipitation and solvent extraction processes are rejected because of their adverse effect on waste management due to the added chemical or because they are not effective in the acid range easily attainable in IAW. Furthermore, radiation decompositions easily occur in the extractant. Since inorganic exchangers and adsorbents usually have high chemical selectivites and high radiation resistance, they have been considered for recovering cesium-137 and strontium-90 in IAW[1-2].

Several exchangers have also been developed for removing cesium from highly acidic solution; these exchangers include the heteropoly acid and acid salts of tungsten and molybdenum, as well as the zirconium, titanium, and tin salts of condensed phosphates.[3-7] As is well known, these inorganic ion exchangers have some shortcomings, for example the acid salts of tungsten and molybdenum are amorphous. The zirconium and

titanium of condensed phosphates easily block up the exchange column, if present in the trivalents state in the feed.

This report presents our preliminary laboratory study on a new complex inorganic cation exchanger titanium phosphate-ammonium molybdophosphate (Tip-AMP), determining its cesium capacities and relative selectivites and capabilities. The results are shown below. The new complex exchanger Tip-AMP possesses unique advantages and show no shortcomings.

Experimental

Preparation of the ion exchanger

The ion-exchanger titaniun phosphate was prepared according to the method of C. Beaudet [8]. Good granules (50-100 mesh) of Tip were obtained in our laboratory, then the exchanger was loaded in glass column or beaker, after being combined with AMP by dynamic or static method; a yellow complex ion-exchanger Tip-AMP was obtained. It was thoroughly washed with distilled water to remove free acid till the effluent pH was neutral, and finally was air-dried for three days.

Determination of breakthrough curves and evaluation of breakthrough capacity

1 gm exchanger was loaded in a glass column (20 cm x 0.5cm) provided with glass wool padding at the bottom, bed volume being 1 ml/g. The loaded column was washed with 10 column volumes of nitric acid of appropriate molarity. The synthetic feed solution containing known amount of carrier and tracer Cs-137 was passed through the exchanger at a fixed flow rate (2.0-3.0 ml/hr) at room temperature. 1 ml fraction were collected with an automatic collector till C/Co reached approx.1. The C/Co value was plotted against the volume of the feed and breakthrough capacity calculated where C/Co reached 0.01 (1 % BT). The exchange capacity is 0.47 meq/g and breakthrough volume is 85 BV. The results are shown in figure 1 and composition of synthetic feed solution in Table I.

Effect of acidity on the cesium capacity of complex exchanger Tip-AMP

The exchange capacity was investigated according to the above static method. Table II shows the results.

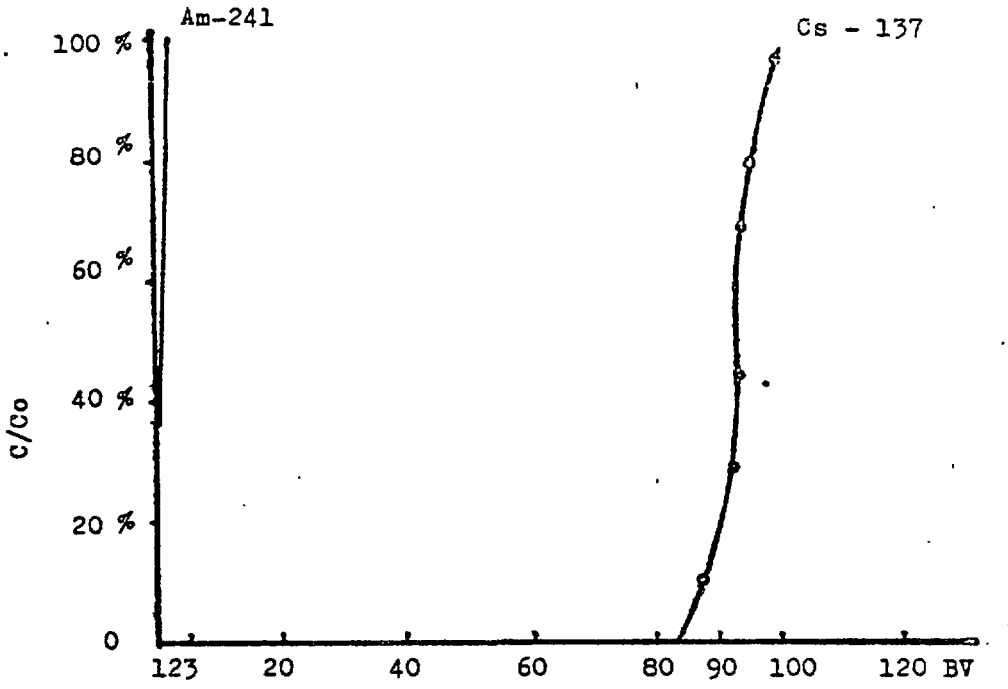

Fig. 1 Breakthrough curves of Am241 and Cs137 from Tip-AMP column

Table I. Composition of synthetic feed solution

Ion	Concentration g/l
Na^{+}	2.5
Cs^{+}	0.75
Rb^{+}	0.075
Sr^{++}	0.5
Ba^{++}	0.25
Ce^{+++}	3.75
Fe^{+++}	2.0
Zr^{++++}	2.0
UO_2^{++}	0.25
HNO_3	1 N

Table II. The exchange capacity of various acidity

Acidity HNO_3 N	0.5	1.0	2.0	4.0
Exchange capacity meq/g	0.50	0.47	0.46	0.45

Effect of sodium ion concentration on the cesium capacity of complex exchanger Tip-AMP

Both sodium and cesium belong to the alkali metals.

It is greatly meaningful to observe the exchange competition between sodium and cesium, hence the exchange capacity was evaluated with dynamic method at different sodium ion concentration. We found that the sodium ion concentration in feed solution slightly influenced the cesium capacity of Tip-AMP as shown in figure II.

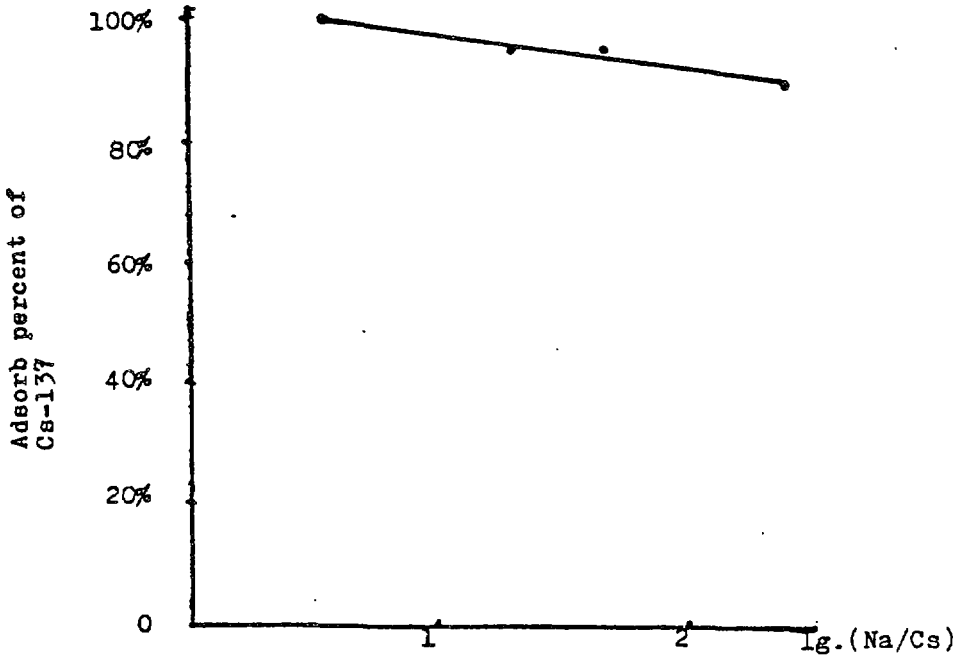

Fig.2 Effect of Na/Cs on the adsorb percent of Cs-137

Table III. Effect of cycle on the Cesium capacity of Tip-AMP

Cycle	Capacity meq/g
1	0.47
2	0.49
3	0.50
4	0.49
5	0.47
6	0.48
7	0.45

Effect of cycle use on the cesium capacity of Tip-AMP

Exchange capacity for cesium was determined under the above condition on the complex exchanger Tip-AMP. When the cesium breakthrough reached 1% in the effluent, cesium elution was started using 5.5 N NH_4NO_3 + 0.5 N HNO_3 at 60°C. Then the exchange column was regenerated with 10 column volumes of 1 N HNO_3. Seven cycles could be used at least with this complex exchanger, and results are shown in Table III.

Recovery of cesium-137 and determination of decontamination factor of Ce-141, Ce-144, Ru-106, Ru-103, Zr-95 and Nb-95

Experiments were also carried out on the decontamination factor of Ce-141, Ce-144, Ru-106, Ru-103, Zr-95 and Nb-95 from feed solution, to which a fresh fission product was added as an indicator. The feed solution passed through the exchanger at a fixed flow rate 2.0-3.0 ml/hr at room temperature. Bed volume was 70. The loaded column was washed with 5 column volumes of 0.5 N HNO_3 and 15 column volumes of 0.5 N $H_2C_2O_4$ + 0.5 N HNO_3 for removing Ce-141, Ce-144, Ru-106, Ru-103, Zr-95 and Nb-95 and the purpose of decontamination was achieved.

Cesium elution was carried out by passing 10 column volumes of 5.5 N NH_4NO_3 + 0.5 N HNO_3 at 60°C. The total cesium eluted was examined on their activity at 4096 channel analyser. The cesium effluent concentration indicated a less than 1% loss in loading the column to essentially 100% breakthrough. Washing liquid of 0.5 N HNO_3 and 0.5 N $H_2C_2O_4$ + 0.5N HNO_3 were collected and examined for their activity by 4096 channel analyser. The results are shown in Table IV and figures 3,4, and 5.

Table IV. Distribution of contaminating nuclides in the process

Nuclides	feed cpm	effluent cpm	HNO_3 0.5N	$H_2C_2O_4$ HNO_3 0.5N	0.5N NH_4NO_3+ 0.5N HNO_3	decontamination factor
Ce-141	230990	228557	516	-	-	-
Ce-144	86110	85600	216	-	-	-
Ru-103	129738	128336	960	-	1226	106
Zr-95	364273	292488	714	313483	403	2300
Nb-95	569940	107765	1022			
Na-22	826670	-	9396	-	710	1164
Sr-85+89	566995	-	2112	-	670	850
Am-241	1164150	-	4198	-	1536	758
Rb-86	760856	-	32680	-	507274	1.5

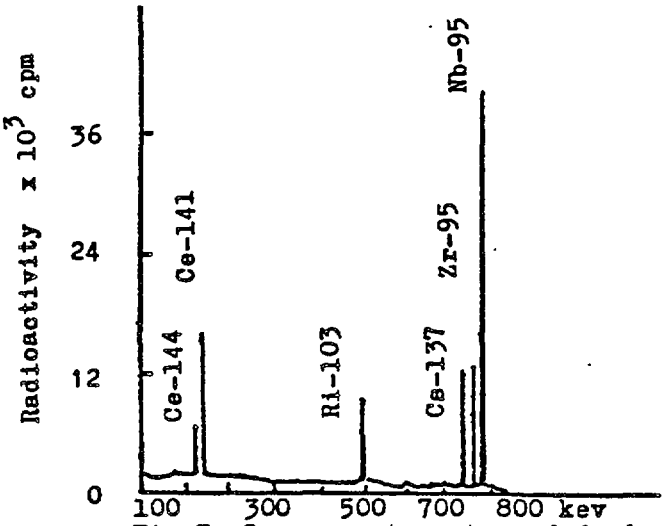

Fig.3. Gama spectrometry of feed

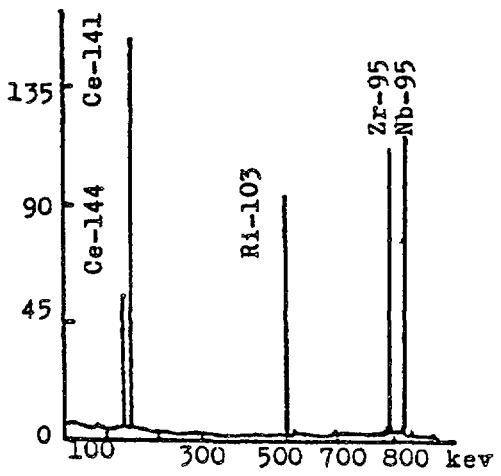

Fig.4. Gama Spectrometry of effluent

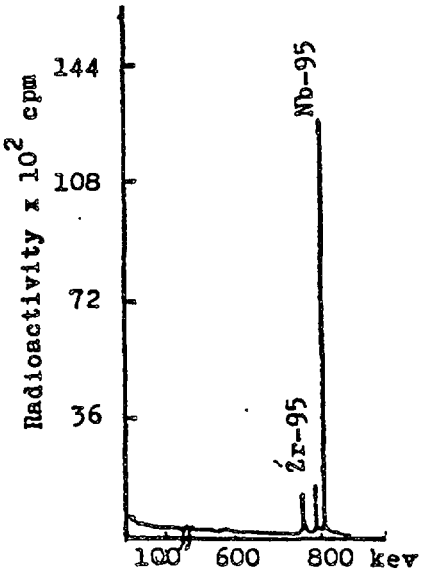

Fig. 5. Gama Spectrometry of washing oxalic acid

Recovery of Cs-137 from IAW using Tip-AMP

The purity of ^{137}Cs is higher than 99% by paper chromatography and loss of Am-241 is less than 1%. The product Cs-137 contained Ce, Sr, Na and Rb with concentration of 0.6%, 0.1%, 0.28% and 6.7% respectively. Therefore, this product might be separate with regard to cesium and rubidium. The results are shown in figure 6,7,8.

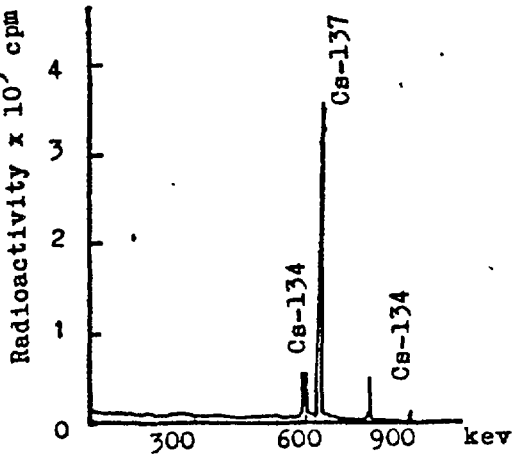

Fig. 6. Gama spectrometry of Recovered ^{137}Cs

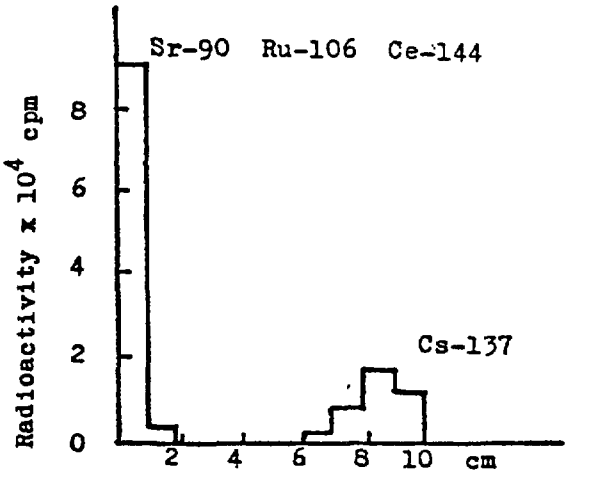

Fig. 7. Paper chromatography of feed

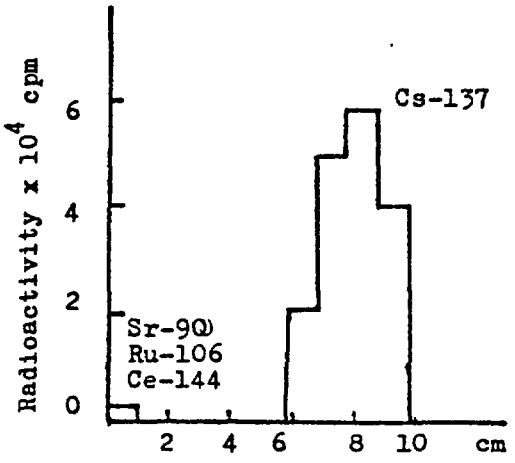

Fig. 8. Paper chromatography of recovered ^{137}Cs

Results and Discussions

1. The results reveal that complex ion exchanger Tip-AMP is much better than titanium phosphate (Tip) or ammonium molybdophosphate (AMP) alone. First, the ion-exchange column block-up when only Tip is used for recovery of Cs-137 from IAW is overcome and the problem of making granulated AMP is solved too. Secondly, the ion-exchange behavior is improved. Although Tip has a high rate of adsorbing Cs, Cs adsorbed is readily eluted; however, it almost loses the ability of adsorbing Cs at high acidity. AMP has a high selectivity capacity for Cs, but Cs adsorbed on it is hard to elute. The new complex exchanger Tip-AMP keeps only the advantages and thus overcomes the demerit.

The complex ion-exchanger Tip-AMP has a higher selectivity capacity for Cs reaching 0.47 meq/g when C/Co = 0.01, and is more readily eluted; only 10 column volumes can remove above 99% Cs from the loaded column.

The product Cs contains other radioactive nuclides, total amount being less than 1% except Rb.

The radioactive purity of recovered Cs-137 by paper chromatography and 4096 channel analyser is higher than 99%.

The complex ion-exchanger does not adsorb Am-241, so the loss of Am-241 is less than 1% in the course of ion exchange. This is very significant.

2. Tip-AMP exchanger is a complex compound and not a stoichiometric compound. This has been confirmed by X ray diffraction analysis.

3. The results indicate that this new complex inorganic ion exchanger has a good ion-exchange performance for Cs in IAW.

On the basis of these experiments, a scheme for Cs-137 recovering process is suggested. It was shown in Figure 9.

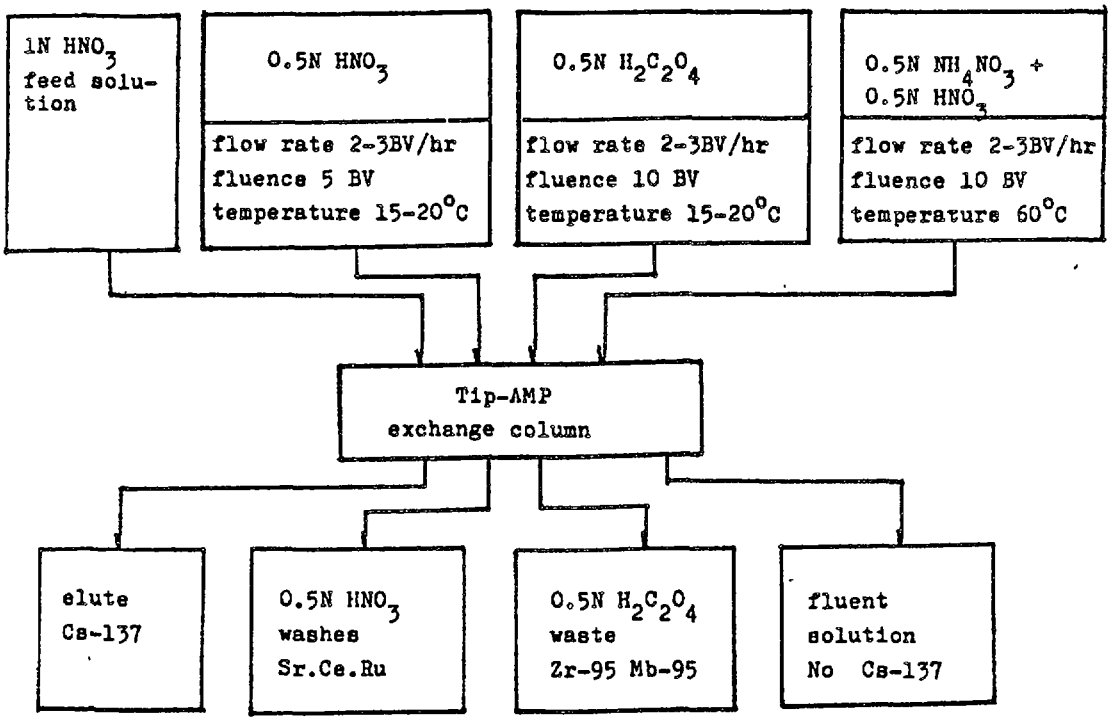

Figure 9. Recovery process of Cs-137 from IAW

References

1. V. Vesley et. al. Talanta 19. 219; 19. 1245 (1972)
2. A. Clearfield,Ed. Inorganic Ion Exchange Materials (1982) CRC Press.
3. V. Kourin et.al. Atomic Energy Review 12(2) 215(1974)
4. L. Baetsle; D. Vam Deyck; D. Hugs and A. Guery
   B. L. G. 2 67 (1964)
5. L. Baetsle; D. Hugs
   B. L. G. 487 (1973)
6. Yvonne M. Jones BNWL - 270 (1964)
7. D.K. Davis; J.A. Partridge; O.H. Koski
   BNWL - 2063 (1977)
8. C. Beaudet et. al.
   Nuclear Application 5(2) 64 (1968)

TREATMENT OF LIQUID WASTES CONTAINING ACTINIDES AND FISSION PRODUCTS USING SODIUM TITANATE AS AN ION EXCHANGER

Y. YING, L. MEIQIONG, F. XIANNUA
Institute of Atomic Energy,
Beijing, China

Abstract

The ion-exchange selectivity and capacity of sodium titanate have been studied as well as the preparation and characterization of this inorganic compound. Sodium titanate has a high selectivity for polyvalent ions (Sr, Ce, Fe, Pu, Am, etc.) but not for monovalent ions (Cs) in neutral and basic radioactive waste solutions. Sodium titanate can be used for the separation and consolidation of these actinides and of fission products into a suitable waste form.

Introduction

New inorganic ion-exchangers of high adsorption selectivity have been developed owing to their ideal irradiation, thermal and chemical stability. They might be used in treating and disposing of high-level radioactive wastes in nuclear energy field. The techniques of solidification by means of Synroc and monazite to fix the high-level wastes or high-level α-wastes all have made considerable headway. Inorganic ion-exchangers can be used as adsorbent and additives in solidification of liquid wastes. Natural inorganic materials which have exchange capacity could be used as back-fill of multiple barrier system for the disposal of nuclear wastes. Among several new ion-exchange materials of hydrous oxide type, sodium titanate is of most interested. In this work, sodium titanate (ST) was used as an adsorbent for decontaminating and separating the liquid wastes which contains actinide nuclides and fission product and satisfactory result were obtained.

Experiment

Preparation and analysis of sodium titanate

Lab-Scale ST has been prepared as follow:

1. Tetra-isopropyl-titanate

   Titanate tetrachloride was allowed to react with iso-

propyl alcohol in anhydrous benzene solution, and the metallic sodium was added later to this reaction mixture with stirring. The reaction mixture was heated and refluxed for 3 hours. The product was centrifuged and isolated by vacuum fractionation.

2. Sodium titanate

Tetra-isopropyl titanate was added to the 10% NaOH in methanol solution with stirring, then hydrolysed and filtered. The product was dried at room temperature.

Sodium in ST's product was determined by atomic adsorption spectrophotometry, and titanium was determined by cupferron reagent.

The components of ST were determined by X-ray diffraction tecnique.

Radioactive measurement:

α, β and γ-activities were measured by silicon surface semiconductor, plastic scintillation detector, and Ge(Li) detector respectively.

Result and discussion

- Analysis product

The determined value in ST product agreed with the feed on Na/Ti ratio(in Mole), but in the case of Na/Ti=1/20 in feed the result for ST product was lower as shown in Table I.

TABLE I

DETERMINATION OF Na/Ti RATIO (IN MOLE) ON ST SAMPLES

NO:	Na/Ti RATIO (IN FEED)	Na/Ti RATIO (ASSAY)
1	1/1	1/1.04
2	1/2	1/1.8
3	1/20	1/15.2

The sample of ST (Na/Ti)=1/1 which were sintered under different temperature were determined by X-ray diffraction technique. These data were roughly similar. The sample seemed to be purer when it had been treated at temperature up to 900°C. The diffraction data of sodium titanate are shown in TableII . These data are very similar to that of $A_2B_2X_7$ such as $(Ca, Fe, Na)_2(Sb, Ti)_2(O,OH)_7$ type of compound.

TABLE II DATA OF X-RAY DIFFRACTION ON ST

RADIATION CONDITION Cu K_{α}(Ni) Al FOIL

EXPOSURE CONDITION 35 KV 15 mA 8.5 Hrs

ST SINTERED 700° C		ST SINTERED 900°C		TYPICAL $A_2B_2X_7$
Q	D	Q	D	D
11.4	3.900	13.5	3.302	3.285
14.2	3.103	14.8	3.018	3.105
16.9	2.959	16.8	2.667	2.964
21.8	2.076	22.6	2.006	2.007
25.1	1.817	24.6	1.852	1.817
27.1	1.692	28.6	1.610	1.716
28.6	1.642	30.7	1.510	1.550
30.9	1.501	31.7	1.467	1.481
32.3	1.443	32.3	1.443	1.440
34.4	1.365	34.3	1.368	1.337
40.0	1.199	39.9	1.202	1.178

In addition, both Na and Ti were uniformly distributed in each micro regions of whole sample when observed under electron-microscope.

- Different way hydrolysis

The ion-exchange performance of ST product depends on different condition of hydrolysis. The product hydrolyzed in pure water formed a hard granules but it's ion-exchange performance is not good enough. The product hydrolyzed in water-acetone solution formed loose granules but it's ability for ion-exchange was 5-6 time greater than in pure water.

The ion-exchange performance of different Na/Ti ratio(in Mole) was shown in Table III. Sodium titanate of Na/Ti=1/1(in Mole) seemed better than Na/Ti=1/2.

- Hydraulics resistance

The liquid flow experiment was carried out using a column with ST bed of 1 Cm in diameter(I.D.) by 11 Cm in height. Distilled water passed through ST column with a flow rate of 6-7 bed volume(B.V.) per hour. After 440 hours(3000 B.V. effluent) opperation no resistance change was observed. This result indicated that ST exchanger has a good performance in column operation.

TABLE Ⅲ

ION EXCHANGE PERFORMANCE OF ST WITH DIFFERENT Na/Ti RATIO (IN MOLE)

NO:	Na/Ti RATIO (M)	ST WEIGHT (g)	FEED VOLUME (ml)	DISTRIBUTION RATIO (Kd)	
1	1/2	0.15	10	4.17×10^{2}	6.6×10^{2}
2	1/1	0.15	10	1.8×10^{3}	1.1×10^{4}
3	1.5/1	0.15	10	$2,9\times10^{3}$	1.8×10^{4}
4	(HTi_2O_5H)	0.15	10	7	15

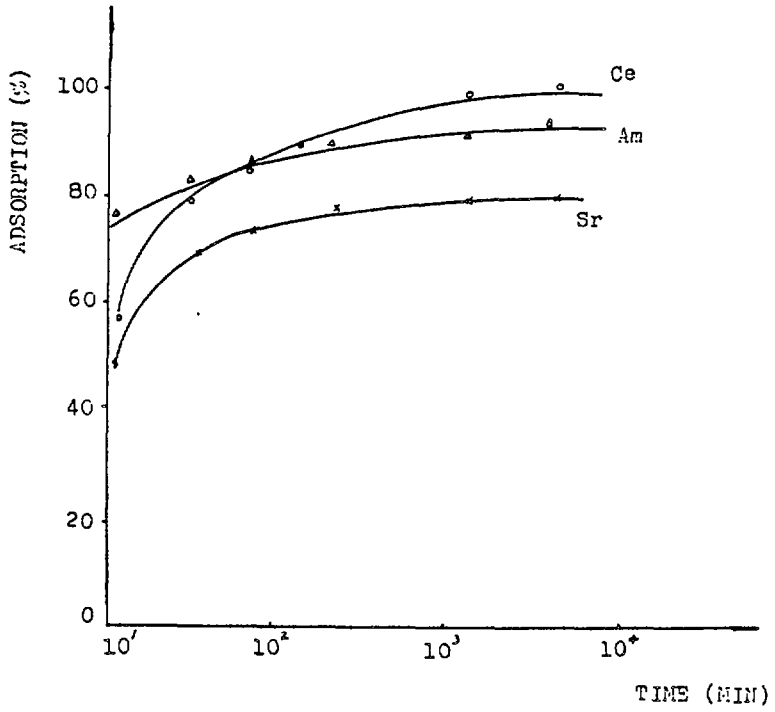

FIG. 1 THE EFFECT OF VARIOUS CONTACT TIME ON ADSORPTION RATIO

- Flow rate of ion-exchange

Like other inorganic ion-exchanger, the flow rate of ST exchanger is slow. In batch adsorption experiment, the effect of various contact time on adsorption ratio for Sr, Ce and Am are shown in Fig.1. The effects of various flow rate on adsorption capacity and the volume of effluent at 1% break-through are given in TableⅣ. In our experiment, the flow rate of ST column was 0.36Cm/min. (4-5B.V./hr.)

- Distribution coefficient, capacity and decontamination factor

Batch adsorption experiment were performed by contacting weighted 0.15 gram of ST sample with 10 ml of $NaNO_3$ feed solution.

TABLE Ⅳ THE EFFECT OF FLOW RATE ON CAPACITY

FLOW		VOLUME OF EFFLUENT AT 1% BREAKTHROUGH		CAPACITY
B.V./hr	Cm/min	ml	B.V.	meq/g
1.5	0.12	25.5	42.5	2.12
4.5	0.36	24	40	2.01
7.5	0.6	20	33.3	1.93
11	0.88	15	25	1.84
16	1.3	12	20	1.5

TABLE Ⅴ

DISTRIBUTION COEFFICIENT (Kd) FOR ST WITH SEVERAL CATION

IONS	FEED COMPOSITION	TRACE NUCLIDE	Kd
Cs^{+}	0.6MNaNO$_3$-0.02M Cs	^{137}Cs	24
Sr^{2+}	0.6MNaNO$_3$-0.02M Sr	$^{85,89}Sr$	1.8×10^{3}
Ce^{3+}	0.6MNaNO$_3$-0.02M Ce	^{141}Ce	1.1×10^{4}
Fe^{3+}	0.6MNaNO$_3$-0.02M Fe	^{59}Fe	3.4×10^{2}
Co^{3+}	0.6MNaNO$_3$-0.01M Co	^{60}Co	1.2×10^{3}
$Pu^{3,4+}$	0.6MNaNO$_3$-2.9×10^{-5}Ci/l Pu	^{239}Pu	8.8×10^{3}
Am^{3+}	0.6MNaNO$_3$-1.3×10^{-6}Ci/l Am	^{241}Am	1.1×10^{4}
Cm^{3+}	0.6MNaNO$_3$-8.6×10^{-6}Ci/l Cm	^{242}Cm	8.6×10^{3}

Each cation to be measured was to feed solution and traced with their radionuclides respectively, and the acidity was adjusted to PH 2. The result shown in Table Ⅴ indicate that ST has a high distribution coefficient for polyvalent cations than for mono-valent cation.

The equilibrium distribution coefficient, Kd, is difined as:

$$Kd = \frac{Co - C_l}{C_l} \times \frac{V\,(ml)}{W\,(g)}$$

Where Co: original concentration in liquid phase

C_l : remained of solution

W : weight of ST

V : volume of solution

The column experiment with a flow rate of 4-5 B.V. per hour are given in TableⅥ. The break-through curves of Sr, Ce, Co and Am on ST column are shown in Fig. 2.

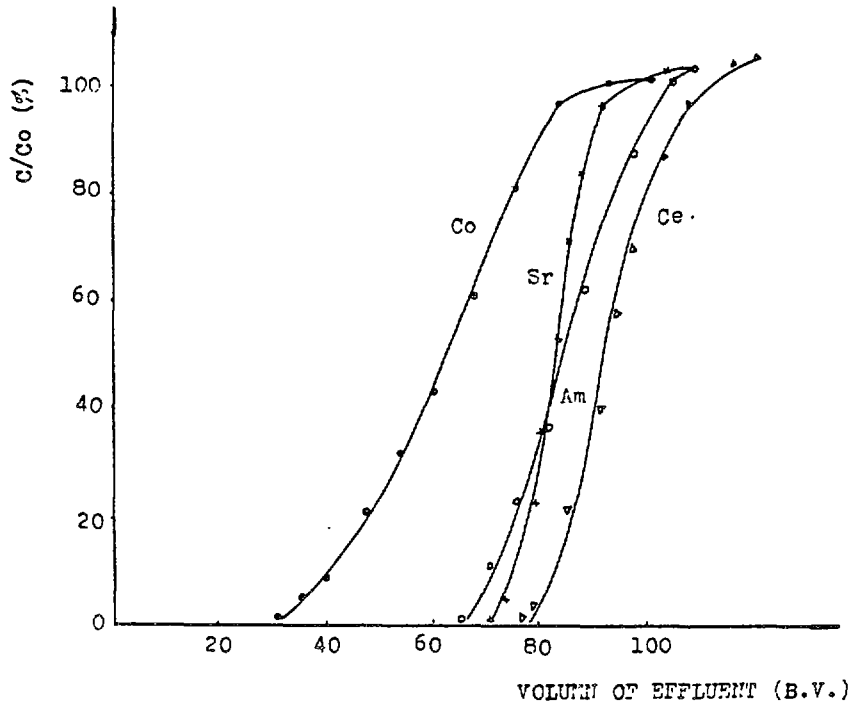

FIG. 2 THE BREAKTHROUGH CURVES OF Sr, Ce, Co, Am

TABLE VI

CAPACITIES AND DECONTAMINATION FACTOR OF ST FOR SEVERAL CATION IN COLUMN OPERATION

NO:	NUCLIDE	FEED COMPOSITION	CAPACITY (meq/g)	D.F.(BEFORE 1% BREAKTHROUGH)
1	Sr	0.6M$NaNO_3$-0.02M Sr	3.9	10
2	Ce	0.6M$NaNO_3$-0.02M Ce	3.8	10
3	Am	0.6M$NaNO_3$-0.02M Nd	4.2	10
4	Co	0.6M$NaNO_3$-0.01M Co	1.9	10
5	Pu	0.6M$NaNO_3$-2.9x10^{-5} Ci/l (^{239}Pu)	D.F.>10^4 in 300 B.V. EFFLUENT.	

- Effect of salt content

The influence of various quantity of Na, Fe, Ca in the feed solution on distribution coefficients of Cs, Sr, and Am for ST are shown in Fig. 3. It indicates that Kd of Cs on ST decreases as the concentration of Na increases. There is no marked change for adsorption of Sr, Ce and Am. While the concentrations of Ca or Fe in the feed solution are more than 2 grams per litre, the

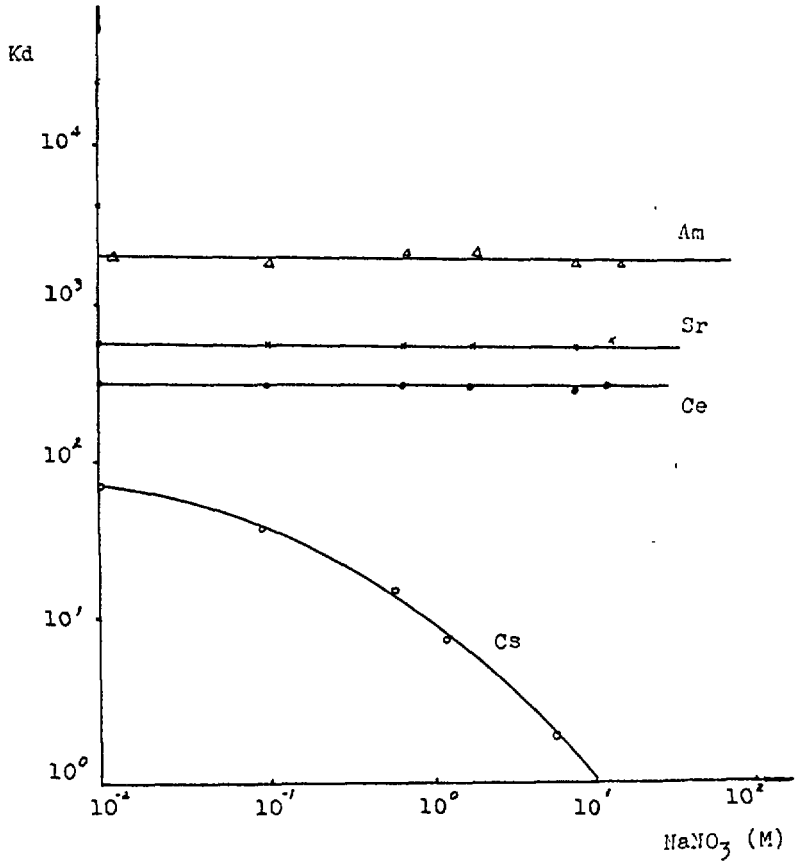

FIG. 3 THE EFFECT OF Na^+ ON ADSORPTION RATIO

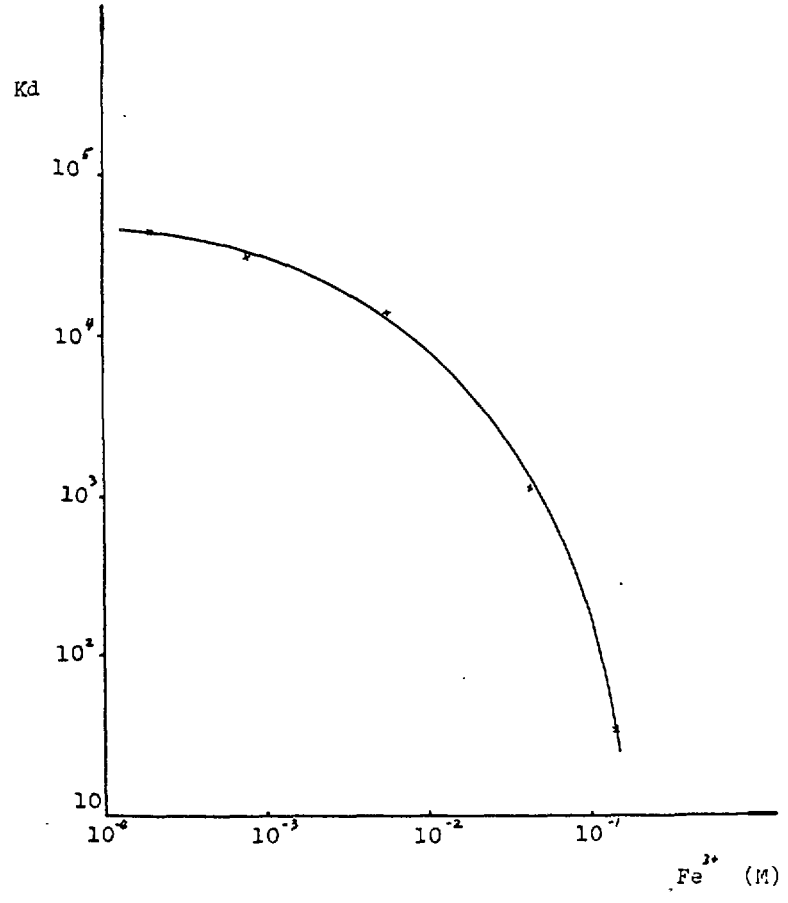

FIG. 4 THE EFFECT OF Fe^{3+} ON DISTRIBUTION RATIO FOR Sr

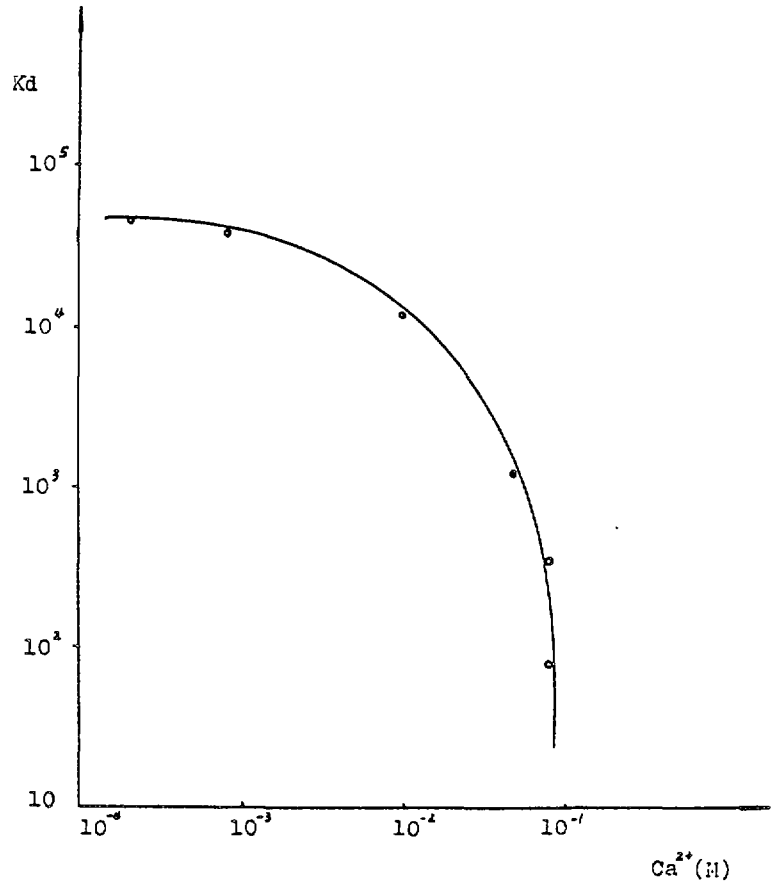

FIG. 5 THE EFFECT OF Ca^{2+} ON DISTRIBUTION RATIO FOR Sr

distribution coefficient of Sr on ST remains greater than 10^3 and there is significant change if it is less than 0.5 grams per litre.(See F.g. 4-5)

- Effect of complexing agent content

With the organic complexing agent in feed, most polyvalent cation formed complex with it. In 10ml feed, containing 0.6M $NaNO_3$ and 0.02M Sr, 0.15 grams of ST, and various quantity of NTA, DTPA or EDTA were added. The curves of Fig. 6-8 showed that these three complexing agent all effected adsorption ratio of cations. In simulated high-level liquid wastes(components listed as TableⅡ.), there was little adsorption if 0.15 grams of ST was added. But when the quantity of ST increase to 0.3 grams, ST showed certain effect on adsorption, even if the concentration of EDTA was much higher than Sr (See TableⅢ).

- Adsorption performance

The adsorption of ST for cation are more suitable in neutral and basic solution than in acidic solution. Take Sr for example, when acidic feed solution (PH 2) passed ST column, a 1% break-through would appear in the effluent at 70-80 B.V. However

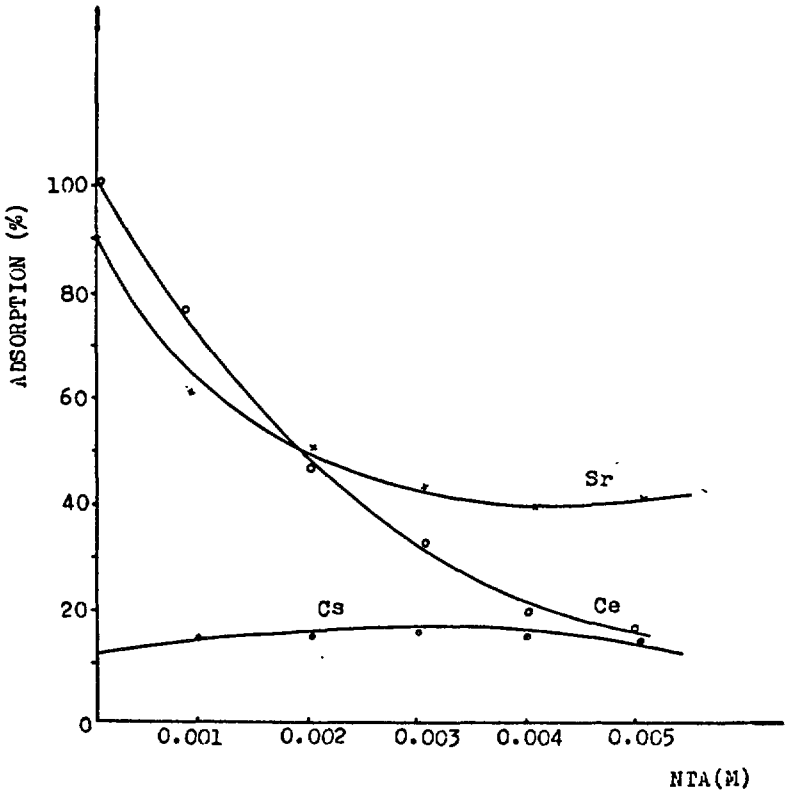

FIG. 6 THE EFFECT OF NTA ON ADSORPTION RATIO

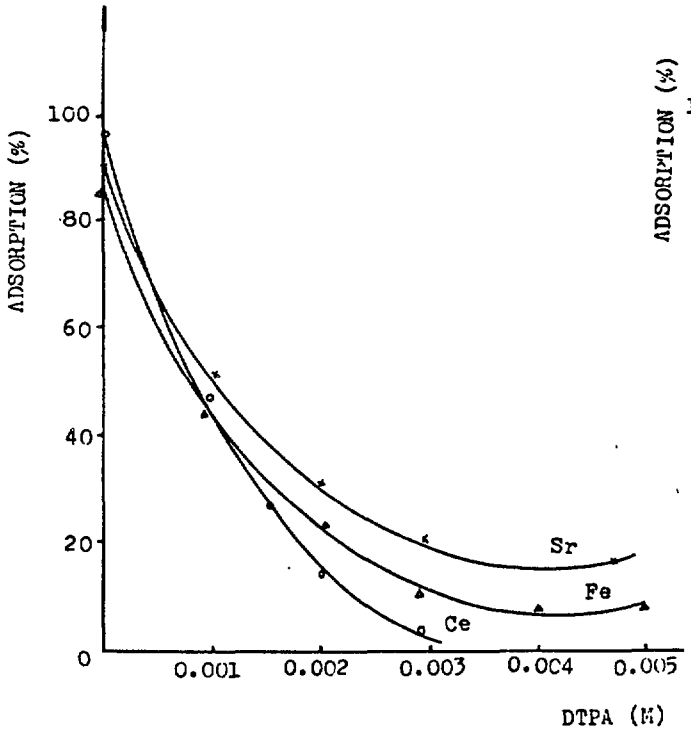

FIG. 7 THE EFFECT OF DTPA ON ADSORPTION RATIO

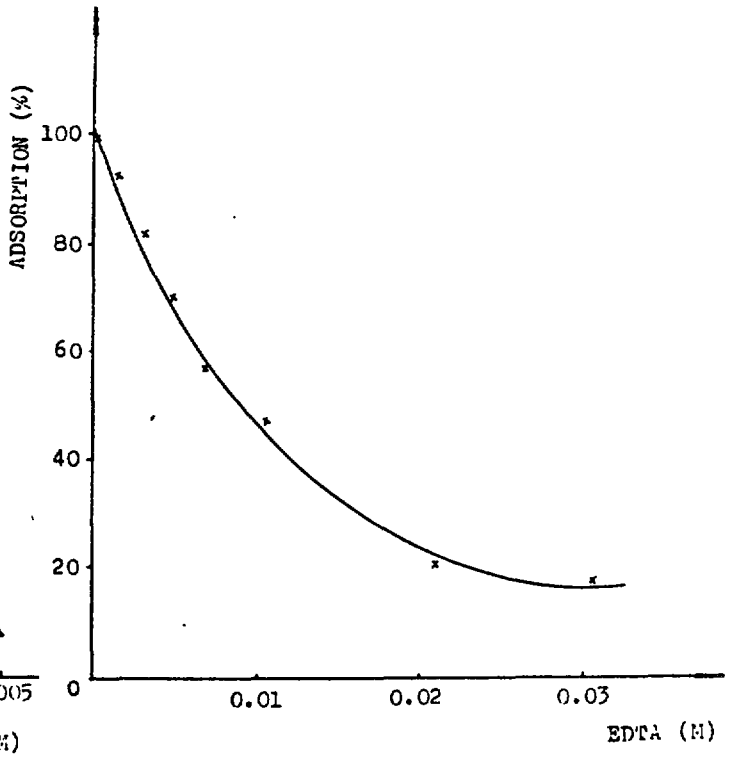

FIG. 8 THE EFFECT OF EDTA ON ADSORPTION RATIO FOR Sr

TABLE VI

THE EFFECT OF EDTA(M) ON ST ADSORPTION (IN SIMULATED HIGH LEVEL LIQUID WASTES)

No:	EDTA (M)	ST WEIGHT (g)	feed volume (ml)	adsorption (%)
1	0	0.3	10	95
2	0.0005	0.3	10	94.1
3	0.01	0.3	10	90.4
4	0.05	0.3	10	89.7
5	0.1	0.3	10	47.2
6	0.15	0.3	10	9.7
7	0.2	0.3	10	7.8
8	0	0.3	10	3

TABLE VII

COMPOSITION OF SIMULATED HIGH LEVEL LIQUID WASTES

COMPOSITION	COMPOUND	WEIGHT (g/l)	CONCENTRATION (M)
Na	$NaNO_3$	50	0.588
Fe	$Fe(NO_3)_3 9H_2O$	18	0.04
Cr	$Cr(NO_3)_3$	32	0.013
Ni	$Ni(NO_3)_3$	1.2	0.0065
Sr	$Sr(NO_3)_2$	1.5	0.007
Zr	$ZrO(NO_3)_2 2H_2O$	9	0.059
Cs	$Cs(NO_3)$	0.14	0.007
Ba	$Ba(NO_3)_2$	1.7	0.0065
Ce	$Ce(NO_3)_2 6H_2O$	21	0.048

then neutral feed (PH 7-8) was passed through, a 0.8 % break-through appeared after 1180 B.V. of effluent.

- Desorption and regeneration

The desorption and regeneration of ST column have been studied. A feed solution which containing 0.6M $NaNO_3$-0.01M Nd^{3+} and Am as tracers passed through column until the effluent reached 80% break-through. Nitric acid (0.2M) was used for desorption. After 10 B.V. acid passed through ST column, the

TABLE Ⅸ

THE COMPARISION OF ADSORPTION PERFORMANCE OF ST BEFORE AND AFTER IRRADIATION

DOSE (rad)	DISTRIBUTION RATIO(IN BATCH) (Kd)		EXCHANGE CAPACITY (IN COLUMN)
	Na/Ti=1/1	Na/Ti=1/2	(meq/g)
0	4.3×10^{2}	6.5×10	2.78
5×10^{7}	5.6×10^{2}	7.0×10	2.73
5×10^{8}	8.4×10^{2}	7.1×10	2.75

desorption ratio was higher than 70%. Then the ST column was regeneration by 3M $NaNO_3$(adding NaOH to PH 10). After two cycle of adsorption-desorption, the adsorption performance of ST column did not show any change.

- Irradiation resistance

Irradiation resistance tests for ST have been accomplished, and the result are presented in Table Ⅸ . It shows that both the exchange capacity and distribution ratio of ST did'nt change after up to 5×10^{8} rad of irradiation.

Experiment of treatment of actual low-level liquid wastes

Feed solution

The low-level liquid wastes were taken from the waste storage tank in Institute of Atomic Energy. The specific of which was $1\text{-}2\times10^{-6}$ Ci/l, calcuted as gross β-activity. Analytical data showed that the nuclides they contained were mainly Sr, Cs and Co. For the ease of measurement, Sr was added to liquid wastes and the PH value of the liquid wastes was adjected to about 7.

Test facility

The column was 5-6mm in internal diameter and 11.5Cm high containing two grams of ST adsorbent. The liquid wastes passed through ST column by peristaltic pump with a flow rate of 3.5-4.5 B.V./hr. The decontamination factor of Sr in 180 B.V. effluent was greater then 10^{4} and remained no less than 10^{3} after 1180 B.V. passing through. The γ-spectra of low-level liquid wastes before and after decontamination are shown in Fig. 9-10.

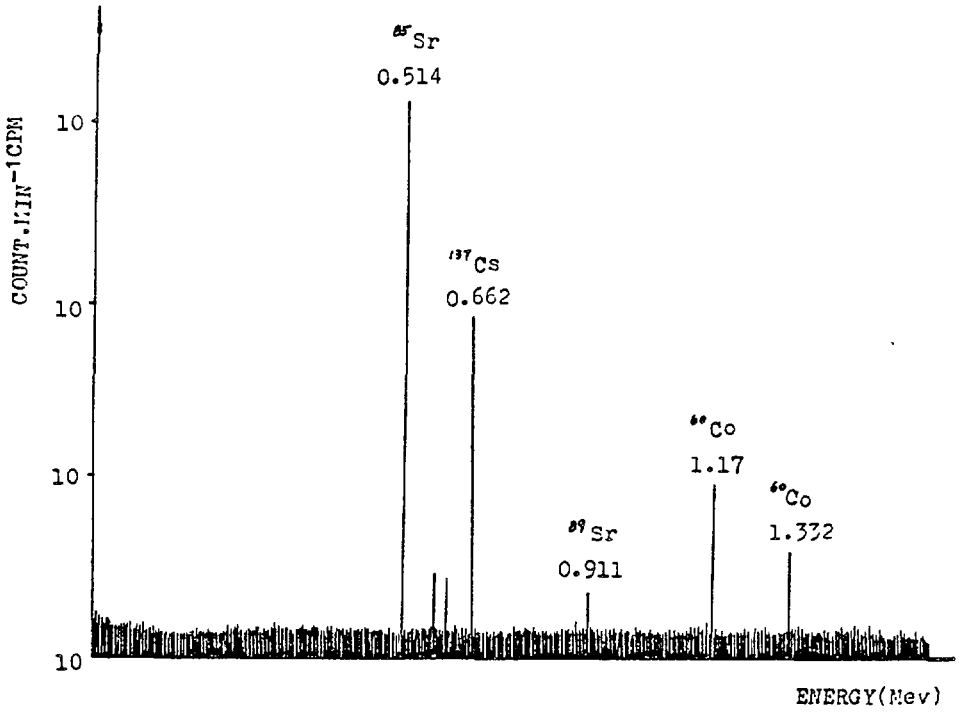

FIG. 9 THE γ-SPECTRA OF LOW-LEVEL LIQAID WASTES BEFORE DECONTAMINATION OF ST COLUMN

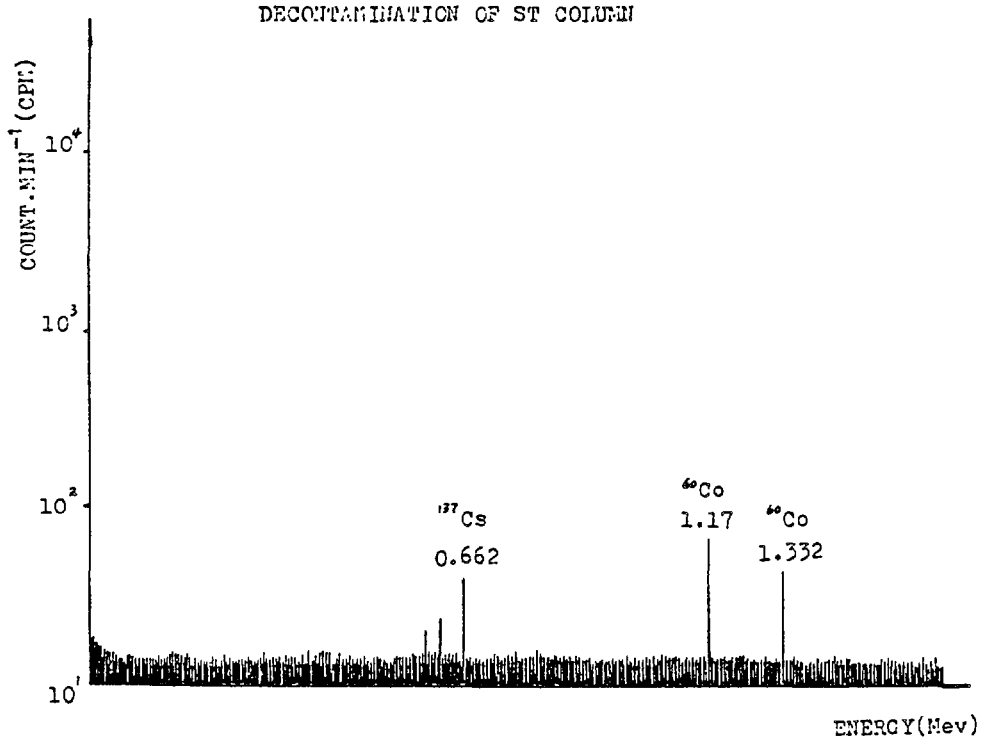

FIG. 10 THE γ-SPECTRA OF LOW-LEVEL LIQUID WASTES AFTER DECONTAMINATION OF ST COLUMN

The adsorption of Cs was interfered by some ions presented in liquid wastes to be treated. After the liquid wastes were treated by flocculation, the decontamination factor(D.F.) of Cs raised. The D.F. of Co in low-level liquid wastes was very poor. However, when the liquid wastes passed through an anionic resin column, more than 95% of cobalt was removed, checking the data of D.F. of Co in Table V, it is appears that cobalt exists as anionic complex state in liquid wastes.

TABLE X

DETERMINATION OF LOW-LEVEL LIQUID WASTES AFTER THREE-COLUMN (AVERAGE EFFLUENT OF 1180B.V.) PURIFICATION

		LOW-LEVEL LIQUID WASTES	
		UNTRATED	PRETREATED WITH FLOCCULATION
D.F. OF ST COLUMN EFFLUENT	Sr	1.8×10^{3}	1.1×10^{3}
	Cs	2.1×10	1.87×10^{2}
	Co	1.1	1.1
D.F. OF ZEOLITE COLUMN EFFLUENT	Sr	4.0	3.5
	Cs	1.53×10	1.2×10
	Co	1	1
D.F. OF ANION RESIN COLUMN EFFLUENT	Co		
	Co	9.7	1.0

The further decomtamination of Cs and Co existing in anionic complex state was accomplished by using a natural zeolite column and a macroporous anionic resin column. A three—column purification system---ST column, zeolite column and anionic resin column --- was assembled for experiment. Table X is the analytical results of effluents of low-level liquid wastes passing through three column system. It was determined by 4096 multi channel γ-ray spectrometer.

After 3-column purification, gross β-activity in effluent dropped down to 1×10^{-10} Ci/l, almost reaching the permissible level of direct discharge, 7×10^{-11} Ci/l.

Conclusion

The cost of ST would be cheaper than other inorganic ion-exchanger and commercial ST would be much cheaper than ST in Lab-scale. After adsorption, ST could be sintered at 1000°C translucent glass-like ceramic form, which reduced volume of waste and facilitated waste treatment, In treating actual liquid wastes, the ST-zeolite-anionic resin column system is simpler and easier to operate as compared with existing evaporation method. Moreover, it can be installed as a small mobile device suitable for liquid wastes treating under local condition.

REFERENCES

1 Lynch, R. W. Dosch R. G. et al., " The SANDIA solidification process-- A broad range aqueous wastes solidification method" IAEA-SM-207/75 361

2 Schwoebel R. L. et al., " An inorganic ion exchange process for partitioning high-level commercial wastes " NR-CONF-001 307

3 Dosch R. G. The use of titanate in decontamination of defence wastes solidification SADD-78-0710 (1978)

4 Johnstone J.K. Headly T.J. Hlava P.F. and Stohl F.V. " Characterization of a titanate based ceramic for high level nuclear waste solidification (Scientific basis for nuclear wastes management) 1 (1979) 211-217

5 Schulz W.W. Koenst J.W. and Tallant D.R. "Application of inorganic sorbents in Actinide separation process " (Actinide Separation) (1980) 17.

6 Forberg S. Westermart T. Arnek R. et al., "Fixation of medium level wastes in titanate and zeolites:progress toward a system for transfer of nuclear reactor activities from spent organic to inorganic ion exchanges" (Science Basis Nuclear Wastes Management) 2 (1979) 867.

ION-EXCHANGE PROPERTIES OF ZEOLITES AND THEIR APPLICATION TO PROCESSING OF HIGH-LEVEL LIQUID WASTE

T. KANNO, H. MIMURA
Research Institute of Mineral Dressing and Metallurgy,
Tohoku University,
Sendai, Japan

Abstract

Zeolites which have framework structures are excellent inorganic ion exchangers having high stabilities to radioactive irradiation.

Their ion exchange properties and thermal transformation have been studied for the purpose of their application to the separation of cesium and strontium from the high-level liquid waste (HLLW). Mordenite, one of the zeolites, selectively exchanged cesium ion with high selectivity coefficient more than 1000, thus cesium ion can be preferentially exchanged into the mordenite even in the acid solution around pH 1, and separate from other metal ions in HLLW. The selectivity for cesium ion decreases in the order, mordenite >> zeolite Y > zeolite X > zeolite A. The cesium exchanged mordenite is transformed to cesium aluminosilicate ($CsAlSi_5O_{12}$) by calcination above 1200°C.

On the other hand, strontium is selectively exchanged into zeolite A and its selectivity is reversed to that of cesium ion, zeolite A > zeolite X > zeolite Y > mordenite. Strontium forms of zeolite A, X and Y are recrystallized to triclinic strontium aluminosilicate ($SrAl_2Si_2O_8$) by calcination above 1100°C.

The leaching rates of cesium and strontium ions from these stable minerals are less than 10^{-9} g cm^{-2} day^{-1}, which are lower by the three orders of magnitude than those from borosilicate glass products. These excellent properties of zeolites for the separation and fixation of cesium and strontium can be applied to the partitioning process in the processing of HLLW and to the solidification.

1. Introduction

Zeolites are crystalline aluminosilicates with framework structures and have excellent cation exchange properties. Zeolite has some cavities occupied by cations such as Na, K, Ca and water molecules. These cations can be exchanged with other cations, and the selectivities of zeolite for cations seem to be different with their structures, Si/Al atomic ratios and the position of ion exchange sites.

Some of zeolites had formed naturally in deep geologic formation by hydrothermal reaction, and also many zeolites are synthesized artificially by various methods. Some of these synthetic zeolites have been used as molecular sieves and catalyzers in petrolium industry and others. Most of the naturally occuring zeolites in Japan are mordenite, clinoptilolite or their mixtures.

In the atomic energy industry, the treatment and management of high-level liquid waste (HLLW) are the most serious problem. In fission products, the most soluble and long lived radioactive isotopes are ^{137}Cs and ^{90}Sr, therefore the fixation of these isotopes to insoluble materials is the most valuable to security against the management of HLLW.

We have studied on the cation exchange properties of zeolites and their application to the fixation of ^{137}Cs and ^{90}Sr, and some interesting results were obtained.

2. Zeolites

Synthetic zeolite A and X used in this study are obtained from Toyo Soda Co. Ltd. and synthetic zeolite Y and synthetic mordenite (Zeolon 900Na, abbreviated as SM) are made by Norton Co. Ltd. Natural mordenite (from Sendai area, Miyagi prefecture, Japan, abbreviated as NM) and clinoptilolites (from Futatsui, Akita prefecture and from Itaya, Yamagata prefecture, Japan, abbreviated as CP) were also used.

3. Ion exchange properties of zeolites for various cations

Effects of pH on the distribution of Cs, Sr and some of transition elements such as Cr, Fe, Co, Ce, Eu and Tb into Na- and H-zeolites from simple cation solutions have been investigated.

Distribution curves of these cations for NaA and NaX are shown in FIG. 1, and these distribution curves of cations except for cesium have maxima around pH 6 - 7. The distribution ratios of these cations at maxima are about 10^4 - 10^5.

The distribution curves for NaY are also similar to those of NaA and NaX zeolites. Decreases of distribution ratios at low and high pH ranges seem to be mainly attributable to competitive exchange with hydrogen ion and hydrolysis of cations respectively. On the other hand, distribution ratio of cesium ion decreases monotonously with decreasing pH.

In the cases of Na- and H-forms of mordenites, cesium ion is selectively exchanged into these zeolites even at low pH range as shown in FIG. 2, therefore cesium ion may be separated from other multivalent cations under this condition.

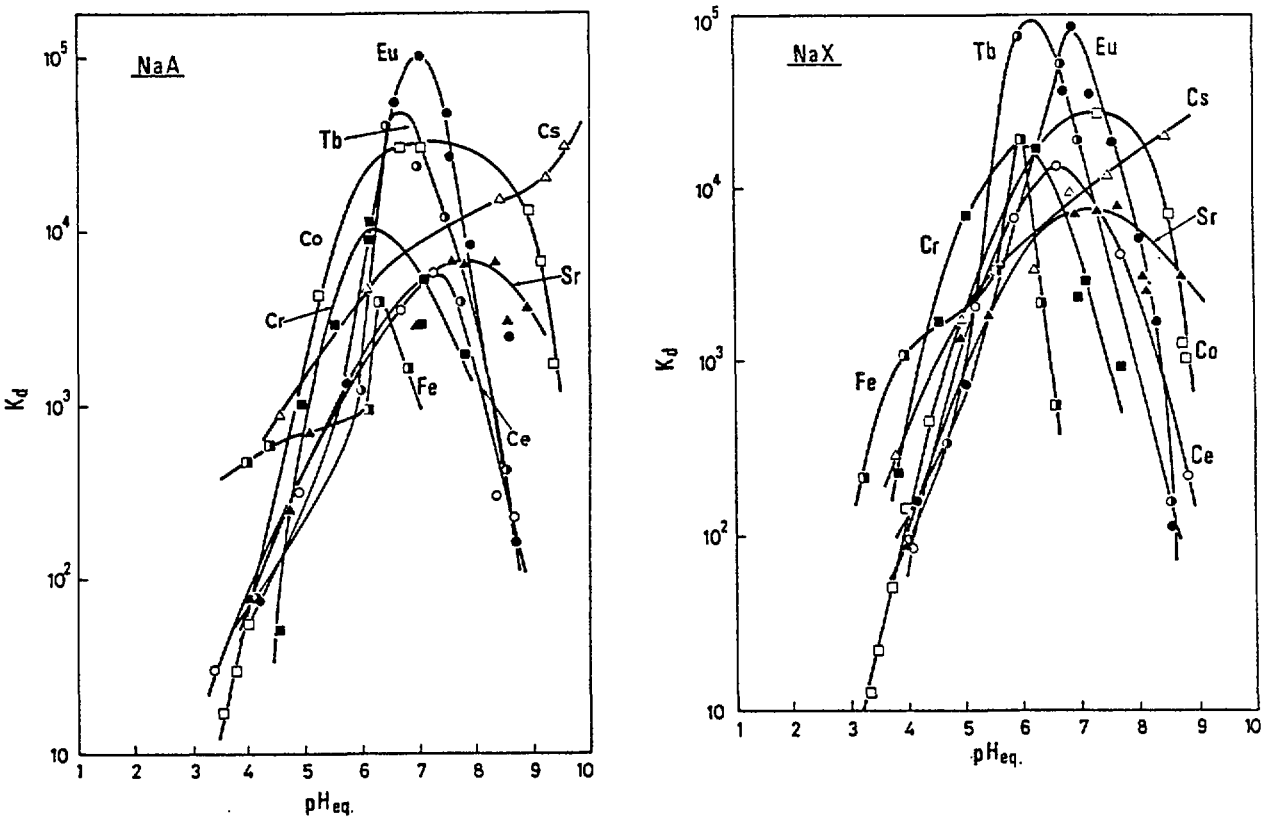

FIG. 1 Cation exchange properties of various cations into NaA and NaX

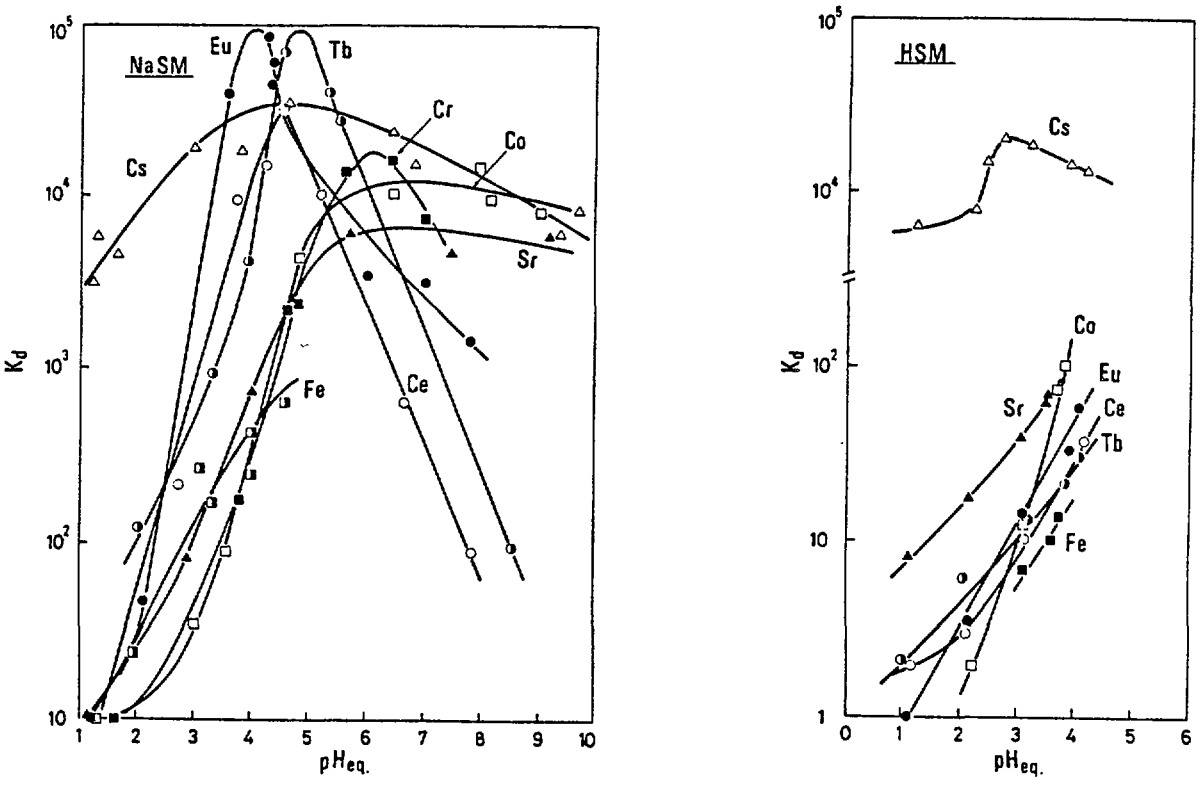

FIG. 2 Cation exchange properties of various cations into NaSM and HSM

4. Selectivity of zeolite for cesium ion

Zeolite has an ability to exchange various cations, but its selectivity is influenced by the structure and the position of ion exchange sites. In the case of exchange of cesium with a large ionic radius, sodium ions located in large cages or large channels can be easily exchanged with cesium, but sodium ions located in narrow channels or frameworks are hardly exchanged with cesium by ion sieve properties of zeolite.

Ion exchange isotherms of NaA for exchange reaction with casium are shown in FIG. 3. The sigmoid curve seems to show the presence of two kinds of site exchangeable with cesium. Plotts of corrected selectivity coefficients against to the equivalent fractions of Cs in NaA for Na - Cs exchange are shown in FIG. 4. In this figure, upper line shows the corrected selectivity coefficients at the sites in large α-cages (site 1), in which cesium is more selective than sodium.

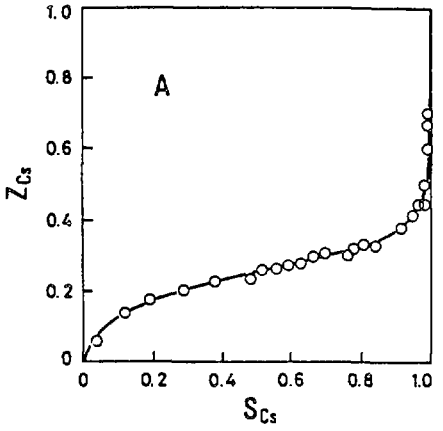

FIG. 3 Ion exchange isotherm of NaA for Cs exchange

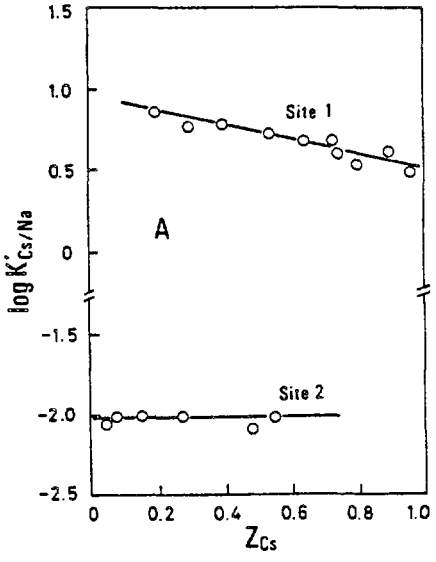

FIG. 4 Ion exchange selectivity of Na-Cs exchange

Lower line shows the corrected selectivity coefficients at the sites in the plane of 6-membered ring (site 2), in which sodium is more selective than cesium.

In NaA, 4 sodium atoms in large α-cage of unit cell are easily exchanged with cesium, while other 8 sodium atoms in the planes of 6-membered ring are hardly exchanged with cesium. From these results, the cations in α-cage and in the plane of 6-membered ring can be considered as hydrated cations and bared cations, respectively.

Ion exchange isotherm of NaSM for exchange with cesium are shown in FIG. 5. This simple curve seems to show that the site exchangeable with cesium is only one. Ion exchange selectivity for Na - Cs exchange in NaSM are shown in FIG. 6, and a simple straight line was obtained.

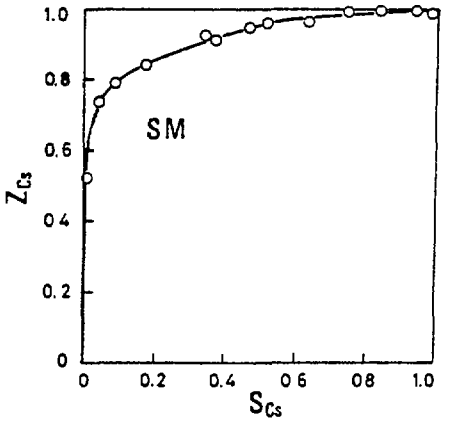

FIG. 5 Ion exchange isotherm of NaSM for Cs exchange

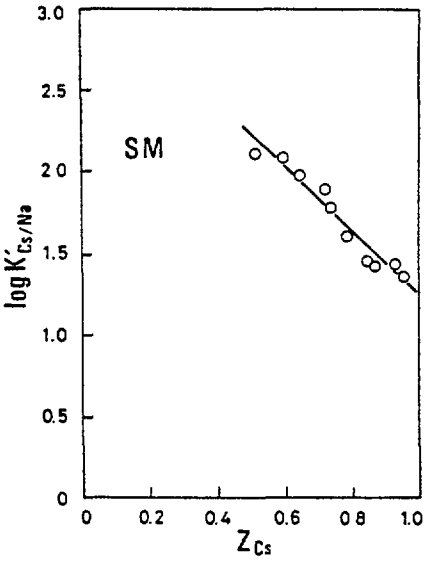

FIG. 6 Ion exchange selectivity of Na-Cs exchange

From this result, it is known that the selectivity coefficient of NaSM for cesium exchange is more than 1,000 at initial exchange with cesium which is very large than that of other zeolites. The order of the selectivities for cesium exchange is NaSM >> NaY > Nax > NaA.

5. Thermal transformation of Na-, Cs- and Sr-zeolites

It is well known that zeolites are aluminosilicates having three dimentional structures, and include the various cations in their framework structures. After zeolite structure are contracted by heating, cations contained in zeolites may become to be insoluble to water, since these cations are located in the aluminosilicate frameworks of zeolites. Zeolites contained cesium and strontium may be also transformed to cesium and strontium aluminosilicates by heating at high temperature.

Thermal transformations of Na-, Cs- and Sr-zeolites are investigated by means of differential thermal analysis (DTA), thermogravimetric analysis (TGA) and X-ray powder diffraction, in order to know the possibility of fixation of ^{137}Cs and ^{90}Sr.

Phase transformation of Na-, Cs- and Sr-forms of zeolites at high temperature are summarized in TABLE I. In the case of Na-A zeolite, the mixture of carnegieite and nepheline was obtained at 900°C, and then changed to a simple nepheline phase. Cs-A zeolite is transformed to the mixture of nepheline and pollucite, one of the cesium aluminosilicate, above 1200°C. Strontium form of A zeolite is transformed to hexagonal strontium aluminosilicate at 1000°C and then changed to triclinic strontium aluminosilicate above 1200°C.

Sodium form of X zeolite changed to amorphous phase at 850°C, and then recrystallized to nepheline above 1000°C. Cesium form of X zeolite is finally transformed to pollucite above 1000°C, through the amorphous phase and in this case no nepheline phase was detected. The thermal transformation of Sr-X zeolites is similar to that of Sr-A zeolite.

Sodium form of Y zeolite was completely destroyed at 800°C and does not formed any crystalline phase. On the other hand, CsY formed pollucite phase above 1100°C, and SrY changed to strontium aluminosilicate ($SrAl_2Si_2O_8$) at 1200°C. Some different results between X- and Y-zeolites may be due to the difference in Si/Al atomic ratios.

Mordenite is most stable zeolite, hence there is no change in its structure until about 900°C. Cesium exchanged synthetic mordenite is transformed to a cesium aluminosilicate

TABLE I Transformation of zeolites at high temperature

Cation / Zeolite	Na	Cs	Sr
A	900° >1000° Carn. + Neph. → Neph.	900° >1000° Carn. → Neph. + Pol.	800° 900-1000° >1100° Am. → Hex. → Tric.
X	850° >1000 Am. → Neph.	800-900° >1000° Am. → Pol.	800-900° 1000° >1100° Am. → Hex. → Tric.
Y	>800° Am.	1000° >1100° Am. → Pol.	900° 1000° 1100° 1200° Am. → ? → Am. → Tric.
SM	>900° Am.	1100° 1200° Am. → R.	1000-1200° >1300° Tric.+C.+Q. → C.
NM	>1000° Am.	>1000° Am.	>1000° Am.
CP	>1000° Am.	>1000° Am.	>1000° Am.

Am.: Amorphous, Carn.: Carnegieite($NaAlSiO_4$),
Neph.: Nepheline($NaAlSiO_4$), Pol.: Pollucite($CsAlSi_2O_6$),
Hex.: Hexagonal($SrAl_2Si_2O_8$), Tric.: Triclinic($SrAl_2Si_2O_8$),
R.: $CsAlSi_5O_{12}$, C.:Cristobalite, Q.: α-Qualtz

($CsAlSi_5O_{12}$) at 1200°C, and strontium exchanged synthetic mordenite changes to the mixture of triclinic strontium aluminosilicate ($SrAl_2Si_2O_8$), cristobalite and α-qualtz at 1000 - 1200°C, and then changes finally to cristobalite over 1300°C. On the other hand, Na-, Cs- and Sr-forms of natural mordenite and clinoptilolite change to amorphous phase over 1000°C, and no crystalline phase is detected.

6. Leachabilities of cesium and strontium from calcined zeolite

The leachability of ^{137}Cs and other radioactive nuclides from the solidified product of HLLW is one of the most important parameters in the safety assessment for the management of HLLW, because the leaching of radioactive nuclide from solid waste is the first step of the nuclide migration with ground water in the repository. In order to realize the ceramic solidification with lower leachability, the authors have investigated the solidification procedure by calcination of zeolites exchanged with cesium and

strontium as mentioned above. Therefore, the leachability of cesium and strontium from these calcined zeolites was investigated.

6.1 Effect of calcining temperature on the leachability of cesium

Alkaline ions such as cesium are the most soluble elements in the HLLW, therefore, the leachability of ^{137}Cs is often measured as one of the parameters for security assessments. FIGURE 7 shows the variation of the leachability of cesium from calcined product into pure water with calcining temperature. Leachability decreased with increasing in calcining temperature, and that from the calcined CsA and CsX decreased rapidly between 900° and 1000°C by the crystallization of pollucite ($CsAlSiO_4$), and nepheline ($NaAlSiO_4$) while the amount of leached cesium from the calcined natural zeolites gradually decreased with increasing in calcining temperature. The leachability from the calcined natural zeolites was a little higher than that from calcied A and X zeolites, since the mordenite and clinoptilolite are more stable at high temperature than A and X zeolites. The leachability of strontium is considerably lower than that of cesium.

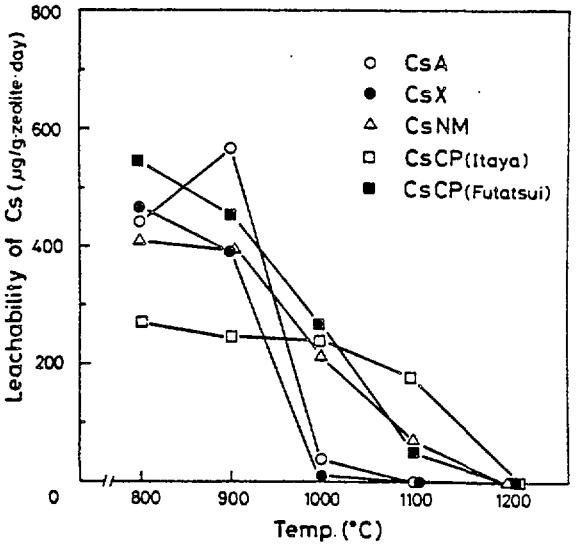

FIG. 7 Variation of leachability of Cs into distilled water with calcining temperature (Calcining time; 3 h)

6.2 Leaching rate

The manners of representation for leaching results were contrived according to the object and method of leaching test. The leaching rate presented by ORNL is available and expressed as follows[1].

$$\text{Leaching rate} = \frac{Y/X}{A/W} \quad (\text{g cm}^{-2}\ \text{day}^{-1})$$

where X: Amount of a constituent present in the sample, g
Y: Quantity leached from the sample in unit time, g/day
A: Surface area of the sample, cm^2
W: Weight of the sample, g

The evaluation of surface area necessary for the calculation of leaching rate were made by means of BET method using nitrogen gas. The measured values of leaching rate are shown in TABLE II. The leaching rates into pure water were about 10^{-8} - 10^{-9} for cesium and 10^{-9} - 10^{-10} for strontium, respectively. The value of leaching rate of cesium into distilled water was very small, and that from the calcined Y zeolite was smallest in the synthetic zeolites by the formation of pollucite. The amount of cesium leached from cesium zeolites calcined at 1200°C and that of strontium leached from calcined A and X zeolites were under the detection limit of atomic absorption analysis.

TABLE II Leaching rate of Cs and Sr for calcined zeolites ($g\ cm^{-2}\ day^{-1}$)

Zeolite	Cs		Sr	
	Distilled water	Sea water	Distilled water	Sea water
A	2.5×10^{-8}	1.2×10^{-7}	$<2.6\times10^{-10}$	1.8×10^{-8}
X	1.7×10^{-8}	6.0×10^{-8}	$<2.6\times10^{-10}$	1.8×10^{-8}
Y	1.3×10^{-8}	1.1×10^{-7}	2.8×10^{-9}	9.7×10^{-9}
SM	7.4×10^{-8}	8.5×10^{-8}	5.0×10^{-9}	1.6×10^{-8}
NM	$<2.3\times10^{-9}$	1.1×10^{-8}	-	-
CP (Itaya)	$<3.8\times10^{-9}$	1.3×10^{-8}	-	-
CP (Futatsui)	$<3.2\times10^{-9}$	1.5×10^{-8}	-	-

Zeolite A, X, Y and SM were calcined at 1100°C for 3 h.
Zeolite CP and NM were calcined at 1200°C for 3 h.

7. Volatility of cesium from zeolites in calcination

Volatilization of Cs-zeolites at high temperature is investigated for the purpose of the safety assessment. As shown in FIG. 8, volatilization curves of cesium are very different with zeolites and the amount of volatilized cesium

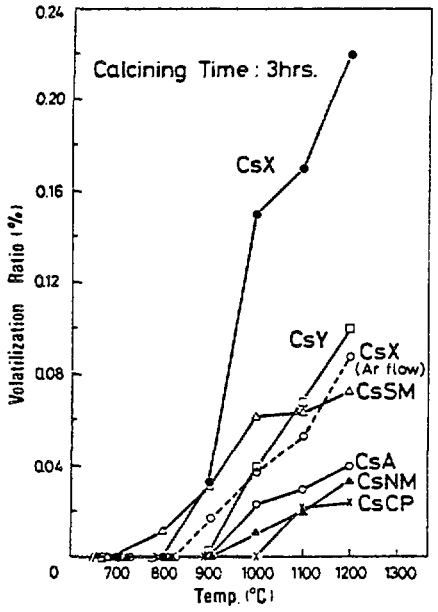

FIG. 8 Variation of volatilization rate with calcining temperature

is increased with increasing temperature. It is shown in FIG. 9 that cesium is volatilized only at the first stage of heating at 1200°C, and except for CsX zeolite volatilization of cesium is depressed after about 40 min-heating. It seems that this depression is owing to the destraction of zeolite structures at high temperature. Volatilized species of cesium was determined as Cs_2O by mass spectrometry. Therefore,volatility of cesium is decreased in inert gas flow such as argon. The volatilized amounts in calcination of Cs-zeolites except for CsX were very little (Table III).

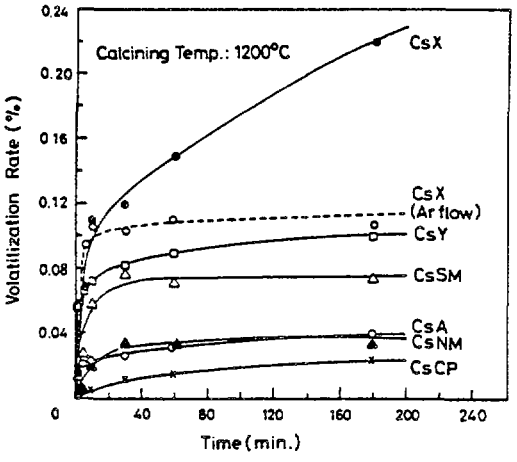

FIG. 9 Variation of volatilization rate with calcining time

TABLE III Volatilization of Cs from zeolites
(Calcining condition: 1200°C, 3 h)

Zeolite	Air	Ar
CsA	4.1×10^{-2}	2.9×10^{-2}
CsX	2.0×10^{-1}	8.8×10^{-2}
CsY	1.0×10^{-1}	8.4×10^{-2}
CsSM	7.3×10^{-2}	1.1×10^{-2}
CsNM	3.4×10^{-2}	4.4×10^{-3}
CsCP	2.4×10^{-2}	5.2×10^{-3}

$$\text{Volatilization rate (\%)} = \frac{\text{Volatilized Cs}}{\text{Total Cs in zeolite}} \times 100$$

8. Conclusion

Zeolites are very excellent materials for adsorption and fixation of radioactive nuclides in HLLW as mentioned above.

Mordenite is most selective to cesium ion in the zeolites, and cesium exchanged synthetic mordenite is transformed to cesium aluminosilicate ($CsAlSi_5O_{12}$) at high temperature, which is very stable and had difficult leachability. Therefore, mordenite is very suitable for solidification of ^{137}Cs.

Zeolite A exchanged with Sr is transformed to strontium aluminosilicate ($SrAl_2Si_2O_8$) by calcination.

Since zeolites have very excellent properties for the treatment of radioactive nuclides in high-level liquid waste, it is necessary to promate the investigation on the application of zeolites for the nuclear fuel cycle in atomic energy development.

REFERENCE

[1] IAEA Technical Report Series, No.82 (1968) 101.

STUDIES ON INORGANIC ION EXCHANGERS – FUNDAMENTAL PROPERTIES AND APPLICATION IN NUCLEAR ENERGY PROGRAMMES

R.M. IYER, A.R. GUPTA, B. VENKATARAMANI
Chemistry Division,
Bhabha Atomic Research Centre,
Bombay, India

Abstract

Investigations on inorganic ion exchangers have been carried out with a view to understand the fundamental properties and to assess their suitability in specific applications in the Nuclear Fuel Cycle.

Method of preparation had a marked influence on the structure and properties of this class of materials, as in the case of crystalline thorium arsenate (TA) and hydrous oxides, especially hydrous titanium oxide (HTiO). The new crystalline modifications of TA, in contrast to the monohydrate, exchanged larger ions like Na^+, K^+ in addition to Li^+; due to the large interlayer spacings. Hysteresis in H^+-Li^+ exchange was observed. The selectivity sequences for alkali, alkaline earth and transition metal ions on hydrous thorium oxide (HThO) and magnetite (MAG) were similar to those observed for other hydrous oxides. While hysteresis in anion exchange involving uni-univalent anions on HThO was observed, cation exchange reactions involving Ca^{2+} and Cu^{2+} were found to be non-reversible.

Preliminary investigations on the usefulness of hydrous oxides in the recovery of uranium from sea water, and purification of reactor coolant water are reported in this paper. Different hydrous oxides having varying acidities were screened for their uranium sorption capacities. On HTiO, the most promising adsorbent among the hydrous oxides, the influence of anions on the sorption of uranium, the possible mechanism of sorption of uranium from carborate solutions and under simulated sea water conditions were studied. Investigations on the sorption of cationic corrosion products on hydrous zirconium oxide (HZrO), HThO and MAG upto 363 K and of anions on mixed oxides, like Bi(III)-Th(IV) mixed oxides, from alkaline solutions were carried out with a view to test their utility in reactor coolant water purification systems.

Adsorbents when used in Nuclear Energy applications are liable to see radiation fields, which can affect and/or influence their sorption properties. With this view, in-vivo γ-radiation effect on the sorption properties of some representative hydrous oxides has been studied and the results will be discussed.

Results of our recent studies on the properties and mechanism of reactions of silver exchanged molecular sieve for the removal of CH_3I are also discussed.

1.0. INTRODUCTION

Investigations on inorganic ion exchangers like thorium arsenate (TA) [1,2], a variety of hydrous oxides and mixed oxides [3-14], ferrocyanide molybdate, ferrocyanide tungstate [15] and sorbents like molecular sieves have been carried out in Chemical Group, BARC, with a view:

1. to understand the fundamental aspects of ion exchange and/or sorption properties of these materials, and

2. to see whether these materials could find possible application in Nuclear Energy Programmes, like purification of reactor coolant water, recovery of uranium from sea water, treatment of radioactive wastes etc.

Salient features of the studies will be summarised in this paper. Results of preliminary experiments on the effect of irradiation on inorganic ion-exchangers are also included.

2.0. BASIC STUDIES ON INORGANIC ION EXCHANGERS

2.1. Influence of Method of Preparation on the Properties of Inorganic Ion Exchangers

In general, the stability, structure and ion exchange and/or sorption properties of inorganic ion exchangers have been found to depend on the conditions of preparation [16]. Our experience has indicated that it is applicable in the case of thorium arsenate (TA) and hydrous oxides also.

In the case of TA, slight variation in the preparation conditions resulted in new crystalline forms of TA viz $Th(HAsO_4)_2$ $2.5\ H_2O$ and $Th(HAsO_4)_2 . 4H_2O$. [1,2], compared to the one reported in the literature, viz, $Th(HAsO_4)_2 . H_2O$. [17]. The interlayer distance of the new crystalline forms were larger - namely, for $TA.2.5H_2O$ it was 8.59 A^0 and $TA.4H_2O$ it was 8.23 A^0 - as compared to the material reported in literature, $TA.H_2O$ (7.05A) [17]. The new crystalline forms were capable of exchanging larger ions like Na^+, K^+ in addition to Li^+, while $TA.H_2O$ could take up only Li^+ [17].

Anion and cation sorption properties of hydrous oxides were found to depend on the nature of the alkali used for precipitation [3,4,7,8,10,11]. Thus, hydrous oxides prepared using NaOH had better cation sorption and the ones prepared using NH_4OH had better anion

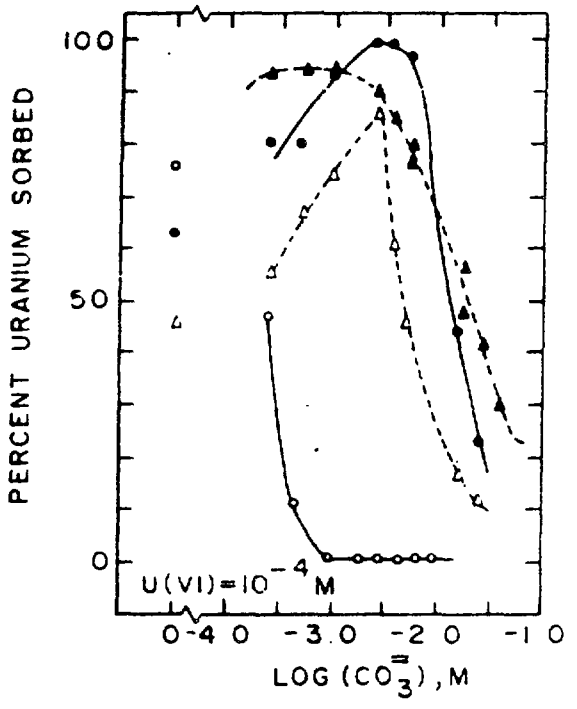

Fig.1 Effect of method of preparation and carbonate ions on the sorption of Uranium on hydrous titanium oxide (HTiO) [13]
o,HTiO(D); ● ,HTiO(H); △ ,HTiO(D-T); ▲,HTiO(H-T)
[D-Direct precipitation; H- Homogeneous precipitation; T- treated]

sorption properties. In the specific case of hydrous titanium oxide [13], it was established that when NaOH was used for precipitation, excess Na^+ was incorporated in the oxide matrix and when urea was used, the hydrolysis of Ti^{4+} was incomplete. As a consequence, the two preparations had different sorption characteristics (Fig.1). However, when excess Na^+ was removed by dilute acid treatment and complete hydrolysis ensured by alkali treatment, the sorption chareacteristics of the two materials were very similar.

Our experience, thus, indicates that for better understanding of the properties of inorganic ion exchangers, conditions of preparations should be carefully chosen and impurities present in the materials should be detected and removed by suitable treatment.

2.2. Properties of Crystalline Thorium Arsenate [1,2]

As mentioned earlier, the thorium arsenate (TA) prepared and studied had the composition, $Th(HAsO_4)_2.2.5H_2O$, and $Th(HAsO_4)_2.4H_2O$. These materials were less stable chemically and thermally than the $Th(HAsO_4)_2.H_2O$ reported in literature [17]. Although both the materials exchanged with Li^+, Na^+ and K^+, $TA.2.5H_2O$ was found to be chemically and thermally more stable than $TA.4H_2O$. The exchangers underwent

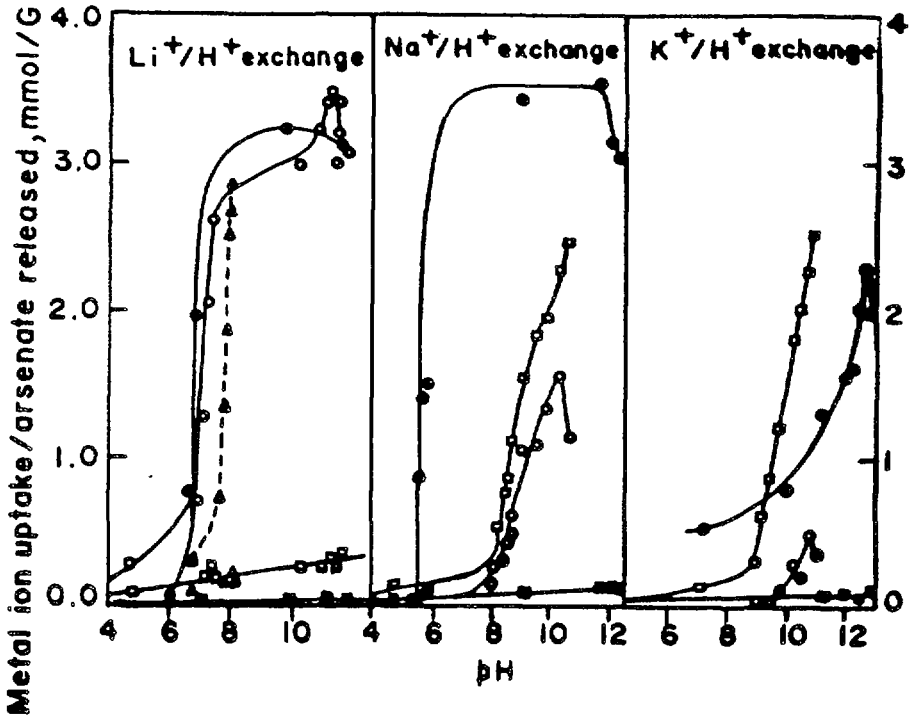

Fig.2 Alkali metal ion/H^+ exchange as a function of pH on TA.2.5H_2O in aqueous and methanolic media [1]
o,metal ion uptake in aqueous medium; •,metal ion uptake in methanolic medium ; □ ,arsenate released in aqueous medium; ■,arsenate released in methanolic medium; ▲,Li^+ uptake in aqueous medium (reverse exchange); △,arsenate released in aqueous medium (reverse exchange)

extensive hydrolysis during exchange. The maximum Li^+ ion uptake and the corresponding arsenate released, respectively, are: 1.75 and 1.20 mmol/g for TA.4H_2O at pH 9.0 and 3.42 and 0.28 mmol/g for TA.2.5H_2O at pH 11.8. In methanolic medium, it was possible to incorporate significant amounts of Na^+ and K^+, ions in TA 2.5.H_2O, without extensive release of arsenate ions. Hysteresis in Li^+-H^+ exchange was observed for TA.2.5H_2O (Fig.2).

The metal ion exchanged materials had different crystal structure as compared to H^+-form. The number of water molecules associated with the metal ion exchanged form followed the same sequence as observed in the various cationic form of synthetic organic ion exchangers [18]: $Li^+ > Na^+ > K^+$. The water was not free, as indicated by the absence of H_2O bending modes in IR spectra, and presumably existed partially hydrolysed structures.

2.3. Properties of Hydrous oxides

As hydrous oxides behave as cation exchangers in alkaline medium and as anion exchangers in acid medium the cation and anion exchange behaviour of some hydrous oxides have been investigated.

2.3.1. Alkali metal ions

Sorption of alkali metal ions from alkaline solutions either decreases with increasing ionic radii of the cations (for example, $Li^+ > Na^+ \geq K^+ > Cs^+ > NH_4^+$ on hydrous thorium oxide [3]), and with increasing hydrated radii of the cations (for example, $Cs^+ \sim K^+ > Na^+ > Li^+$, on magnetite [5])(Table I). This indicates that on hydrous thorium oxide, cations are partially or fully dehydrated on sorption, while on magnetite hydration of the exchanging ions is more or less unaffected.

TABLE I: Sorption of alkali metal ions on hydrous thorium oxide (HThO) and magnetite(MAG) from 0.1M MeOH solutions(Me= Li^+, Na^+, K^+, Cs^+, NH_4^+)[3,5]

Metal ion	Crystal ionic radii A^0	Amount sorbed (meq/g)	
		HThO	MAG
Li^+	0.68	1.15	0.54
Na^+	0.97	1.03	0.68*
K^+	1.33	1.04	0.78
Cs^+	1.67	0.96	0.71
NH_4^+	1.43	0.46	-

* From 0.13M solution.

2.3.2. Alkaline earth metal ions

Sorption of alkaline earth metal ions is a complicated process because of the contribution to the sorption from hydrolysis of the cations. As a result of this, sorption show an abrupt increase over a narrow pH range [12].

2.3.3. Transition metal ions

Sorption of transition metal ions from neutral solutions on hydrous thorium and zirconium oxides, magnetite, La(III)-Fe(III) mixed oxides, followed the sequence: [3,4,5,9,14],

$$Cu^{2+} > Zn^{2+} > Ni^{2+} > Co^{2+} > Mn^{2+}$$

The sequence parallels the Irwing-William series observed in the case of stability of metal complexes.

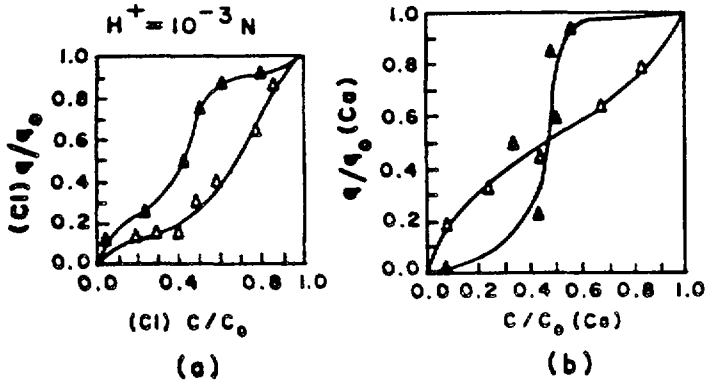

Fig.3(a) NO_3^---Cl^- Exchange isotherms on HThO[7]
▲, $\overline{NO_3}^- \rightarrow \overline{Cl}^-$; ▲, $\overline{Cl}^- \rightarrow \overline{NO_3}^-$

(b) NH_4^+--Ca^{2+} Exchange isotherms on HThO[9]
▲, $\overline{NH_4}^+ \rightarrow \overline{Ca}^{2+}$; ▲, $\overline{Ca}^{2+} \rightarrow \overline{NH_4}^+$

This indicates that surface hydroxyl groups of the hydrous oxides could be considered as ligands and sorption of cations viewed as surface complex formation.

2.3.4. Hysteresis in ion exchange isotherms

Hysteresis in anion exchange involving simple anions like NO_3^-, Cl^-, CNS^- and SO_4^{2-}, at constant solution acidity and ionic strength on hydrous thorium oxide (HThO) has been observed for the first time [7] (Fig.3a). Subsequent to our reporting, hysteresis in anion exchange on commercially available hydrous oxides has been reported [19], although, in general, it is claimed that anion exchange reactions on hydrous oxides are reversible [20,21,22]. The reason for the hysteresis in anion exchange is not yet clear. One could, however, tentatively suggest the differences in the structure of the exchanging sites (for example, $\equiv Me\text{-}OH_2^+ NO_3^-$, $\equiv Me\text{-}OH_2^+ Cl^-$, where $\equiv Me\text{-}OH$ is a surface hydroxyl group), in the forward and reverse exchange as the cause of the observed phenomenon. Further investigations are needed in this area to clearly understand the anion exchange behaviour on hydrous oxides.

Certain cation exchange reactions on HThO have been found to be non-reversible [9], for example, between alkali metal ions and Ca^{2+}, pairs of transition metal ions, like Cu^{2+}-Zn^{2+}, Cu^{2+}-Ni^{2+}, Cu^{2+}-Co^{2+}. The non-reversibility could be due to selective binding of ions as in the case of Ca^{2+} or due to specific sorption, which include electrolyte sorption, as in the case of Cu^{2+}. However, NH_4^+-Ca^{2+} exchange exhibited hysteresis (Fig. 3b). A combination of buffering action of NH_4^+ and precipitation of Ca^{2+} in solution, has been proposed to explain the observed behaviour.

2.4. Effect of γ-radiation on the sorption of Metal Ions on Hydrous Oxides

The impetus gained in the study of inorganic ion exchangers is due to the radiation stability of these materials [23]. It is to be expected that these materials, when exposed to radiation in dry conditions, would not appreciably change their physical and chemical characteristics. However, when exposed to radiation in contact with aqueous solutions, as in actual applications, the inorganic ion exchangers could undergo some changes and hence behave differentially as a result of formation and interaction of radiolytic products of water such as H, OH, e^- H_2O_2 etc. [24]. Not many studies have been reported with regard to the influence of in-situ radiation on the sorption properties of inorganic ion exchangers.

Some preliminary investigations have been carried out with HTiO and magnetite (MAG) (representing hydrous oxides of varying acidities) (Fig.4), to find out the influence of γ-radiation field on their sorption properties. These hydrous oxides also find possible application in radioactive waste disposal (HTiO) and in reactor coolant water systems (MAG). Sorption of Li^+ was studied, because it is a non-specific ion and its sorption would indicate the changes in the oxides due to γ-radiation.

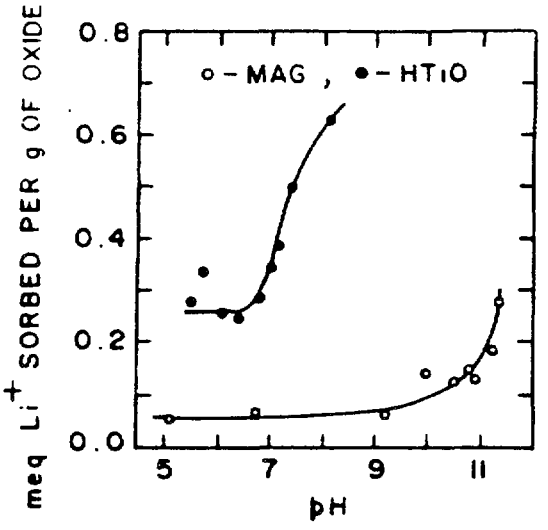

Fig.4 Sorption of Li^+ on magnetite(MAG) and hydrous titanium oxide(HTiO) from LiCl+LiOH(~0.01M)solutions.

The salient results of the investigations are listed in Table II. Within the limits of the experimental error, there appears to be no change in the uptake of Li^+ on the two hydrous oxides even after in-situ γ-dose of >17 Mrad. The significant observation in the study was that in presence of radiation, the pH of the supernatant solution in contact with HTiO was higher than the unirradiated samples, in contrast to the pH of the supernatant

TABLE II: Effect of γ -radiation on the sorption of Li^+ on magnetite (MAG) and hydrous titanium oxide (HTiO).

Time*	No irradiation			With irradiation		
h	pH Initial	pH Equil.	Amt.of Li^+ sorbed meq/g (±0.02)	pH Initial	pH Equil.	Amt. of Li^+ sorbed meq/g (±0.02)
MAGNETITE						
4	11.27	10.92	0.05	11.27	10.90	0.07
24	11.27	10.95	0.07	11.27	10.77	0.06
48	11.27	10.72	0.05	11.27	10.38	0.06
67	11.28	10.76	0.08	11.28	10.4	0.10
HTiO						
4	11.57	9.57	0.58	11.57	10.11	0.56
24	11.57	8.15	0.58	11.57	9.00	0.57
48	11.61	7.76	0.60	11.61	8.50	0.57
68	11.61	8.00	0.60	11.61	8.27	0.60

* Time of equilibration or irradiation..
Conditions+ Oxide 0.4g; Soln. 25ml; for MAG a mixture of LiOH+LiCl (0.01M); for HTiO 0.01M LiOH. Strength of γ-source 0.26M rad/h.

solution in contact with MAG, which was lower. There was no apparent change in the physical nature of MAG. HTiO changed its colour to yellow on exposure to radiation, presumably due to the interaction of H_2O_2 (a product of radiolysis) with Ti of HTiO.

Further work is needed in order to understand better the pH changes observed in this study.

3.0. APPLIED STUDIES WITH RESPECT TO NUCLEAR ENERGY PROGRAMMES

3.1. Purification of Reactor Coolant Water

One of the envisaged application of inorganic ion exchangers was their use as possible purification materials for the reactor coolant water, because of the expected thermal stability of this class of materials [25]. Magnetite (MAG) appeared to be an attractive material as it is already present in the reactor and its use could not add a new component to the reactor coolant system. Sorption studies with MAG would also lead to a better understanding of the activity transport phenomenon in reactor coolant systems.

TABLE III: Sorption of corrosion product cations on hydrous oxides from a mixture of ions at 363 K under flow conditions [4]

Hydrous oxide	Influent		Amount of traced ion sorbed, µg/g			
	Total amt. of ions present in mixture (µg)	Amt. of traced ion present in the mixture (µg)	Cr^{3+}	Fe^{3+}	Mn^{2+}	Co^{2+}
HZrO	6400	1600	816	560	256	224
HThO	4000	1000	350	340	70	50
MAG	6400	1600	1184	688	0	13

Conditions: Hydrous oxide 1g; Soln. pH ~6; Concn. of each ion 1 µg/ml; flow rate 50 ml/h.

3.1.1. Sorption of corrosion product cations

Sorption of corrosion product cations (Fe^{3+}, Cr^{3+}, Co^{2+}, Mn^{2+}) in trace concentrations on hydrous zirconium oxide (HZrO), HThO and MAG under dynamic conditions upto 363 K was investigated [4]. The performance of the hydrous oxides is given in Table III. At higher pH, the sorption of Co^{2+} and Mn^{2+} on these hydrous oxides increased, presumably due to presence of hydrolysed species.

3.1.2. Studies on mixed oxides

With a view to develop an adsorbent capable of sorbing anions from alkaline solutions, different hydrous mixed oxides were prepared by incorporating a metal ion of higher valency into the bulk oxide matrix. Among the several combination of mixed oxides tested, like Bi(III)-Th(IV), Bi(III)-Zr(IV), Bi(III)-Ti(IV), Ti(IV)-Sb(V) etc. Bi(III)-Th(IV) mixed oxide was found to be most promising, sorbing Cl^- ions from alkaline solutions [6].

Attempts were made to improve the halide ion sorption of Bi(III)-Th(IV) mixed oxide by incorporating Ag^+ ion in the matrix [8]. By loading Ag^+ ion on Bi(III)-Th(IV) mixed oxide, by equilibrating with $AgNO_3$ solution, no beneficial effect was observed. However, sorption of halide ion increased with increasing Ag^+ content in the mixed oxide, when the oxide was prepared by coprecipitating Ag^+ along with Bi(III) and Th(IV) (Table IV).

These materials may find possible use in the removal of halide ions from reactor coolant water and from spent fuel storage tank water.

3.2. Removal of Organic Radioiodine using Ag^+ Molecular Sieve

Another aspect of our current interest is in evaluating the basic properties of silver exchanged

TABLE IV: Sorption of halide ions on hydrous Bi(III)-Th(IV) mixed oxides (Bi/Th = 4) [8]

Test Solution	Sorption capacity, meq/g					
	Bi-Th mixed oxide		Bi-Th-Ag coprecipitated oxide			
	Pure oxide	Ag^+ loaded oxide	Ag^+ present in the mixed oxide, meq/g			
			0.10	0.29	0.57	1.38
0.1M NaCl	1.07	0.91	0.16	0.46	0.70	1.38
0.1M NaBr	1.04	0.90	0.12	0.72	0.84	1.76
0.1M KI	0.94	1.05	0.17	0.50	0.79	1.46
0.05M KI	1.0	1.01	0.16	0.45	0.77	1.46
0.05M KI + 10^{-5} M NaOH	0.98	1.05	0.15	0.47	0.77	1.51
0.05M KI + 10^{-4} M NaOH	0.96	0.89	0.19	0.47	0.77	1.54
0.05M KI + 10^{-3} M NaOH	0.92	0.90	-	-	-	-
0.05M KI + 10^{-2} NaOH	0.42	0.49	-	-	-	-

(a) Mixed oxide precipitated using NH_4OH; (b) Ag^+ loading on the mixed oxide = 0.08 meq Ag^+/g of oxide; (c) precipitation effected using NaOH.
Conditions: Oxide 0.5 g; solution 25 ml; equil.time 24 h.

TABLE V: Quantity of CH_3I adsorbed/consumed [26] (x 10^{-4} + 0.5 ml)

Temperature (K)	A Hydrated 13X	B Dehydrated 13X	C Hydrated Ag^+ 13X	D Dehydrated Ag^+ 13X
298	0.84	23.6	13.8 (16.5)*	31.5 (36.2)*
323	0.56	21.1	18.2	30.1
375	0.42	16.5	23.3	28.2
423	-	13.1	21.7	26.2

Molecular sieve used 1g; Silver content in Ag^+ 13X, 1.5 mmol g^{-1}
( )* with concommittent γ dose of 0.4M rad h^{-1}.

molecular sieves used for the removal of volatile organic radioactive iodine species from off gas streams of nuclear installations. The development of an efficient and at the same time less expensive adsorbent than silver loaded matrices demands a knowledge of the basic chemical processes involved in the chemisorption-decomposition of CH_3I and of the role of silver.

Our studies [26] covered identity and yields of chemical products formed in the reaction of CH_3I over plain and silver exchanged (16%) 13X molecular sieve as a function of temperature, humidity and γ-radiation field. Mechanistic aspects of the reaction were inferred from supportive evidence from X-ray photoelectron spectroscopy. The main results are given below:

(i) Hydrated (18%) plain 13X permits only negligible physiabsorption of CH_3I which is uninfluenced by concommittent γ-radiation field (Table V).

(ii) Dehydrated (at 575 K for 6 hours) plain 13X shows significant adsorption capacity for CH_3I which decreases with increasing temperature and the capacity is unaffected by γ-irradiation (Table V). No reaction products are observerd at temperatures below 500 K and the adsorbed CH_3I could be desorbed at 600 K. Repeat use of the same matrix for upto 5 cycles (adsorption and regeneration) shows no measurable change in its behaviour. Ingress of moisture during adsorption cycle drastically reduces the adsorption capacity.

(iii) Exposure of CH_3I to hydrated (18%) silver exchanged (16%) 13X produces two products namely, CH_3OH and CH_3OCH_3, the yields of which increase with increasing temperature. The adsorption capacity increases with temperature and γ-radiation dose (Table V). It appears that more CH_3I is consumed than is required for a stoichiometric reaction between CH_3I and silver which is particularly noticeable at higher temperatures (Table V, Column C). The reaction products CH_3OH and CH_3OCH_3 do not react with bound iodine if present in Ag^+ 13X to regenerate again volatile organic iodides under the influence of temperature and/or γ-radiation field.

(iv) In the case of dehydrated Ag^+ 13X, although as expected no oxygenated reaction products are produced, small amounts of the hydrocarbons CH_4 and C_2H_6 are released, the yields of which increase with temperature. Beyond 575 K free iodine is also released from the matrix.

A few significant conclusions drawn from this study are

(i) more CH_3I is consumed over Ag^+ 13X than is required for a stoichiometric reaction between CH_3I and silver indicating participation of Na^+ of molecular sieve in the fixation of iodine.

(ii) CH_3I interaction with hydrated Ag^+ 13X is through the formation of methyl carbonium ion and

(iii) use of two dehydrated plain molecular sieve beds in series followed by a small bed of hydrated Ag^+ molecular sieve could be considered as an attractive alternative to the use of a single Ag^+ molecular sieve adsorber for the removal of radioactive CH_3I.

TABLE VI: Sorption of uranium on hydrous oxides from different uranyl salt solutions [11]

Hydrous oxide	Salt → used	Uptake of uranium, mmol U/g of oxide			
		Nitrate	Chloride	Sulphate	Tricarbonate
HTiO(H)		0.86	0.75	0.77	0.44
HTiO(Am)		0.66	0.52	0.56	0.34
HTiO(So)		0.81	0.68	0.60	0.26
HCeO(Am)		0.31	0.16	0.42	0.17
HCeO(So)		0.43	0.29	0.33	0.25
HZrO(Am)		0.20	0.12	0.29	0.13
HZrO(So)		0.33	0.14	0.36	0.17
HThO(Am)		0.05	0.02	0.09	0.01
HThO(So)		0.15	0.09	0.08	0.05

(H) Oxide homogeneously precipitated. (Am) Oxide precipitated using NH_4OH. (So) Oxide precipitated using NaOH.
Conditions: UO_2^{2+} - 0.01M; pH 3.5; for tricarbonate soln. ~9; oxide 0.3g; soln. 25 ml; contact time 24 h.

3.3. Recovery of Uranium from Sea-water

In recent years there has been a growing interest in developing sorbents for the recovery of uranium from sea-water. With this view in mind, different hydrous oxides, HTiO, hydrous cerium oxide (HCeO), HZrO, and HThO were screened in order to find a suitable sorbent for uranium [10]. In general sorption of uranium decreased with decreasing acidic nature of the oxide. Moreover, on acidic oxides like HTiO, HCeO, uranium was sorbed as uranyl ion and on less acidic oxides like HZrO, HThO, electrolyte sorption, involving uranyl ion and anion, was predominant [10]. Uranium sorption also depended on the salt used for the sorption experiment [11] (Table VI). Sorption was high when a nitrate was used and was low when carbonate was used. Among the hydrous oxides investigated, HTiO and HCeO were found to be more suitable for the sorption of uranium from carbonate solutions [11].

More detailed investigations were carried out with HTiO using uranium in millimolar concentrations [13]. HTiO prepared using NaOH did not exhibit good sorption characteristics as Na^+ was present in the material. The sorption characteristics improved on removing the Na^+ impurity (Fig.1). HTiO prepared using urea had large surface area and had only partially hydrolysed Ti^{4+}, and exhibited good sorption property as such. In large scale preparation and operation, this particular material could prove useful, unlike the NaOH-precipitated material, because the partially

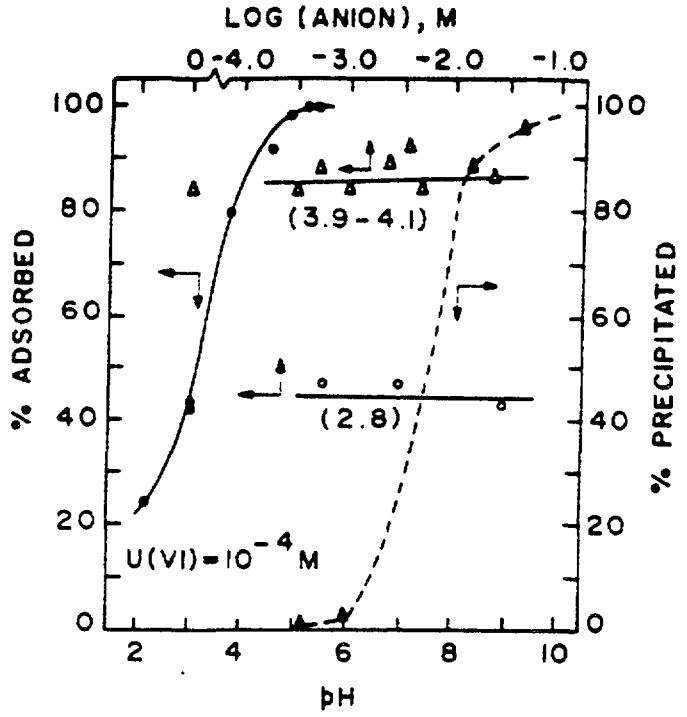

Fig.5 Sorption of Uranium on HTiO[13]

as a function of : •,pH; ○, NO_3^- concentration; △,SO_4^- concentration. Equilibrium pH values for anions are given in brackets.▲,Precipitation of uranium as a function of pH.

hydrolysed Ti^{4+} sites could also act as acidic sites, in addition to the surface hydroxyl groups, and bind more uranyl ions.

pH of the solution had a marked influence on the sorption of uranyl ion (Fig.5) than the added anions like Cl^-, NO_3^-, SO_4^-. Sorption of uranium from carbonate solutions was limited by the acidity of the surface groups, because the sorption involved breaking of the uranium-carbonate complex present in solution [13] (Fig.1). The sorption of uranium from simulated sea-water was restricted by the competive sorption of Ca^{2+}, Mg^{2+} present in solution.

REFERENCES

[1] SARPAL, S.K., GUPTA, A.R., J. Inorg. Nucl. Chem., 43 (1981) 1347.

[2] SARPAL, S.K., GUPTA, A.R., J.Inorg. Nucl. Chem., 43 (1981) 2043.

[3] VENKATARAMANI, B., VENKATESWARLU, K.S., SHANKAR, J., Proc. Indian Acad. Sci., 87A (1978) 409.

[4] VENKATARAMANI, B., VENKATESWARLU, K.S., SHANKAR, J., BEATSLE, L.H., Proc. Indian Acad. Sci., 87A (1978) 415.

[5] VENKATARAMANI, B., VENKATESWARLU, K.S., SHANKAR, J., J.Collois. Inrterf. Sci., 67 (1978) 187.

[6] VENKATARAMANI, B., VENKATESWARLU, K.S., SHANKAR, J., BEATSLE, L.H., J.Colloid Interf. Sci., 76 (1980) 1.
[7] VENKATARAMANI, B., VENKATESWARLU, K.S., J. Inorg. Nucl. Chem., 42 (1980) 909.
[8] VENKATARAMANI, B., VENKATESWARLU, K.S., Proc. Indian Acad. Sci., (Chem. Sci.), 89 (1980) 241.
[9] VENKATARAMANI, B., VENKATESWARLU, K.S., J. Inorg. Nucl. Chem., 43 (1981) 2549.
[10] MAHAL, H.S., VENKATARAMANI, B., VENKATESWARLU, K.S., J. Inorg. Nucl. Chem., 43 (1981) 3335.
[11] MAHAL, H.S., VENKATARAMANI, B., VENKATESWARLU, K.S., Proc. Indian Acad. Sci., (Chem. Sci.), 91 (1982) 321.
[12] MAHAL, H.S., VENKATARAMANI, B., Unpublished work.
[13] VENKATARAMANI, B., GUPTA, A.R., Paper presented at the Int. Meeting on the Recovery of Uranium from Sea Water, Tokyo, Japan (Oct. 17-19, 1983)), Paper No. 32.
[14] MAHAL, H.S., VENKATESWARLU, K.S., Indian J. Chem., 16A (1978) 712.
[15] BHARGAVA, S.S., VENKATESWARLU, K.S., Indian Chem., 14A (1976) 800.
[16] CLEARFIELD, A., NANCOLLAS, G.H., BLESSING, R., "Ion Exchange and solvent Extraction" (MARINSKY, J.A., MARCUS, Y. Eds.) Vol.5, Marcel Dekker, New York, NY (1973) 1.
[17] ALBERTI, G., MASSUCCI, M.A., J.Inorg.Nucl.Chem., 32 (1970) 1719.
[18] NANDAN, D., GUPTA, A.R., Indian J. Chem., 12 (1974) 808.
[19] DYER, A., MALIK, S.A., J. Inorg. Nucl. Chem., 43 (1981) 2975.
[20] NANCOLLAS, G.H., PATERSON, R., J.Inorg.Nucl.Chem. 29 (1967) 565.
[21] RUVARAC, A. Lj., TRSTANJ., M.I., J. Inorg. Nucl. Chem., 34 (1972) 3893.
[22] MISAK, N.Z., MIKHAIL, E.M., J.Inorg. Nucl. Chem., 43 (1981) 1903.
[23] EGROV, E.V., NOVIKOV, P.D., "Action of Ionizing Radiation on Ion Exchange Materials", Israel Progr. Sci., Transl., Jerusalem (1967).
[24] SELLERS, R.M., "The Radiation Chemistry of Colloids - A Review", Central Elect. Gen. Board, Berkeley Nucl. Labs., Report, RD/B/N 3707 (1976).
[25] VENKATARAMANI, B., VENKATESWARLU, K.S., "Water Chemistry Studies VI: Role of Inorganic Ion Exchangers in the Purification of Reactor Coolant Water", Bhabha Atomic Research Centre Rep. BARC/I-123 (1971).
[26] BELAPURKAR, A.D., ANNAJI RAO, K., GUPTA, N.M., IYER, R.M., Surf. Technol., 21 (1984) 263.

ION-EXCHANGE SELECTIVITIES ON ANTIMONIC ACIDS AND METAL ANTIMONATES

M. ABE
Department of Chemistry,
Tokyo Institute of Technology,
Ookayama, Meguro-ku,
Tokyo, Japan

Abstract

Antimonic acids and metal antimonates as the inorganic ion-exchangers exhibit extremely high selectivity for a certain element or group of elements for comparison with sulfonated polystyrene ion-exchange resin. Various antimonic acid materials have been obtained with different compositions and ion-exchange properties, depending on the method of their preparations as well as on aging. The species can be divided into three groups -crystalline, amorphous and glassy. The affinity sequence for alkali metal ions shows Li < Na< K < Rb< Cs on the amorphous and glassy acid, while Li < K < Cs< Rb < Na on the crystalline acid. However, slightly different affinity series have been reported by other authors, Cs< Li< Rb< K< Na or Rb=Cs < Na on the crystalline acid. Similar disagreement between various authors exists for alkaline earth metal cation series: Mg < Ca < Sr< Ba, Ra- Ba< Ca< Sr, Mg < Ba < Ca< Sr. These selectivities for various metal ions on the crystalline antimonic acid are discussed in the terms of rate of adsorption, steric effect, and host-guest co-relations.

The antimonates of quadrivalent metal, such as Ti, Zr, and Sn, act as cation exchangers. The selectivity sequences for alkali metal ions show Li< Na< K < Rb < Cs on Zirconium antimonate, Na < K < Rb < Li < Cs on titanium antimonate and Na < K < Rb < Cs < Li on tin antimonate with microamount of metal ions in acid media. However, titanium and tin antimonates exhibit a regular selectivity sequence for alkaline earth metal cations; Mg < Ca < Sr < Ba. The selectivity on the tin antimonate varies with the loading of the alkali metal ions on the exchanger for steric effect. The selectivity sequence for macro amounts shows Li > Na > K > Rb > Cs. These selectivities are discussed in the terms of steric effect and entropy changes of the ion-exchange reactions.

1. INTRODUCTION

Synthetic inorganic ion exchangers have both thermal resistance and radiation stability and have been applied in reactor chemistry such as reprocessing of irradiated nuclear fuel. Much attention has been paid recently to the selective adsorption properties which are not found with the commercial organic resins.

During the last two decades, new inorganic ion exchangers have been synthesized and studied extensively for their ion exchange properties by various authors [1-7].

Some of the inorganic ion exchangers exhibit excellent selectivities with respect to certain element or group of elements. The selectivity on the inorganic ion exchangers increases usually with decreasing concentration of the element to be separated. However, the change in the selectivity is much depended on chemical species of the elements, co-ion present, and on the crystallinity of the adsorbent. In the chemical processing of nuclear reactor cycle, the separation of the radionuclides may be needed from a large amount of the bulk components. Overall ion exchange reaction from microamount to macroamounts of the elements should be studied for this porpose. Furthermore, high stability in the acidic solution at high concentration may be required otherwise in high resistance to high temperature and radiation field.

Various antimonic acid materials have been obtained with different chemical compositions, characteristics, and cation exchange properties. The species can be divided into three groups- crystalline(C-SbA), amorphous(A-SbA), and glassy(G-SbA) [8-11]. Compounds similar to C-SbA have been reported as polyantimonic acid (PA) and hydrated pentoxide (HAP) by different authors [12, 13].

Quadrivalent metal antimonates as ion exchangers have been studied first by Abe and Ito [14]. A number of metal antimonate has been reported by various authors. Especially, antimonates of titanium(Ti-SbA) and tin(Sn-SbA) exhibit an excellent selectivity for lithium ions [15, 16].

This paper describes comparison of the selectivity of cations on various antimonic acid and metal antimonates.

2. Experimental

2. 1. Preparations of antimonic acid cation exchangers.

The antimonic acid cation exchangers of different species were prepared as described previously [10].

2. 1. 1. Crystalline antimonic(V) acid(C-SbA).

A 75 mL of antimony pentachloride was preliminarily hydrolyzed by 75 mL of cold water, and was then hydrolyzed by 5 L of water. The precipitate obtained was kept in the mother solution at 40 °C over 20 days, and then washed with cold demineralized water until free from chloride ions using a centrifuge (about 10000 rpm). After drying the precipitate, the product was ground and sieved in the appropriate fraction of 100-200 mesh size. The collected sample was rewashed with cold demineralized water in order to remove any adherent fine particle and to obtain a clear supernatant solution in the subsequent experiments.

2. 1. 2. Amorphous antimonic acid (A-SbA).

Similar procedures to those for C-SbA were carried out, except aging overnight in cold mother solution. The subsequent procedures are the same as above.

2. 1. 3. Glassy antimonic acid (G-SbA).

The washed amorphous antimonic acid with cold demineralized water was dissolved in a hot water and cooled rapidly. The water in the solution was as quickly evaporated as possible by using fan. After drying, the subsequent procedures are the same as above.

2. 2. Preparation of metal antimonate.

The SnSbA exchanger was prepared as described previously[15].

2. 2. 1. Preparation of tin antimonate(SnSbA).

A liquid antimony(V) chloride was prehydrolyzed with an equal amount of demineralized water in order to prevent fractional precipitation of antimonic acid by further procedures. The 3.9M antimony(V) chloride solution obtained was mixed with 4.5M tin(IV) chloride solution at 80 °C. The mixed solution was immediately hydrolyzed in 50-fold volume of demineralized water at 80°C. The white precipitate was kept in the mother solution overnight, then was filtered and water-washed by using a centrifuge(about 10000 rpm) until the pH value of the supernatant solution was higher than 1.5. After drying at 60°C, the product was ground and sieved to 100-200 mesh size. The collected samples were rewashed with water in order to remove adherent fine particle of SnSbA, and finally dried to 60°C.

2. 2. 2. Preparation of titanium antimonate(TiSbA) and zirconium antimonate(ZrSbA)

Similar procedures to those for SnSbA were carried out. The solutions of titanium(IV) chloride and zirconium oxide chloride were used instead of tin(IV) chloride.

2. 3. Distribution coefficients(Kd).

The equilibrium Kd values of metal ions for microamounts were determined with a batch technique. The exchanger was immersed in the metal salt solution containing hydrochloric acid or nitric acid at different concentrations in thermostatted bath. The initial concentrations of metal ions were adjusted mainly to 10^{-4} M. The concentration of the metal ions in the exchanger and in the solution was deduced from the concentration relative to the initial concentration in the solution. The concentration of metal ions were determined by flame photometry or atomic absorption spectrometry. The Kd values were calculated as follows;

$$Kd = \frac{\text{Amounts of metal ions in exchanger}}{\text{Amounts of metal ions in solution}} \times \frac{\text{mL of solution}}{\text{g of exchanger}}$$

The Kd vakues of metal ions for comparison were normalized to a 1M nitric acid solution by extrapolating the Kd values determined.

2. 4. Overall ion exchange reactions

In the forward reactions, the exchanger(0.10 or 0.20g) in H^+ form was immersed in 10.0 or 20.0 mL of a mixed solution of varying ratio of the metal nitrate/ nitric acid in a sealed glass tube with intermittent shaking at different temperatures. The ionic strength in the mixed solution was adjusted to 0.1 after attainment of the equilibrium.

In the reverse reaction, the ion exchanger in various metal ion forms, corresponding in weight to 0.10 or 0.20 g of the exchanger in H^+ form was immersed in 10.0 or 20.0 mL of the mixed solutions with ionic strength of 0.1 after equilibriation. The concentration of the metal ions in the exchanger and in the solution was deduced from the concentration relative to the initial concentration in the solution.

2. 5. Preparation of the exchanger in metal ion form.

A 0.1M metal nitrate solution was charged continuously at the top of the column of the exchanger in the hydrogen ion form until the change in the concentration of the metal ions was negligible between the effluent and feed.

2. 6. Reagents. The antimony(V) chloride (Yotsuhata Chemical Co. Ltd.) and tin(IV) chloride (Wako Chemical Co. Ltd.) were used without further purification. The other reagents used were all of analytical grade.

3. Theoretical Aspects

The ion exchange reactions of metal ions/H^+ exchange system on the exchanger can be represented by the following expression;

$$\overline{n\,H^+} + M^{n+} \rightleftharpoons \overline{M^{n+}} + n\,H^+ \qquad (1)$$

where bar refers to exchanger and M^{n+} is metal ions with valency n.

The thermodynamic equilibrium constant, K, of the above reaction can be difined as:

$$K = \frac{m_{H^+}^n \,\overline{X}_{M^{n+}}\, \gamma_{H^+}^n \,\overline{f}_{M^{n+}}}{m_{M^{n+}} \overline{X}_{H^+}^n \,\gamma_{M^{n+}}\, \overline{f}_{H^+}^n} = K_H^M \frac{\overline{f}_{M^{n+}}}{\overline{f}_{H^+}^n} \qquad (2)$$

where K_H^M is the selectivity coefficient, m_{H^+} and $m_{M^{n+}}$ are the molalities of HNO_3 and $M(NO_3)_n$ in solution, and γ_{H^+} and $\gamma_{M^{n+}}$ are the ionic activity coefficients of H^+ and M^{n+} in solution. $\overline{X}_{H^+}$ and $\overline{X}_{M^{n+}}$ are the equivalent fractions of the exchanging H^+ and M^{n+} in the exchanger phase and $\overline{f}_{H^+}$ and $\overline{f}_{M^{n+}}$ are the activity coefficients of H^+ and M^{n+} in the exchanger phase, respectively.

The contribution of the ionic activity coefficiens in solution to the thermodynamic equilibrium constant can be neglected for uni-univalent exchange reactions, while not for uni-multivalent reactions. The values of the ionic activity coefficient ratio ($\gamma_{H^+}^n / \gamma_{M^{n+}}$) in solution have been used in the following equation [17]:

$$\log \frac{\gamma_{H^+}^n}{\gamma_{M^{n+}}} = \log \frac{\gamma_{\pm HNO_3}^{2n}}{\gamma_{\pm M(NO_3)_n}^{1+n}} = \frac{n\,S\,\sqrt{I}}{1 + 1.5\sqrt{I}}$$

$$S = 1.8252 \times 10^6 \left(\frac{\rho}{\varepsilon^3 T^3} \right)^{1/2} \qquad (4)$$

where ρ is the density of water, ε the dielectric constant of water, and T the absolute temperature of the system.

The thermodynamic equilibrium constant can be evaluated by using the simplified treatment of Gains-Thomas equation [18], assuming that the change of water content in the exchanger and entrance of anion from solution phase are negligible.

$$\ln K_H^M = -(Z_M - Z_H) + \int_0^1 \ln K_H^M \, d\overline{X}_M \qquad (5)$$

When the $\ln K_H^M$ versus $\overline{X}_M$ are linear, the $\ln K_H^M$ is given by

$$\ln K_H^M = 4.606\, C\, \overline{X}_M + \left(\ln K_H^M \right)_{\overline{X}_{M^{n+}} \to 0} \qquad (6)$$

where the C is the Kielland coefficient [19], and $(\ln K_H^M)_{\bar{X}_M \to 0}$ is a value of $\ln K_H^M$ obtained by extrapolating X_M to zero. The change in the free energy of the ion exchange reaction, ΔG° , was calculated per cation equivalent,

$$\Delta G^\circ = -(RT/Z_M Z_H) \ln K \qquad (7)$$

The change in the enthalpy, ΔH°, and the entropy, ΔS° , were calculated in the usual way [20].

The theoretical cation capacity(5.057 meq/g) of the exchangers was evaluated by assuming that one antimony gives one hydrogen ion available for cation exchange reaction.

4. Result and Discussion

4. 1. Selectivities on different antimonic acids.

4. 1. 1. Distribution coefficient(Kd) of microamounts.

The determination of the Kd values gives useful information for the separation of trace and microamounts of the elements in the fields of analytical chemistry, radiochemistry, environmental chemistry, and biochemistry. Nitric acid media have been used in order to obtain fundamental ion exchange data in the less complexing media, which are useful for application to the reprocessing of nuclear fuel.

Equilibrium distribution coefficients of alkali metal ions on C-SbA, A-SbA, and G-SbA were plotted in Fig. 1, values on Bio-Rad AG 50W-X8 being included for comparison. The Kd values for alkali metal ions on their inorganic exchangers, except C-SbA, increase in the order Li< Na < K < Rb < Cs as shown with sulfonate-type organic resins. The separation factors are more favorable than

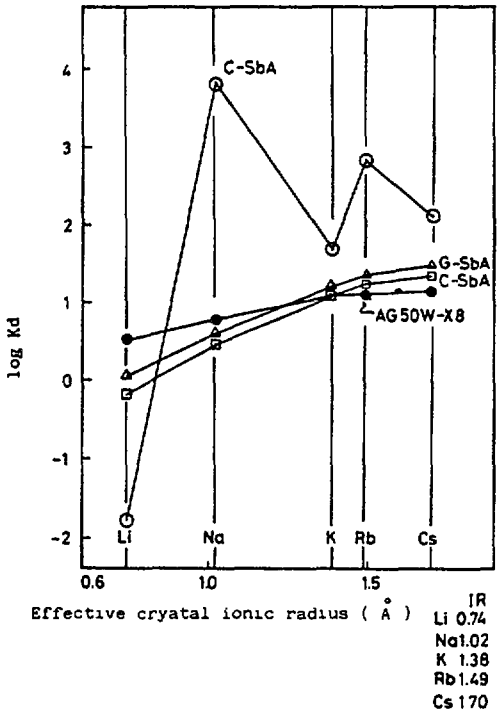

Fig. 1. The log Kd values of alkali metal ion on different antimonic acids

C-SbA; crystalline, A-SbA; amorphous, G-SbA; glassy alkali metal ions; 10^{-4}M, HNO_3 1 M, total vol. 25 mL, exchangrer; 0.25 g.

those obtained on Bio-Rad AG 50W-X8. The Kd values of metal ions on the Bio-Rad AG 50W-X8 are taken from the data reported by Strelow [21]. The increased selectivity was observed as Bio-Rad AG50W-X8 < A-SbA < G-SbA. The adsorptive properties on the G-SbA showed essentially the same as those on the A-SbA, while the differences in the selectivity may be due to that the apparent density of the G-SbA is higher that of A-SbA. However, C-SbA showed an unusual selectivity for alakli metal ions Li < K < Cs < Rb < Na.
An extremely low adsorption properties was observed for Li on C-SbA, while an extremely high Kd value was determined for Na even in a concentrated nitric acid solution.

Similar unusual selectivity was also found for other metal ions on the C-SbA: an extremely low selectivity for Mg, Ni, and Al and an extremely high for Ca, Sr, Pb, Cd, and Hg (Fig. 2).

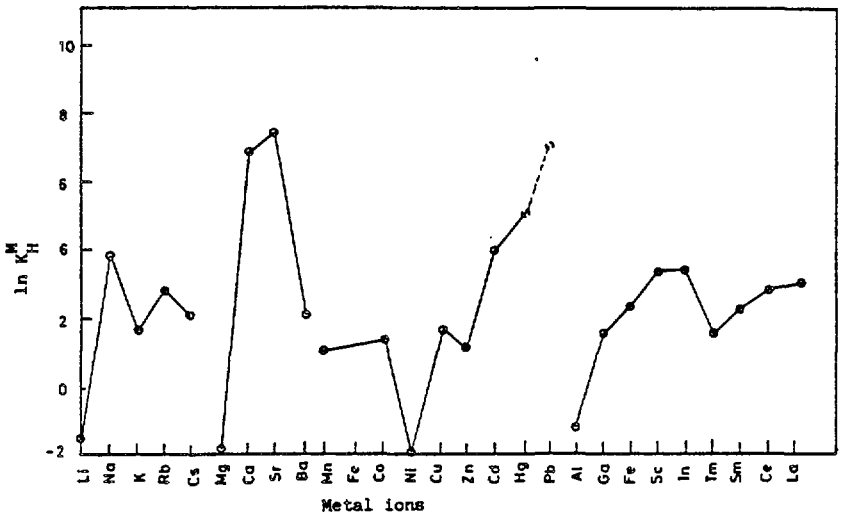

Fig. 2. The ln K_H^M of various metal ions on C-SbA in 1M HNO_3

Conditions; same as Fig. 1.

On the organic ion exchange resins, the Kd values of alkali metal ions are nearly constant for the solution containing alkali metal ion at the concentration lower than 1 m mol/L in a relatively high concentration of acid(> 0.1 M). However, it has been known that the kd values change with the concentration of the metal ion loaded on some inorganic ion exchangers, although the acid concentration is unity and relatively high, because of their steric effects. The log-log plotts of the Kd values vs $[H^+]$, were demonstrated on Fig. 3, with the change in the concentration of Mg and Ba [22]. The ion exchange ideality is maintained up to relatively high concentration of 10^{-3}M, indicating that the slopes, d log Kd/ d log $[H^+]$, are about 2. The Kd values increase with decreasing the concentration of the metal ions even in the same concentration of hydronium ions.

A systematic study of the distribution coefficient of metal ions on C-SbA has been reported by Abe and co-workers. Girardi and co-workers have reported that about 3,000 adsorption and elution cycle were carried out in a

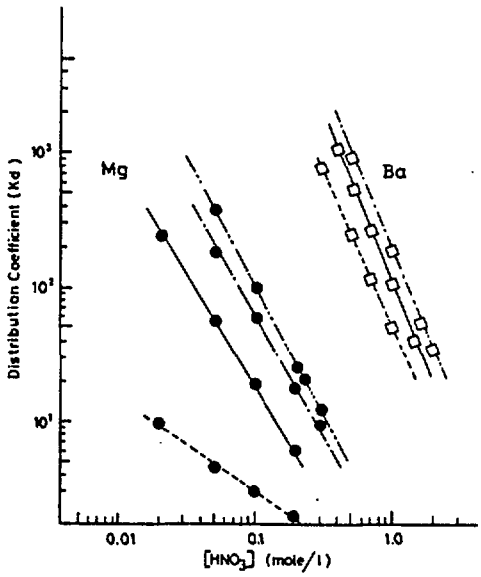

Fig. 3. The Dependence upon the initial concentration of the metal ions for the Kd of Mg and Ba on C-SbA.

Initial concn.; (- - -)10^{-2}M, (——)10^{-3}M, (—.—)10^{-4}M, (—···—)10^{-5}M

standardized way over eleven adsorbents(including 9 inorganic ion exchangers) from various media for preliminary screening of possible material to use for radiochemical separation [12]. A comparative study of ion exchange selectivity between C-SbA and HAP reported by Girardi et al. was carried out by Abe. The evaluated selectivities on HAP are essentially compatible with those of C-SbA for 18 but out of 4 metal ions [23].

4. 1. 2. maximum uptake of metal ions on C-SbA

The maximum uptakes were determined by the column technique mentioned at the section 2. 5. The maximum uptakes on inorganic ion exchangers have been known to vary extensively with the nature of cation species, temperature, concentration of cation in solution, and co-ion present, while the organic ion exchange resins have fairly constant capacity due to their elastic structure. The maximum uptakes for alkali and alkaline earth metal ions, except Li and Mg on the C-SbA decrease with increasing effective ionic crystal radii [23] (Fig. 4). This can be explained by the effect of steric effect. The maximum uptakes of Mn, Cd, and Pb was about 6 meq/g, which is higher than the theoretical capacity of 5.057 meq/g. The additional capacity may be explained by assuming the adsorption of hydroxo-aquo species or polynuclear species in the exchanger at high concentration of these metal ions in high pH media [23]. The metal ions having small crystal ionic radii show strong tendency to be more highly hydrated than the larger ions. This causes weak electrostatic force on the surface of the hydrated shell of the small cations.

4. 1. 3. Ion exchange isotherms on C-SbA.

Ion exchange isotherms have used to represent graphically experimental data pertinent to steric and ion sieve effect. The ordinate of these plots, $\overline{X_M}$, is the

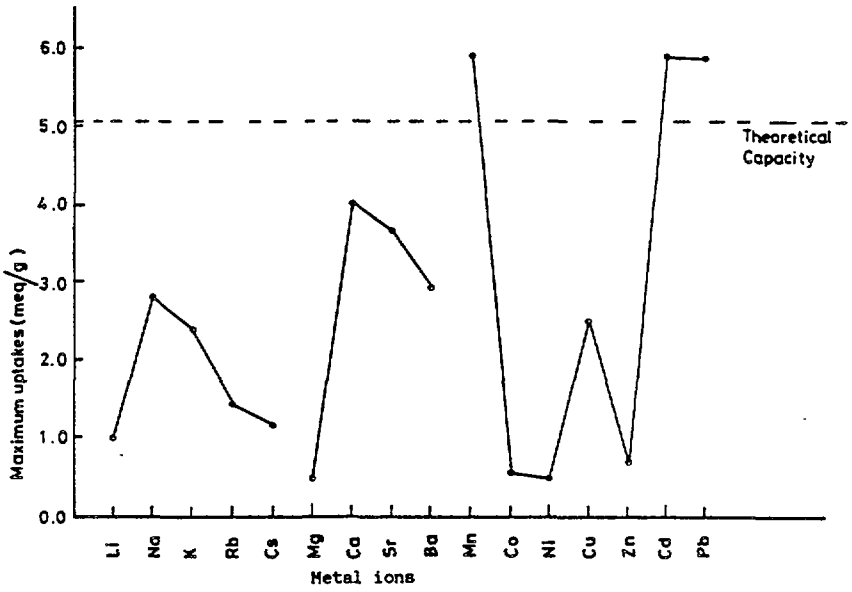

Fig. 4. Maximum uptakes of metal ions on C-SbA

equivalent fraction of the ion M^{n+} in the exchanger phase and the abbcissa, X_M , is in the solution. Cation exchange resins of strong acid type have essentially elastic structure and display swelling and shrinking depending upon the nature of the exchanging cations with hydration. They display isotherms which do not deviate greatly from the ideal ones. Inorganic ion exchangers generally have rigid structures and display curve in which K_H^M varies greatly with the ion exchanging cations. When small cations are exchanged with large cations, the ingoing cation is initially preferred, and the degree of exchange gives a value lower than unity. Thus, the ion exchange isotherm shows S shape curve for rigid exchanger, indicating reversal selectivity, and the selectivity coefficient decrease progressively with increasing concentration of metal ions in exchanger.

Figs. 5-a) and 6-a) showed the typical ion exchange isotherms for alkali metal, alkaline earth metal , and Pb /H^+ systems. The selectivity reversal was observed for the metal ions/ H^+ ion exchange reactions listed, except for Li^+ and Mg^{2+}/ H^+ reactions [25, 26].

The plots of ln K_H^M vs X_M , which are referred to Kielland plots, are shown in Figs. 5-b and 6-b. The selectivity coefficients decrease with increasing the concentration of metal ions in the exchanger. A fairly good linearlity was observed for the Kielland plots of the all ion exchange system listed, except of Ba^{2+}/H^+ and Pb^{2+}/H^+ systems. It has been known that the absolute values of the Kielland coefficient, C, indicate degree of the steric effect in the exchangers. The C values for different exchange systems are plotted as a function of the effective crystal ionic radius in Fig. 7, including the results for our earlier results. These plots show that cations with an effective crystal ionic radius of 1.0-1.2 Å enter the exchanger with minimum steric hindrance. The C-SbA has a rigid structure without swelling or shrinking; the change in the lattice constant is less than 2% for the conversion

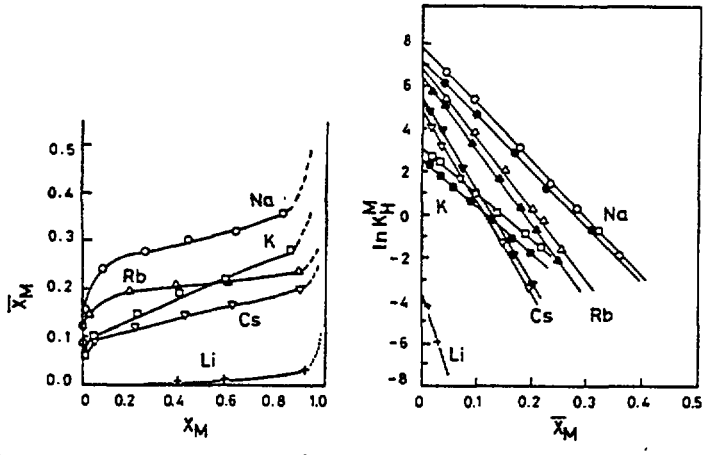

Fig. 5. Ion exchange isotherms (a) and plots of ln K_H^M vs $\overline{X}_M$ (b) for the system of alkali metal ions/H^+ on C-SbA.

Open mark; 30°C, closed mark; 45°C.

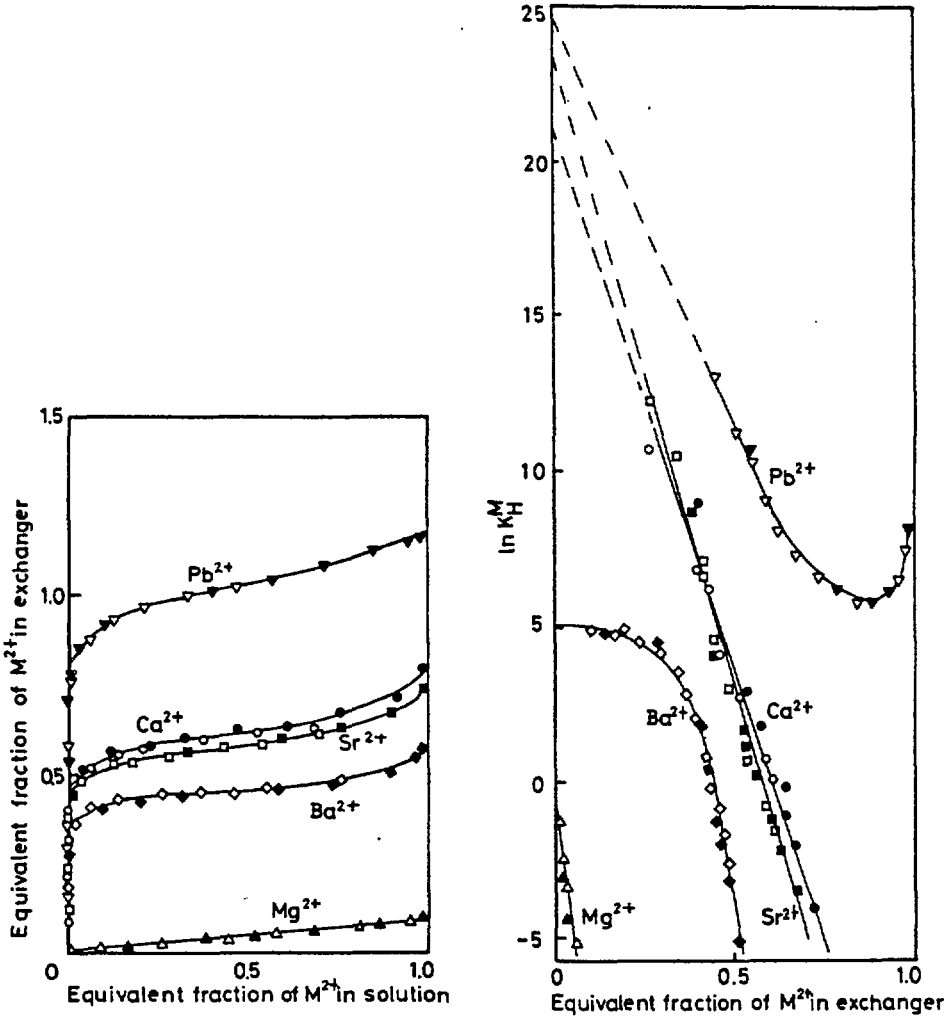

Fig. 6. Ion exchange isotherms (a) and plots of ln K_H^M vs $\overline{X}_M$ (b) for the systems of alkaline earth metal ions and Pb^{2+}/H^+ on C-SbA at 30°C

Open mark; forward reaction,
closed mark; reverse reaction

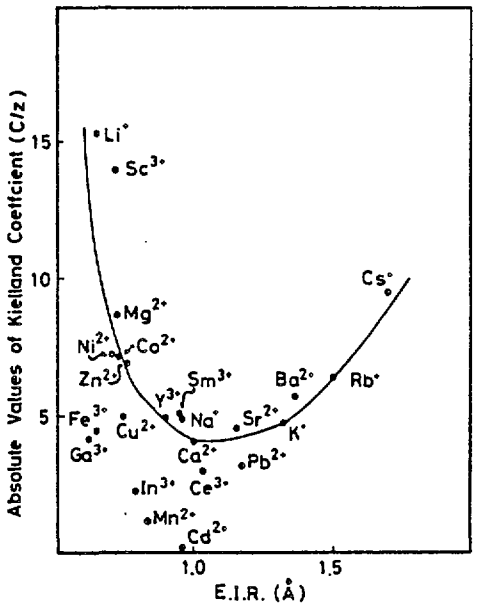

Fig. 7. Plots of absolute value of Kieland coefficient vs effective crystal ionic radius of various metals.

from the hydrogen ion form to metal ion forms. The small cations, Li^{+}, Mg^{2+} and Ni^{2+} are hydrated strongly in the aqueous solution and may be exchanged in keeping with their hydration shell or in leaving a few hydrated water from hydration shell. This brings large steric effects in the rigid structure of the C-SbA. The exchange reaction of H^{+} by the large cations with less hydrated becomes progressively difficult in the rigid structure. Thus, the minimum steric effect of the C-SbA may be interpreted in the both contributions.

4. 2. Ion exchange selectivity of metal antimonates.

Quadrivalent metal antimonates as ion exchangers have been studied first by Abe and Ito [14]. Especially, tin(IV) and Titanium antimonates(SnSbA and TiSbA, respectively) behave as the cation exchangers with relatively high exchange capacity, and show the excellent selecivities for alkali metal ions in the order: Na< K <Rb< Cs < Li on SnSbA and Na< K < Rb< Li < Cs on TiSbA, which are not included in 11 Eisenman's selectivity series predicted [27].

4. 2. 1. Selectivity of SnSbA for microamount of metal ions.

Equilibrium distribution coefficients of alkali, alkaline earth, and transition metal ions on SnSbA with a mole ratio(Sb/Sn) of 1.86 were plotted in Fig. 8, values on Bio-Rad AG 50W-X8 being included for comparison. The Kd values for alkali and alkaline earth metal ions on SnSbA, except Li, increase in the order; Na< K <Rb < Cs and Mg< Ca < Sr < Ca, as shown with sulfonate-type organic resins. The separation factors are more favorable than those obtained on Bio-Rad AG 50W-X8 [28]. The increased selectivity, except Na and Mg, was observed to be higher than that on Bio-Rad AG 50W-X8. Much high selectivity and Kd values for transition metal ions were also observed with comparison of organic ion exchange resins. The selective sequence of transition metal showed Ni < Mn < Cd < Co< Cu < Zn on the SnSbA [28], and Mn < Zn < Cu < Ni < Co < Cd < on Bio-Rad AG 50W-X8.

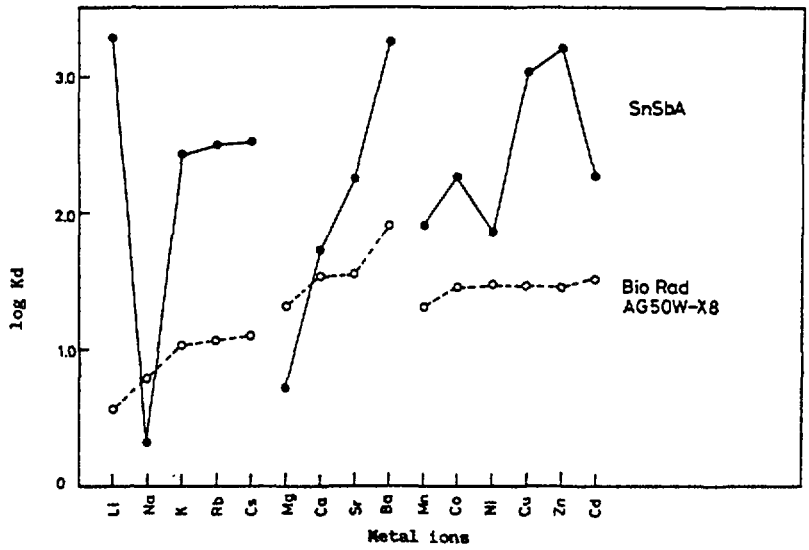

Fig. 8. The Kd values of various metal ions on SnSbA in 1 M HNO_3

It has been known that the ion exchange properties including their selectivities are much dependendt on their preparetive conditions and compositions. The Kd value of Li^+ shows a maximum at about 1.7 of the Sb/Sn ratio, while increase with increasing Sb/Sn ratio for other alkali metal ions [15]. The selectivity sequences of alkali metal ions maintain in a range from 0.5 to 2.5 of Sb/Sn ratio. An extremely high selectivity was observed for Li , which was a good advantage for separation of Li from other alkali metal ions like seawater [29].

4. 2. 2. Selectivity of TiSbA for microamount of metal ions.

On the TiSbA, slightly different selectivities with the SnSbA was observed; Na < K < Rb < Li < Cs for alkali metal ions [16], and Ni < Mn < Co < Cd < Zn < Cu for transition metal ions [30]. An usual selectivity sequence was obtained for alkaline earth metal ions. The Kd values on the TiSbA were smaller than those on the Bio-Rad AG 50W-X8. The Kd value increases with increasing mole ratio of Sb/Ti. The low Kd values for these metal ions, compared with SnSbA and Bió-Rad AG 50W-X8, are due to lower value (0.64) on the Sb/Ti ratio (see Fig. 9).

4. 2. 3. Ion exchange isotherms and Selectivity coefficients for alkali metal ions/ H^+ system.

The ion exchange isotherms observed at 30°C are shown in Fig.10. Each plot of the results of the reverse reaction can be plotted on the isotherm curves of the forward reaction. Thus, reversible exchange reactions are established and no hysteresis effect is observed. The isotherms observed showed the S shape curves, indicating the selectivity reversal [31].

The Kielland plots showed inflection points at about 0.04 and 0.14 of $\overline{X_M}$ for Li^+/H^+ and other metal ions / H^+ systems. An extremely high selectivity was observed for Li at the concentration lower than X = 0.04. This indicates that preference sites for Li are present at lower exchange composition. Other alkali metal ions can not approach to the sites because of large crystal ionic radius. The

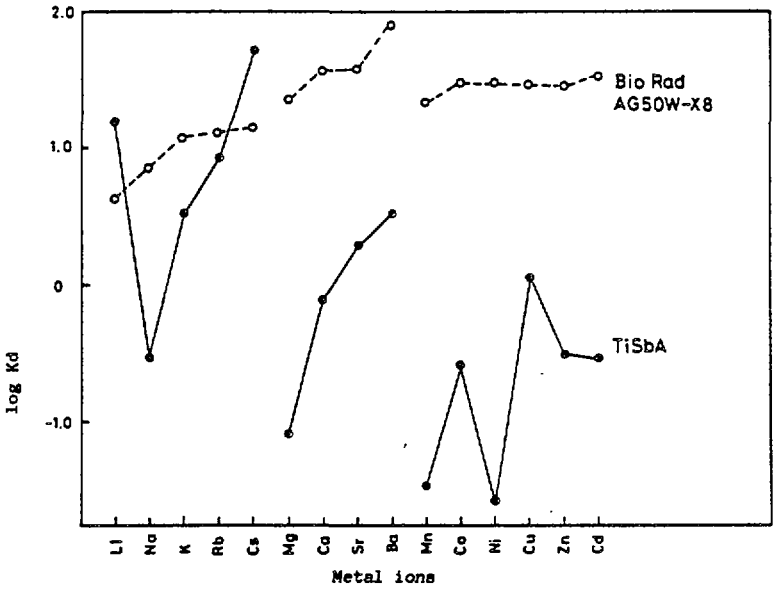

Fig. 9. The Kd values of various metal ions on TiSbA in 1 M HNO_3

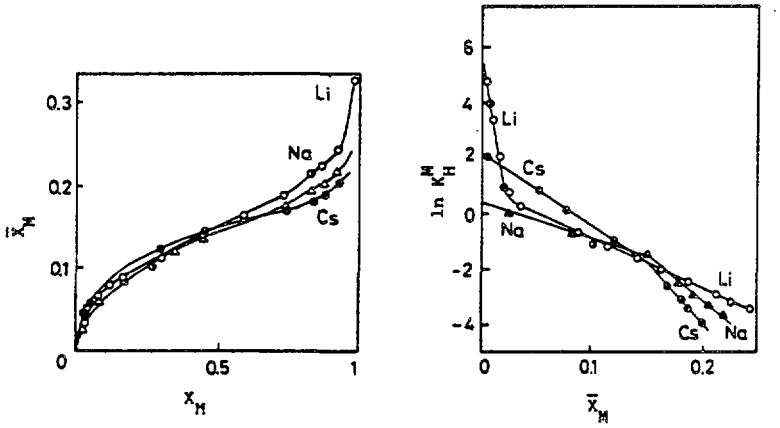

Fig. 10. Ion exchange isotherms (a) and plots of ln K_H^M vs $\bar{X}_M$ (b) for the systems of alkali metal ions on SnSbA at 30°C.

maximum uptake was found to be 1.13, 0.98, 0.77, and 0.73 meq/g for Li, Na, K, Rb, and Cs, respectively. This behavior can be explained in the terms of the selectivity reversal at these infection points.

REFERENCES

[1] AMPHLETT, C. B., Inorganic Ion Exchangers, Elsevier, Amsterdam, 1964.
[2] FULLER, M.J., Chromatogr. Rev., 14 (1971) 45.
[3] VESELY, V., Pekarek, V., Talanta, 19 (1972) 219,1245.
[4] ABE,M., Bunseki Kagaku, 23 (1974) 1254, 1561.
[5] ALBERTI, G., Acc. Chem. Res.,11 (1978) 163.
[6] De, A. K., Sen, A. K., Sep. Sci. Technol., 13 (1978) 517.
[7] CLEARFIELD, A., Inorganic Ion-exchange Materials, CRC Press, Inc., Boca Raton Fl., (1982).

[8] ITO, T., ABE, M., Nippon Kagaku Zasshi, 87 (1966) 1174.
[9] ABE, M., ITO,T., Bull. Chem. Soc. Jpn., 40 (1967)1013.
[10] ABE, M., T. ITO, Bul. Chem. Soc. Jpn., 41 (1968) 333.
[11] ABE, M., Bull. Chem. Soc. Jpn., 42 (1969) 2623.
[12] GIRARDI, F., SABBIONI, E., J. Radioanal. Chem., 1 (1968) 169.
[13] BAETSLE, S., HUYS, D., J. Inorg. Nucl. Chem., 30 (1968) 242.
[14] ABE, M., ITO, T., Kogyo Kagaku Zasshi, 70 (1967) 440.
[15] ABE, M., HAYASHI, K., Solv. Extract. Ion Exch., 1 (1983) 97.
[16] ABE, M., TSUJI, M., Chem. Lett. 1983, 1561.
[17] KRAUS, K. A., RARIDON, R. J., J. Phys. Chem., 63(1959) 1901.
[18] GAINS Jr.,G. L., THOMAS, H.C., J. Chem. Phys.,41(1953) 714.
[19] BARRER, R. M., FALCONER, J. D., Proc. R. Soc., A236 (1956) 227.
[20] BARRER, R. M.,et al., Proc. R. Soc., A273 (1963) 180.
[21] STRELOW, F. W. E., et al., Anal. Chem., 37 (1965) 106.
[22] ABE, M., UNO, K., Sepn. Sci.,Technol. 14, (1979) 355.
[23] ABE, M., Sepn. Sci. Tech., 15 (1980) 23.
[24] SHANNON, D. D., PREWITT, C. T., Acta Crystallogr. B23 (1969) 925.
[25] ABE, M., J. Inorg. Nucl. Chem., 41 (1979) 85.
[26] ABE, M., SUDOH, K., J. Inorg. Nucl. Chem., 43 (1981) 2537.
[27] EISENMAN, G., Biophys. J., 2, 259 (1962).
[28] ABE, M., FURUKI, N., The 44th Annual Meeting of Jpn. Chem. Soc., paper 2F19, Okayama (1981)
[29] ABE, M., HAYASHI, K., Hydrometallgy, 12 (1984) 83.
[30] ABE, M., CHITRAKAR, R., Unpublished Result.
[31] ABE, M., FURUKI, N., The 47th Annual Meeting of Jpn. Chem. Soc., paper 3T15 Kyoto (1983)

PANEL DISCUSSION

Chairman: H.J. Ache (Federal Republic of Germany)

SUMMARY AND RECOMMENDATIONS

I. Summary of the discussion

Inorganic ion exchangers and adsorbents have proved their potential usefulness in various areas of nuclear fuel cycle technology such as:

1) In the separation of fission products and actinides from medium- and high-activity wastes.

2) In the treatment of effluents from nuclear power plants.

3) As chemical barriers (backfill material) in underground repositories of radioactive wastes.

Improvements can be made in some techniques that are already being used by the industry, such as:

1) The adsorption of iodine from dissolver off-gases, and

2) The fixation of krypton-85 and $^{14}CO_2$.

Further research and development should be directed towards the optimization of the chemical and physical properties of these inorganic compounds for their application in the fields listed above. Considerable fundamental research is still necessary to have a better understanding of the mechanisms involved in adsorption and ion-exchange and of the correlation between structure and efficiency.

II. Recommendations

Regarding future activities, the participants recommend that international cooperation should be encouraged on the main topic of research on inorganic ion-exchangers and adsorbents for the separation of fission products and actinides from medium-and high-activity wastes and

for the treatment of effluents from nuclear power plants, including the following sub-topics:

a) Preparation;
b) Characterization;
c) Applications;
d) Process and engineering aspects, and
e) Economics.

Special efforts should be made to promote a greater exchange of information and closer cooperation between the specialists who are working in basic research and those who are primarily concerned with the practical applications of these compounds in nuclear fuel cycle technology.

LIST OF PARTICIPANTS

BELGIUM

Baetsle, L.
Chef du Department Chimie
CEN/SCK
B-2400 Mol, Belgium

Centner, B.
Ingenieur au bureau d'etude
d'Electrobel S.A.
Place du trone 1
1000 Bruxelles, Belgium

Jacqmin, J.
Belgonucleaire
25, Rue du Champ de Mars
B - 1050 Brussels, Belgium

CHINA, PEOPLE'S REPUBLIC OF

Weng Haomin
Beijing Normal University
Division of Radiochemistry
and Radiation Chemistry
Beijing, China, People's Republic of

Zhu Yong-jun
Institute of Nuclear Energy Technology
Tsinghua University
Beijing, China, People's Republic of

EGYPT

Misak, N.Z.
Prof. of Physical Chemistry
Nuclear Chemistry Department
Atomic Energy Post 13759
101 Kasr El Einy Street
Cairo, Eygpt

FINLAND

Lehto, J.
University of Helsinki
Department of Radiochemistry
Unioninkatu 35
Helsinki, Finland

FRANCE

Dozol, J.F.
CEA/Centre d'Etudes Nucleaires de
Cadarache
Services d'Effluents et Dechets de
Faible et Moyenne Activite
F-13115 St. Paul Les Durance, France

Madic, C.
CEA, Section des Transuraniens
B.P. No. 6
F-92260 Fontenay-aux-Roses
France

Regnaud, F.	CEA/DCAEA/Service Etudes Analytiques B.P. No. 6 F-92260 Fontenay-aux-Roses France

GERMANY, FEDERAL REPUBLIC OF

Ache, H.J.	Nuclear Research Center Karlsruhe Institute of Radiochemistry Postfach 3640 D - 7500 Karlsruhe Germany, Federal Republic of
Merz, E.	Institute of Chemical Technology Kernforschungsanlage Julich GmbH D-5170 Julich, POB 1913 Germany, Federal Republic of
Sameh,A.A.	Nuclear Research Center Karlsruhe Institute of Radiochemistry Postfach 3640 D - 7500 Karlsruhe Germany, Federal Republic of

HUNGARY

Szirtes, L.	Institute of Isotopes of the Hungarian Academy of Sciences P.O.Box 77 H-1525 Budapest Hungary

INDIA

Iyer, R.M.	Head of Chemistry Division Bhabha Atomic Research Coentre Trombay Bombay 400 085, India

ITALY

Alberti, G.	Dipartimento di Chimica Universita di Perugia Via Elce di Sotto 10 I-06100 Perugia, Italy

JAPAN

Abe, M.	Department of Chemistry Tokyo Institute of Technology 2-12-1 Ookayama Meguro-ku Tokyo, Japan
Ito, T.	Deputy Director Department of Radioisotope Production Radioisotope Center, JAERI Tokai-mura, Ibaraki-ken, Japan

Kanno, T.	Research Institute of Mineral Dressing and Metallurgy Tohoku University 1 1 Katahira-Chome Sendai, Japan
Sakurai, T.	General Manager, Physical Chemistry Lab. Department of Chemistry Tokai Research Establishment JAERI Tokai-mura, Ibaraki-ken Japan

PAKISTAN

Chaudhri, S.A.	Alternate to the Resident Representative Permanent Mission of Pakistan to the IAEA Hofzeile A-1190 Vienna

SWEDEN

Airola, C.	Nuclear Division, Waste Systems Studsvik Energiteknik AB S - 61182 Nykoeping Sweden

UNITED KINGDOM

Harding, K.	UKAEA ABE Winfrith Dorchester Dorset DT2 8DH U. K.
Hooper, E.W.	Separation Processes Group Chemical Technology Division AERE Harwell Oxon OX11 ORA U. K.
Eccles, H.	Building 643, BNFL Springfield Works Salwick Preston, Lancs., PR4 OXJ U. K.

UNITED STATES OF AMERICA

Carl, D.	Senior Engineer/Solidification Engineer West Valley Nuclear Services Co. Inc. P.O. Box 191 West Valley, New York 14171-0191, U.S.A.

Clearfield, A.	Department of Chemistry Texas A&M University College Station, TX 77843 U.S.A.
Collins, E.D.	Manager Three Mile Island Assistance Programs Oak Ridge National Laboratory Oak Ridge, TN 37831 U.S.A.

YUGOSLAVIA

Ruvarac, A.	The Boris Kidric Institute of Nuclear Sciences 11001 Belgrade P. O. Box 522 Yugoslavia

ORGANIZATIONS

INTERNATIONAL ATOMIC ENERGY AGENCY (IAEA)

Ajuria, S.	Division of Nuclear Fuel Cycle
Rybalchenko, I.	Division of Nuclear Fuel Cycle
Ugajin, M. (Scientific Secretary)	Division of Nuclear Fuel Cycle